THE
PHYSICAL REVIEW
A Journal of Experimental and Theoretical Physics Established by E. L. Nichols in 1893
VOL. 54, NO. 12 DECEMBER 15, 1938 SECOND SERIES

On World-Wide Changes in Cosmic-Ray Intensity

S. E. FORBUSH
Department of Terrestrial Magnetism, Carnegie Institution of Washington, Washington, D. C.
(Received October 11, 1938)

Continuous cosmic-ray records for periods of 17 months or more obtained by Compton-Bennett meters at Cheltenham (United States), Teoloyucan (Mexico), Christchurch (New Zealand), and Huancayo (Peru) are reduced to a constant barometric pressure at each station. After deducting a 12-month wave from the data at each of these stations except at Huancayo, where none is found, a high correlation ($r \doteq 0.90$) is obtained between the means of cosmic-ray intensity for each one-third month for any two of the four stations. This high correlation, based on all available data for each pair of stations, is definite evidence that, except for the 12-month waves, the major changes in cosmic-ray intensity are world-wide. With published data from a Steinke instrument on the Hafelekar, near Innsbruck, the world-wide changes, when expressed in percent of the absolute intensity at each station, are found to increase rapidly with altitude for stations at the same latitude. A large increase in the world-wide effect for stations at high altitudes occurs between the equator and geomagnetic latitude 30° north, while no further very large increase occurs up to latitude 47° north. Results for Christchurch and Cheltenham indicate that the magnitude of the world-wide effect is symmetrical about the equator, and its connection with effects observed during certain magnetic storms is discussed. The amplitude of the 12-month wave, which in the Northern Hemisphere has its maximum near mid-January, increases from zero at the equator to about 1.0 percent at Teoloyucan, 1.6 percent at Cheltenham, and 1.9 percent on the Hafelekar. At Christchurch, its maximum occurs near the end of July, its amplitude being about 0.8 percent of the total intensity. Accordingly, it seems that the 12-month wave may not be ascribed to a solar-magnetic moment.

INTRODUCTION

THE decrease of several percent in cosmic-ray intensity which occurred[1–4] simultaneously at Cheltenham (United States), Huancayo (Peru), on the Hafelekar (Germany), Christchurch (New Zealand), and Teoloyucan (Mexico) during the magnetic storms which began April 24, 1937, and January 16, 1938, provided definite evidence that these changes were world-wide. The fact that the decrease in cosmic-ray intensity began within an hour or two after the sudden commencements of these magnetic storms led us to hypothesize[1, 4] that the change in cosmic-ray intensity resulted from the magnetic field of the current-system responsible for magnetic storms. The nature of the field-changes which occur over the earth's surface during magnetic storms is such that the world-wide characteristics of the storm field can be ascribed either to a system of westward currents forming a spherical current-sheet, concentric with the earth, in the upper atmosphere or to a westward current-system approximated by a ring concentric with the earth and in the plane of the earth's geomagnetic equator.[5]

[1] S. E. Forbush, Phys. Rev. **51**, 1108–1109 (1937).
[2] V. F. Hess and A. Demmelmair, Nature **140**, 316–317 (1937).
[3] V. F. Hess, R. Steinmaurer and A. Demmelmair, Nature **141**, 686–687 (1938).
[4] S. E. Forbush, Terr. Mag. **43**, 203–218 (1938).
[5] S. Chapman, Terr. Mag. **40**, 349–370 (1935).

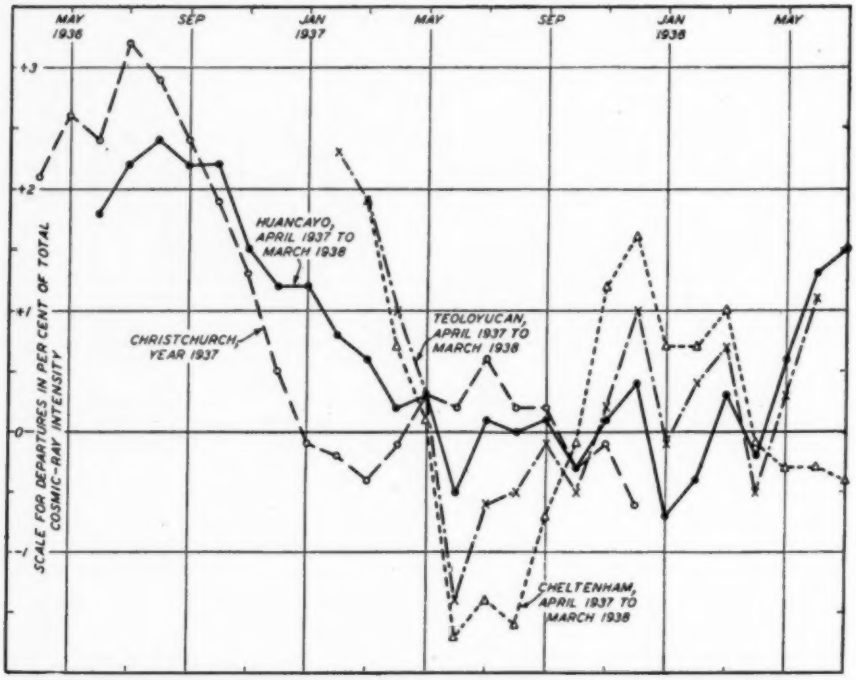

FIG. 1. Departures monthly means cosmic-ray intensity from mean for year indicated.

Further investigation[4] showed, however, two magnetic storms of equal intensity at the earth's surface, during one of which a world-wide decrease of about six percent in cosmic-ray intensity was observed, while no detectable change occurred in the other. Assuming the world-wide part of the storm field to arise from the above-mentioned ring-current system, we attempted[4] to calculate, using magnetic data from several observatories, the radius of the assumed ring for the two storms. Although this analysis provided no convincing evidence that the radius of the ring was significantly different for the two storms, it did indicate that a necessary condition for the existence of such a ring-current was satisfied by the magnetic data. We concluded that the radius for neither storm could be much less than about twice that of the earth, although the possibility of an indefinitely larger radius for either of the storms was not excluded.

We also found that, while there was close correlation between changes in daily means of cosmic-ray intensity and of the horizontal magnetic component at the equator during individual magnetic storms, the ratio between the two was significantly different even for storms accompanied by world-wide changes in cosmic-ray intensity. We therefore concluded that, if the major current-system for magnetic storms were approximated by an equatorial ring, its radius must be different even for the different storms accompanied by changes in cosmic-ray intensity.

Evidence is presented in the present investigation that the world-wide character of changes in

TABLE I. *Location and elevation of cosmic-ray stations and magnitude of world-wide effect, relative to Huancayo, for each.*

STATION	GEOGRAPHIC LATITUDE	GEOGRAPHIC LONGITUDE	GEOMAGNETIC LATITUDE	ELEVATION ABOVE SEA LEVEL	WORLD-WIDE EFFECT RELATIVE TO HUANCAYO
Cheltenham, United States	38.7N	76.8W	50.1N	72	1.11
Teoloyucan, Mexico	19.2N	99.2W	29.7N	2285	1.58
Huancayo, Peru	12.0S	75.3W	0.6S	3350	1.00
Christchurch, New Zealand	43.5S	172.6E	48.0S	8	1.05
Hafelekar, Germany	47.3N	11.3E	48.4N	2300	1.59

cosmic-ray intensity is found throughout the data available to us, and hence is not restricted to periods of intense magnetic storms.

Table I indicates the location and elevation of the several cosmic-ray meters. Those at the first four locations are Compton-Bennett[6] precision recording instruments operated under the auspices of the Committee on Coordination of Cosmic-Ray Investigations of the Carnegie Institution of Washington. Data from these were obtained with a total shielding equivalent to 12 cm of lead. Data for the last station of Table I were obtained from publications by V. F. Hess[2, 3, 7] and his co-workers who used a Steinke apparatus at constant temperature, shielded on all sides with ten cm of lead and seven cm of iron. Observed values of ionization were corrected for bursts and for changes in barometric pressure, by applying to all data at each station a constant barometric coefficient.[8] The percentage changes in cosmic-ray intensity for each station were determined on the basis of the total ionization, corrected for residual, given by the meter at that station.

[6] A. H. Compton, E. O. Wollan and R. D. Bennett, Rev. Sci. Inst. **5**, 415–422 (1934).
[7] A. Demmelmair, Ber. Akad. Wiss. Wien, **146**, IIa, 643–659 (1937).
[8] S. E. Forbush, Terr. Mag. **42**, 1–16 (1937).

Analysis of Data

In Fig. 1 are plotted, for four stations, the departures of observed monthly means of cosmic-ray intensity from the indicated annual means. It is evident that, in general, no particularly close correspondence exists between the departures for the different stations. From the 13 monthly mean departures for Cheltenham, beginning with April, 1937, we obtained by harmonic analysis[9] the 12-month wave which best fits the departures in this interval corrected for noncyclic change, which was assumed linear and was taken as the departure for April, 1938 minus that for April, 1937. The smooth function plotted in Fig. 2 is the sum of this wave and the linear change. This function, indicated in Fig. 2 by a dashed line where extrapolated, departs considerably from the observed departures.

The dashed curve in Fig. 2 indicates the ordinates of the 12-month wave deducted from the observed departures for Cheltenham. This curve resembles closely that for the observed departures for Huancayo. The correlation between the two ($r=0.90$) is shown in Fig. 10. This indicates that the variations in cosmic-ray intensity which occur at Huancayo also occur with about the same amplitude at Cheltenham, where they are superposed upon a 12-month wave.

[9] J. Bartels, Beitr. Geophysik **28**, 1–10 (1930).

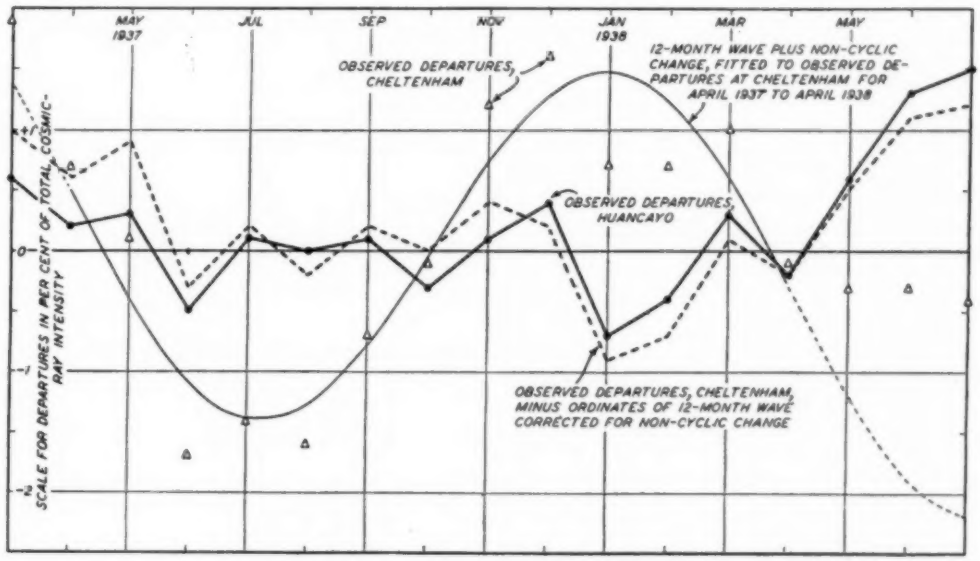

FIG. 2. Departures cosmic-ray intensity from Fig. 1, for Huancayo, and for Cheltenham before and after deducting 12-month wave.

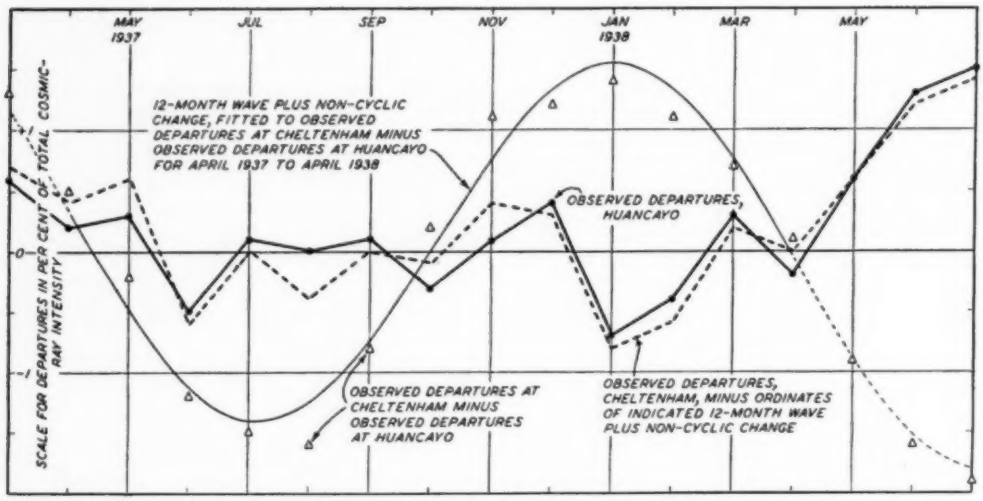
MAY 1937
JUL
SEP
NOV
JAN 1938
MAR
MAY
12-MONTH WAVE PLUS NON-CYCLIC CHANGE, FITTED TO OBSERVED DEPARTURES AT CHELTENHAM MINUS OBSERVED DEPARTURES AT HUANCAYO FOR APRIL 1937 TO APRIL 1938
OBSERVED DEPARTURES, HUANCAYO
OBSERVED DEPARTURES AT CHELTENHAM MINUS OBSERVED DEPARTURES AT HUANCAYO
OBSERVED DEPARTURES, CHELTENHAM, MINUS ORDINATES OF INDICATED 12-MONTH WAVE PLUS NON-CYCLIC CHANGE
SCALE FOR DEPARTURES IN PER CENT OF TOTAL COSMIC-RAY INTENSITY
+1
0
-1

FIG. 3. Departures cosmic-ray intensity from Fig. 1, for Huancayo, and for Cheltenham after deducting departures for Huancayo.

When the departures at Huancayo for the interval April 1937 to April 1938 are corrected for noncyclic change and subjected to harmonic analysis, the amplitude of the resulting 12-month wave is practically zero. Thus, although the changes in cosmic-ray intensity at Huancayo are also found at Cheltenham superposed on a 12-month wave, our determination of the 12-month wave for Cheltenham is not materially affected by their presence. If, obscured by the changes which also occur at Cheltenham, a 12-month wave in cosmic-ray intensity existed at Huancayo, then the differences, taken month by month, between the two irregular curves of departures in Fig. 2 should determine the 12-month wave for Huancayo. In this way no significant amplitude for this wave is found.

If the indication is correct that changes in cosmic-ray intensity occur simultaneously at Huancayo and at Cheltenham superposed on a 12-month wave, then a 12-month wave should fit quite closely the differences obtained by subtracting the monthly mean departures of cosmic-ray intensity for Huancayo from those at Cheltenham. The result is shown in Fig. 3 in which the better approximation to the 12-month wave is evident.

To obtain a better indication of the relation

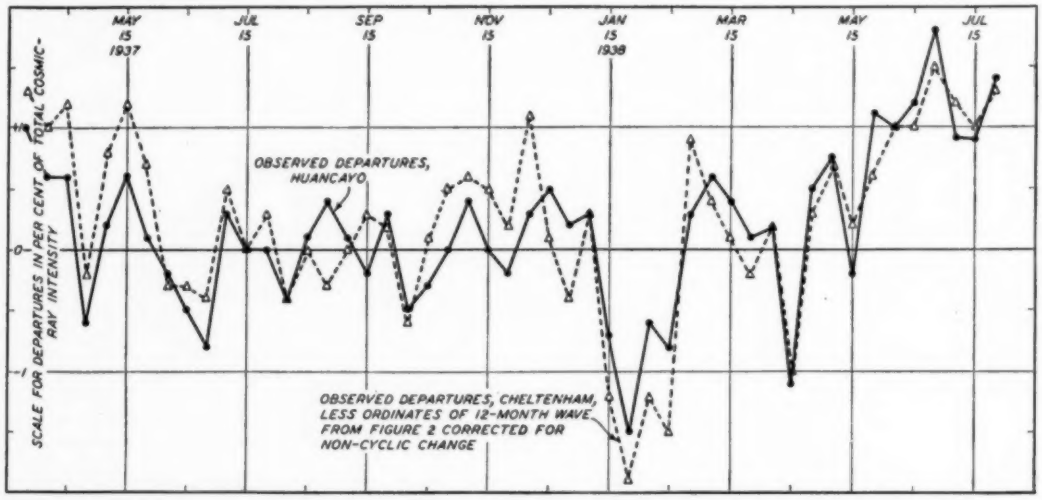

FIG. 4. Departures cosmic-ray intensity for each one-third month from mean April, 1937 to March, 1938 for Cheltenham after deducting 12-month wave, and for Huancayo.

between the world-wide changes at Huancayo and Cheltenham, the departures from the annual mean of those of cosmic-ray intensity for each one-third month were computed. From these means for Cheltenham were subtracted the ordinates of the 12-month wave of Fig. 2 and the result is shown in Fig. 4. The correlation between the two curves is 0.86 (see Fig. 12-*A*).

Figure 5 shows the close approximation of a 12-month wave to the result obtained by subtracting the monthly mean departures of cosmic-ray intensity at Huancayo from those at Christchurch. The dashed curve, which is remarkably similar to that for the observed departures at Huancayo, results from deducting the ordinates of this 12-month wave from the observed de-

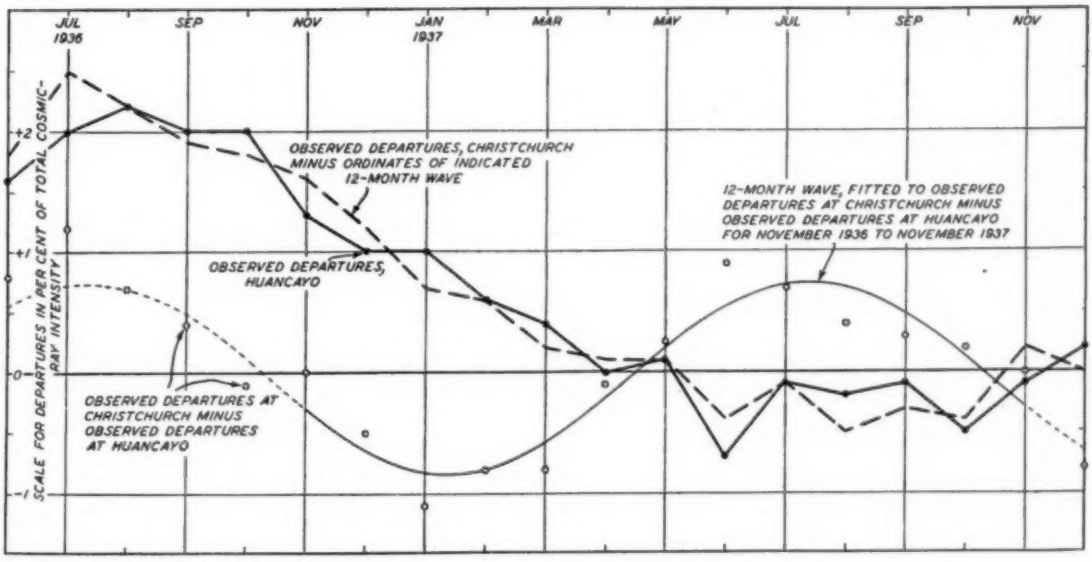

FIG. 5. Departures monthly means cosmic-ray intensity from mean for 1937 for Huancayo and for Christchurch after deducting departures for Huancayo.

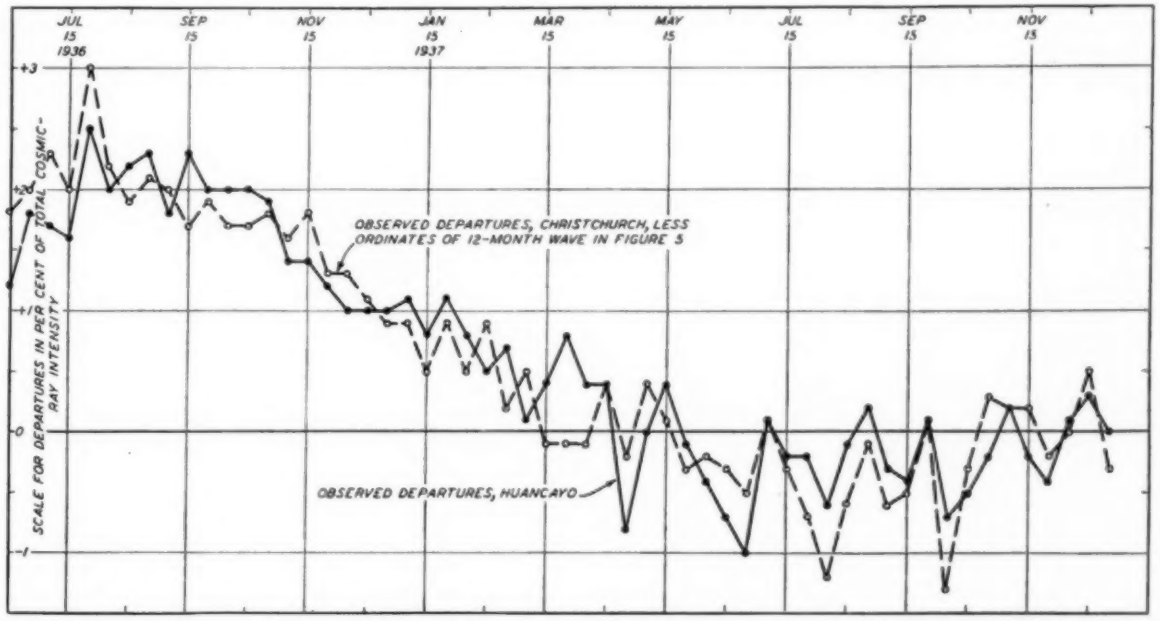

FIG. 6. Departures cosmic-ray intensity for each one-third month from mean for 1937, for Christchurch with 12-month wave deducted, and for Huancayo.

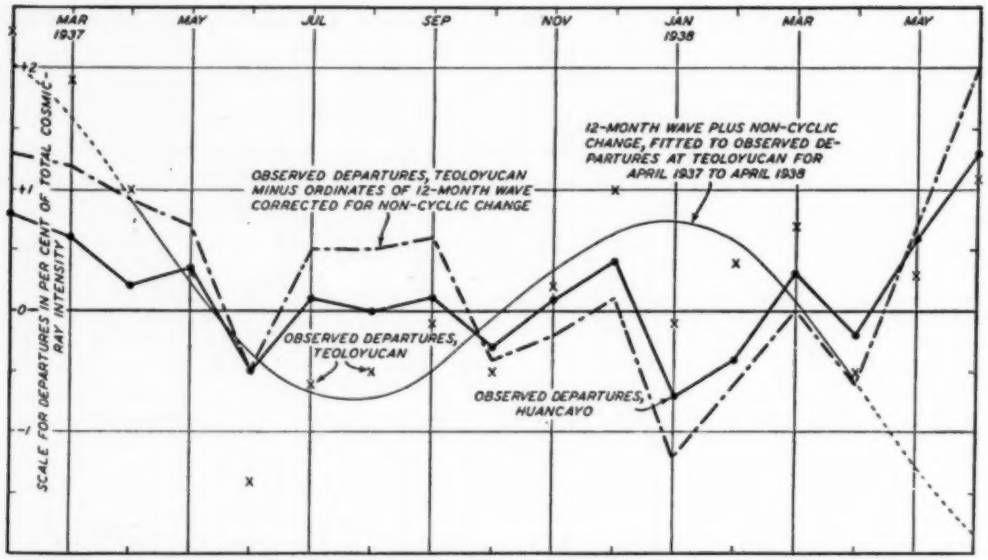

FIG. 7. Departures cosmic-ray intensity from Fig. 1, for Teoloyucan after deducting 12-month wave, and for Huancayo.

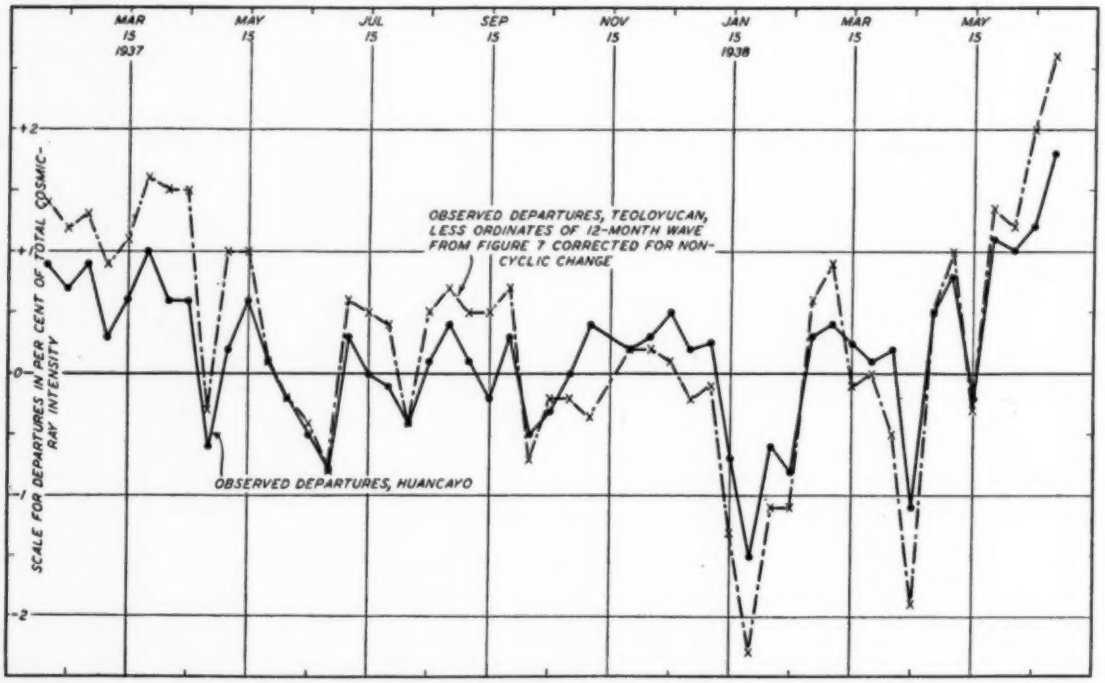

FIG. 8. Departures cosmic-ray intensity for each one-third month from mean for year beginning April 1937, for Teoloyucan after deducting 12-month wave, and for Huancayo.

partures (see Fig. 1) at Christchurch. The high correlation ($r=0.97$, see Fig. 10) between these curves results from the similarity in their trends rather than from correspondence of individual changes. However, a parallelism between changes in the means of cosmic-ray intensity for each one-third month at Christchurch, after deducting the 12-month wave, and those at Huancayo is evident in Fig. 6.

The similarity between the observed departures of monthly means of cosmic-ray intensity at Huancayo and those obtained by deducting

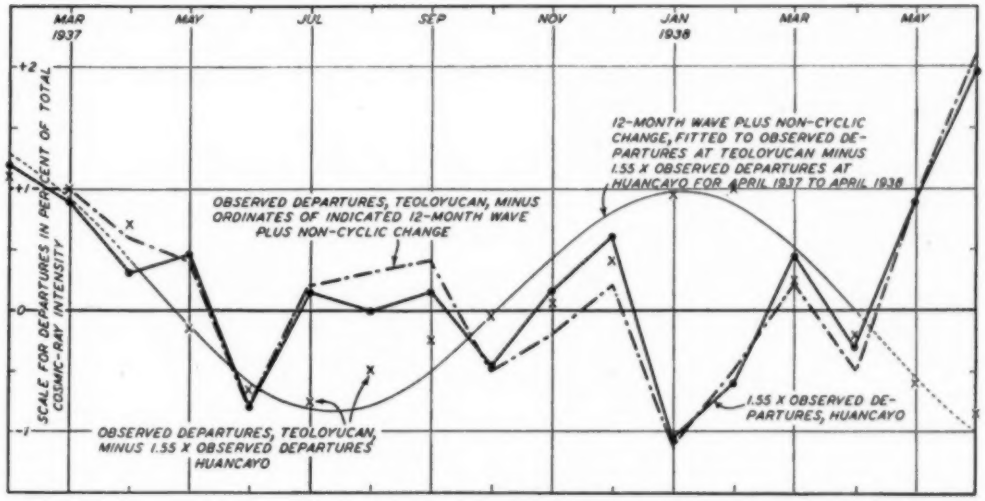
MAR 1937
MAY
JUL
SEP
NOV
JAN 1938
MAR
MAY
+2
+1
0
-1
SCALE FOR DEPARTURES IN PER CENT OF TOTAL COSMIC-RAY INTENSITY
12-MONTH WAVE PLUS NON-CYCLIC CHANGE, FITTED TO OBSERVED DEPARTURES AT TEOLOYUCAN MINUS 1.55 X OBSERVED DEPARTURES AT HUANCAYO FOR APRIL 1937 TO APRIL 1938
OBSERVED DEPARTURES, TEOLOYUCAN, MINUS ORDINATES OF INDICATED 12-MONTH WAVE PLUS NON-CYCLIC CHANGE
1.55 X OBSERVED DEPARTURES, HUANCAYO
OBSERVED DEPARTURES, TEOLOYUCAN, MINUS 1.55 X OBSERVED DEPARTURES HUANCAYO

FIG. 9. Departures cosmic-ray intensity from Fig. 1, times 1.55 for Huancayo, and for Teoloyucan after deducting 1.55 times departures for Huancayo.

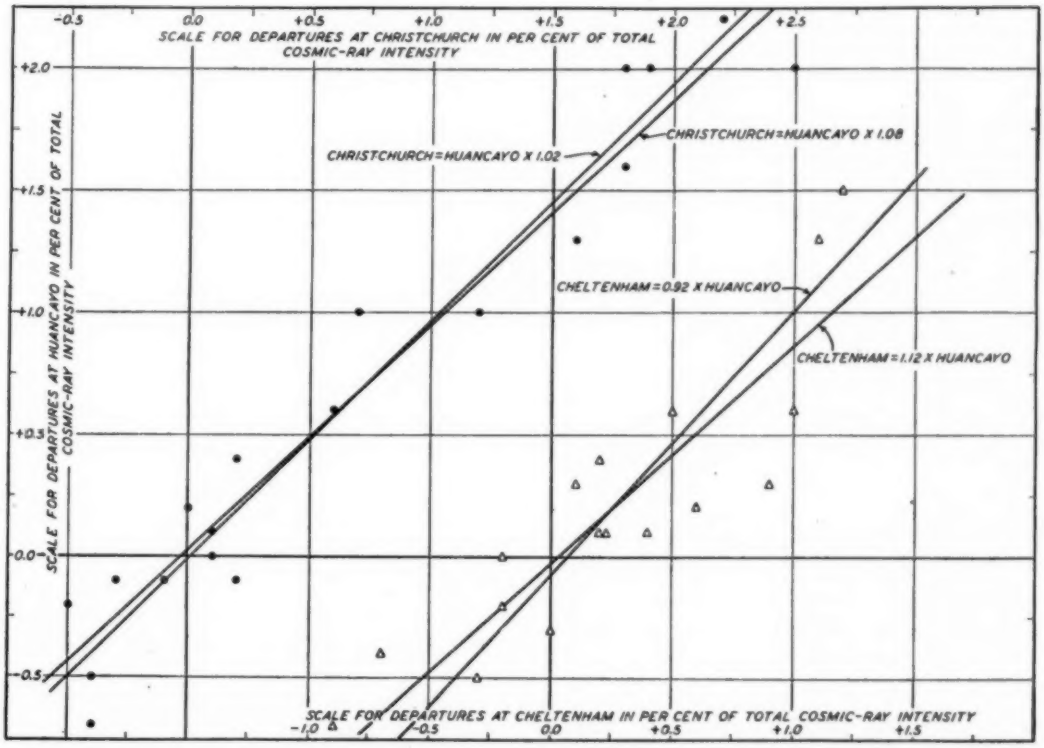

FIG. 10. Correlation between departures cosmic-ray intensity from Fig. 1, after deducting 12-month waves for Christchurch and Cheltenham.

the 12-month wave at Teoloyucan is shown in Fig. 7. The correlation between the two ($r=0.92$) is shown in Fig. 11-*A*, which indicates that the world-wide changes at Teoloyucan are between 50 and 80 percent greater than at Huancayo. This is also evident from the curves in Fig. 8, the correlation between which is 0.92 (see Fig. 12-*B*). It will later be shown that the world-wide changes in cosmic-ray intensity at Teoloyucan are about 55 percent greater than at Huancayo.

The close approximation of a 12-month wave, plus a linear change, to the result obtained by

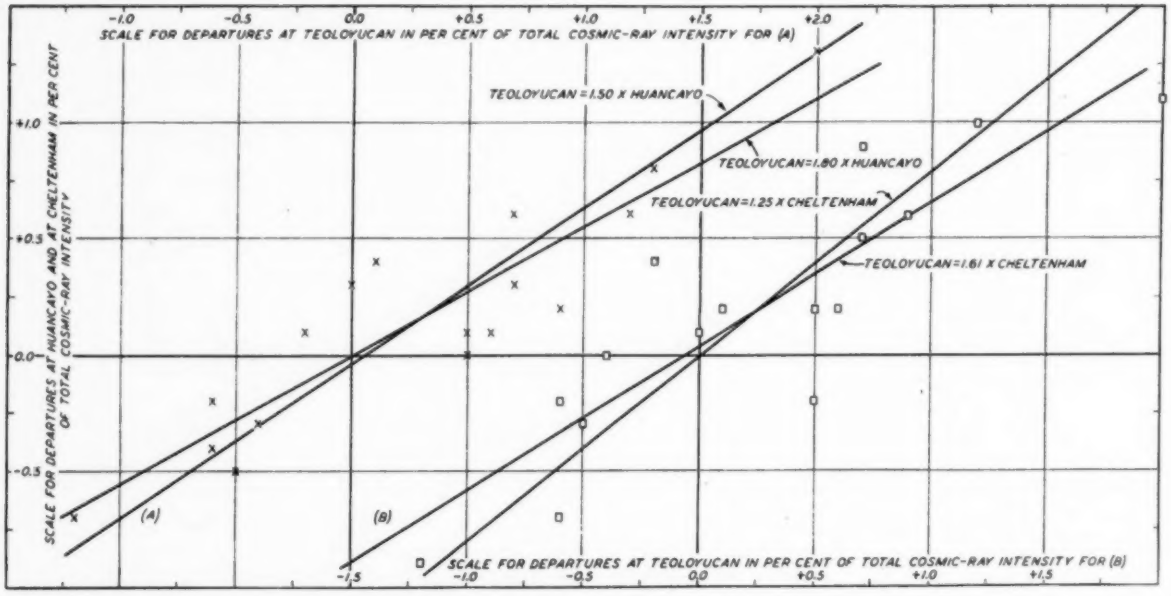
SCALE FOR DEPARTURES AT TEOLOYUCAN IN PER CENT OF TOTAL COSMIC-RAY INTENSITY FOR (A)
TEOLOYUCAN = 1.50 X HUANCAYO
TEOLOYUCAN = 1.80 X HUANCAYO
TEOLOYUCAN = 1.25 X CHELTENHAM
TEOLOYUCAN = 1.61 X CHELTENHAM
SCALE FOR DEPARTURES AT HUANCAYO AND AT CHELTENHAM IN PER CENT OF TOTAL COSMIC-RAY INTENSITY
(A)
(B)
SCALE FOR DEPARTURES AT TEOLOYUCAN IN PER CENT OF TOTAL COSMIC-RAY INTENSITY FOR (B)

FIG. 11. Correlation between departures cosmic-ray intensity from Fig. 1, after deducting 12-month waves for Teoloyucan and Cheltenham.

subtracting 1.55 times the departures at Huancayo from those at Teoloyucan is shown in Fig. 9. The dashed curve, which so closely parallels the curve for 1.55 times the observed departures at Huancayo, results from deducting the ordinates of the indicated wave from the observed departures at Teoloyucan.

Relative Magnitude of World-Wide Changes in Cosmic-Ray Intensity at Different Latitudes and Elevations

In Fig. 11-*B* is shown the correlation between monthly means of cosmic-ray intensity at Teoloyucan and Cheltenham after deducting the respective 12-month waves. If one arbitrarily assumes the best relation between the world-wide changes at any two stations to be the average of the two factors indicated for the regression lines in Figs. 10 and 11, it is found that (1) the world-wide changes at Cheltenham and at Christchurch are each a few percent greater than those at Huancayo, and (2) the world-wide changes at Teoloyucan are about 65 percent greater than at Huancayo and about 43 percent greater than at Cheltenham. However, these factors for the three relations, of which only two are independent, between Cheltenham, Teoloyucan, and Huancayo are mutually only roughly consistent. This is to be expected since the factors were selected somewhat arbitrarily.

To obtain more reliable values for these relations, assumed linear, between world-wide changes at different stations, use is made of the data in Fig. 12. *C* of Fig. 12 indicates the correlation between world-wide changes in the means for each one-third month at Teoloyucan and Cheltenham. For Figs. 12, 4, 6 and 8, only those days were used in each one-third month for which simultaneous data were available from both stations; there are, however, but few cases in which all days were not available for all stations.

The slopes of the lines indicated in Fig. 12 represent the most probable values, in the sense of least squares, consistent with the assignment of weights[10, 11] 1, 2 and 3, respectively, to the departures at Cheltenham, Teoloyucan, and Huancayo. Since these weights were assigned in an objective manner, there is nothing arbitrary, except the use of least squares, in the method used to obtain the slopes indicated.

The correlation coefficients for *A*, *B*, and *C* of Fig. 12 are 0.86, 0.92, and 0.86, respectively.

[10] W. E. Deming, Phil. Mag. **11**, 146–158 (1931); **17**, 804–829 (1934).
[11] H. S. Uhler, J. Opt. Soc. Am. **7**, 1043–1066 (1923).

The slopes of the regression lines, which result if infinite weight is given to one or the other of the two coordinates, are 1.01 and 1.36 for *A*, 1.42 and 1.68 for *B*, and 1.11 and 1.50 for *C*. Any slope between these limits may be obtained by least squares depending upon the relative weights assigned to the two coordinates. Suppose a slope midway between that for the two regression lines is arbitrarily adopted for *A* and *B*. With these slopes, values for the departures for Huancayo can be calculated separately from those at Cheltenham and at Teoloyucan. The variance (square of standard deviation) for single differences in each of the two sets of differences between the observed and calculated departures for Huancayo is computed. With the same arbitrary slopes, the variance is now determined for single differences between the two series of calculated departures for Huancayo. Since each of these three computed values of variance is the sum of two separate variances because of independent statistical variations at the two stations involved, one obtains three equations from which the variance, because of statistical fluctuations, at each of the stations is readily obtained. The variance thus obtained of statistical variations at each station is measured in terms of the original unit for Huancayo, and thus in terms of units, which are larger (on account of the arbitrary factors used for calculating departures for Huancayo) for Cheltenham and Teoloyucan than the original units for those two stations. Correcting for this change of units, one obtains the variance for statistical variations at each station in terms of the original units used for that station. The weights are then assigned to each station in inverse proportion to the variance of statistical fluctuations at that station. The slopes indicated for the lines in Fig. 12 were obtained with these weights. These slopes were then used to obtain a closer approximation to the weights; these second approximations differed so little from the previous ones that the slopes calculated from them were not significantly different from those in Fig. 12.

The three slopes given in Fig. 12 are mutually quite consistent. Also the weights, thus objectively assigned, are not surprising since variations in daily means of barometric pressure are in general largest at Cheltenham and practically absent at Huancayo.

To determine the magnitude of the world-wide

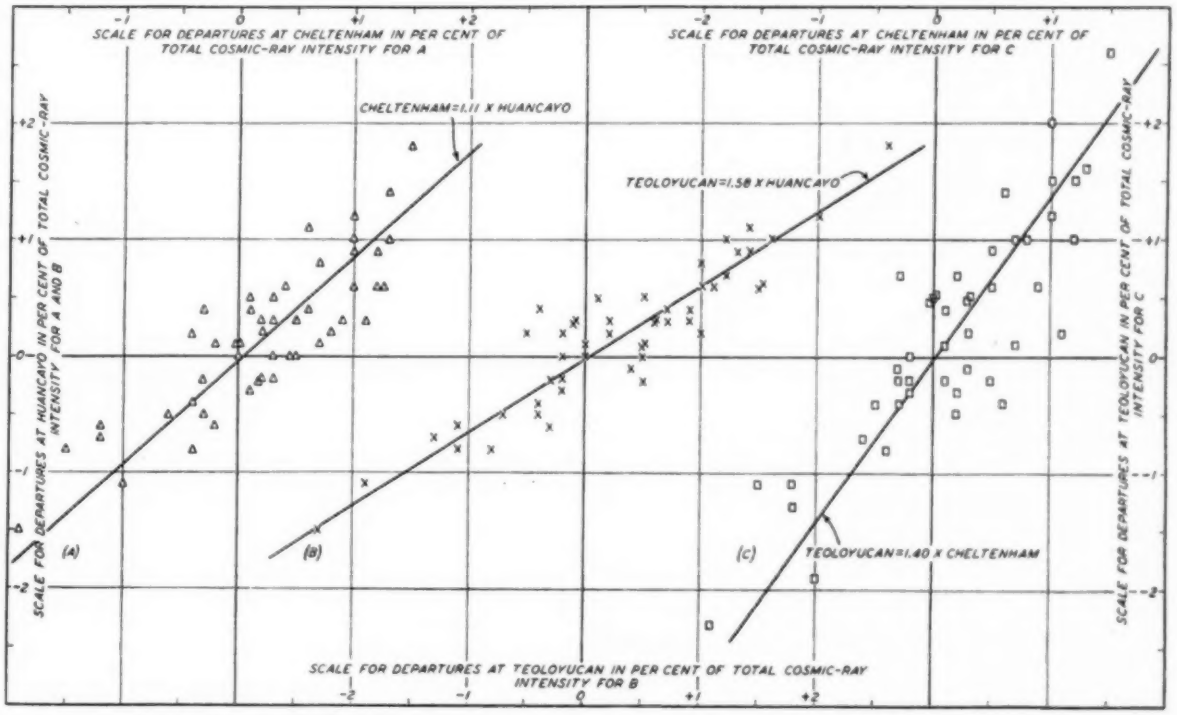
SCALE FOR DEPARTURES AT CHELTENHAM IN PER CENT OF TOTAL COSMIC-RAY INTENSITY FOR A
CHELTENHAM=1.11 X HUANCAYO
SCALE FOR DEPARTURES AT HUANCAYO IN PER CENT OF TOTAL COSMIC-RAY INTENSITY FOR A AND B
(A)
(B)
SCALE FOR DEPARTURES AT CHELTENHAM IN PER CENT OF TOTAL COSMIC-RAY INTENSITY FOR C
TEOLOYUCAN=1.58 X HUANCAYO
TEOLOYUCAN=1.40 X CHELTENHAM
(C)
SCALE FOR DEPARTURES AT TEOLOYUCAN IN PER CENT OF TOTAL COSMIC-RAY INTENSITY FOR C
SCALE FOR DEPARTURES AT TEOLOYUCAN IN PER CENT OF TOTAL COSMIC-RAY INTENSITY FOR B

FIG. 12. Relation between departures cosmic-ray intensity from Figs. 4 and 8.

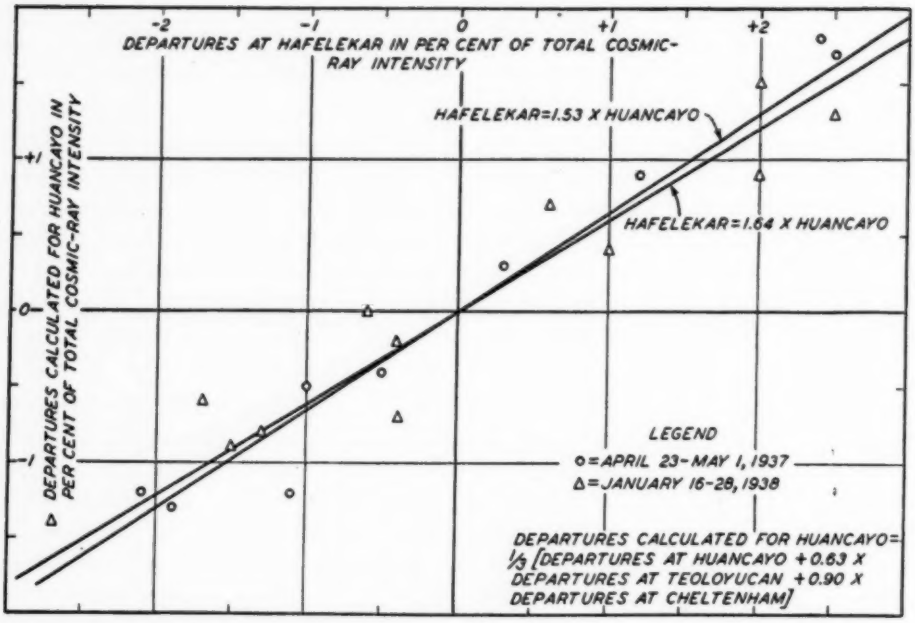

FIG. 13. Correlation between observed departures daily means cosmic-ray intensity from average during two magnetic storms for Hafelekar and calculated departures for Huancayo.

effect in cosmic-ray intensity for a station at great elevation and high latitude, data published by V. F. Hess[2, 3] and his co-workers for the Hafelekar during two intense magnetic storms were used. Departures of the scaled daily cosmic-ray intensity (75° west meridian day) from the means for each of the storms are plotted in Fig. 13. Daily (75° west meridian) means of cosmic-ray intensity were then computed separately for Huancayo, Teoloyucan, and Cheltenham. Their departures from the means for the respective storms were used in the equation of Fig. 13 to compute calculated departures for Huancayo; the high correlation of $r=0.96$ between the two departures is evident. The indicated regression lines fit the separate data for the two periods of magnetic storms about equally well. The correlation in Fig. 13 is considerably higher than that found when the *observed* departures at Huancayo were used as ordinate. Since the factors used in the equation for calculated departures at Huancayo are those indicated in Fig. 12, we assumed that the ratio between the world-wide effects at different stations during individual magnetic storms is the same as that for means for each one-third month. However, this point was carefully tested for each station in the same manner as for the Hafelekar in Fig. 13. While the correlation in most cases is not so high as for Fig. 13, no evidence was found indicating that the relations in Fig. 12 do not also apply to changes in cosmic-ray intensity at the other stations during the same magnetic storms. Thus for the magnitude of the world-wide effect at different stations relative to that for Huancayo, the values of Table I are adopted. In the case of the station on the Hafelekar the average of the two slopes in Fig. 13 was taken since any reasonable weighting will not appreciably alter the result.

SUMMARY AND DISCUSSION OF TWELVE-MONTH WAVES IN COSMIC-RAY INTENSITY AT DIFFERENT STATIONS

In Fig. 14 are summarized the results for the 12-month waves in cosmic-ray intensity at different stations after deducting the world-wide effects. Each vector in the harmonic dial[12] of Fig. 14 points to the date of the wave maximum and its length represents the amplitude. The world-wide effects were determined, as previously described, from the data for Huancayo, where

[12] J. Bartels, Terr. Mag. 40, 1–60 (1935).

the 12-month wave is absent. The world-wide effects at each of the other stations, except Hafelekar as noted below, were computed from those at Huancayo with the factors given in Table I.

The 12-month wave at the Hafelekar was based on monthly means, corrected only for barometric pressure, for April 1936 to March 1937 obtained from Table III of A. Demmelmair's paper.[7] Since no data for Huancayo prior to June 1936 were available, the world-wide changes for April and May 1936 were determined from the data at Christchurch (see Fig. 15). Fig. 14 also indicates the 12-month waves in temperature of outside air based, except for Teoloyucan, on data for the same intervals used to obtain the 12-month waves in cosmic-ray intensity. For Teoloyucan the temperature-wave is the average for the five years,[13] 1917–1921.

The phase of the 12-month wave in temperature at each station differs, except for Teoloyucan, by about 180° from that of the 12-month wave in cosmic-ray intensity. The ratio of the amplitude of the 12-month wave in cosmic-ray intensity to that in temperature is about the same for Cheltenham and Christchurch, which have similar elevations and geomagnetic latitudes. However, this ratio is quite different for the other stations, excluding the possibility that the variation in cosmic-ray intensity is, in general, closely connected with temperature. Whether or not the 12-month wave in cosmic-ray intensity is the result of the 12-month wave in temperature, the fact that the two are about opposite in phase would necessarily lead to a correlation between the two, which has been reported by Hess[14] and others. Possibly the cause for the apparent seasonal wave in cosmic-ray intensity may be associated with the seasonal variation[15] in the distribution of air-density with height in the earth's atmosphere, as was implied by Schonland.[16]

If we arbitrarily assume a seasonal wave in cosmic-ray intensity having the same amplitude but opposite phase at Cheltenham and Christchurch, the observed 12-month waves in cosmic-ray intensity at these two stations could then be attributed to an annual wave, with the same phase and amplitude at both stations, superposed upon the seasonal waves. It is readily seen from Fig. 14 that this annual wave would have its maximum in January. This is just opposite in phase to that of the annual wave which, according to the calculations of Vallarta,[17] would arise if the sun had a magnetic moment. Thus it seems impossible to ascribe the 12-month wave in cosmic-ray intensity to a solar magnetic moment,

[13] Bol. Obs. Astr., Tacubaya, No. 10, Table 11 (1928).

[14] V. F. Hess, Terr. Mag. **41**, 345–350 (1936).

[15] W. J. Humphreys, *Physics of the Air*, second edition (1929).

[16] B. F. J. Schonland, B. Delatizky and J. Gaskell, Terr. Mag. **42**, 137–152 (1937).

[17] M. S. Vallarta, Nature **139**, 839 (1937).

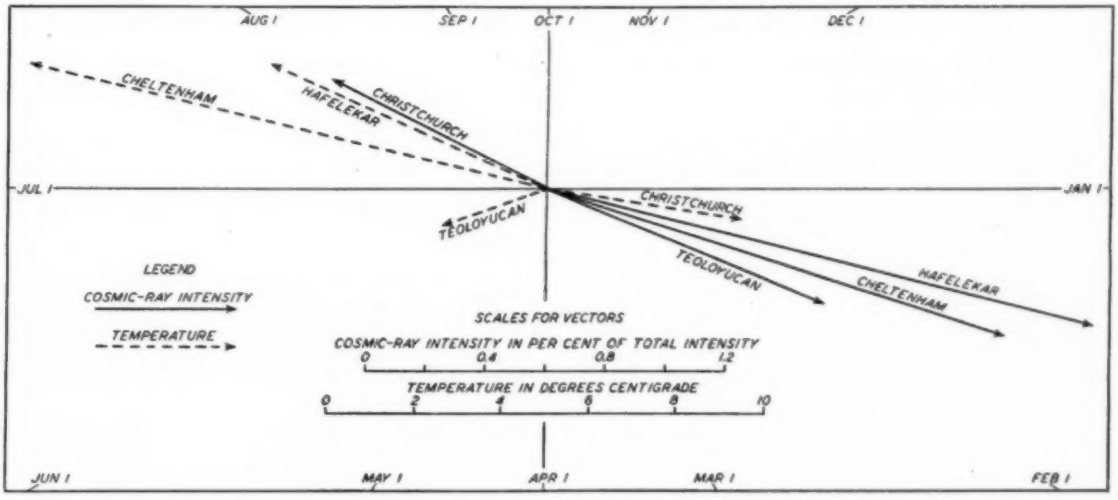

FIG. 14. Harmonic dial for 12-month waves in cosmic-ray intensity after deducting world-wide changes and in temperature showing dates and amplitudes of wave-maximum.

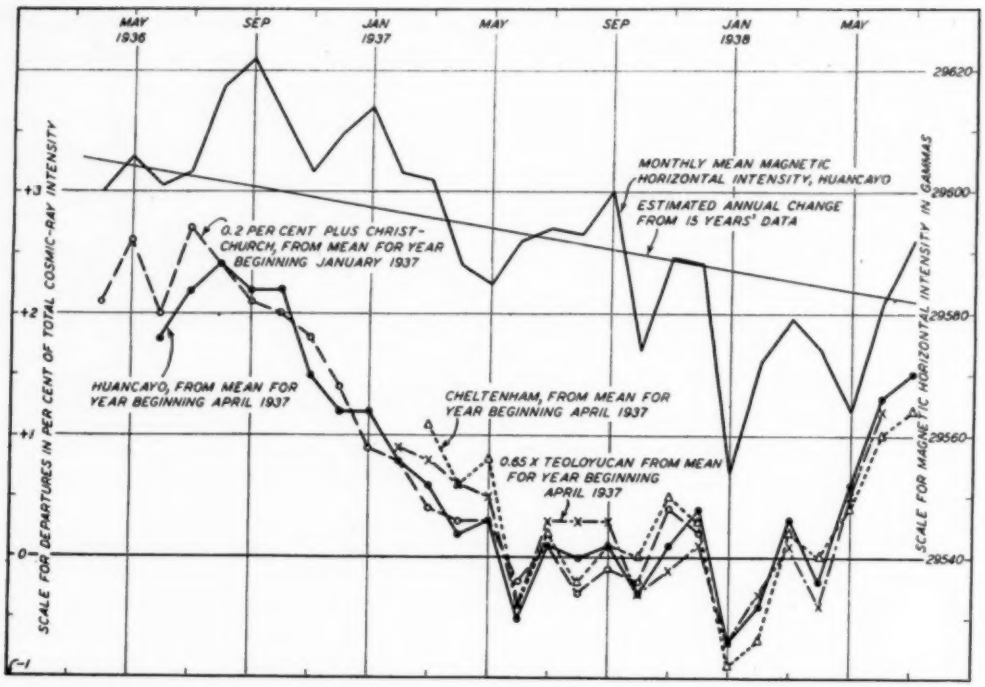

FIG. 15. Departures cosmic-ray intensity from Fig. 1 after deducting 12-month waves.

unless perhaps the annual variation in the angle between the earth's magnetic axis and the ecliptic introduces an unsuspected variation. This latter, however, would seem to be excluded on the basis that the diurnal variation of about 12° in the angle between the earth's magnetic axis and the ecliptic should then be expected to result in a diurnal variation in cosmic-ray intensity with amplitude many times that actually observed.[8]

Since the relative amplitudes of the 12-month waves are quite different from those of the world-wide changes at the different stations, the two effects must be ascribed to different causes. It would seem impossible to obtain the excellent agreement indicated in Figs. 4, 6, 8 and 12 unless the fundamental mechanism for the 12-month wave at each station varied almost perfectly sinusoidally.

It should be added that by varying the temperature of the Compton-Bennett meter at Cheltenham over a range of 15°C and comparing results over a period of many weeks with those from two Millikan-Neher electroscopes at constant temperature, the Compton-Bennett meter is found to be unaffected by temperature.

DISCUSSION OF THE WORLD-WIDE EFFECT IN COSMIC-RAY INTENSITY

The high correlation which exists between changes in cosmic-ray intensity at any two stations definitely establishes the fact that the major changes in cosmic-ray intensity, after eliminating the 12-month wave, are world-wide. The relative amplitude of the world-wide changes at different stations derived from data extending over periods of more than a year is not significantly different from that derived from two short periods of intense magnetic storms. This suggests that the mechanism responsible for changes occurring over longer periods of time is similar to that which causes the decrease of intensity during certain individual magnetic storms.

The world-wide character of changes in monthly means of cosmic-ray intensity, after removing the 12-month wave, is summarized in Fig. 15. If the hypothesis that the decrease in intensity during certain magnetic storms is due to alteration of trajectories of cosmic-ray particles resulting from the magnetic field of an equatorial ring-current, or its equivalent, is correct, then the more or less continued world-

wide changes in intensity evident in Fig. 15 would imply the continued existence of such a current-system with changing strength or radius. Störmer[18] concluded that such a current-system was necessary to account for the large diameter of the auroral zones.

For comparison, the monthly means of magnetic horizontal intensity are indicated in Fig. 15. The average rate of decrease, derived from fifteen years of data, of the horizontal magnetic intensity at this station is indicated by the slope of the straight line. Any correspondence between the trend in this line and that in cosmic-ray intensity must therefore be regarded as accidental. However, the correspondence between departures of monthly means in horizontal intensity from this line and those in cosmic-ray intensity is doubtless significant. That the correspondence in some instances is more marked than in others is not surprising in view of the fact[4] that some magnetic storms are not accompanied by significant changes in cosmic-ray intensity.

Since the period of minimum values for the departures in cosmic-ray intensity in Fig. 15 agrees roughly with that of maximum magnetic activity, and since we have also indicated[4] the existence of a 27-day wave, probably quasi-persistent,[12] in cosmic-ray intensity, it would not be unexpected to find, when adequate data are available, the 11-year cycle of sunspot-activity reflected in cosmic-ray intensity.

From values for the relative magnitudes of the world-wide effect in cosmic-ray intensity given in Table I, the effect at the Hafelekar, where the instrument had somewhat greater shielding than at the other stations, is about 40 percent greater than at Cheltenham. This indicates that the intensity of the cosmic-ray component which is affected by the mechanism causing the world-wide changes increases much faster with altitude than does the total intensity. This is consistent with the fact that Clay and Bruins[19] found, in an instrument shielded by 110 cm of iron, no measurable change in cosmic-ray intensity during the magnetic storm which began April 24, 1937. They were thus enabled to set an upper limit to the energy of particles affected by the field of the magnetic storm.

Table I also indicates for high altitude stations a rapid increase in the magnitude of the world-wide effect between the equator and geomagnetic latitude 30° north. While the value for the Hafelekar indicates no further increase up to latitude 47° north, the additional shielding may have somewhat reduced the ratio in Table I for that station. Since no data are available for a sea-level station at the equator, it is not possible to determine the latitude variation in the world-wide effect at sea level. However, the agreement between Cheltenham and Christchurch indicates that the variation with latitude is probably symmetrical about the equator. Whether the world-wide changes in cosmic-ray intensity are due to the magnetic field of an equatorial ring-current system, or its equivalent, can only be answered when the difficult problem of finding the trajectories of cosmic-ray particles in such a field superposed on that of the earth's doublet has been solved.

The world-wide effects indicated in Fig. 15 imply that special precautions are necessary to obtain accurate determinations of the longitude effect. Also, if the magnitude of the world-wide effect increases as rapidly with altitude and latitude as the results in Table I suggest, then the results for latitude variations at extreme altitudes may also be materially affected if the mechanism responsible for the world-wide effect operates somewhat continuously but with varying intensity. Although this suggests a possible explanation for the exclusion of low energy cosmic-ray particles from the top of the earth's atmosphere at high latitudes, it is open to the serious objection that it would also be expected to exclude the auroral particles.

Finally, it should be emphasized that the results of this investigation could not have been secured without remarkable stability in the several cosmic-ray meters by which the data were obtained. Thus the estimated probable error for each entry in the last column of Table I is roughly ± 0.03. Although an examination of barometric coefficients at the separate stations does not indicate the existence of appreciable instrumental differences, it may be desirable to obtain further

[18] C. Störmer, Terr. Mag. **35**, 193–208 (1930).
[19] J. Clay and E. M. Bruins, Physica **5**, 111–114 (1938).

confirmation of this through an intercomparison of instruments at some of the stations.

Acknowledgments

We are indebted to the Committee on Coordination of Cosmic-Ray Investigations of the Carnegie Institution of Washington for providing the assistance of W. R. Maltby, without whose aid the reduction of the data here used would have been long delayed.

We are also under obligation to G. Hartnell and the staff of the Cheltenham Magnetic Observatory of the United States Coast and Geodetic Survey for operation of a cosmic-ray meter at that station, to J. W. Beagley of the Christchurch Magnetic Observatory for operation of a meter and reduction of records, to Professor J. Gallo, Director of the National Astronomical Observatory at Tacubaya, Mexico, for supervising the operation of the meter at Teoloyucan, and to the staff of the Huancayo Magnetic Observatory of the Department of Terrestrial Magnetism of the Carnegie Institution of Washington for operating the meter at that station. We are also especially indebted to Professor A. H. Compton and his assistants for making available to us the reduced data from Teoloyucan, and to the National Carbide Company, Incorporated, for providing all batteries for operating the Compton-Bennett meters.

Finally, it is a pleasure to acknowledge the encouragement received from Dr. J. A. Fleming, Director of the Department of Terrestrial Magnetism of the Carnegie Institution of Washington.

DECEMBER 15, 1938 PHYSICAL REVIEW VOLUME 54

Anomalous Dispersion of X-Rays in Calcite

ROBERT M. WHITMER* AND GEORGE A. LINDSAY
University of Michigan, Ann Arbor, Michigan

(Received October 11, 1938)

The index of refraction of calcite ($CaCO_3$) for x-rays has been investigated in the wave-length range from 2880 to 3550 x.u., which includes the K absorption edge of calcium. The method is such that all of the incident beam enters the crystal through an artificial face, ground so that after reflection from the (100) planes a part of the beam emerges through this face at a sufficiently small angle to be refracted appreciably. At the same time another part of the beam emerges from a cleavage face at a large angle and is refracted only a little. The separation between the two is a measure of the index. The continuous spectrum is used rather than emission lines, thus enabling measurements to be made as closely spaced in wave-length and as near the absorption edge as is desired. The absolute accuracy of the method in its present form is probably not great, but the relative accuracy is sufficient to show a distinct dip in δ/λ^2 in the vicinity of the absorption edge. A comparison is made with Hönl's theoretical curve.

Introduction

BECAUSE the index of refraction of all substances for x-rays is very nearly unity, the refractive bending of an x-ray beam has a measurable magnitude only when the angle between the beam and the interface is very small. Bergen Davis first suggested grinding an artificial face on a crystal in order that an x-ray undergoing Bragg reflection might make a small angle with the surface. The experiments of Davis and Hatley[1, 2] gave the first quantitative determinations of the index of refraction. Variations of this method have been used by Lindsay and his collaborators[3, 4] to measure the index of cerussite ($PbCO_3$). Retaining the idea of a small angle at the interface, but not using Bragg

* Now at Purdue University.

[1] C. C. Hatley and Bergen Davis, Phys. Rev. **23**, 290 (1924).
[2] C. C. Hatley, Phys. Rev. **24**, 486 (1924).
[3] H. C. Hoyt and G. A. Lindsay, Phys. Rev. **49**, 498 (1936).
[4] J. E. Field and G. A. Lindsay, Phys. Rev. **51**, 165 (1937).

reflection, Lärsson[5] and Bearden and Shaw[6] have obtained accurate results with right-angled prisms of various substances.

Outline of the Present Method

In this investigation the index of refraction of calcite ($CaCO_3$) was studied in the region of the K absorption edge of calcium. A new adaptation of Davis' method was employed. A crystal with an artificial or bevelled face was used, the entire x-ray beam entering the crystal through this face. Upon emerging, one component came through the bevelled face at a sufficiently small angle to be refracted appreciably, while the other came out through a cleavage face at a large angle and was bent only a little. The second component furnished a reference from which the bending of the first could be measured. This is illustrated in Fig. 1.

The crystals were prepared by grinding off a corner and optically polishing the resulting face AB (Fig. 2).[7] This makes an angle φ with the (100) planes, as shown in Fig. 1. After the bevelled face had been polished the crystal was cleaved along CD. It was necessary that the edge at D between the cleavage and bevelled faces be sharp and distinct for a distance of at least a few millimeters. The crystals were prepared by the Bryden Company of Waltham, Massachusetts.

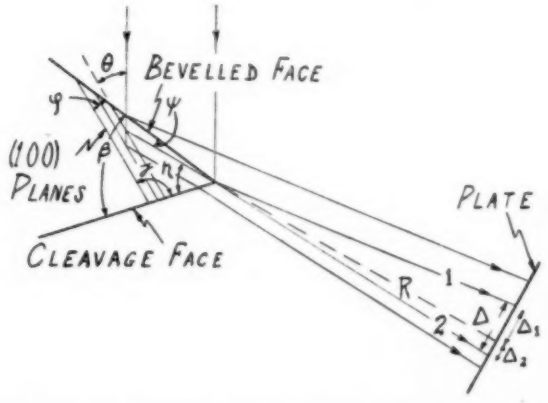

FIG. 1. Geometry of the x-rays in the crystal. This shows the quantities used in the derivation of the expression for $\delta = 1 - n$.

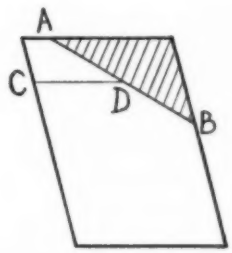

FIG. 2. In preparing the calcite crystals, the shaded part was ground off and the face AB polished. Then the crystal was cleaved along CD.

The investigation was carried out with a Siegbahn vacuum spectrometer having a radius of 181.6 mm and a slit width of 0.10 mm. Before being mounted in the instrument each crystal was examined microscopically in order to be certain that the edge was sufficiently sharp for use. It was then set up with the sharp part of the edge accurately in the axis of the spectrometer. Thus the distance from the edge of the crystal to the photographic plate remained constant as the crystal was rotated about the axis of the instrument. Only radiation reflected from the best parts of the edge was considered.

All measurements were made with the continuous x-ray spectrum, with known emission lines for reference to determine the wave-length being refracted. This permits one to take many points at very small wave-length intervals, and in particular it allows an indefinitely close approach to the wave-length of the absorption edge, where the unit decrement falls off sharply.

Optics and Geometry of the Problem

The emerging ray *1* makes a small angle $\psi = \theta - \varphi$ with the bevelled face (Fig. 1). Throughout the work this angle ranged from about 1° to 5°, and in the following development we may with sufficient accuracy take its cosine to be unity and its sine and tangent equal to the angle. Ray *2* emerges from the cleavage face at a much larger angle η. If there were no refraction both rays would follow the direction of the broken line from the edge of the crystal to the plate. We see that the angular deviation of ray *1* is Δ_1/R, where R is the radius of the spectrometer, and the deviation of ray *2* is Δ_2/R. If now $\delta = 1 - n \ll 1$,

[5] Axel Lärsson, *Dissertation*, Uppsala (1929).
[6] J. A. Bearden and C. H. Shaw, Phys. Rev. **46**, 759 (1934).
[7] Emission lines reflected from the bevelled face were as sharp as those from the cleavage face, which shows that the polish was satisfactory and that there was very little powder or mosaic structure on the surface.

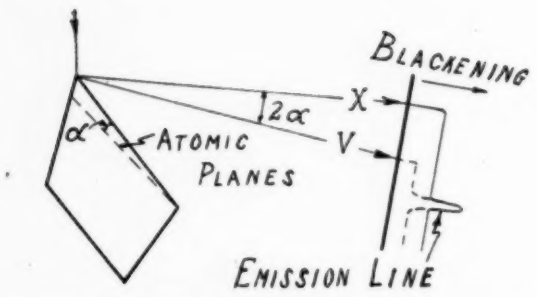

FIG. 3. Ray diagram illustrating the measurement of the deviation angle α by means of x-radiation and visible light.

where n is the index of refraction, it may easily be shown that $\Delta_1=\delta R/\psi$, and $\Delta_2=\delta R/\tan\eta$. The separation actually measured on the photographic plate is

$$\Delta_1+\Delta_2=\delta R(1/\psi+1/\tan\eta).$$

Solving this equation for δ and dividing by λ^2 we see that

$$\delta/\lambda^2=(\Delta/R\lambda^2)(\psi\tan\eta/(\psi+\tan\eta)). \qquad (1)$$

The Bragg equation, $\lambda=2d\sin\theta$, will furnish the value of θ when the wave-length is known.[8] The measurement of φ will be described below. The angle made with the cleavage face is given by $\eta=180°-\theta-\gamma$. The value of γ obtained by Beets[9] was used.

Because ψ is very small, it is necessary to know both θ and φ with great accuracy. Bearden and Roseberry[10] have reported deviations of the cleavage faces of calcite from the atomic planes supposedly parallel to them. If such a deviation existed here the simple relation $\varphi=180°-\beta-\gamma$ would not be accurate. In order to measure this deviation angle for crystal D the crystal was turned for reflection from the cleavage face. An x-ray exposure was made, the crystal being in such a position that an emission line appeared on the plate. The plate was also blackened by the continuous spectrum, the intensity of which fell off sharply at ray X (Fig. 3), the ray reflected just at the edge of the crystal. Next, a second plate was exposed to x-rays, but for a shorter time—sufficient to show the line but not the continuous background. While this second plate was still in position, the anode was removed and visible light allowed to fall on the crystal through the slit. As with the x-radiation, the blackening decreased rapidly beyond the ray V coming from the edge. Since the x-rays were reflected by the atomic planes and the visible light by the actual surface of the crystal, the angular separation between the two extreme rays (as measured on the plates, with the emission line as reference) is just twice the deviation angle α between the planes and surface. α was found to be 43″. β was measured with a goniometer. We may now calculate $\varphi=180°-(\alpha+\beta+\gamma)$. The angle η is of the order of magnitude of 45°, so there was no need to correct it for the deviation angle.

For crystals E and F, φ was obtained directly in a manner very similar to that described above. Here it was necessary to turn the plate through a large angle approximately equal to 2φ between the x-ray and visible light exposures. By a proper choice of this angle the two blackened regions could be made to occur several millimeters apart, so that one plate was sufficient and no reference emission line was necessary. The plate circle of the spectrometer was observed through two microscopes about 180° apart, and the average of the differences between the initial and final readings taken as the angle through which the plate was turned. If we call this angle A, and the separation between the blackened regions D, then $\varphi=\frac{1}{2}(A\pm D/R)$; the sign is determined by the relative placing of the two regions.

DETERMINATION OF THE REFRACTED WAVE-LENGTH

The wave-length of the ray refracted at the edge of the crystal was determined from that of a known emission line. This line was reflected according to the Bragg Law, but emerged through the bevelled face at some distance from the edge. The difference in wave-length $d\lambda$

[8] With the continuous spectrum, it is possible to measure refraction only for first-order reflection. If radiation which would be reflected in second order were present, it would emerge at the same angle, but δ would be only one-fourth as great, so that at the plate the ray would fall between the refracted and reference components of the first-order radiation. The result would be merely to blur the position of ray *1*. To prevent this the tube voltage was always kept so low as barely to excite radiation of this wave-length.

[9] H. N. Beets, Phys. Rev. 25, 624 (1925).

[10] J. A. Bearden and H. H. Roseberry, Phys. Rev. 48, 110 (1935).

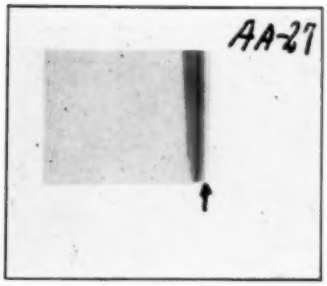

FIG. 4. Plate taken with Crystal *F* at 2813 x.u. The sharp line at the extreme right is caused by the radiation emerging from the cleavage face (ray *2* of Fig. 1). The arrow points to the separation Δ between the reference and refracted components. The line in the center is Sb $L\gamma_1$, λ2845 x.u., reflected from the bevelled face. Wave-length increases from right to left.

between this line and the ray emerging from the bevelled face just at the edge is given by

$$d\lambda=(d\cos\theta/R)(1+\tan\varphi/\tan\theta)ds, \qquad (2)$$

where ds is the separation on the plate. The wave-length of the ray at the edge is obtained by subtracting $d\lambda$ from the wave-length of the line. It was found that sufficient accuracy was obtained if the value of θ for the line were used in the expression (2), and the $d\theta$ corresponding to $d\lambda$ was neglected. Corrections for refraction were negligible even when the line was observed in the second order. The wave-lengths of the lines and the value of the grating constant $d(=d_{(100)})$ were taken from Siegbahn.[11]

METHODS OF ASSEMBLING DATA

Figure 4 is a photograph of one of the plates. The dark background is the blackening due to the continuous spectrum emerging from the bevelled face. Near the right-hand edge is seen a white line; this is the region between the rays *1* and *2* of Fig. 1. Beyond is a distinct dark line, caused by the radiation which passed through the crystal and out through the cleavage face. The width of the white line is the quantity Δ in the development above. It was measured on a comparator. For ψ less than about 1° the left side of the white line was too indistinct for measurement, and for ψ greater than about 5° the width was too small. These limits determined the wave-length range over which any one crystal could be used.

For each crystal the coefficient of Δ in (1) was computed for a few wave-lengths within the useful range and plotted graphically. When the wave-length for one plate or a group of plates had been determined, the value of this coefficient was read from the curve and multiplied by the measured Δ to find δ/λ^2.

With crystal *D*, points were taken at very small wave-length intervals from 2986 x.u. to 3267 x.u. The value of δ/λ^2 was found for each plate, then they were grouped and averaged. The wave-length range included in a group was 5 x.u. near the absorption edge, increasing to more than 40 x.u. at some distance away. For the work with crystals *E* and *F*, whose useful wave-length ranges were higher and lower, respectively, than that of crystal *D*, plates were taken in groups. Each group covered a wave-length range of some ten or twenty x.u., but was separated from its neighboring groups by considerably more. Within each group, the wave-lengths and Δ's were averaged, and a single value of δ/λ^2 was obtained. The averaged values appear in Table I, and they are plotted in Fig. 5.

The solid curve of Fig. 5 represents Hönl's theoretical expression[12] for δ/λ^2. This was obtained from the classical value by multiplying the term which represents the dispersion due to the *K* electrons by the hydrogenic oscillator strength as developed by Sugiura.[13] This is then integrated over the continuous spectrum from the frequency of the absorption edge to infinity. Analytically the result is given by

$$\delta/\lambda^2=\frac{Ne^2}{2\pi mc^2}\left\{1+\frac{N_{Ca}}{N}\frac{2^7\exp(-4)}{9}\lambda^2\right.$$
$$\times\left[\frac{4}{(1-\Delta_k)^2}\left(1+x^2\log\left|1-\frac{1}{x^2}\right|\right)\right.$$
$$\left.\left.-\frac{1}{(1-\Delta_k)^3}\left(\frac{2}{3}+2x^2+x^3\log\left|\frac{x-1}{x+1}\right|\right)\right]\right\}. \qquad (3)$$

Here e and m are the charge and mass of the electron, c the velocity of light, and $x=\lambda/\lambda_k$, where λ_k is the wave-length of the absorption

[11] M. Siegbahn, *Spektroskopie der Röntgenstrahlen*, Berlin (1931).

[12] H. Hönl, Zeits. f. Physik **84**, 1 (1933).

[13] Y. Sugiura, J. de phys. et le rad. **8**, 113 (1927).

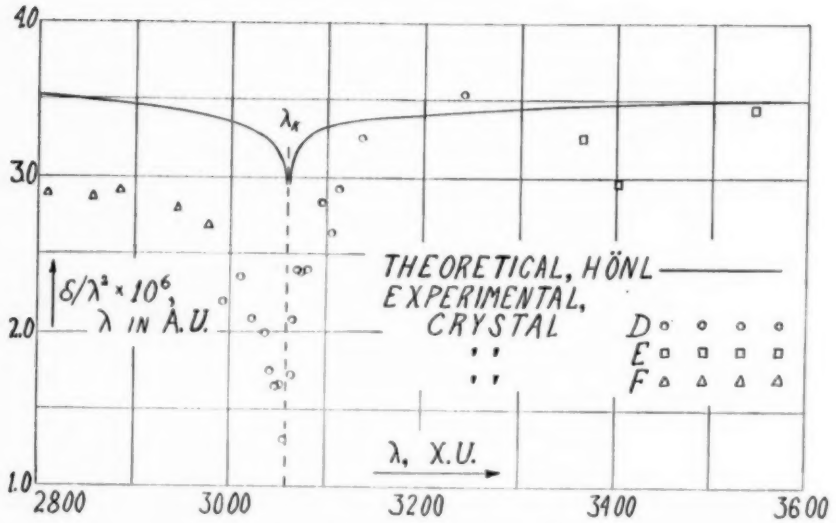

FIG. 5. The averaged experimental points, together with Hönl's theoretical curve, Eq. (3).

edge. N_{Ca} is the number of calcium atoms per cm³ and $N=\Sigma N_i Z_i$. Here N_i is the number per cm³ of atoms having the effective atomic number Z_i. By effective atomic number is meant the number of electrons which do not contribute to the K dispersion. This term thus includes all the electrons of carbon and oxygen, the L, M, etc. electrons of calcium, plus 0.59 K electrons per calcium atom which, from the value of the integrated oscillator strength, do not take part in K dispersion. Δ_k is a term containing screening and relativity corrections.

RESULTS AND DISCUSSION OF ERRORS

The values of δ/λ^2 obtained experimentally fall below Hönl's curve, especially on the short wave side of the absorption edge. Also the dip in the region of the edge is wider and deeper. Lärsson's[5] experimental results are the only ones which have been published with which a comparison may be made. His values agree very well with Hönl's on the short wave side, but fall a little low for longer wave-lengths. Because of uncertainties in the measurement of the separation between the refracted and reference components, it may well be that the present method does not give the absolute magnitude of the refraction. However, in regions in which data were obtained with two different crystals the separation and distinctness of the two components differed considerably on the plates taken with one crystal from those with the other.

TABLE I. *Average values of δ/λ^2. To show the spread of values for the individual plates there are given in the right-hand section of the table the individual values of δ/λ^2 for the group at 3094 x.u.*

Number of plates averaged	Wave-length (x.u.)	$\delta/\lambda^2\times10^6$	Number of plates averaged	Wave-length (x.u.)	$\delta/\lambda^2\times10^6$	Number of plates averaged	Wave-length (x.u.)	$\delta/\lambda^2\times10^6$	Plate	Wave-length (x.u.)	$\delta/\lambda^2\times10^6$
Crystal F, $\varphi=26°\ 29.3'$			3	3024	2.09	6	3094	2.84	*Y*-19	3093	2.70
4	2811	2.89	4	3037	1.99	5	3107	2.63	20	3093	2.90
4	2858	2.87	4	3042	1.75	2	3113	2.93	*X*-72	3094	2.57
1	2886	2.91	3	3048	1.65	3	3139	3.26	71	3095	2.84
5	2947	2.80	3	3052	1.66	4	3241	3.54	73	3095	2.93
1	2978	2.69	4	3056	1.30				*Y*-18	3096	3.07
			4	3064	1.72	*Crystal E, $\varphi=32°\ 4.5'$*					
Crystal D, $\varphi=28°\ 28.3'$			4	3066	2.08	6	3365	3.25			
2	2993	2.20	2	3071	2.40	8	3404	2.96			
3	3011	2.35	2	3076	2.39	7	3546	3.43			
			2	3081	2.40						

Yet the values of δ/λ^2 obtained from the two agree well. This shows that the plates were all measured in the same manner, and indicates that the form of the dependence of refraction on wave-length is correct.

The principal source of error is in the comparator measurement of the position of the refracted component of the beam, which always appeared fuzzy. This position corresponds to ray *1* in Fig. 1. The causes of this fuzziness are as follows: In Fig. 6, *S* represents the slit of the spectrometer. Two parallel rays *A* and *B* of the same wave-length strike the bevelled face of the crystal and are reflected as rays *A'* and *B'*. Actually, of course, there is a finite beam incident upon the crystal; these rays merely define its limits. All the rays in this beam are reflected from the crystal. At the same time a ray *C* of slightly shorter wave-length may be incident upon the crystal at a smaller angle and be reflected as ray *C'*, which falls outside the beam defined by *A'* and *B'*. The blackening at *C'* will be less than that at *A'* because it is caused by radiation coming from only a part of the slit. Thus as we go from *A'* toward shorter wave-lengths, the blackening diminishes not sharply, but gradually, as less and less of the slit contributes to it.

Also, since beams of longer wave-lengths reflected from the bevelled face do not emerge at the edge, the extent of the crystal contributing to their intensities is determined by absorption rather than by a limiting ray passing through the edge. These beams are therefore stronger than *A'B'*, and we have a second effect producing a gradual diminution of the blackening. Moreover, the area *abc* contributing to the beam *A'B'* diminishes rapidly as the crystal is turned to refract shorter wave-lengths, while the absorption-limited regions contributing to the longer wave-lengths do not. Thus the indistinctness of the position of ray *A'* (the same as ray *1* of Fig. 1) increases as the refracted wave-length is decreased. At the same time the separation from the unrefracted component increases, so that the relative accuracy of measuring Δ does not change rapidly, but eventually, as was mentioned above, a lower limit of ψ is reached beyond which measurements cannot be made.

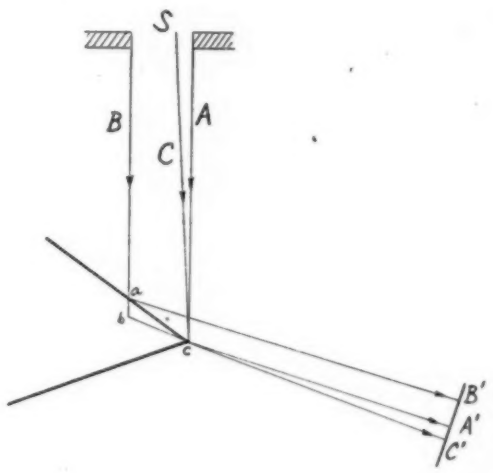

FIG. 6. A ray *C* having a wave-length slightly less than that of *A* and *B* causes a gradual decrease in blackening at *A'*.

Microphotometer curves were taken for a few plates, but measurements of Δ obtained from them were no more consistent than those from the comparator. Positions on the plate would probably have been more distinct if a narrower slit had been used, but that would have increased the required exposure times unreasonably. As it was, most of the plates were exposed for about twenty hours, and few for as long as forty hours.

From the method described in this paper, refraction may be measured at any wave-length desired, in substances which form good single crystals having linear dimensions of at least a few millimeters. The faces used may be natural or artificial, provided only that it is possible to obtain a sharp edge between them parallel to some set of atomic planes.

The Absorption of X-Rays of Wave-Length $1.5 \leq \lambda \leq 8.3$A

C. Luther Andrews*
Cornell University, Ithaca, New York
(Received September 27, 1938)

The mass absorption coefficients for Be (4), C (6), Al (13), Cu (29), Ag (47) and Au (79) have been determined in the wave-length region $1.5 \leq \lambda \leq 8.3$A. Only characteristic line radiation obtained with a vacuum spectrometer was used. Because of the presence of about 1 percent of heavier impurities in the Be (4), the apparent absorption coefficients for Be (4) may be as much as 100 percent higher than for the pure element. This large effect of a small amount of impurity on the apparent absorption coefficient of Be (4) leads to a suggested method of microanalysis for heavy impurities in elements of low atomic number. Following Jönsson's procedure, a universal absorption curve is plotted.

Introduction

THE determination of the laws of absorption of x-rays is complicated by the presence of two types of absorption, fluorescence absorption and absorption by scattering. With increase in wave-length, however, absorption by scattering becomes much smaller than photoelectric absorption. For wave-lengths above 1.5A and absorbing elements heavier than Al 13, absorption by scattering is negligible compared with photoelectric absorption. Above 2.5A absorption caused by scattering by elements heavier than C (6) is negligible. Thus accurate absorption measurements at the longer wave-lengths give important data for the developement of the laws of photoelectric absorption.

In 1928 Jönsson[1] measured absorption coefficients at wave-lengths as high as 10A, using a crystal spectrometer as monochromator and measuring intensity photographically. Woernle[2] made measurements from 2 to 10A on gases of low atomic number employing a vacuum spectrometer for monochromatization. The gases to be studied were placed in a special ionization chamber; an electrometer was used as a null instrument. Recently Biermann,[3] employing the Ross[4] balanced filter method to produce a monochromatic beam and measuring intensities with an ionization chamber and electrometer, covered the same range of wave-lengths, using seven elements and Cellophane as absorbers. His values are higher than Jönsson's above 3A for Al (13) and Ag (47), the spread increasing until at 10A for Ag (47) they differ by 45 percent.

This investigation was undertaken with the view of checking some of Jönsson's measurements by use of a more modern and entirely different technique, and of extending the measurements to more elements. While this work was in progress, Biermann's[3] results were published. Since Jönsson, Biermann and the author each employed different methods and each studied absorption by Al and Ag, a comparison of the results should indicate something of the accuracy of measurements in this wave-length region. A plot of all the absorption data by Jönsson's procedure for a universal absorption curve[1] should indicate whether the curve is constantly decreasing in slope or is made up of a series of broken lines, with the absorption coefficient depending on some constant power of the wave-length within any region not including an absorption discontinuity.

Apparatus

To eliminate any doubt concerning the purity of the monochromatic radiation, characteristic lines of various elements were obtained in a modified Siegbahn-Thoraeus[5] vacuum spectrometer (see Fig. 1). The target arm and ionization chamber arm were each 105 cm long, with slits of such width as to give a resolving power of about 500, resolving power being defined as the ratio of

* Now with the Department of Physics, New York State College for Teachers, Albany, New York.

[1] E. Jönsson, Thesis, Uppsala (1928).
[2] B. Woernle, Ann. d. Physik **5**, 475 (1930).
[3] H. Biermann, Ann. d. Physik **26**, 720 (1936).
[4] P. A. Ross, J. Opt. Soc. Am. and Rev. Sci. Inst. **16**, 433 (1928).
[5] M. Siegbahn and R. Thoraeus, J. Opt. Soc. Am. and Rev. Sci. Inst. **13**, 235 (1926).

the wave-length to the observed full width of the line at half-maximum. Since, at the long wave-lengths and correspondingly large Bragg angles employed, characteristic line radiation is far more intense than the continuous radiation, high geometric resolving power is not necessary to secure a highly monochromatic beam. The main purpose in the degree of resolution is to reduce radiation of other lines in that wave-length region. Thus, in using $K\alpha_1$-radiation, most of the $K\alpha_2$-radiaton must be eliminated. Since the absorption coefficients for $K\alpha_1$- and $K\alpha_2$-radiation in this wave-length region differ by only a small amount, a small portion of $K\alpha_2$ may be tolerated in the $K\alpha_1$-radiation.

The targets were wedged or soldered to a water-cooled holder. Targets of Cu, Ni, Fe, Ag, Pd, Mo and Al were made from sheet metal. Cr, Va and Ti targets were made by evaporation onto an Ag backing; Si by evaporation onto Al. For Sc, Ca, and Cl targets, Sc_2O_3, CaO, and KCl respectively were pressed into sheets of Ag.

$K\alpha_1$-radiation was used from Cu, Ni, Fe, Cr, Va, Ti, Sc and Ca; the whole $K\alpha$-radiation from Cl, Si and Al; $L\alpha_1$-radiation from Ag, Mo and Zr; $L\beta_1$ from Ag and Mo.

The absorbing foils were mounted on disk A Fig. 1, which could be turned by a ground cone G so as to bring any desired foil into the path of the beam. Since the maximum Bragg angle with this instrument is about 25°, crystals of calcite, selenite and mica were employed to cover the desired wave-length range.

X-ray intensities were measured with an ionization chamber. A Cellophane window separated the argon in the ionization chamber from the evacuated spectrometer. An FP-54 Pliotron tube amplified the ionization current. Control grid shunts as high as 5×10^{10} ohms were used. To balance out the effects of small changes in the Pliotron filament current, a Brown and DuBridge[6] circuit was employed. Tests at regular intervals showed the amplification to be always linear in the range used.

Preparation of Absorbers

In this long wave-length region, a major portion of the problem was to produce sufficiently thin absorbers of known and uniform thickness.

The Be (4) absorbers for use at the shorter wave-lengths and the C (6) absorbers were granular cakes. To form the Be (4) cakes, the smallest grains were sifted from the supply of flakes and pressed together in a mold. The C (6) absorbers were made by turning out a disk from a stick of regraphitized graphite and scraping it down with an apparatus designed for scraping parallel surfaces.

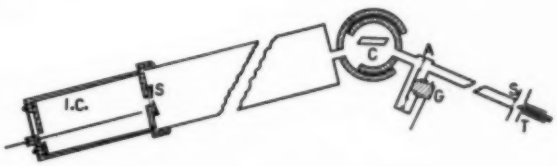

Fig. 1. Diagram of vacuum spectrometer.

All other absorbers used in this work were produced by evaporating the metal in high vacuum from a tungsten spiral basket onto a glass plate. The foils were removed mechanically with a razor blade. Fortunately the thinnest foils rolled into a tight roll as they were peeled from the glass plate. The smallest rolls, or "pipes," thus formed were just large enough to permit a small needle to be inserted. Such foils were more convenient to weigh and mount than those produced by rolling. Moreover, evaporation provided a means of producing foils of hard brittle metals, like Be (4), which could not be rolled. To mount the foils, one edge of the roll was stuck to the holder and the holder inclined until the weight of the needle unrolled the foil.

The absorbers were weighed on microbalances designed to weigh to a thousandth of a milligram. The weights were calibrated by the National Bureau of Standards.

To detect variations from point to point in the thickness of an absorber, the absorber was moved across the x-ray beam. Not one of the metal foils or carbon disks showed a variation of more than one percent in the intensity of the beam transmitted. The Be (4) cakes, however, showed a variation in transmitted intensity as high as 3 percent. To eliminate error caused by variation in thickness of an absorber, the absorbers were moved across the beam during measurements of intensity.

[6] L. A. DuBridge and H. Brown, Rev. Sci. Inst. **4**, 532 (1933).

TABLE I. *Purity of the absorbers.*

ELEMENT	PURITY	IMPURITIES	REMARKS
Au	99.975%		Purchased from Baker and Company.
Ag	99.97%	Au 0.00034% Cu 0.0036% O 0.028%	Donated to F. K. Richtmyer by the Raritan Copper Works.
Cu	99.962%	Ag 0.00028% Pb 0.0009% Fe 0.0014% S 0.0025% O 0.033%	Purchased from Am. Brass Company.
Al	99.975%	Si 0.009% Fe 0.008% Cu 0.008%	Donated to F. K. Richtmyer by the Aluminum Company of America and tested in the Aluminum Research Laboratory, New Kensington, Pa.
C	99.9%	Ca	Regraphitized graphite from the Achison Graphite Company. Spectral analysis made by the Cornell University Chemistry Department.
Be (Granular)		Fe 0.4%	Purchased from and tested by Siemens & Halske.
Be (Evaporated foil)		Cu Fe Si W	Tested by spectral analysis by Cornell University Chemistry Department.

The tested purity of each metal, the amount of impurity, and the company responsible for the test are given in Table I.

METHOD OF TAKING DATA

During measurements of intensity, small fluctuations in tube current and tube voltage were controlled manually.

A contour of each characteristic line was constructed to see if there was any background of scattered radiation from the walls of the spectrometer. In no case was a background of half of one percent detected as the chamber was turned to either side of the line in use.

The intensity readings for the measurement of absorption were taken in the order: zero, absorber-out, absorber-in, absorber-out, and zero. The absorber-in reading consisted of a set of ten readings for ten uniformly spaced positions of the absorber as it was moved across the beam.

For each absorber and wave-length, about twenty such determinations of the absorption were made under different conditions of tube voltage and tube current.

RESULTS

In Table II are given the mass absorption coefficients for Au (79), Ag (47), Cu (29), Al (13), C (6), and the apparent mass absorption coefficients for flakes and foils of Be (4). The results for Au (79), Ag (47), Cu (29) and C (6) are plotted in Fig. 2, the results for Al (13) and Be (4) foils in Fig. 3.

Measurements of absorption by Au (79) were extended out beyond the five M absorption discontinuities to the N_1 absorption region. The only other measurements ever made beyond the M limits are those by Jönsson[1] on Pt (78). The plot of $\log \mu/\rho$ against $\log \lambda$ in Fig. 2 reveals a decrease in slope as the plot is extended to the long wave-length side of the M absorption limits. The slopes computed from the data are 2.537 below the M limits and 2.225 above.

Likewise a plot for Ag (47) shows a decrease in slope from the short to the long wave-length side of the L absorption discontinuities. The computed slopes are 2.655 and 2.478.

The measurements for Cu (29) are entirely within the L_1 absorption region. The computed slope is 2.744. It is to be noted that the slopes decrease with increase in the atomic number of the absorber.

The measurements for Al (13) are within the K absorption region except for one at 8.3A just beyond the K discontinuity for Al. In Fig. 3 a straight line is drawn through the points of data although the data actually lie along a curve of constantly decreasing slope. This curve for Al is the only one in this work extending over a sufficiently long wave-length region to give definite evidence of a decreasing slope within a region not containing an absorption discontinuity. The computed slope, assuming a linear relation between $\log \mu/\rho$ and $\log \lambda$ is 2.741.

The measurements for C (6) are entirely within

the K absorption region. The computed slope is 2.834.

For the absorbers Au (79), Ag (47), Cu (29) and Al (13) and for wave-lengths below 3A, the estimated experimental error is less than 2 percent. For wave-lengths above 3A, the estimated experimental error is less than 3 percent. As the C (6) absorber was moved across the beam, no measurable variation of transmitted intensity was exhibited. However, because of the granular nature of graphite, there may have been a variation of transmitted intensity from point to point of the absorber. The experimental error for C (6) is therefore estimated as not more than 4 percent. However, since all the data, except that at 0.7078A, were taken with the same absorber, the slope for C (6) is as accurately determined as that for any of the metal foil absorbers.

A comparison of the results of Jönsson,[1] Biermann,[3] and the author in Fig. 4 may give some idea of the precision of absorption measurements in this wave-length region. Each observer used distinctly different methods. The close agreement between the results of the author and those of Biermann, and the large variation from those by Jönsson is significant of the modern improvements in the methods of measuring x-ray intensities. As Biermann has suggested, much of the discrepancy is no doubt caused by scattering from Jönsson's crystal, but also to the inherent difficulties of making precise intensity measurements by photographic means

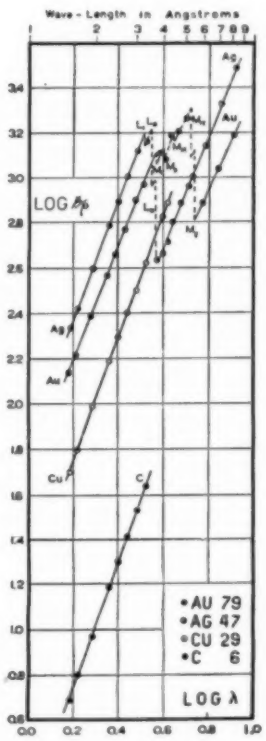

FIG. 2. Mass absorption coefficients for Au, Ag, Cu and C.

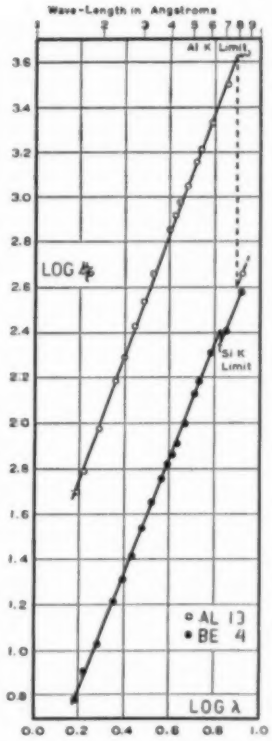

FIG. 3. Mass absorption coefficients for Al and Be.

Since the Be (4) contained nearly 1 percent of higher atomic-number impurities, the values

TABLE II. *The mass absorption coefficients, μ/ρ, in* $cm^2\ g^{-1}$.

λ	Au (79)	Ag (47)	Cu (29)	Al (31)	C (6)	Be (4)* FLAKES	Be (4)* FOILS
0.7078A		27.1		5.08	0.594		
1.537	216	217	50.0	49.7	4.87	4.87	6.0
1.655	259	264	63.0	61.3	6.18	6.04	8.15
1.753						5.04	
1.932	387	394	96.7	93.5	9.38	6.55	10.5
2.285	585	612	155	153	15.5	10.1	16.3
2.498	720	779	198	194	20.0		20.4
2.743	925	1007	256	268	26.1		25.8
3.025	1252	1320	319	346	34.0		34.7
3.352	1470	1450	439	459	43.8		45.1
3.694		431					57.2
3.927	2050	459	673	710			66.0
4.146	1910	517	773	822			73.2
4.395	2450	629		941			90.8
4.718	2550	764		1108			99.0
5.167	2910	905		1430			134
5.395		1012		1630			152
6.057	1210	1380		2130			203
7.111	1730	2145		3170			257
8.321	2450	3070		459			381

* No corrections have been made for the impurities in the Be (4). Siemens and Halske found the flakes to contain 0.4 percent of Fe (27). Spectral analysis of the foils revealed traces of Fe (27), Cu (29), Si (14) and W (74).

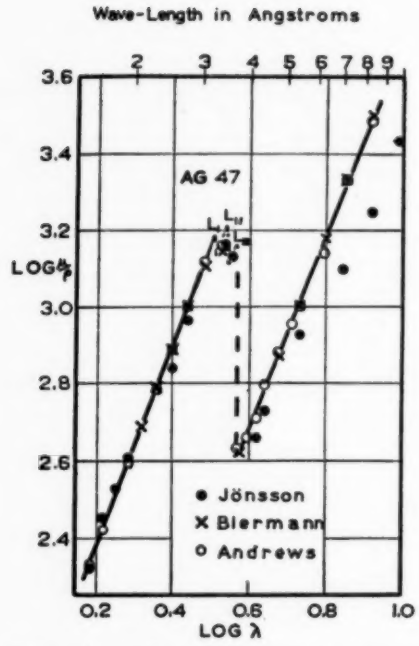

FIG. 4. Comparison of mass absorption measurements of Jönsson, Biermann and the author.

obtained for the mass absorption coefficients are possibly as much as 100 percent higher than they would be for pure Be (4). However, the results are given because some of the experimental difficulties may be pointed out.

So great is the effect of a heavy impurity on the apparent mass absorption coefficient of a light element such as Be (4), that measurements of the absorption coefficients in the neighborhood of an absorption limit of an impurity provide a means of microanalysis for that impurity.

Be (4) flakes were obtained from Siemens and Halske and were estimated by that company to contain 0.4 percent of Fe (27). The mass absorption coefficients given in Table II for a cake of Be (4) flakes were plotted against the cube of the wave-length in Fig. 5 and the Fe K discontinuity revealed 0.44 percent of Fe impurity.[7]

[7] If the masses per unit area of the total absorber, the Be, the Fe, and all the other combined impurities are represented respectively by m_T, m_{Be}, m_{Fe}, and m_I and if, at the Fe K absorption limit, the maximum and the minimum absorption coefficients for the total absorber and for Fe are, respectively, $(\mu/\rho)_T$, $(\mu/\rho)_T'$, $(\mu/\rho)_{Fe}$, and $(\mu/\rho)_{Fe}'$ and for Be and the other combined impurities are $(\mu/\rho)_{Be}$ and $(\mu/\rho)_I$, then

$$(\mu/\rho)_T m_T=(\mu/\rho)_{Fe}m_{Fe}+(\mu/\rho)_{Be}m_{Be}+(\mu/\rho)_I m_I \quad (1)$$

and

$$(\mu/\rho)_T' m_T=(\mu/\rho)_{Fe}'m_{Fe}+(\mu/\rho)_{Be}m_{Be}+(\mu/\rho)_I m_I. \quad (2)$$

Subtracting Eq. (2) from Eq. (1) and solving for m_{Fe}/m_T, we obtain, independently of any knowledge of the other impurities or of the absorption coefficient of pure Be, the fraction of Fe present.

$$\frac{m_{Fe}}{m_T}=\frac{(\mu/\rho)_T-(\mu/\rho)_T'}{(\mu/\rho)_{Fe}-(\mu/\rho)_{Fe}'}=\frac{6.80-5.00}{460-54}=0.0044.$$

The mass absorption coefficients for Fe were taken from Allen's tables in Compton and Allison's book, *X-rays in Theory and Experiment*.

Even if the Be is pure, cakes of flakes are much too granular to permit accurate absorption measurements in this wave-length region. For the first time, Be foils have been produced to permit an attempt at measurement at long wave-lengths. With considerable difficulty, for Be (4) is much more brittle and clings more firmly to the glass plate than do the other metals, thirty-seven foils were produced. This stack of foils was sufficient to absorb half of the intensity at 4A.

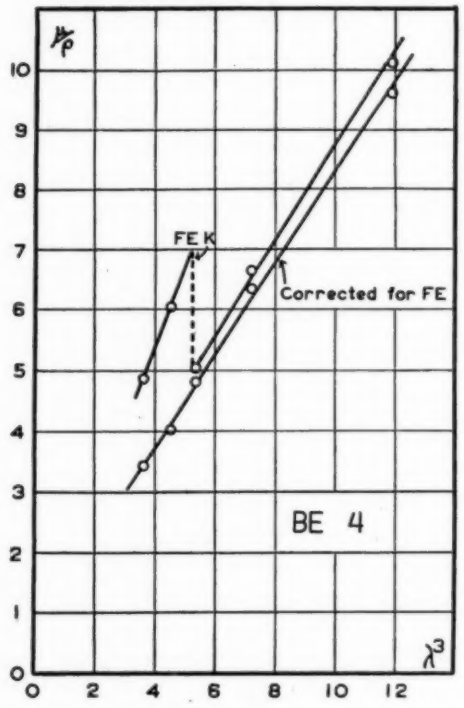

FIG. 5. Plot of mass absorption coefficients of beryllium which shows the Fe K absorption discontinuity caused by 0.44 percent of Fe impurity.

The measurements of the apparent mass absorption coefficients for Be (4) foil are given in Table II and plotted in Fig. 3. This stack of the thickest foils that could be produced without the formation of bubbles behind them, was too thin to permit accurate measurements below 2A. Thus

no attempt was made to analyze for Fe (27) at its K limit.

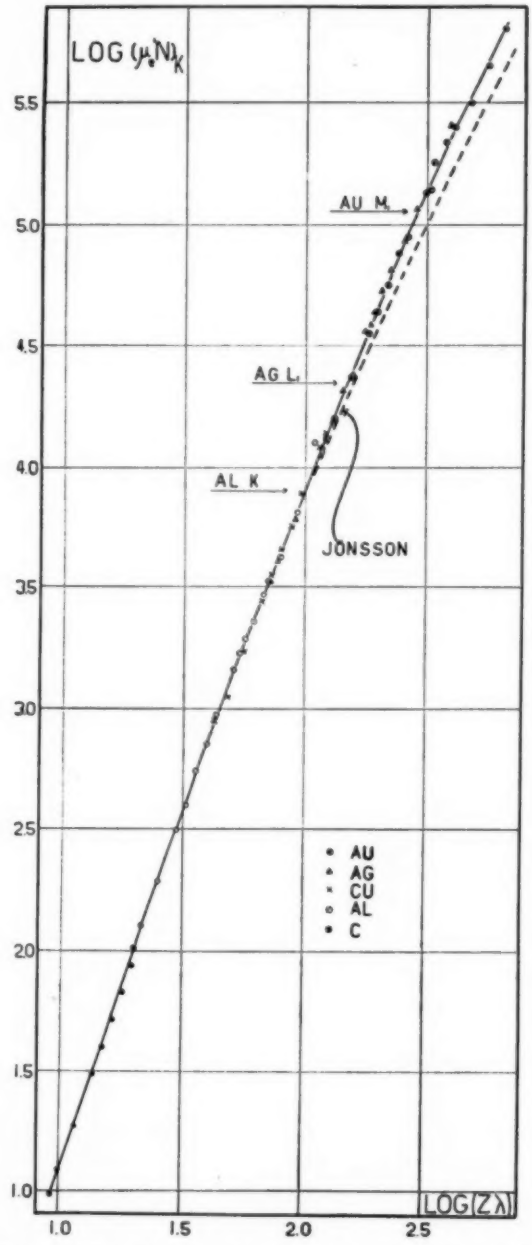

FIG. 6. Plot of electronic absorption coefficients which verifies Jönsson's conclusion that they are simple functions of the product $Z\lambda$.

Such foils of Be (4) could be of considerable value as x-ray windows and as backings on which to evaporate heavier elements for absorption measurements at still longer wave-lengths.

UNIVERSAL ABSORPTION CURVE

The electronic absorption coefficient, μ_e, is defined by the expression

$$\mu_e = (\mu/\rho)(A/ZN), \tag{1}$$

where N is the number of atoms per gram atom, A the atomic weight of the absorber, and Z the atomic number of the absorber. As a means of eliminating the absorption discontinuities, Jönsson[1] has suggested multiplying the absorption coefficient by E_K/E_x. E_K is the energy of the K state of an atom of the absorber and E_x is the energy of that state of an atom of the absorber corresponding to the first absorption discontinuity on the long wave-length side of the wave-length under consideration. $\mu_e NE_K/E_x$ may, without confusion, be expressed by the abbreviation $(\mu_e N)_K$.

In Fig. 6 the author's values of log $(\mu_e N)_K$ are plotted against log $Z\lambda$. Although this curve lies above Jönsson's, most of the data for the five elements lie along a sufficiently smooth curve to confirm, within the limits of experimental error, Jönsson's conclusion that the electronic absorption coefficient is some simple function of the product $Z\lambda$.

ACKNOWLEDGMENTS

The author wishes to express his appreciation of the constant encouragement and advice which he has received from Dean F. K. Richtmyer during the course of this problem, of valuable suggestions from Professor L. G. Parratt, and of help from Dr. S. Kaufman who had previously designed much of the apparatus.

The Effect of Chemical Combination on *K* Fluorescent X-Ray Emission Lines

LEONARD OBERT AND J. A. BEARDEN
Johns Hopkins University, Baltimore, Maryland

(Received September 23, 1938)

The width and index of asymmetry of the fluorescent $K\alpha_1$, $K\alpha_2$ and $K\beta_1$ emission lines of pure Zn, Cu, Fe, Mn, Cr and 26 compounds, including the halides and sulfides of Cu and Fe, have been measured with a double crystal spectrometer. The changes between the shapes of the lines of the metals and their oxides are in good agreement with those determined by Roseberry and Bearden for the same emission lines produced by direct excitation (electron impact), and indicate that the method of excitation does not influence the shape of the lines. A study of the Cu and Fe halide and sulfide lines shows some regularities in the change of the width and index of asymmetry with the percentage composition, the most outstanding of which are for the iron sulfides FeS, Fe_2S_4, Fe_2S_3, FeS_2. As the percentage of sulfur increases, both the width and the index of asymmetry decrease for all lines, the maximum change being of the order of 40 percent for the width of the $K\alpha_1$ lines.

INVESTIGATIONS[1] previously carried out on the effect of chemical combination on x-ray emission lines have been made with direct excitation by electron bombardment. That the chemical composition can and does change under these conditions has been realized by all investigators and directly demonstrated by Parratt[2] in the case of iron sulfate. This difficulty has been overcome in the present work, as shown by the results, through the use of fluorescent excitation. The present developments have made it possible to study all the commonly available compounds of copper and iron, many of which could not have been used inside an x-ray tube.

The production of sufficient intensity of fluorescent radiation presented some difficulty, for it was found in preliminary experiments that it is impossible to use many of the compounds inside of the tube, due to their appreciable vapor pressure. If the compounds were placed outside of the ordinary x-ray tube, the distance from the primary to the secondary target would become so large that the fluorescent radiation would be insufficiently intense. To overcome this difficulty, a metal-walled x-ray tube was designed with a thin aluminum window. The fluorescent target was placed directly outside of the window and the focal spot was deflected, by means of suitable electrostatic baffles, to a point on the gold or tungsten anode directly inside of the window. The distance from the primary focal spot to the fluorescent target was then less than one cm. The upper limit on the power which can be dissipated in the tube is about 500 watts, and is fixed by the heating of the aluminum window due to the absorption of scattered electrons.

The fluorescent targets were made from the compounds by pressing the powdered crystals, without binder, into rectangular wafers 1 cm by 0.5 cm which were cemented with Duco cement to a microscopic cover glass. The Fe targets were made by electro-plating the metal on copper. The Mn, Cr and Zn targets were made from the pure metals.

The advantages of using a metal x-ray tube with the fluorescent target outside are: first, the targets can be easily interchanged without disturbing the x-ray tube; second, there is no danger of decomposition or chemical change due to bombardment or heating; third, there is no tungsten deposited on the target; fourth, the compound does not evaporate, as sometimes happens when it is placed inside the tube.

The source of high voltage was a 100,000-volt transformer. A two-kenotron full-wave rectifier and a 0.5-mf Pyranol condenser were used to produce the d.c. voltage. Between the condenser and x-ray tube a kenotron was used to limit the possible current from the high voltage source to about 50 ma. The high voltage was measured with a 25×10^6-ohm wire-wound resistor. The kenotrons, high voltage transformer, condenser and resistance were all immersed in transformer oil in a steel tank.

The x-ray intensities were measured with either an ionization chamber in conjunction with a Western Electric D 96475 electrometer tube

[1] Roseberry and Bearden, Phys. Rev. **50**, 204 (1936).
[2] Parratt, Phys. Rev. **49**, 14 (1936).

and a Barth Pliotron circuit, or with an argon-filled Geiger counter and scale of eight recorder.[3] The linearity of the Geiger counter was determined by plotting the number of counts per minute as a function of the x-ray tube current at constant potential. The counter and circuit were found linear within one percent up to 3000 counts per minute. All measurements were made at rates lower than this value.

The spectrometer and crystals have been previously reported by Roseberry and Bearden.[1] The width of the Cu $K\alpha_1$ line in the (1−1) position was 9.8 seconds, and in the (1+1) position 39.2 seconds. This gives a physical resolving power of 11,000. The geometrical resolving power, determined by the height and separation of the slits, was 40,000 for the first order. Since the crystals were always used in the first order, the resolving power was determined by the perfection of the crystals and not by the geometry of the instrument.

Experimental Procedure

The procedure followed for obtaining the data was essentially the same as that described by Roseberry and Bearden,[1] except that no correction had to be made for the base line because fluorescent lines do not have any background due to continuous spectrum. The points on the curves in the neighborhood of the half maximum or above were measured within a probable error of 3 percent for the $K\alpha_1$ lines and 4 percent for the $K\alpha_2$ and $K\beta$ lines. After running each line, it was immediately checked once or more to increase the accuracy. Taking into account the integrating effect of the curve, the widths (the full width at half-maximum) were determined with an estimated error of 1.5 percent for the $K\alpha_1$ lines, and 2.0 percent for the $K\alpha_2$ and $K\beta$ lines, and could always be repeated within these limits. The index of asymmetry cannot be determined as accurately, due to the error in locating the maximum ordinate of the curve. The values are given with an estimated error of 8 percent.

Results

A comparison of the results obtained in this investigation of the fluorescent $K\alpha_1$, $K\alpha_2$, $K\beta$

[3] Giarratana, Rev. Sci. Inst. **8**, 390 (1937).

TABLE I. *Comparison of line widths, widening and asymmetry for fluorescent and direct excitation. The* Cu $K\alpha_1$, α_2 *lines are compared for different methods of recording.*

Compound	Width in Seconds		Index of Widening		Index of Assymmetry	
	$K\alpha_1$					
Cr	76.0	(75.5)	—	—	1.39	(1.37)
Cr_2O_3	100.4	[102.0]	1.32	[1.35]	1.46	[1.36]
Mn	73.6	[76.5]	—	—	1.56	[1.54]
MnO	88.9	[93.7]	1.21	[1.22]	1.52	[1.42]
Mn_3O_4	94.4	[100.2]	1.28	[1.31]	1.33	[1.43]
Fe	65.2	(68.4)	—	—	1.51	(1.61)
Fe_2O_3	82.4	[85.2]	1.26	[1.25]	1.55	[1.61]
Fe_3O_4	83.2	[85.5]	1.27	[1.25]	1.52	[1.58]
FeS	75.2	[79.3]	1.15	[1.16]	1.52	[1.58]
Zn	36.0	(36.9)	—	—	1.14	(1.12)
ZnO	35.6	[38.5]	0.99	[1.02]	1.15	[1.12]
Cu	39.0	(39.9)	—	—	1.15	(1.13)
Cu*	39.2	—	—	—	1.15	—
Cu**	39.2	—	—	—	1.14	—
	$K\alpha_2$					
Cr	84.1	(90.4)	—	—	1.01	(1.03)
Cr_2O_3	113.2	[115.0]	1.35	[1.27]	1.00	[1.03]
Mn	89.4	[89.3]	—	—	1.17	[1.17]
MnO	100.0	[97.5]	1.12	[1.09]	1.28	[1.21]
Mn_3O_4	102.8	[103.3]	1.15	[1.15]	1.11	[1.14]
Fe	76.6	(80.1)	—	—	1.25	(1.26)
Fe_2O_3	83.2	[84.8]	1.08	[1.06]	1.15	[1.24]
Fe_3O_4	83.6	[85.0]	1.09	[1.06]	1.20	[1.24]
FeS	78.8	[81.2]	1.02	[1.01]	1.26	[1.20]
Zn	40.8	(43.1)	—	—	1.32	(1.33)
ZnO	38.4	[42.6]	0.94	[0.99]	1.21	[1.33]
Cu	51.4	(51.5)	—	—	1.33	(1.31)
Cu*	51.2	—	—	—	1.26	—
Cu**	51.4	—	—	—	1.28	—
	$K\beta$					
Mn	76.0	(76.5)	—	—	1.40	(1.40)
MnO	76.8	[76.5]	1.01	[1.00]	1.94	[1.75]
Mn_3O_4	79.2	[76.3]	1.04	[1.00]	1.63	[1.75]
Fe	73.0	(73.2)	—	—	1.62	(1.75)
Fe_2O_3	84.0	[85.2]	1.15	[1.16]	1.62	[1.79]
Fe_3O_4	83.6	[85.0]	1.14	[1.16]	1.73	[1.75]
FeS	82.8	[84.0]	1.13	[1.15]	1.63	[1.74]
Zn	66.8	(63.5)	—	—	1.34	(1.48)
ZnO	66.8	[66.3]	1.00	1.04	1.48	[1.46]
Cu	72.8	(72.5)	—	—	—	—

For numbers in ( ) see J. A. Bearden and C. H. Shaw, Phys. Rev. **48**, 18 (1935). And those in [ ] see H. H. Roseberry and J. A. Bearden, Phys. Rev. **50**, 204 (1936).

emission lines with those obtained by Roseberry and Bearden,[1] and Bearden and Shaw,[4] for the same primary lines, is given in Table I. In this table width in seconds is the uncorrected full width of the line at half-maximum, and the index of widening is the ratio of the width of the line for the compound to the width of the same line for the pure metal in the solid state. In this table no corrections have been made for resolving power of crystals or overlapping of lines.

The lines are, in general, narrower than those obtained by Roseberry and Bearden[1] or Bearden and Shaw,[4] giving differences that exceed the combined experimental errors in numerous instances. It should be pointed out, however, that the widths of the Cu $K\alpha$ lines, determined by both direct and fluorescent radiation, give values less than those of Bearden and Shaw, indicating that the crystals used in this work have a somewhat higher resolving power. Moreover, Parratt[5] has shown that differences of this amount are usually found between different pairs of crystals or when crystals are reground and etched. In view of these conditions the narrowings are not considered significant.

The widths of the Cu $K\alpha$ doublet were determined in three ways: first, with primary radiation and an ionization chamber (Table I**); second, with fluorescent radiation and the same ionization chamber (Table I*); and third, with fluorescent radiation and a Geiger counter (Table I Cμ). The close agreement between these methods, both for the line widths and the asymmetries, indicates that there is no difference due to either the method of excitation or the method of recording.

The index of widening, which is a measure of the change in the width due to chemical effects, is practically independent of the differences in the crystals. A comparison of the indices of widening shows that the relative widenings for the primary and fluorescent lines agree within the experimental error except for the $K\beta_1$ line of Mn_3O_4, the $K\alpha_2$ line of Cr_2O_3 and the K lines of Zn, for which the differences are of the order of 5 percent. The indices of asymmetry for all lines agree within the combined experimental errors.

[4] Bearden and Shaw, Phys. Rev. **48**, 18 (1935).
[5] Parratt, Rev. Sci. Inst. **6**, 387 (1935).

TABLE II. *Widths, indices of widening R_W, indices of asymmetry R_A for the $K\alpha_1$, $K\alpha_2$ and $K\beta$ lines of* Cr, Mn, Fe, Cu, *and* Zn *and for the same lines in chemical combination.*

	$K\alpha_1$				$K\alpha_2$				$K\beta$				
	Width Sec.	Width Volts	R_W	R_A	Width Sec.	Width Volts	R_W	R_A	Width Sec.	Width Volts	R_W	R_A	Crystal Structure and Type
Cr	76.0	2.00	—	1.39	84.1	2.21	—	0.98	—	—	—	—	Body Centered Cubic *A*-2
Cr_2O_3	100.4	2.89	1.44	1.46	113.2	2.98	1.35	0.96	—	—	—	—	Hexagonal *D*-51
Mn	73.6	2.40	—	1.56	89.4	2.88	—	1.20	76.0	3.04		1.40	Cubic *A*-12
MnO	88.9	3.00	1.25	1.52	100.0	3.26	1.13	1.32	76.8	3.08	1.01	1.94	Cubic *B*-1
Mn_3O_4	94.4	3.20	1.33	1.33	102.8	3.40	1.18	1.15	79.2	3.18	1.04	1.63	Tetragonal *H*-11
αFe	65.2	2.53	—	1.51	76.6	2.98	—	1.28	73.0	3.55	—	1.62	Body Centered Cubic *A*-2
FeO	81.6	3.29	1.30	1.47	81.6	3.19	1.07	1.30	85.5	4.25	1.20	2.09	Face Centered Cubic *B*-1
Fe_3O_4	83.2	3.37	1.33	1.52	83.6	3.30	1.11	1.24	83.6	4.17	1.17	1.73	Cubic (Wyckoff)
Fe_2O_3	82.4	3.34	1.32	1.55	83.2	3.27	1.10	1.19	84.0	4.17	1.17	1.62	Rhombohedric *D*-51
FeS	75.2	2.99	1.18	1.52	78.8	3.06	1.03	1.29	82.8	4.09	1.15	1.63	Hexagon *B*-8
Fe_3S_4	68.8	2.70	1.07	1.39	75.4	2.93	0.98	1.22	73.6	3.59	1.01	1.27	
FeS_2	67.6	2.64	1.04	1.36	75.6	2.91	0.98	1.08	74.0	3.59	1.01	1.31	
FeS_2	53.2	1.97	0.78	1.22	68.8	2.64	0.88	1.10	74.4	3.63	1.02	1.19	Cubic (Pyrites) *C*-2
FeF_3	82.4	3.34	1.32	1.64	90.2	3.76	1.26	1.15	88.4	4.41	1.24	1.85	Rhombic *DO*-12
$FeBr_3$	80.0	3.22	1.27	1.56	82.1	3.24	1.09	1.24	76.4	3.71	1.04	1.55	
$FeCl_3 \cdot 2H_2O$	85.7	3.50	1.38	1.51	85.6	3.37	1.13	1.33	83.6	4.17	1.17	1.58	Rhombic C-19
$Fe_2(SO_4)_3$	81.8	3.29	1.30	1.46	84.0	3.30	1.11	1.16	88.0	4.41	1.24	2.15	
Cu	39.0	2.38	—	1.15	51.4	3.28	—	1.33	72.8	6.01	—	1.07	Face Centered Cubic *A*-1
Cu_2O	39.7	2.43	1.02	1.20	48.1	3.04	0.93	1.36	69.2	5.69	0.95	1.14	Cubic *C*-3
CuO	39.4	2.41	1.01	1.13	48.4	3.06	0.93	1.31	72.0	5.95	0.99	1.02	Face Centered Cubic *B*-1
Cu_2S	40.1	2.46	1.03	1.14	52.3	3.34	1.02	1.30	68.5	5.62	0.94	1.12	Face Centered Cubic *C*-1
CuS	40.6	2.50	1.05	1.20	52.4	3.35	1.02	1.29	70.4	5.82	0.97	1.09	Hexagon *B*-18
CuCl	39.6	2.42	1.02	1.19	49.2	3.12	0.95	1.13	68.2	5.60	0.93	1.00	Face Centered Cubic *B*-3
$CuCl_2 \cdot 2H_2O$	42.5	2.64	1.11	1.25	49.8	3.16	0.96	1.38	75.2	6.20	1.03	1.01	Rhombic (?)
CuBr	40.1	2.46	1.03	1.17	50.0	3.17	0.97	1.39	70.4	5.83	0.97	1.18	Face Centered Cubic *B*-3
$CuBr_2$	43.0	2.68	1.13	1.22	55.0	3.54	1.08	1.37	80.4	6.71	1.11	1.05	Monoclinic
CuF_2	42.8	2.66	1.12	1.14	48.8	3.09	0.94	1.33	68.6	5.63	0.94	1.20	Face Centered Cubic *C*-1
CuI	39.0	2.38	1.00	1.12	51.2	3.26	0.99	1.39	69.8	5.74	0.96	1.00	Face Centered Cubic *B*-3
$CuSO_4 \cdot 5H_2O$	41.6	2.57	1.08	1.21	48.8	3.09	0.94	1.26	74.8	6.20	1.03	1.12	Triclinic *H*(?)
Zn	36.0	2.55	—	1.14	40.8	2.96	—	1.32	66.8	6.38	—	1.34	Hexagonal *A*-3
ZnO	35.6	2.51	0.98	1.15	38.4	2.76	0.93	1.21	66.8	6.38	1.00	1.48	Hexagonal *B*-4

* Width in seconds are the only results not corrected for overlapping of lines and resolving power of crystals.

The results shown in Table I indicate that the method of excitation has no significant effect on the shape of the emitted x-ray line. This fluorescent method makes it possible to study the shapes of x-ray lines when the emitter is in any physical state whatever.

Table II gives the measured width in seconds, the width in volts corrected for both resolving power of crystals[6] and overlapping of lines, the index of asymmetry, and the index of widening of the $K\alpha_1$, $K\alpha_2$ and $K\beta$ lines of Cr, Mn, Fe, Cu, Zn, and their simple compounds. The asymmetries and indices of widening were calculated from the true widths in volts. In the last column is given the corresponding crystal structure insofar as it is known.

The results may be summarized as follows:

(1) In general the effect of chemical combination on the width of the $K\alpha_1$ line for the compounds of Cr, Mn, Fe, Cu, and Zn, tends to decrease as the atomic number increases. All of the $K\alpha_1$ lines have an index of widening greater than one, with the exception of ZnO and FeS_2, which is decidedly less than one. The $K\alpha_2$ lines show a similar change with the atomic number. The index is greater than one for the compounds of Cr, Mn and Fe, with the exception of FeS, but for Cu and Zn most of the indices are less than or approximately equal to one. The $K\beta$ lines show no regular change with the atomic number. The indices of widening for the Mn oxides are slightly greater than one; all of the iron compounds are appreciably greater than one; most of the copper compounds are less than one; and ZnO is equal to one. No general conclusions can be drawn for the effect of chemical combination on the index of asymmetry.

(2) The $K\alpha_1$ and $K\alpha_2$ lines of the iron sulfides, FeS, Fe_3S_4, Fe_2S_3, and FeS_2 are unique in that they show a progressive but not linear change in the width and asymmetry as the relative atomic concentration is varied. As the relative percentage of the sulfur is increased, the index of widening decreases. This is best shown by the $K\alpha_1$ line, which changes from 2.99 volts for FeS (which is 18 percent wider than pure Fe) to 1.97 volts for FeS_2 (which is 22 percent narrower than pure Fe). A similar change in width is exhibited by the $K\alpha_2$ line. The asymmetries of the $K\alpha_1$, $K\alpha_2$ and the $K\beta_1$ lines show a corresponding change, the index of asymmetry decreasing as the percentage of sulfur is increased.

(3) The iron oxides, FeO, Fe_3O_4, and Fe_2O_3 show large indices of widening for all lines which are practically independent of the relative percentages of the atomic constituents. The indices of asymmetry are unchanged within the experimental error.

(4) The copper compounds show a general effect, namely, the divalent compounds yield wider lines than the monovalent compounds, or in terms of the concentrations, the smaller the concentration of Cu in the compound, the wider the lines. This effect is particularly noticeable for the bromides and chlorides, and is the reverse of what was found for the iron sulfides.

Conclusions

The effect of chemical combination on the widths of the lines studied is small compared with the energy of excitation, producing a change amounting to about 1.5 volts at most and usually much less. Compared to the excitation energy, the effect is at most one part in five thousand.

The fact that in several instances the widths of the $K\alpha_1$ and $K\alpha_2$ lines changed in opposite directions, that is, the $K\alpha_1$ line widened while the the $K\alpha_2$ line narrowed or *vice versa*, together with the fact that Roseberry and Bearden[1] found no widening for the $K\beta_5$ line ($K-M_{IV}M_V$) indicates that the width of the K level is not influenced by chemical combination. Hence the change in the widths of the L levels must be responsible for the change in the widths of the $K\alpha_1$ and $K\alpha_2$ lines. If one takes the results from the present work on the $K\alpha_1$ lines ($K-L_{III}$) together with those of Roseberry and Bearden[1] and Gwinner[7] on the $K\beta_5$ lines ($K-M_{IV}M_V$) and $L\alpha$ lines ($L-M_{IV}M_V$), respectively, it should be possible to calculate the widths of the K, L_{III} and $M_{IV}M_V$ levels from the widths of these lines, assuming that the width of a line is equal to the

[6] The most satisfactory formula for correcting the widths for the finite resolving power of the spectrometer, given by Parratt, Rev. Sci. Inst. **6**, 387 (1935) is $W_t = W_0 - 2.9W_R^{1.7}$, where W_0 is the measured width in the (1+1) position, W_R is the measured width of the (1−1) curve, and W_t is the true width, all in x.u.

[7] Gwinner, Zeits. f. Physik **108**, 523 (1938).

sum of the widths of the levels. If this is done for Fe, the results give

K level$+L_{III}$ level
$=3.15$ volts (width of $K\alpha_1$ line),
L_{III} level$+M_{IV}M_V$ level
$=3.5$ volts (width of $L\alpha$ line),[8]
K level$+M_{IV}M_V$ level
$=6.9$ volts (width of $K\beta_1$ line).

The solution of these equations gives

$$K \text{ level} = 3.28 \text{ volts},$$
$$L_{III} \text{ level} = -0.12 \text{ volt},$$
$$M_{IV}M_V \text{ level} = 3.6 \text{ volts}.$$

If these calculations are carried out for other elements the results are similar. The negative width of the L_{III} level, of course, is physically meaningless; in fact it would be expected that the width of the L_{III} level is at least comparable with those of the K or $M_{IV}M_V$ levels. These results should not be interpreted as a failure of the theory, that is, that the width of line is equal to the sum of the widths of the levels, but rather that the lines are made up of unresolved components. This is further substantiated by the asymmetry of the lines.

If this is so, one should, in view of the foregoing, look for some factor that might cause the splitting of the $L_{II}L_{III}$ levels to account for the change in the widths of the $K\alpha_1$, $K\alpha_2$ lines.

The following factors are discussed as possible explanations of the effect:

(1) *Multiple ionization.* The presence of relatively strong satellites in the $L\alpha$ and $L\beta$ lines, as found by Gwinner,[7] is attributed to multiple ionization of the outer levels. This causes displacements of the levels in the direction of higher energy, the effect being greater for the M than the L level, accounting for the fact that the satellites are on the short wave-length side of the parent line. This displacement of the L levels in those atoms doubly ionized will also displace the K lines and, as a result, the K lines may have unresolved components. The multiple ionization of the outer levels containing the valence electrons would be influenced by the chemical binding, hence it is possible that the binding can influence the shape of the K lines. On the basis of this reasoning it is, however, impossible to explain why the $K\beta_5$ line is not influenced and why the $K\beta_1$ line is influenced only for certain elements.

(2) *Splitting due to couplings between the L and M levels.* The L shell with one electron missing has an angular momentum equal to that of the missing electron. This can couple with the angular momentum of the M level and cause a splitting of both levels which would produce a multiple line structure. This splitting would be small and it is very possible in the case of the $K\alpha$ lines that the components are unresolved. The changes in the width of the $K\beta_1$ line can be attributed to a coupling between the p-electrons in the M_{III} level and the d-electrons in the partially filled $M_{IV}M_V$ level. That the $K\beta_5$ line does not widen is explained by the fact that for the production of the line the ($M_IM_{II}M_{III}$ and L_IL_{II} and L_{III}) levels are fully occupied, hence there is no possibility for coupling. The coupling with the K level would be small because of the screening of the L shell. In this manner the coupling between the outer levels could be influenced by the chemical binding and thus produce chemical effects.

A study of the effect of chemical combination on the K and L absorption edges, as well as a measurement of the Auger coefficients of the different levels, might yield valuable information for the explanation of this problem.

The authors are greatly indebted to Professors James Franck, G. H. Dieke and Dr. M. Goeppert-Mayer for helpful discussions on possible theoretical explanations of the results; and to Dr. C. H. Shaw for many helpful suggestions and for assistance in developing the apparatus. The double crystal spectrometer was a generous loan of the Naval Research Laboratory.

[8] The uncorrected widths of the lines are used in this calculation, because sufficient data were not given (reference 7) to correct the $L\alpha$ line for the resolving power of the crystal.

Further Tests of the Validity of X-Ray Crystal Methods of Determining *e*

V. L. BOLLMAN, *Occidental College, Los Angeles, California*

AND

J. W. M. DUMOND, *California Institute of Technology, Pasadena, California*

(Received July 20, 1938)

The authors have continued their efforts to absolve the x-ray method of determining the electronic charge of the criticism that Bragg reflection determines the lattice dimensions in only a very shallow surface region whereas the density determinations have been made on a much larger volume of crystal. In earlier work by a powder method we were able to show that the above-mentioned superficiality criticism could not explain the discrepancy between $e=4.803$ (the "x-ray value") and $e=4.770$ (computed by the oil-drop method with Harrington's value of air viscosity). The powder method, necessarily somewhat less precise than the macroscopic calcite method, yielded a mean of $e=4.799$, agreeing with the macroscopic calcite value well within the precision of the powder method. The present work gives a still more precise absolution of the macroscopic calcite results from the above-mentioned criticism. In the earlier work we abandoned efforts to measure lattice dimensions in the interior of a thin-cleaved slab of calcite by means of Laue reflection in a precision transmission spectrometer because photographs with the crystal adjacent to the slit, but on the same side as the photographic plate showed most of the Laue reflection coming from regions close to the front and back surfaces of the slab. Also strange unexplained fluctuations of intensity along the lengths of the spectral "lines" were observed with the crystal in this position. In a continuation of this work two thin crystal slabs have been studied. Each has been etched with HCl rather heavily all over one of its faces and over half the height of its opposite face. The upper half of the spectral lines selectively reflected to the photographic plate had thus traversed a crystal slab etched on both sides, while the lower half had traversed a slab etched on only one side. With this arrangement, and with the crystal on the side of the slit nearest the photographic plate, we are able to show that the enhanced Laue reflection from regions near the surface is completely suppressed by sufficient etching and that fainter reflection can then be definitely observed from the interior regions of the crystal. With the crystal on the opposite side of the slit from the plate we are able to compare very accurately on one and the same photographic plate the reflection angles for the enhanced surface reflection with the reflection angles for the interior planes. These angles turn out to be very precisely equal, thus furnishing clinching justification for the validity of the well-known precise determinations of *e* by Bragg reflection from the surface of macroscopic pieces of calcite. The density fluctuations along the length of the lines are absent for the interior reflection and we conclude that they are probably the result of local variations of surface disturbance set up in the process of cleavage.

I. INTRODUCTION

THE present paper describes the continuation of a program of investigation of the criticisms of the x-ray crystal method of determining the electronic charge *e*. In a previous paper[1] the authors have tried chiefly to answer the following criticism, namely, that while the density measurements on a macroscopic crystal are averages

[1] DuMond and Bollman, Phys. Rev. **50**, 524 (1936). The schematic view, Fig. 5 of this paper, shows the precision transmission or "Laue reflection" type spectrometer. The slit and crystal are mounted on a turntable whose axis of rotation coincides accurately with the center line of the slit. The reflecting planes of the thin calcite crystal parallel to its narrow cleavage surface are used and the table and crystal are set by optical adjustments so that these planes stand accurately normal to the photographic plate holder surfaces. These latter are two in number (not shown in Fig. 5) and the distance between their accurately parallel plane surfaces has been measured by means of scratches on a bar in the same comparator used for measuring the line separations on the plates. Movable lead shields are provided to protect the plate from the straight-through transmitted beam on the side opposite to that on which the spectrum lines are being photographed. Lead x-ray shielding and light-tight housings are shown in Fig. 4. The Mo target of the x-ray tube has its surface nearly parallel to the plane of Fig. 5 so that the projected height of the focal spot (normal to the plane of the drawing) is very small. The focal spot is of large enough diameter in the direction parallel to the plane of the figure to furnish radiation of appropriate direction for the entire *K* spectrum. In Fig. 5 the crystal and slit are shown in the normal *A* position for making sharp spectrum lines and for determining Laue reflection angles with precision. Fig. 7 of the same reference shows schematically the position of slit and crystal after turning the turn table one-half revolution away from the normal position of Fig. 5. Only the first of the two photographic plate positions is shown. Before etching the exit or entry cleavage surfaces of the calcite, reflection from the regions near these surfaces predominated so strongly as to form intense lines on the plate at A_1 and B_1 or at A_2 and B_2 with the appropriate separations d_1 and d_2 easily computed from the thickness of the crystal and the geometry of the arrangement. (See Fig. 8.) After etching, these lines are extinguished and a uniform band of reflection by the interior planes of the crystal throughout the triangle *OAB* can be seen on the photographic plate filling the regions

of a large volume, say 10 cc of crystal, the x-rays are diffracted from a thin surface layer (Bragg reflection) which is limited by "extinction" to about 4×10^{-4} cm thickness, a very small fraction of the total volume in an entirely specialized location.

In the earlier work an effort was made to measure by means of Laue reflection the calcite lattice dimensions for the *interior* of a thin crystal slab. A precision transmission spectrometer, whose arrangement is schematically evident in Fig. 5 of the above-mentioned previous paper,[1] was used. Normally the slit is situated on the same side of the crystal as the photographic plate, so as to form sharp spectral lines. We shall designate this as the *A* position. We found, however, upon turning the circular table halfway round so that the crystal stood between the slit and the photographic plate, (hereafter called *B* position) as indicated in Fig. 7 of the previous paper, that the Laue reflection from those parts of the internal planes closely adjacent to the front and back surfaces of the crystal slab (at *O*, *A* or *B*) strongly predominated over the reflection from the interior of the slab. See Fig. 8 of the previous paper. The results of the *A* arrangement could, therefore, not be regarded as representative of the crystal interior. Also in the *B* position there were observed certain mysterious fluctuations of intensity along the lengths of the spectral lines reflected by the regions of the planes near the front and back surfaces of the crystal.

These difficulties led us to the adoption of the powder method for determining e with the result, $e=4.799\times10^{-10}$ e.s.u. slightly lower than the value 4.803 obtained by ordinary methods with macroscopic calcite. We did not attach any especial significance to this slight difference of four units in the third decimal place which is within the limits of accuracy of the powder method. Rather the result was interpreted as a corroboration in favor of the value 4.803 obtained by Bragg reflection on macroscopic calcite and against the much lower value 4.770. The powder method is necessarily somewhat less precise (as judged by internal consistency of the measurements) than the macroscopic calcite method and it is therefore desirable to increase, if possible, the precision with which the macroscopic calcite results may be absolved of the criticism regarding their superficiality.[2] We believe the work here reported accomplishes this.

II. Effect Upon Laue Reflection of Etching Exit and Entry Surfaces

K. V. Manning[3] has described specifications for etching a cleaved or polished calcite surface with HCl in order to reduce the "rocking curve" widths of the crystal as observed with the two-crystal spectrometer. We have etched one side of our thin slab of cleaved calcite and have found that the enhanced Laue reflection from the regions near the surface can be completely suppressed if the etching be continued considerably longer than Manning specifies for his purpose. We found some 20 minutes with 0.7 normal HCl were necessary. With the spectrometer set in the *B* position and a prolonged exposure,

d_1 and d_2. (See Fig. 7.) In this position the spectrometer is useless for precise measurements on the lines as these are too broad. Its use is solely to show which regions of the crystal are active or predominant in reflection. The exposure in Fig. 8 was made with the plate in the more remote plate holder (see Fig. 1) so that the α-doublet spectral separation would be sufficient to avoid confusion with the doublet character of the lines caused by enhanced reflection near the crystal surfaces. Because of the large plate distance the fluctuations of intensity along the lengths of the lines are spread so far apart that they are few in number and do not show clearly in this reproduction.

[2] In a paper entitled "The Most Probable 1938 Values of the Electron and Related Constants," R. A. Millikan, Ann. d. Physik **32**, 42 (1938), the question as to a slight residual "mosaic effect" is again raised as a possible justification for a value of $e=4.796$ very appreciably lower than 4.803, the mean of the best x-ray results obtained with macroscopic calcite. Millikan in this paper has frankly attempted to harmonize the best experimental values of e, e/m, and h/e so that when these are substituted into the Bohr formula for the Rydberg constant a value in accord with the spectroscopic determinations of that constant shall be obtained. In our opinion this required doing some violence both to the most reliable values of h/e as measured by means of the short wave-length limit of the continuous x-ray spectrum and to the value of e obtained by the x-ray crystal method. The results reported in the present paper, we believe, remove any justification for revising downward the x-ray crystal value, $e=4.803$, obtained with macroscopic calcite. For the purpose of determining *the most probable values of the constants, e, m, and h in 1938* such an effort to harmonize these discrepancies is perhaps the best compromise that can be made. We take the stand, however, that the discrepancy between the measured values of these constants and the requirements of the Bohr-Rydberg formula is something interesting in itself which may lead to important revisions of theory. Whether such revisions must be made in the form of the Bohr-Rydberg formula itself or in the theory governing some of the experimental determinations we, of course, do not pretend to know. Experiments are now under way which we hope may answer such a question.

[3] K. V. Manning, Rev. Sci. Inst. **5**, 316 (1934).

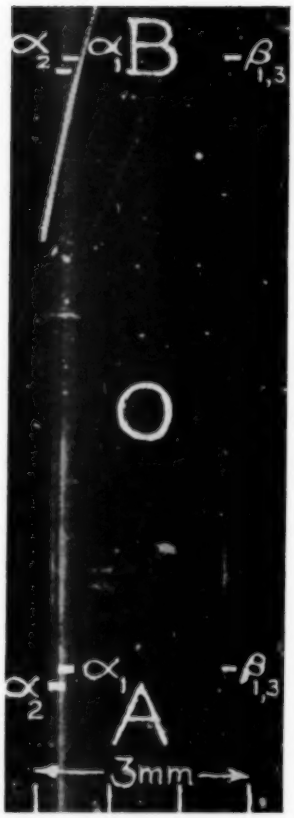

FIG. 1. Showing an enlargement of the reflected Mo K spectrum from an etched crystal slab (spectrometer in B position). In this case the exit surface of the crystal slab has been rather strongly etched with HCl and the entry surface has been similarly etched over its upper half. That segment of the spectrum lines marked AO came from the part of the crystal with one unetched face. The segment OB came from the region with both faces etched. The etching has caused the intensified surface reflection to disappear completely. The fainter reflection from the interior of the crystal can now be seen as a uniform band and in the region AO it is bounded on one side only by the enhanced reflection from the single remaining unetched part of the entry face. In the region OB each line can be seen spread out as a uniform band of reflection from the crystal interior (region, OAB, Fig. 7 previous paper) with no enhancement at the edges. The apparent width of the enhanced region is mainly caused by the finite width of the spectrometer slit and should not be understood as indicating any great depth for the crystal region from which the enhanced reflection comes. This exposure was taken with the plate in the nearer of the two plate holders and there is, therefore, some slight overlapping of the bands from $K\alpha_1$ and $K\alpha_2$. The band from $K\beta_{1,3}$ is also clearly visible in the original. Also because of the closer plate distance several of the fluctuations of intensity along the length of all the enhanced surface lines are visible in the original in the region AO. These fluctuations are completely absent for the reflection from the interior of the crystal (segment OB). The reader is asked to disregard the accidental scratch in the region OB of the alpha-lines. The scale indicates the magnification.

reflection from the interior of the crystal could now be brought out on the photograph as a band of the appropriate breadth bounded on one side only with the sharp intense line from the region of the crystal near the remaining unetched face. This remaining surface line still exhibited the marked fluctuations of intensity along its length which characterize all such surface lines in all the samples we have observed.

Next the crystal slab was etched in the same way on the upper half of its opposite face (the face nearest the slit). The boundary line between the etched and unetched regions of this face was horizontal and cut across the slit at very near the midpoint of its height. By carefully adjusting the

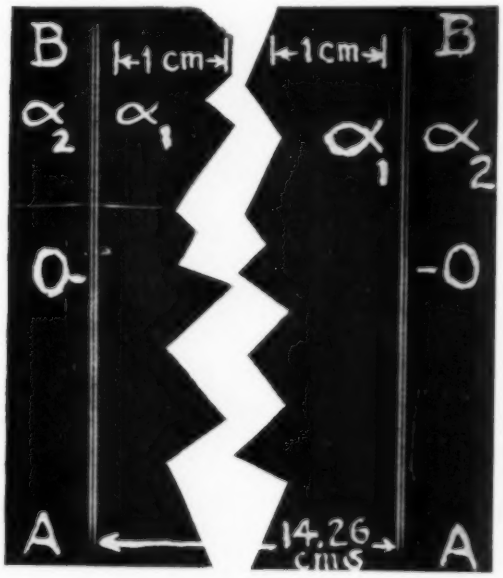

FIG. 2. Enlarged reproduction of spectral lines (Mo $K\alpha_1$, α_2) taken with the spectrometer i n the A position. (Normal arrangement to give sharp lines for accurate angle determinations, the crystal being on the opposite side of the slit from the photographic plate.) Here the crystal slab has been etched completely over its entry face and over the upper half of its exit face (the face nearest the slit). Thus the somewhat fainter upper half of the spectrum line (segment here indicated as OB) has been formed by Laue reflection throughout the entire interior of the crystal slab, while the stronger lower half (segment here indicated as OA) has been formed chiefly by Laue reflection from the regions near the unetched surface. On the original the fluctuations of intensity along the length of the line can be seen in the segment OA. Attention is called to the complete absence of any jog or offset at the junction of the line segments OA and OB. Careful measurements, on lines such as these, of the separation between left- and right-hand reflected images for the top and bottom segments (OB and OA) showed the reflection angles for the interior of the crystal to be accurately identical with the reflection angles for the regions near the surface.

height of the focal spot of the x-ray tube it was easy to arrange so that the upper half of the spectral lines selectively reflected to the photographic plate had thus traversed a crystal slab etched on both sides while the lower half has traversed a slab etched on only one side. Fig. 1 is an enlarged reproduction of an exposure with the spectrograph in the *B* position and with the crystal etched fully on one side and halfway down on the other side. The band reflected from the interior of the crystal is clearly visible and its lower half is bounded on one side by the enhanced reflection from the unetched part of one face of the crystal.

Now with the above-described crystal and with the spectrometer in the *A* position (slit between crystal and photographic plate) a number of exposures were taken for the purpose of comparing precisely the diffraction angle for the reflection near the surface with the diffraction angle from the interior planes. Both α_1- and α_2-lines of the molybdenum *K* spectrum were measured. The upper part of the spectral lines formed by Laue reflection in a crystal with both entry and exit surfaces etched appears of uniform density over its length but considerably less intense than the lower part of the spectral lines formed by Laue reflection chiefly from the part of the crystal with one unetched surface. This latter part of each line exhibits the fluctuations of intensity along its length and clearly comes mainly from Laue reflection near the unetched surface which strongly predominates over the reflection from the interior. The sharp boundary between the part of the line where surface reflection predominates and the part formed by interior reflections is clearly visible, the difference in reflected intensity being marked. Fig. 2 is an enlarged reproduction of one such spectrum line.

TABLE I. *Line separations in cm on plate for* Mo$K\alpha_1$ *and* $K\alpha_2$.

PLATE No.	$\Delta\alpha_1$ FOR INTERIOR	$\Delta\alpha_1$ FOR SURFACE	$\Delta\alpha_2$ FOR INTERIOR	$\Delta\alpha_2$ FOR SURFACE	
1	4.4155	4.4162	4.4431	4.4430	Nearer plate holder
2	4.4124	4.4112	4.4392	4.4378	
3	4.4141	4.4135	4.4406	4.4403	
Average	4.4140	4.4136	4.4410	4.4404	
4	14.2612	14.2610	14.3480	14.3483	Farther plate holder
5	14.2568	14.2579	14.3435	14.3437	
6	14.2565	14.2560	14.3444	14.3432	
Average	14.2582	14.2583	14.3453	14.3436	

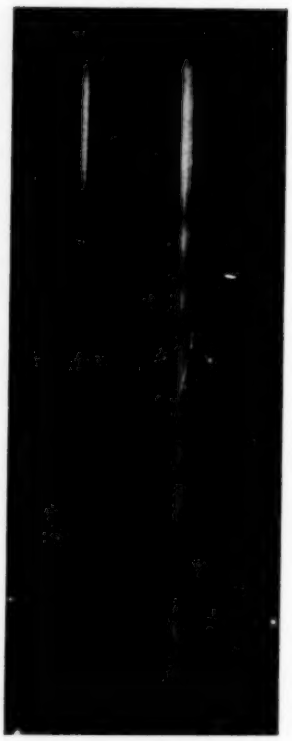

FIG. 3. Illustrating the fluctuations of intensity along the lengths of the lines. Enlarged reproduction of an entire *K* spectrum formed by Laue reflection from an unetched crystal with the spectrometer in the *B* position and with the plate on the nearer of the two plate holders. The broadening and doubling of the lines combined with the low dispersion because of the proximity of plate to slit has caused the alpha-doublet to overlap confusingly. This proximity of plate to slit permits a large number of the intensity fluctuations to appear in good contrast on the plate.

Precise measurements of the diffraction angles could be made by measuring the separation of the images formed by Laue reflection both to left and to right. The angles for surface and interior reflection were very accurately compared by use of the measurements between the top halves of the lines and the bottom halves on one and the same plate. The absolute angles themselves were also measured precisely by successively photographing spectra on plates mounted in two plate holders (visible in Fig. 4 of the previous paper)[1] one of which was much nearer the slit than the other and whose separation was accurately measured (by means of a trammel bar) on the same comparator as was used for measuring the plates. Table I gives the comparison of line separations for surface and interior reflections, while Table II gives the absolute angles we have

TABLE II. *Laue reflection angles for interior and surface reflection.*

θ_{α_1} interior	θ_{α_1} surface	θ_{α_2} interior	θ_{α_2} surface
6° 42′ 21″	6° 42′ 22″	6° 44′ 47″	6° 44′ 45″
Comparison with Larsson's results in Bragg reflection			
θ_{α_1} = 6° 42′ 35″		θ_{α_2} = 6° 45′ 2″	

TABLE III. *Measured Laue reflection angles for second crystal sample before etching.*

θ_{α_1}	θ_{α_2}
6° 42′ 35″	6° 44′ 59″

measured compared with those observed by Larsson,[4] whose results were given highly satisfactory confirmation by Compton,[5] Tu,[6] and Bearden.[7]

The first thin slab we studied, while showing satisfactory agreement between surface and interior reflection angles, gave the absolute values for the angles of Laue reflection about six-hundredths of one percent smaller than the results observed by Larsson in Bragg reflection. This discrepancy is only slightly decreased by the correction for index of refraction and as it is a little too large to be interpreted as an error of measurement, we concluded that our first sample of calcite was perhaps slightly imperfect. We therefore selected another thin slab of calcite which, before etching, as shown in Table III, gave for the absolute Laue angles excellent agreement with the accepted Bragg values, and we repeated on this sample all the studies we have just described for our first sample with the completely satisfactory results as regards agreement between the line separations for the surface and for the interior reflections as shown in Table IV. Table V shows the absolute angles for surface and interior Laue reflections for the second calcite. Comparison with the results of Larsson (Table II) shows excellent agreement with the Bragg values.

The very slight differences between the Laue reflection angles for surface and interior reflection are entirely within the limits of observational error and quite without significance, for both crystal samples.

Regarding the absolute values of the reflection angles, the correction for refractive index of 3.25 seconds of arc must be subtracted from Larsson's value but is entirely negligible in our case because in our Laue reflection the entry and exit beams are nearly normal to the surface of the calcite. The deviation from Larsson's corrected results is inside the limit of our observational error for the second crystal sample.

The important conclusion from these observations is that when Laue reflection is used with a calcite crystal etched on both faces in the *A* arrangement the observed diffraction angle *representative of the entire interior of the crystal* is just the same as the diffraction angle for reflection occurring near the surface so that the validity for the purpose of determining *e* of the well-known precision measurements made in Bragg reflection is now, we believe, firmly established to about the same order of precision as could be claimed for the observational precision of those measurements themselves.

III. Probable Cause of the Intensity Fluctuations Along the Length of the Spectral Lines

We think the fluctuations of intensity along the length of the spectral lines in the case of Laue reflection near the exit or entry surface of a calcite crystal may be explained as follows. We suppose that in spite of the remarkable uniformity of calcite both as regards density and lattice perfection as revealed by x-rays there exists in the body of the crystal a multitude of regions where the cleavage planes do not resist rupture quite as strongly as elsewhere. An incipient crack is too strong a term to describe such a weak region. We have no reason to think that these regions exhibit any marked regularity

TABLE IV. *Line separations in cm on plate for* Mo $K\alpha_1$ *and* $K\alpha_2$ *(second crystal sample).*

PLATE No.	$\Delta\alpha_1$ FOR INTERIOR	$\Delta\alpha_1$ FOR SURFACE	$\Delta\alpha_2$ FOR INTERIOR	$\Delta\alpha_2$ FOR SURFACE	
7	4.4149	4.4138	4.4416	4.4407	Nearer plate holder
8	14.2646	14.2630	14.3518	14.3504	Farther plate holder

TABLE V. *Measured Laue angles for surface and interior reflections, second crystal sample.*

θ_{α_1} interior	θ_{α_1} surface	θ_{α_2} interior	θ_{α_2} surface
6° 42′ 35″	6° 42′ 33″	6° 45′ 1″	6° 44′ 59″

[4] Larsson, Phil. Mag. (7) **3**, 1136 (1927).
[5] A. H. Compton, Rev. Sci. Inst. **2**, 365 (1931).
[6] Y. C. Tu, Phys. Rev. **40**, 662 (1932).
[7] J. A. Bearden, Phys. Rev. **38**, 1389 (1931).

of distribution but feel tempted to regard them as accidents in the detailed history of the crystal growth. These regions though numerous enough to insure fairly ready cleavability of a macroscopic piece of calcite in almost any portion of its structure are, we suppose, separated by strong homogeneous domains which constitute the overwhelmingly preponderant volume of the entire crystal. This volumetric preponderance of the homogeneous strong domains is necessary to explain the remarkably reproducible density and the x-ray structural perfection of this crystal. It also agrees with the annoying difficulty sometimes encountered in inducing cleavage in calcite at some exactly specified point. A further fact supporting this picture is that a large piece of calcite, if hit or dropped, will almost always cleave along cleavage planes whereas when finely powdered calcite is examined with a microscope one sees many curved irregular and conchoidal fractures. It seems reasonable to suppose that when calcite is cleaved, the tearing action progresses by a sort of propagation of stress from one weak region to another lying as nearly as possible in the same plane. The lattice structure is greatly disturbed by the tearing action in the strong regions and little disturbed in the weak regions. Hence the surface after cleavage has patches of greater and less disturbance. Indeed something of this sort seems frequently visible under close scrutiny with a low power microscope. The more disturbed regions will reflect more x-ray energy than the less disturbed regions.[8] The fluctuations of intensity along the length of the spectral lines we have observed are, we think, a direct result of this. It is interesting to note that the above phenomenon is less pronounced in the case of our second crystal sample whose reflection angle showed it to be the more perfect of the two samples.

Figure 3 is an enlargement of a K spectrum of lines exhibiting these fluctuations of intensity taken with the first crystal sample.

Acknowledgments

It is a pleasure to express our gratitude for the financial assistance from the Watters Memorial Research Fund established by Dr. Leon L. Watters of New York City which has supported this research work, establishing the validity of the x-ray crystal method of determining the electronic charge.

[8] That mechanical disturbance of the crystal lattice produces stronger reflected spectral lines is well known. We believe it can be easily understood in the present case of Laue reflection in calcite as follows: Two-crystal spectrometer studies show calcite to be such a perfect crystal that the angular domain over which selective reflection occurs in a good undisturbed sample is very small (only a few seconds of arc). As a result, the solid angle into which a source of x-rays (say any atom radiating in the target) must radiate a given wave-length in order to have it selectively reflected by the crystal is very restricted. Now if the calcite lattice structure is mechanically disturbed, new, slightly differing orientations will be set up in different regions of the crystal so that a larger solid angle of radiation from each atom in the source can find regions appropriately oriented for selective reflection and the total energy reflected will be greater but will cover a wider angular domain. In a spectrometer of high resolving power (such as the two-crystal spectrometer) this results in an angular broadening of the lines rather than in an intensification of them. But in a spectrometer such as the one here described where the breadth of the spectral lines is determined chiefly by the breadth of the slit this latter masks to a large extent the angular broadening set up by mechanical disturbance and the overlapping of the broadened diffracted images transmitted through different regions of the slit width builds up a more intense spectral line.

The Scattering of Alpha-Particles by Argon, Oxygen and Neon*

GORDON BRUBAKER
Sloane Physics Laboratory, Yale University, New Haven, Connecticut

(Received October 13, 1938)

Data on the scattering of alpha-particles by argon, oxygen and neon have been obtained with a novel experimental arrangement developed for the purpose. Anomalies were found in the scattering by all three elements. Irregularities in the course of the anomalies in the cases of oxygen and neon have been interpreted as resonance phenomena. Estimates of the radii of the various nuclear barriers, based on the assumption that the penetrability of the barrier is appreciable at the lowest energy for which an anomaly is apparent, give the values $4.5(10^{-13})$ cm for O^{16}, $4.6(10^{-13})$ cm for Ne^{20}, and $7.5(10^{-13})$ cm for A^{40}. The first two are lower than values calculated from the formula $R=2.05(10^{-13})A^{\frac{1}{3}}$ and the last is somewhat higher. The latter result agrees with deductions of Pollard, Schultz, and Brubaker from data on the A-α-n reaction.

INTRODUCTION

THE scattering of alpha-particles by the gases argon, oxygen and neon has been investigated to some extent by Rutherford and Chadwick[1] and by Riezler.[2] Rutherford and Chadwick found that the number of particles scattered by argon agreed closely with the number calculated from the geometry of the apparatus, under the assumption of inverse square forces, up to 7.3 Mev alpha-particle energy in the angular range 40°–50° and 8.4 Mev in the range 29°–44°. Riezler found that argon and neon scattered classically into the angular range 55°–90° for energies as high as 5.2 Mev. For oxygen he found an anomaly in the scattering consisting of a decrease in numbers scattered below the classical value, beginning at 4.6 Mev. From his results Riezler estimated the radius of the oxygen potential barrier to be $4.5(10^{-13})$ cm and that of the neon barrier to be less than $4.6(10^{-13})$ cm.

The present work was undertaken to extend the data on alpha-particle scattering by these three gases to higher alpha-particle energies and other angles of scattering. In the case of argon, the discovery by Pollard, Schultz and Brubaker[3] that neutrons are emitted from argon under bombardment by alpha-particles of energy as low as 4.5 Mev, and the deduction that the nuclear radius of argon is exceptionally large, made it seem likely that anomalies in the scattering of alpha-particles by argon might exist at lower energies than previously suspected.

A novel experimental arrangement, in which the scattered particles were detected by two proportional counters of toroidal shape developed for the purpose, was used for the work. The scattering into four ranges of angles, whose mean angles were approximately 53°, 65°, 89° and 104°, was investigated with Ra C′, and in some cases Th C′, alpha-particles. In the case of oxygen some data were obtained on the scattering into a third range of angles, of mean angle 78°.

Anomalies were found in the scattering by all three elements. The number of particles scattered by argon was found to decrease below the classical value at the higher energies, the decrease beginning at lower energies and being more marked at the higher angles. Irregularities were found in the anomalies in scattering by oxygen and neon which are explainable as reasonance phenomena. Estimates of the various nuclear radii were made from the results.

APPARATUS

The apparatus used in the experiments, a cross section of which is shown in Fig. 1, differed considerably from the usual "annular ring" arrangement. The incident beam of particles was defined by a circular aperture in front of the source disk, and the scattered particles were detected by proportional counters of toroidal

* Part of a dissertation presented to the Faculty of the Graduate School of Yale University in candidacy for the degree of Doctor of Philosophy.

[1] E. Rutherford and J. Chadwick, Phil. Mag. **4**, 605 (1927).

[2] W. Riezler, Ann. d. Physik **23**, 198 (1935).

[3] E. Pollard, H. L. Schultz and G. Brubaker, Phys. Rev. **53**, 351 (1938).

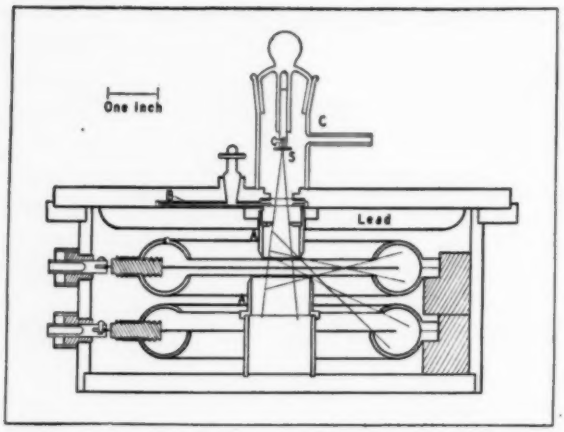

FIG. 1. Cross section of scattering chamber and counters.

shape. The beam of scattered particles was defined by the beveled ends of the brass tubes, *A*,*A* and the edges of the openings in the counters. The use of two counters, mounted one above the other, made it possible to count particles scattered into two angular ranges simultaneously. Two sets of tubes *A*,*A* of different lengths were used to investigate the scattering into four ranges of angles. The counters were contained in a cylindrical chamber on top of which was mounted a short glass tube which contained the source disk. Chamber and tube were separated by a thin foil. The chamber was filled to a pressure of ten cm with the gas being investigated.

The type of counter which was developed for this work consisted of a hollow toroid of aluminum (large radius, 5.2 cm; small radius, 1.0 cm) inside of which was supported a circular loop of ten-mil wire. Details of the counter and of the supports for the wire are shown in Fig. 2. The aluminum toroid, which formed the negative electrode of the counter, was constructed in two parts, a top and a bottom half-shell, for ease in construction and assembly. Through the peripheral flange of the toroid passed amber plugs, fitted with grounded guard sleeves, which served as insulating supports for the wire. The two ends of the wire, which led to the input of an amplifier, passed to the outside of the toroid through one of the amber insulators. Particles to be counted entered the counter through a slot in the toroid, as indicated in Fig. 1.

Two of these counters, with the entrance slots in different places, were mounted on hard rubber blocks in the scattering chamber and the wire of each connected to a separate amplifying and recording system. The amplifiers used consisted of three stages, resistance-capacity coupled, having a total amplification factor of about 50,000. The third stage operated a single thyratron recording circuit. This type of circuit was sufficiently fast since seldom did the counting rate approach sixty per minute.

Since the counters had no foils over their entrance slots, they were filled with the gas in the scattering chamber to a pressure of ten cm. Under these conditions they were found to operate quite satisfactorily as proportional counters for alpha-particles. As in all such counters the negative voltage applied to the toroids was not critical; the value to be used depended upon the sensitivity of the associated amplifier. As is to be expected from the various lengths and directions of possible paths of particles through the counter, the resultant impulses were not uniform. They varied in height, as measured by a cathode-ray oscillograph, from twice to about eight times the height of the background due to gamma-rays. This relatively large ratio of heights of background to impulse is thought to have been caused by the considerable length of the counter and the large solid angle which it subtended at the alpha-particle source, plus the fact that photoelectrons are able to pass parallel to the wire while the alpha-particle paths are perpendicular to the wire. Little difference was apparent in the operation of the counter when filled with different gases, except as to the electrode voltage necessary.

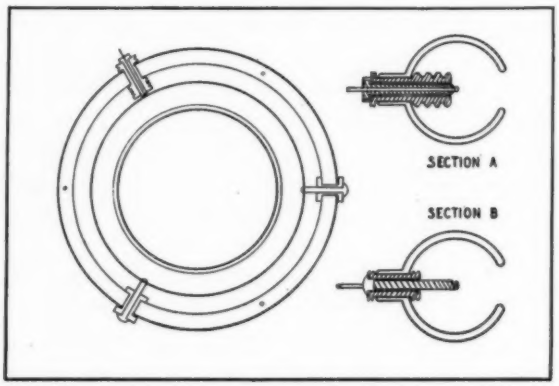

FIG. 2. Details of construction of counters. Lower shell of counter and cross sections of two insulators are shown.

The scattering chamber was a steel cylinder having a steel bottom and a brass flange around its top. Into a depression in this flange was fitted the flat brass plate which formed the top of the chamber. The joint was made airtight by stopcock grease between the flange and plate, and Apiezon putty around the edge of the plate. On the underside of the top was fastened a lead plate a little over a centimeter thick which supported the upper section of edges defining the alpha-particle beams. A disk, B, turned through a metallic ground joint, carried a set of mica foils with which the alpha-particle energy could be varied. The stopping power of the foils was determined both by weighing and by calibration with alpha-particles. The same disk served to prevent particles from entering the scattering chamber during determinations of the background count.

The hole in the center of the chamber top was covered by a thin foil. At first celluloid foils of about one mm stopping power were used, and the upper chamber connected to the lower through a long tube fitted with an adjustable leak. By the exercise of considerable care the chambers could be emptied and filled without straining the foil. However, considerable trouble was experienced with contamination of the counters in spite of glass wool filters and a liquid-air trap placed in the tube connecting the two chambers. The celluloid foils were, therefore, abandoned in favor of mica foils thick enough to withstand at least ten cm pressure and the two chambers were connected to different pumping systems.

The gas being investigated was stored in a reservoir, into which it was introduced through a liquid-air trap, under a pressure of about 25 cm when not in use. It was introduced into the evacuated scattering chamber through a capillary leak, and was removed and returned to the reservoir by a mercury pump. To eliminate the possibility of spurious results through admixture of the small amount of air left in the scattering chamber after each evacuation, fresh oxygen and argon were placed in the reservoir after each five or six runs. In the case of neon a charcoal trap immersed in liquid air was used to speed and make more complete the evacuation.

For most of the work the alpha-particles of Ra C′ were used, although some work was done with Th C′ sources. The Ra C′ sources were prepared by exposing charged disks, nine mm in diameter, to radon. The strength of the sources was measured by counting the alpha-particles emitted into a small solid angle normal to the disks.

Experimental Method and Treatment of Data

After a source disk had been placed in the apparatus and the chamber filled with gas, a series of five minute counting periods, including at least two with each available alpha-particle energy and at least three background counts, were taken. This procedure was repeated with subsequent sources until a number of particles ranging from about four hundred in the case of the larger angles to several thousand at the smaller angles had been counted. These data were reduced to the average number of particles scattered into the counter per minute per millicurie source strength for each incident alpha-particle energy, and a plot made of these numbers against energy.

It is known from the experiments of Rutherford and Chadwick[1] and of Riezler[2] that argon scatters alpha-particles of energies below about five Mev through the angles investigated in this work according to the Rutherford-Darwin law. A curve of $1/E^2$ against E should therefore fit the experimental curve of number against energy for argon up to $E=5$ Mev. Such a curve was fitted to the experimental points. Deviations of the points from the curve at energies above five Mev then indicated departure from classical scattering. By use of this theoretical curve and the Rutherford-Darwin formula similar curves applying to oxygen and neon were constructed. Deviations of the experimental points for each gas from the corresponding theoretical curve indicated departures from classical scattering. The results were finally exhibited as plots of the ratio of observed to classically expected numbers against the energy of the alpha-particles. These curves are shown in Figs. 4, 5 and 6. The lengths of the vertical lines through the experimental points, intended to indicate the relative probable errors of the points, were obtained by dividing the ordinate of the point by the square root of the number of particles counted.

Angular Conditions

Four different angular ranges were investigated in the case of each gas except oxygen, for which a fifth range was investigated. The ranges were quite large and somewhat overlapping. The extent of overlap is indicated by the histograms of Fig. 3, which indicate the angular distributions of detectable scattered particles which would exist if the particles were classically scattered. The histograms were derived by dividing the source disk and scattering volume into small sections and calculating the relative number of scattered particles associated with each pair of sections in source disk and scattering volume which would enter a small section of the counter aperture. The appropriate angle of scattering was also calculated. The total area in each histogram is proportional to the experimental number of alpha-particles of 2.5 Mev energy scattered by argon per minute per millicurie into that range of angles. The average angles of scattering given in Figs. 4, 5 and 6 are derived from the histograms. These average angles are 53°, 65° 30′, 88° 45′ and 104°.

Experimental Results

Argon

An anomaly in the scattering by argon in the form of a decrease below the classically expected number was observed (Fig. 4). The decrease persists to the highest energies used. At the smallest angles (mean 53°) the least energy for which the anomaly is apparent is about 6.5 Mev. This least energy decreases as the angle of scattering is increased, being about five Mev at the highest angles for which observations were taken.

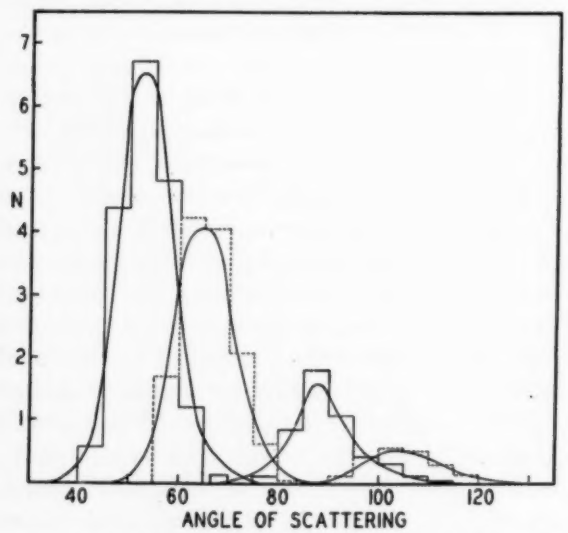

Fig. 3. Calculated angular distribution of detectable scattered particles on assumption of Coulomb forces. Distributions for the four angular ranges whose mean angles are 55°, 65° 30′, 88° 45′ and 104° are shown.

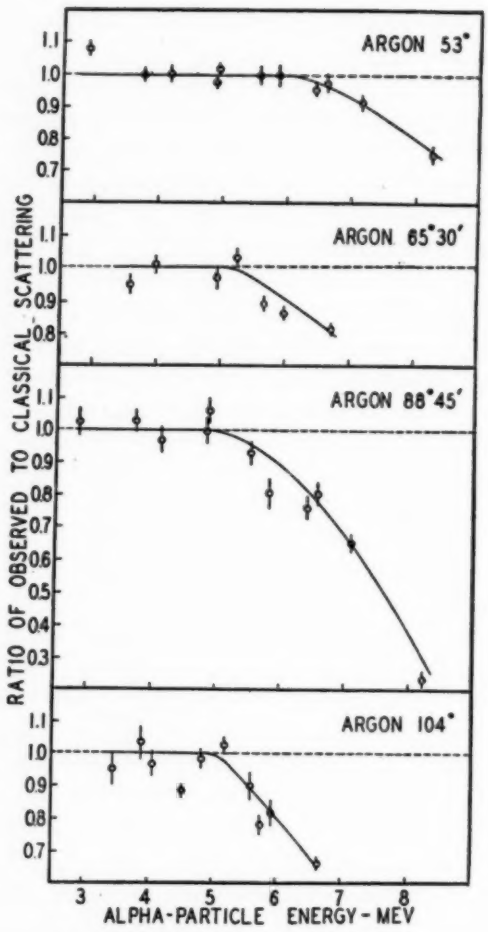

Fig. 4. Experimental results for argon.

An apparent anomaly of this type would be caused if fast alpha-particles produced impulses only as high as, or a little higher than, the impulses of the gamma-ray background, not large enough to be recorded. That the observed decrease was not due to this cause was shown in the following way. First, the counting level was lowered until some of the background impulses were being counted, but no increase in the net count was observed. Second, a cylindrical foil was placed in front of the counter openings to reduce the energy of the particles entering.

Failure again to observe an increased net count showed that the counters were responding properly to fast alpha-particles.

The character of the anomaly observed makes it likely that it is caused by penetration through the top of the argon potential barrier. If we assume that this is true, and that the penetrability of the barrier for particles of zero angular momentum becomes appreciable ($\sim$10 percent) at the minimum energy at which the anomaly becomes apparent, the Gamow probability formula leads to a radius for the argon potential barrier of about 7.5 (10^{-13}) cm. This is about eight percent higher than the radius (7.0×10^{-13} cm) calculated from Bethe's formula, $R=2.05\ (10^{-13})A^{\frac{1}{3}}$ cm.[4]

This large radius is in agreement with the deductions of Pollard, Schultz, and Brubaker[3] concerning the A-α-n reaction. Attempts to fit their experimental yield pressure curves theoretically, based on the assumption that the emission of neutrons was governed by the penetrability of the argon barrier for alpha-particles, were successful only when a large radius was assumed for the argon barrier. That the two experiments should lead to similar estimates of the radius is apparent from the fact that the lowest energy for which neutrons were observed (4.5 Mev) is only slightly less than the minimum energy at which the scattering anomaly becomes apparent.

Oxygen

The anomalies found in the scattering by oxygen are shown in the curves of Fig. 5. At the smaller angles the anomaly consists of a decrease below the classically expected number followed by a slight rise. As the angle of scattering increases the decrease first becomes more marked, then, as the angle increases further, becomes less marked and the increase in number scattered at high energies becomes the most prominent feature of the anomaly. At the highest angles the number of scattered particles reaches five times the expected number.

The results for the mean angle 65° 30′ are in fair agreement with those of Riezler[2] who investigated the scattering of polonium alpha-particles at angles between 55° and 90°. A calculation of the radius of the oxygen potential barrier, made on the assumption that the penetrability becomes appreciable at the least energy (4.6 Mev) at which the scattering anomaly becomes apparent, leads to a value of 4.5 (10^{-13}) cm, in agreement with the estimate made by Riezler. If the radius is calculated from Bethe's formula, the result is 5.17 (10^{-13}) cm, about 15 percent higher.

In the two largest angular ranges the ratio of observed to classically expected numbers rises rapidly above unity as the energy of the alpha-particles is increased. The curves show no decrease below unity, although one may exist between four and five Mev, where no data were taken.

At about six Mev there is an irregularity in the curves. It is quite marked in the curve for the mean angle 88° 45′, although very slight in the curve for the larger angles. Since oxygen is not disintegrated by alpha-particles, and there is, consequently, no question of competition of nuclear processes, this irregularity is attributed to a resonance level. Further, because of the small abundance of the isotopes of oxygen other than O^{16}, the resonance level must be in the Ne^{20} nucleus. If the alpha-particle energy at resonance is taken to be 5.8 Mev, the resonance level is about 9.3 Mev above the ground state of Ne^{20}.

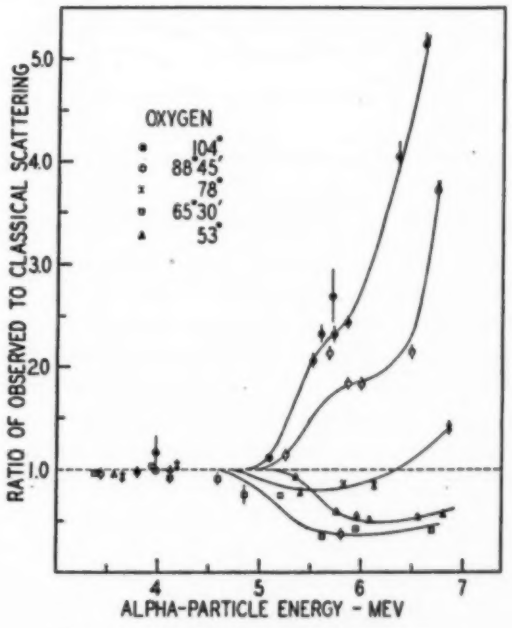

FIG. 5. Experimental results for oxygen.

[4] H. A. Bethe, Rev. Mod. Phys. 9, 172 (1937).

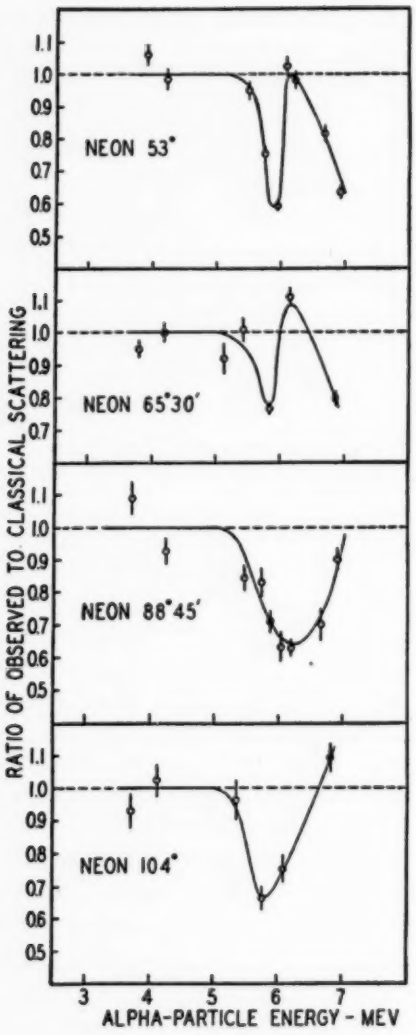

FIG. 6. Experimental results for neon.

This does not correspond to any level previously found.

Since we are dealing with scattering by an element not disintegrated by alpha-particles, we may apply the theoretical results of Wenzel.[5] According to the curves given by him, the maximum ratio of observed to classical scattering of alpha-particles of zero angular momentum and 5.7 Mev energy which can be produced by oxygen is three. Since the irregularity in the curves does not rise above the ratio three, it may be attributed to resonance scattering of particles of zero angular momentum. The subsequent rise to ratios greater than three must be attributed to particles of higher angular momentum. It is to be expected that such particles would contribute to the anomaly since the higher energies are above the top of the oxygen barrier.

[5] P. Wenzel, Zeits. f. Physik 90, 754 (1934).

Neon

The most striking feature of the results for the scattering by neon (Fig. 6) is a very sharp irregularity in the curves for the mean angles 53° and 65° 30′ which is not present in the other two curves. The irregularity consists of a decrease from unity at about 5.3 Mev to a minimum at 5.9 Mev, followed by a rapid rise to approximately unity at 6.1 Mev and a subsequent fall. For the two higher angular ranges the course of the curves is a decrease at 5.2 Mev to a minimum, followed by a rise. There is no sign of the irregularity present in the first two curves.

It was established that the peculiarities observed are not caused by protons produced by the disintegration of neon. A foil was placed in the apparatus to prevent alpha-particles, but not protons, from reaching the counters. No protons were detected.

Because of the relatively large yield of protons from neon under alpha-particle bombardment, it is not certain whether the observed irregularity is caused by a resonance level of the compound nucleus or to a rapid variation in the relative probabilities of emission of protons and alpha-particles. No data on the variation of proton yield with alpha-particle energy are available to help in deciding this question. A possible explanation of the curves for the two lower angular ranges is that the initial decrease is caused by penetration of the barrier, and that the subsequent peak at 6.1 Mev is caused by a resonance level of Mg^{24}. Because of the magnitude of the peak, it seems improbable that it could be caused by Ne^{22}, which composes ten percent of neon.

From the calculated classical angular distribution of detected particles, it may be deduced that, since no evidence of an irregularity is apparent in the curve for the mean angle 88° 45′, only particles scattered at angles less than about 75° contribute appreciably to the observed irregularity. The fact that the irregularity does not appear at all angles does not preclude its assignment to a resonance phenomenon, since, according to Mott[6] and to Bethe,[7] the magnitude

[6] N. F. Mott, Proc. Roy. Soc. 133, 228 (1931).
[7] H. A. Bethe, Rev. Mod. Phys. 9, 175 (1937).

of a scattering anomaly due to a resonance level may vary rapidly with the angle of scattering.

A calculation of the nuclear radius based, as before, on the energy at which the first decrease began leads to a value of 4.6 (10^{-13}) cm. This also is lower than the value calculated from Bethe's formula. Since the barrier height corresponding to this radius is 6.2 Mev, the assumed resonance energy is just below the top of the barrier. The excitation energy of the Mg^{24} nucleus at resonance is 14.7 Mev. This is higher than any resonance level previously found.

Conclusion

Data gathered on the scattering of alpha-particles by argon, oxygen and neon show the existence of anomalies in all three cases. Irregularities in the variation of the anomalies with energy in the cases of oxygen and neon are thought to be due to resonance levels of the associated compound nuclei. Calculations of radii of the scattering nuclei, based on the penetrability of the barriers, lead, in the cases of oxygen and neon, to values smaller than those calculated from Bethe's formula, but, in the case of argon, to a value higher than that given by the formula. This latter result agrees with the deductions of Pollard, Schultz, and Brubaker[3] from data on the disintegration of argon by alpha-particles.

The writer wishes to express his thanks to Professor A. F. Kovarik for his helpful advice and suggestions, and to Professor E. C. Pollard for assistance in some of the work.

DECEMBER 15, 1938 PHYSICAL REVIEW VOLUME 54

The Resonance Processes in the Disintegration of Boron by Protons

B. Waldman,* R. C. Waddel, D. Callihan† and W. A. Schneider
Washington Square College, New York University, New York, New York

(Received October 17, 1938)

The yields of long range alpha-particles and gamma-rays from the disintegration of boron by protons having energies from 150 to 195 kev were measured simultaneously. The shapes of the yield curves indicate that the yields for the two processes are proportional and that the resonances occur at the same voltage, to within 1 kev. A determination of the alpha-particle yield places the resonance point at 165±4 kev. Thus it is highly probable that both resonance processes involve the same level in the excited C^{12} nucleus. The unsatisfactory findings of Oppenheimer and Serber are therefore probably not due to their assumption concerning the association of the resonances with the same energy level of the compound nucleus. The half-breadth of the alpha-resonance was estimated to be 6 kev, and could be accounted for by the spread in energy of the ion beam. Thus the estimates of Oppenheimer and Serber concerning the sharpness of the resonance processes are here supported.

Introduction

VARIOUS workers have reported conflicting data concerning the long range alpha-particle and gamma-ray resonances observed when boron is bombarded with protons. Williams, *et al.*,[1] observed a resonance of the long range alpha-particles at 180 kev. Bothe and Gentner[2] reported that gamma-rays were emitted which also indicated a resonance at 180 kev. Later Williams and associates,[3] using thin targets of boron, placed the alpha-particle resonance at 159 kev with a half-breadth of 10 kev. They also observed the gamma-ray resonance at about the same voltage. The spectrum of the gamma-rays was found to consist of three lines: 4.3 Mev, 11.8 Mev, 16.6 Mev with relative intensities of 1 : 1 : 1/7, respectively.[4]

These resonance processes are attributed to the following reactions:

$$B^{11}+H^{1}\rightarrow C^{12*}\rightarrow C^{12}+\gamma, \quad (1)$$

$$B^{11}+H^{1}\rightarrow C^{12*}\rightarrow Be^{8}+He^{4}. \quad (2)$$

---

* Now at the University of Notre Dame.
† Now at the College of the City of New York.
[1] Williams, Wells, Tate and Hill, Phys. Rev. **51**, 434 (1937).
[2] Bothe and Gentner, Zeits. f. Physik **104**, 685 (1937). Gentner, Zeits. f. Physik **107**, 354 (1937).
[3] Allen, Haxby and Williams, Phys. Rev. **53**, 325 (A) (1938).
[4] Fowler, Gaerttner, and Lauritsen, Phys. Rev. **53**, 628 (1938).

Recently Oppenheimer and Serber[5] in a theoretical discussion of this problem have shown that it is not possible to obtain a satisfactory description of the above reactions if it be assumed that: (a) The alpha-particles and gamma-rays originate from the same excited state of C^{12}; (b) the disintegration is caused by p proton capture; and (c) the angular distribution is that observed by Neuert.[6] They also conclude that the half-breadths of both alpha- and gamma-resonances should be less than 100 volts, in disagreement with the reported value of 10 kev.[3]

In view of the above it appeared that a further investigation of the locations and widths of the boron resonance processes was justified.

Experimental

With a voltage rectifying and doubling set of conventional design[7] and a low voltage hydrogen arc,[8] proton currents of the necessary energy were obtained. The voltmeter design was similar to that of Hafstad, Heydenberg and Tuve,[9] consisting of 400 ten-megohm IRC type BT1 resistors in series with a 20,000-ohm standard resistor, across which a potentiometer was connected. This voltmeter was calibrated under working conditions against one constructed of 100.5 megohms of Taylor wire-wound corona-free resistance units, manufactured by Shallcross, in series with a calibrated Weston model 1 microammeter. A completely independent calibration was made by measuring the voltmeter resistance (4.23×10^9 ohms) on a Wheatstone bridge and by determining the current-resistance characteristic of the type of resistor used. At 165 kev these independent calibrations agreed to within 1.6 percent. The first calibration was used since it was obtained under working conditions. The high voltage was maintained at given values to within one percent by continuous manual adjustment.

After magnetic analysis the proton beam of 0.7 to 2.5 microamperes was directed on a thick target of pure amorphous boron (Eimer and Amend). The target chamber, the design of which is shown in Fig. 1, was arranged so that

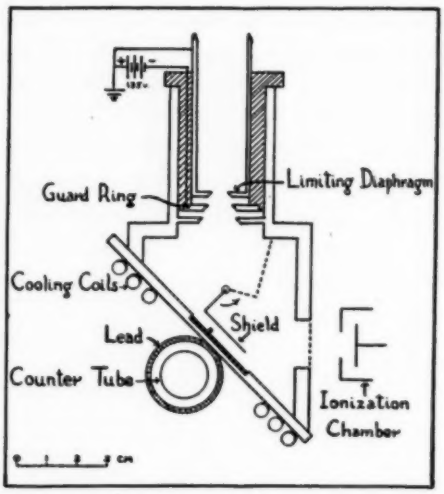

FIG. 1. Target chamber. Simultaneous runs were made with both counter tube and ionization chamber but without the cooling coils. The counter tube was removed for the experiments on alpha-particles alone and the water cooling coils added to keep wax seals cool during the preliminary target heating.

alpha-particle and gamma-ray counting could be done simultaneously. Such a procedure eliminates to a large degree errors in the relative positions of the alpha- and gamma-resonance points. As indicated in Fig. 1, a guard ring whose potential was 135 volts negative was used to minimize secondary electron effects. A brass shield was arranged so that it could be made to intercept the ion beam directly above the target while taking backgrounds on the gamma-ray counting system. Since only the long range (4.4 cm) alpha-particles exhibit the resonance phenomena it was necessary to interpose about 4 cm of stopping power between target and ionization chamber. This was provided by a suitable mica window and air path.

The proton current was read at short intervals (5 to 15 seconds) from a galvanometer, and averaged. The average deviation from the mean for a typical run was 4 percent.

The alpha-counting system consisted of an ionization chamber, linear amplifier, scale of four counter, and recorder. This scaling system could follow more than 400 regular pulses per second and was never used on random counts above 300 per minute.

The gamma-counting system consisted of a thin-walled glass Geiger-Müller counter covered with 1 mm lead, a Neher-Harper extinguishing circuit, a vacuum tube scale of sixteen circuit,[10]

[5] Oppenheimer and Serber, Phys. Rev. **53**, 636 (1938).
[6] Neuert, Physik. Zeits. **38**, 122 (1937).
[7] Cockcroft and Walton, Proc. Roy. Soc. **136**, 619 (1932).
[8] Tuve, Hafstad and Dahl, Phys. Rev. **48**, 334 (1935).
[9] Hafstad, Heydenberg and Tuve, Phys. Rev. **50**, 504 (1936).
[10] Lifschutz and Lawson, Rev. Sci. Inst. **9**, 83 (1938).

and recorder. This scaling circuit was tested at 15,000 cycles per second and was never used above 500 per minute. The gamma-ray background was determined immediately after making a count at a particular voltage by inserting the brass shield in the path of the ion beam. This method eliminates the effects of weak x-rays generated by the ion beam and by the rectifier tubes. Both counting systems were controlled by a common switch and times were read from a stopwatch.

A typical set of data obtained from three runs (two increasing the voltage, one decreasing the voltage), in which alpha-particles and gamma-rays were counted simultaneously, is plotted in Fig. 2. The curves were normalized at 193.5 kev. Each point represents, on the average, about 2000 counts.

A number of these simultaneous runs were made, *all* of which gave curves similar to Fig. 2, indicating coincidence of the resonance voltages for gamma-rays and alpha-particles. The actual value of the resonance voltage, however, was not the same for all runs. These changes in the value of the resonance potentials can be explained by:

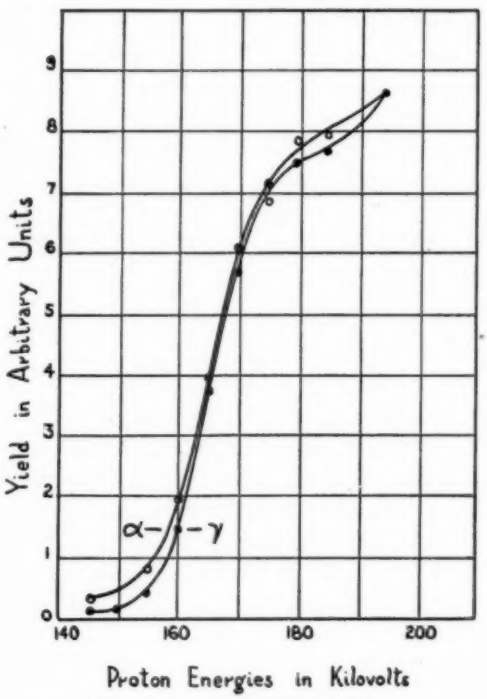

FIG. 2. Yield curves of alpha-particles and gamma-rays counted simultaneously from the disintegration of boron by protons. The ordinates have been adjusted so that both yields coincide at the maximum voltage.

(1) changes in the voltmeter resistance, (2) changing of the target surface due to the deposition of a carbon layer during bombardment (decomposed oil vapor from pumps).

In order to determine the resonance point more precisely, a number of changes were made in the apparatus. Resistance bridge measurements showed that the resistance of the voltmeter varied with the humidity. This difficulty was eliminated by paraffining the isolantite spacers and the reconstructed voltmeter was then calibrated as mentioned before. Fresh boron targets were inserted for each run and were heated to drive off any condensed oil.[11] The time necessary for a run was reduced to a minimum by counting only alpha-particles, and the geometry was improved by reducing the aperture which limited the proton beam from 7 mm to 4 mm. As a consequence of these changes consistent data were obtained. The results of two alpha-particle runs (one increasing, the other decreasing the voltage) are shown in Fig. 3. Each point represents about 1500 counts. This yield curve was then differentiated with respect to the three-halves power of the voltage and is shown in Fig. 4.

DISCUSSION

An examination of the simultaneously determined alpha- and gamma-yield curves, Fig. 2, shows that the steepest portions of both curves, which represent the resonance points, lie at the same voltage to within 1 kev. Further, the alpha- and gamma-yields are proportional, within experimental error.

The position of the peak of the differentiated curve, Fig. 4, shows the resonance voltage to be 165 kev. From a consideration of the various errors involved, the precision of the measurement is set at 2.5 percent, or 4 kev.

The half-breadth of the alpha-particle resonance is estimated to be 6 kev. To determine whether this half-breadth is real or instrumental a careful measurement of the ripple in the accelerating voltage was made. A ripple measurement was made by connecting a 10,000-ohm resistor between the large voltmeter resistance and ground, and determining the peak ripple content by means of a calibrated oscilloscope.

[11] Hatch, Phys. Rev. **54**, 165 (1938).

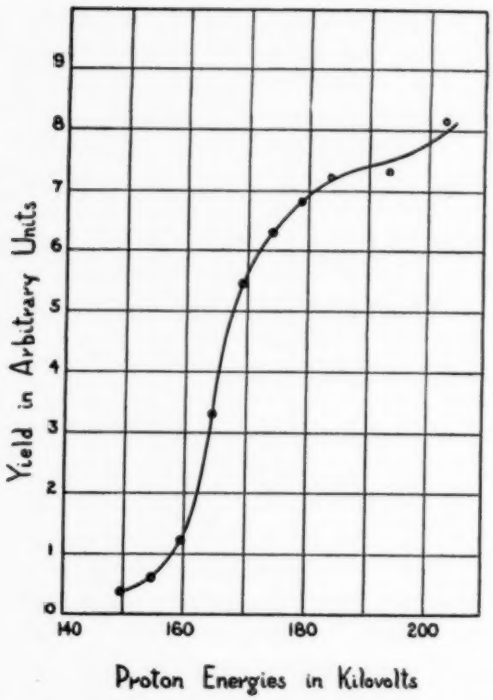

FIG. 3. The yield curve of alpha-particles from a thick target of boron under proton bombardment.

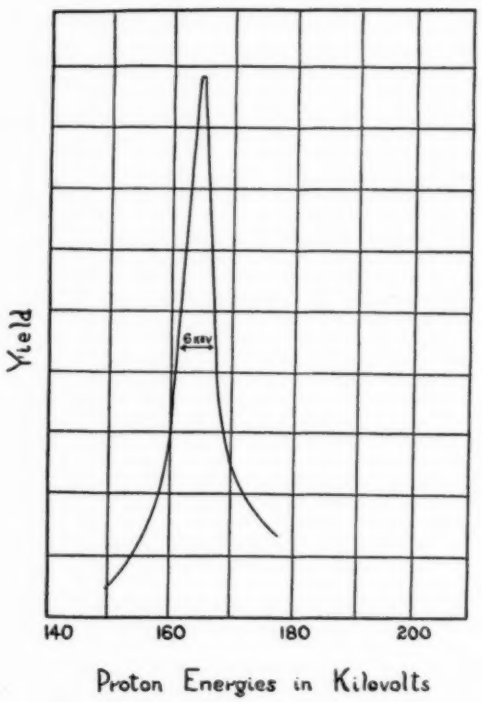

FIG. 4. The yield curve of alpha-particles to be expected from a thin boron target. This curve was obtained by differentiating the observed thick target curve (Fig. 3) with respect to the voltage to the three-halves power.

In this connection it should be pointed out that for the method to be valid, the input impedance of the amplifier-oscillograph combination must be large compared with the value of the auxiliary (10,000-ohm) resistor. Further, it is necessary to take into account the fact that the sectionalized construction of this type of voltmeter resistance introduces a considerable shunt capacitance, which results in exaggerating the ripple. The shunt capacitance was measured and calculation showed that it was sufficient to reduce the 60-cycle impedance of the circuit from a nominal value of 4.23×10^9 ohms to 2.35×10^9 ohms. After applying the necessary correction to the apparent peak value of the ripple at 165 kev a value of 3.6 percent, or 6 kev, was obtained. This is in good agreement with a value of 2.8 percent which was obtained when an alcohol-xylol high resistance was used instead of the voltmeter resistance, although this resistor was not entirely satisfactory.

Thus the *maximum* spread in the ion beam energy was about 12 kev, and since the ripple wave form was peaked in nature, the *effective* spread in the ion beam was undoubtedly considerably less. In any event, it appears that the observed half-breadth (6 kev) of the alpha-resonance process can be attributed entirely to instrumental causes.

The authors wish to thank Dr. C. B. Braestrup of the Bellevue Hospital Physical Laboratory for the loan of the wire-wound high resistance voltmeter and Mr. W. Turnbull of the machine shop for his suggestions and interest in the construction of the apparatus.

Proton Induced Radioactivities

II. Nickel and Copper Targets

CHARLES V. STRAIN
The University of Rochester, Rochester, New York

(Received October 14, 1938)

Nickel bombarded with 6.3-Mev protons shows activities of half-lives of 10.5±0.6 min., 3.4±0.3 hr., and 12.8±0.8 hr., corresponding to known periods of Cu^{62}, Cu^{61} and Cu^{64}, respectively. The reactions are principally of the p-n type but there is evidence that in the case of Cu^{62} proton capture occurs at energies below the p-n threshold. The maximum β-ray energies obtained by absorption method are 2.8, 1.2 and 0.68 Mev for Cu^{62}, Cu^{61} and Cu^{64}, respectively. Thick target excitation curves are given. Copper bombarded with 6.3-Mev protons shows two activities of half-lives 38.3±0.5 min. and 235±20 days due to Zn^{63} and Zn^{65}, respectively. Both must be formed by p-n reactions. The Zn^{63} positrons have a maximum energy of 2.3±0.15 Mev. Thick target excitation curve shows a threshold proton energy of 4.1±0.1 Mev in good agreement with the energy relations. Average (thick target) cross section for the $Cu^{63}(p,n)Zn^{63}$ reaction is 0.28×10^{-25} cm². For protons of energy 6.1 Mev it is 0.95×10^{-25} cm.

INTRODUCTION

THIS work is a continuation of the studies[1] being made in this laboratory of the nuclear reactions produced by high energy protons. The present paper summarizes the results obtained when targets of nickel and copper are bombarded by protons of energies up to 6.3 Mev accelerated in the cyclotron. The proton beam currents were of the order of 0.5μa which is sufficient to produce large activities. Thus a 30-minute bombardment of a copper target by this beam produces an initial activity of about one millicurie and with the ionization chamber and d.c. amplifier this activity (38 min.) can be followed for about 16 half-lives.

I. RADIOACTIVE Cu FROM Ni TARGETS

Periods

Nickel bombarded with 6.3-Mev protons shows Cu activities with half-lives of 10.5±0.6 min., 3.4±0.3 hr., and 12.8±0.8 hr. (cf. Fig. 1). The 10.5-minute positron emitting activity has been shown by Heyn,[2] Bothe and Gentner[3] and Ridenour and Henderson[4] to be due to Cu^{62}. The 3.4-hour positron emitting activity has been shown by Ridenour and Henderson[4] to be due to Cu^{61}. Each of these could be formed either by a proton-neutron (p-n) reaction or by proton capture. The 12.8-hour period is known[5] to be assigned to Cu^{64} which can be formed only by the p-n reaction.

The absorption curves in aluminum of the positrons emitted by Cu^{62} and Cu^{61} show maximum positron energies[6] of 2.8±0.3 and 1.2±0.2 Mev respectively (cf. Figs. 2 and 3). Cu^{64} decays as a branch reaction,[5] emitting either a positron going to Ni^{64} or an electron going to Zn^{64}. Cloud-chamber photographs of the β-rays from an aged sample showed 210 electron tracks and 138 positron tracks giving a branching ratio of 1.5 electrons per positron, in agreement with VanVoorhis'[5] data. Absorption measurements (Fig. 3) show a maximum energy of 0.68±0.1 Mev, also in agreement with VanVoorhis' cloud-chamber data, which showed about the same energy for positrons and electrons.

Excitation curves

Thick target excitation data were obtained by bombarding identical targets for the same length of time with known proton currents, reducing the beam energy in steps by aluminum foils of known stopping power. The decay curves were followed

[1] L. A. DuBridge, S. W. Barnes, J. H. Buck and C. V. Strain, Phys. Rev. **53**, 447 (1938).
[2] F. A. Heyn, Nature **138**, 723 (1936).
[3] W. Bothe and W. Gentner, Naturwiss. **25**, 90 (1937).
[4] L. N. Ridenour and W. J. Henderson, Phys. Rev. **51**, 1102 (1937).
[5] S. N. VanVoorhis, Phys. Rev. **50**, 895 (1936).
[6] The relation obtained by E. E. Widdowson and F. C. Champion, Proc. Phys. Soc. **50**, 185–195 (1938), was used to obtain the maximum energies from the aluminum ranges of the beta-rays.

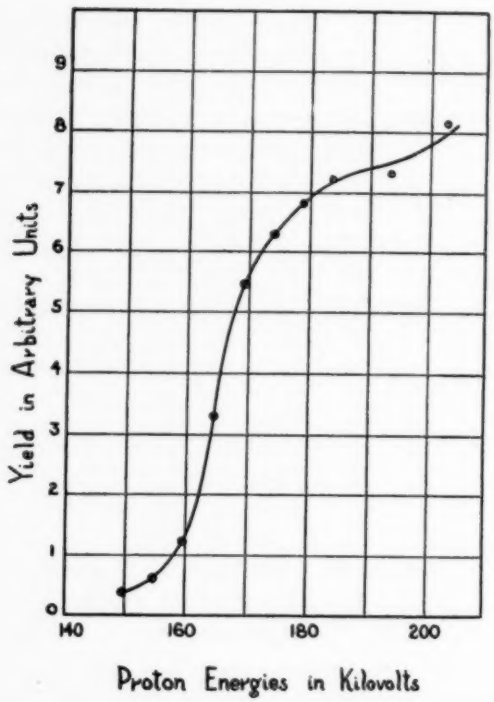

FIG. 3. The yield curve of alpha-particles from a thick target of boron under proton bombardment.

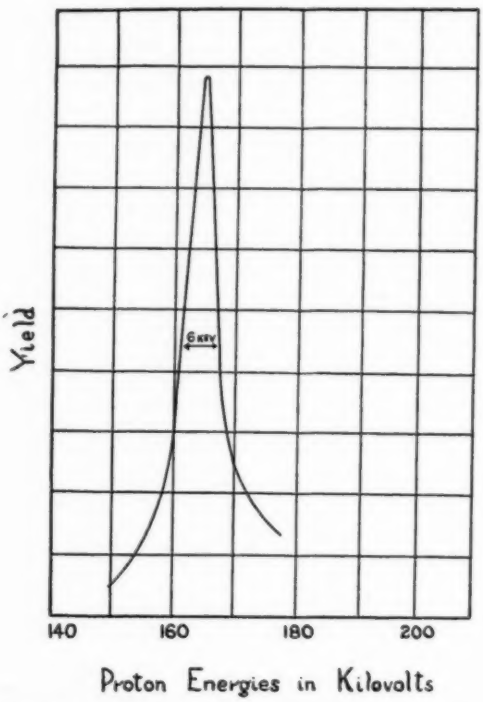

FIG. 4. The yield curve of alpha-particles to be expected from a thin boron target. This curve was obtained by differentiating the observed thick target curve (Fig. 3) with respect to the voltage to the three-halves power.

In this connection it should be pointed out that for the method to be valid, the input impedance of the amplifier-oscillograph combination must be large compared with the value of the auxiliary (10,000-ohm) resistor. Further, it is necessary to take into account the fact that the sectionalized construction of this type of voltmeter resistance introduces a considerable shunt capacitance, which results in exaggerating the ripple. The shunt capacitance was measured and calculation showed that it was sufficient to reduce the 60-cycle impedance of the circuit from a nominal value of 4.23×10^{9} ohms to 2.35×10^{9} ohms. After applying the necessary correction to the apparent peak value of the ripple at 165 kev a value of 3.6 percent, or 6 kev, was obtained. This is in good agreement with a value of 2.8 percent which was obtained when an alcohol-xylol high resistance was used instead of the voltmeter resistance, although this resistor was not entirely satisfactory.

Thus the *maximum* spread in the ion beam energy was about 12 kev, and since the ripple wave form was peaked in nature, the *effective* spread in the ion beam was undoubtedly considerably less. In any event, it appears that the observed half-breadth (6 kev) of the alpha-resonance process can be attributed entirely to instrumental causes.

The authors wish to thank Dr. C. B. Braestrup of the Bellevue Hospital Physical Laboratory for the loan of the wire-wound high resistance voltmeter and Mr. W. Turnbull of the machine shop for his suggestions and interest in the construction of the apparatus.

Proton Induced Radioactivities

II. Nickel and Copper Targets

CHARLES V. STRAIN
The University of Rochester, Rochester, New York

(Received October 14, 1938)

Nickel bombarded with 6.3-Mev protons shows activities of half-lives of 10.5±0.6 min., 3.4±0.3 hr., and 12.8±0.8 hr., corresponding to known periods of Cu^{62}, Cu^{61} and Cu^{64}, respectively. The reactions are principally of the p-n type but there is evidence that in the case of Cu^{62} proton capture occurs at energies below the p-n threshold. The maximum β-ray energies obtained by absorption method are 2.8, 1.2 and 0.68 Mev for Cu^{62}, Cu^{61} and Cu^{64}, respectively. Thick target excitation curves are given. Copper bombarded with 6.3-Mev protons shows two activities of half-lives 38.3±0.5 min. and 235±20 days due to Zn^{63} and Zn^{65}, respectively. Both must be formed by p-n reactions. The Zn^{63} positrons have a maximum energy of 2.3±0.15 Mev. Thick target excitation curve shows a threshold proton energy of 4.1±0.1 Mev in good agreement with the energy relations. Average (thick target) cross section for the $Cu^{63}(p,n)Zn^{63}$ reaction is 0.28×10^{-25} cm². For protons of energy 6.1 Mev it is 0.95×10^{-25} cm.

INTRODUCTION

THIS work is a continuation of the studies[1] being made in this laboratory of the nuclear reactions produced by high energy protons. The present paper summarizes the results obtained when targets of nickel and copper are bombarded by protons of energies up to 6.3 Mev accelerated in the cyclotron. The proton beam currents were of the order of 0.5μa which is sufficient to produce large activities. Thus a 30-minute bombardment of a copper target by this beam produces an initial activity of about one millicurie and with the ionization chamber and d.c. amplifier this activity (38 min.) can be followed for about 16 half-lives.

I. RADIOACTIVE CU FROM NI TARGETS

Periods

Nickel bombarded with 6.3-Mev protons shows Cu activities with half-lives of 10.5±0.6 min., 3.4±0.3 hr., and 12.8±0.8 hr. (cf. Fig. 1). The 10.5-minute positron emitting activity has been shown by Heyn,[2] Bothe and Gentner[3] and Ridenour and Henderson[4] to be due to Cu^{62}. The 3.4-hour positron emitting activity has been shown by Ridenour and Henderson[4] to be due to Cu^{61}. Each of these could be formed either by a proton-neutron (p-n) reaction or by proton capture. The 12.8-hour period is known[5] to be assigned to Cu^{64} which can be formed only by the p-n reaction.

The absorption curves in aluminum of the positrons emitted by Cu^{62} and Cu^{61} show maximum positron energies[6] of 2.8±0.3 and 1.2±0.2 Mev respectively (cf. Figs. 2 and 3). Cu^{64} decays as a branch reaction,[5] emitting either a positron going to Ni^{64} or an electron going to Zn^{64}. Cloud-chamber photographs of the β-rays from an aged sample showed 210 electron tracks and 138 positron tracks giving a branching ratio of 1.5 electrons per positron, in agreement with VanVoorhis'[5] data. Absorption measurements (Fig. 3) show a maximum energy of 0.68±0.1 Mev, also in agreement with VanVoorhis' cloud-chamber data, which showed about the same energy for positrons and electrons.

Excitation curves

Thick target excitation data were obtained by bombarding identical targets for the same length of time with known proton currents, reducing the beam energy in steps by aluminum foils of known stopping power. The decay curves were followed

[1] L. A. DuBridge, S. W. Barnes, J. H. Buck and C. V. Strain, Phys. Rev. 53, 447 (1938).
[2] F. A. Heyn, Nature 138, 723 (1936).
[3] W. Bothe and W. Gentner, Naturwiss. 25, 90 (1937).
[4] L. N. Ridenour and W. J. Henderson, Phys. Rev. 51, 1102 (1937).
[5] S. N. VanVoorhis, Phys. Rev. 50, 895 (1936).
[6] The relation obtained by E. E. Widdowson and F. C. Champion, Proc. Phys. Soc. 50, 185–195 (1938), was used to obtain the maximum energies from the aluminum ranges of the beta-rays.

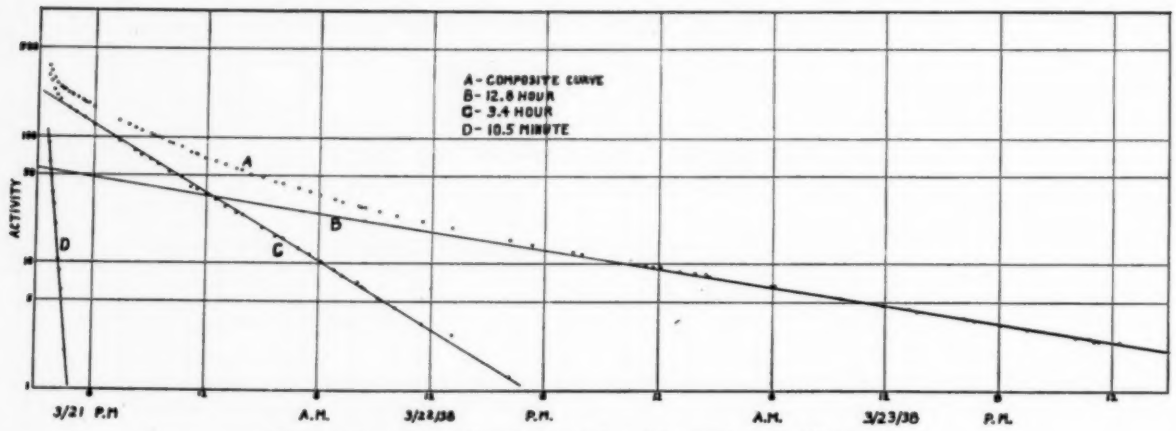

FIG. 1. Decay of radioactivity induced by protons in Ni targets.

to obtain the activity associated with each period. The initial activities corrected to infinite bombardment are shown as a function of proton energy in Fig. 4. Since Cu^{64} can be formed only by a proton-neutron reaction in this case the excitation curve is that for the single process, Ni^{64} $(p\text{-}n)$ Cu^{64}. The theoretical threshold[7] for this reaction is rather low (2.5 Mev). Some activity could be detected below three Mev but it was weak because of the low penetration factor and the low abundance of Ni^{64}. A consideration of the stable isotopes of nickel shows that both Cu^{61} and Cu^{62} might be formed by either a proton-neutron reaction or by simple proton capture. Although at sufficiently high energy the p-n reaction seems more probable, it is interesting to determine whether the capture process does occur. This can be done by determining whether Cu^{62} is formed below the p-n threshold. In the case of Cu^{62} the positron energy is 2.8 ± 0.3 Mev and hence the threshold[7] for the p-n reaction must be 4.6 ± 0.3 Mev. However, the excitation curve for this period (Fig. 4) shows activity at proton energies below three Mev. This must be ascribed either to the occurrence of proton capture or to contamination. Carbon impurity from which N^{13} (11.0-min. half-life) is formed is suggested and no other impurity of the correct half-life seems possible. The positron absorption curves, however, for samples activated at four Mev and at six Mev were the same within limits of error (Fig. 2), and showed no evidence of the much softer (1.25-Mev) positrons from N^{13}. It is evident then that the Cu^{61} $(p\text{-}\gamma)$ reaction is occurring at low energies, though the activity rises sharply above 4.6 Mev where the p-n reaction sets in. The cross section for capture at four Mev is approximately 0.7 percent of the total cross section at 6.3 Mev when corrected for isotopic abundance.

In the case of Cu^{61} the predicted threshold is 2.9 Mev (positron energy 1.1 Mev) and our data show no detectable activity below three Mev. However, White, Delsasso, Sherr and Ridenour[8]

[7] For a discussion of the energy relation see reference 1.

[8] M. G. White, L. A. Delsasso, Rubby Sherr and L. N. Ridenour, Phys. Rev. **54**, 314 (1938).

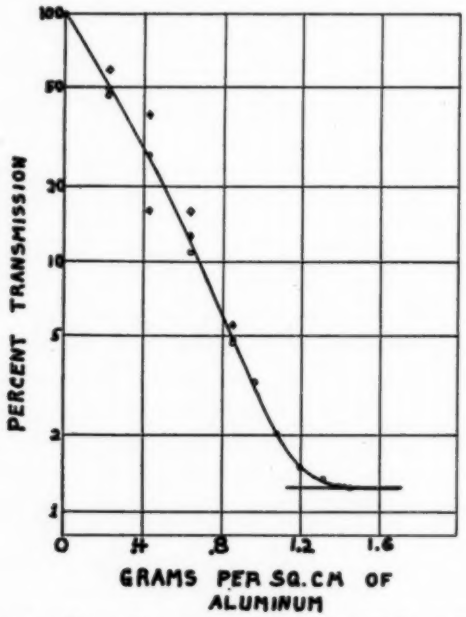

FIG. 2. Absorption curve in Al for Cu^{62} positrons. Circles are for nickel sample bombarded at 6.3 Mev. Squares are for nickel sample bombarded at 4.0 Mev.

find that Cu^{61} (3.4 hr.) is formed by protons of energy less than 1.9 Mev. However, they also report a low value (2.1 Mev) for the threshold of the $Ni^{64}(p\text{-}n)Cu^{64}$ reaction which has a computed threshold of 2.5 Mev, which is difficult to understand. However, even if one assumes that their energy values are 0.4 Mev low there is still evidence that proton capture is effective in forming Cu^{61}.

Cross section

The d.c. amplifier and ionization chamber were calibrated as follows. The deflection produced by one beta-particle per second traversing the chamber was computed from the depth of the chamber, the specific ionization of the particle and the measured current sensitivity of the amplifier. The effective solid angle subtended by the chamber was measured and the number of beta-particles per second, emitted in all directions, required to produce a centimeter deflection was computed. This ranged from 80 to 160 β/sec. depending upon the β-ray energy. This value was checked with a standard uranium source. With this calibration and with the value of the stopping power of nickel for protons computed from the data of Livingston and Bethe[9] the cross sections for the reactions for protons of energy between 0 and 6.3 Mev and also for energy between 6.0 and 6.3 Mev were computed. The results are given in Table I.

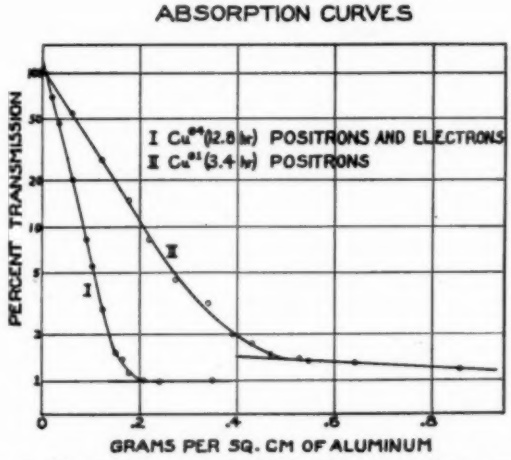
ABSORPTION CURVES
I Cu64(12.8 hr) POSITRONS AND ELECTRONS
II Cu61(3.4 hr) POSITRONS
PERCENT TRANSMISSION
GRAMS PER SQ. CM OF ALUMINUM

FIG. 3. Absorption curve in Al for Cu^{61} and Cu^{64} β-rays.

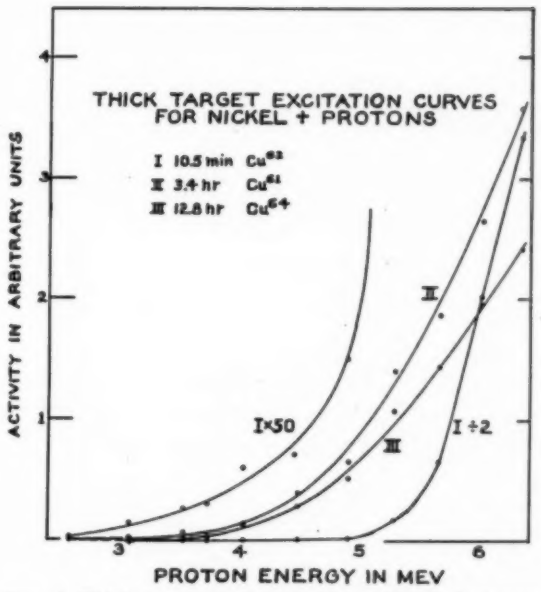

FIG. 4. Thick target excitation curves for Cu isotopes.

The value for Cu^{61} and Cu^{64} are uncertain since the isotopic abundances of Ni^{61} and Ni^{64} are not well known. Also it is assumed that proton capture plays a negligible role. Consequently the values for Cu^{61} and Cu^{62} may be high. Cu^{61} will be affected most since the isotopic abundance of Ni^{60} is approximately 30 times that of Ni^{61}.

Radioactive Zn Isotopes from Cu Targets

For short proton bombardments of copper a strong activity is observed with a half-life of

[9] M. S. Livingston and H. A. Bethe, Rev. Mod. Phys. 9, 261–272 (July, 1937).

TABLE I. *Proton induced radioactivities in* Cu *and* Zn.

Assumed Process	Half-life	Yield* Rad. atoms per 10^6 protons		Cross section† $\times 10^{26}$ cm^2	
		Obs.	for single isotope	Av.	6.3–6.0 Mev
$Ni^{61}(p\text{-}n)Cu^{61}$ (and $Ni^{60}(p\text{-}\gamma)Cu^{61}$)	3.4 hr.	0.48	29.	0.29	1.05
$Ni^{62}(p\text{-}n)Cu^{62}$ (and $Ni^{61}(p\text{-}\gamma)Cu^{62}$)	10.5 min.	1.11	30.	0.30	1.50
$Ni^{64}(p\text{-}n)Cu^{64}$	12.8 hr.	0.24	26.	0.26	0.78
$Cu^{63}(p\text{-}n)Cn^{63}$	38.3 min.	18.4	27.	0.28	0.95

* For a thick target at 6.3 Mev

† Assuming p-n reactions.

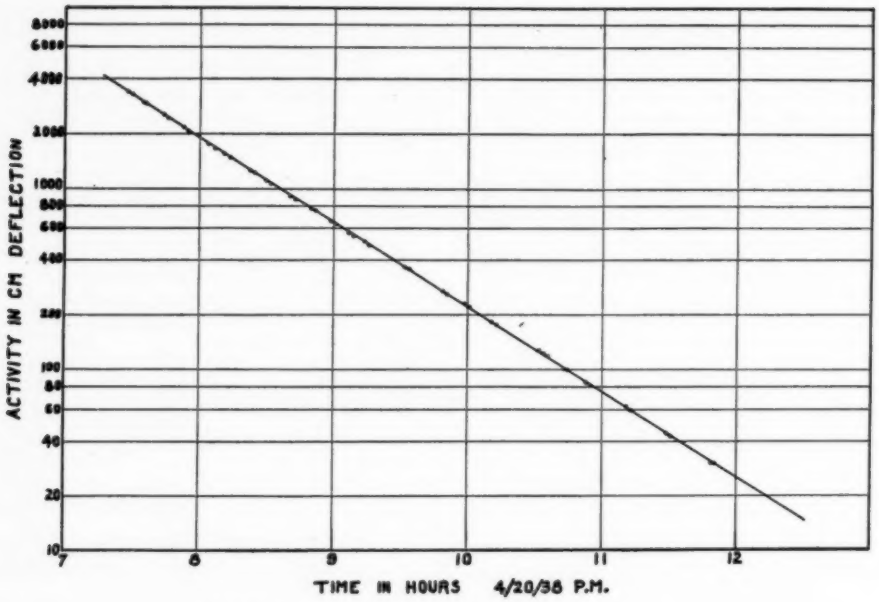

FIG. 5. Decay curve for Zn^{63}. Copper+protons.

38.3±0.5 min. (cf. Fig. 5). The absorption curve for the positrons emitted (cf. Fig. 6) show a maximum energy of 2.3±0.15 Mev. This activity has been shown by Pool, Cork and Thornton[10] and by Bothe and Gentner[11] to be due to either Zn^{63} or Zn^{65}. However, a long lived activity has since been definitely assigned to Zn^{65} and consequently the 38-minute activity can be assigned to Zn^{63}.

The thick target excitation curve is shown in Fig. 7. The samples showed no detectable contamination and only the Zn^{63} period is excited in short bombardments so that it was possible to fix the proton threshold energy at 4.1±0.1 Mev. This is in agreement with the computed threshold of 4.1±0.17 Mev. The cross section for this

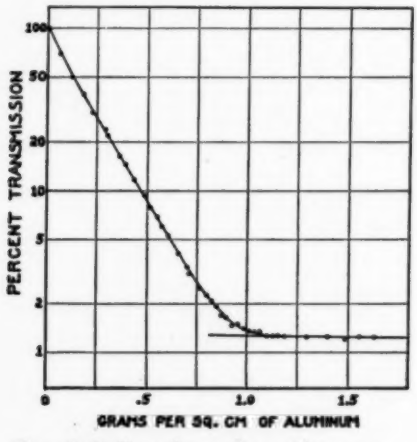

FIG. 6. Zn^{63} positron absorption curve.

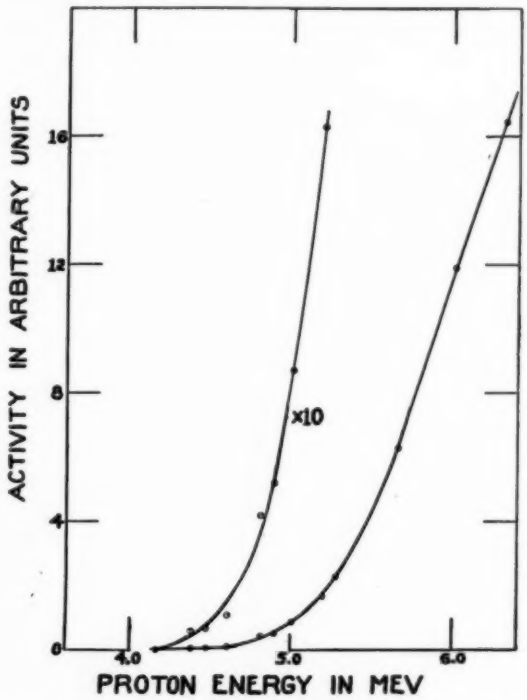

FIG. 7. Thick target excitation curve for $Cu^{63}(p\text{-}n)Zn^{63}$.

[10] M. L. Pool, J. M. Cork and R. L. Thornton, Phys. Rev. 52, 239 (1937).
[11] W. Bothe and W. Gentner, Naturwiss. 25, 191 (1937).

reaction for proton energies ranging from 6.0 to 6.3 Mev is 0.95×10^{-25} cm² (cf. Table I).

A long lived activity is observed in copper samples which have been subjected to long bombardments. The decay curve (cf. Fig. 8) shows a single half-life of 235±20 days. A cloud-chamber investigation made by Mr. George Valley[12] shows that the radioactive decay takes place either by positron emission of K electron capture. The negative electrons which are observed are identified as internal conversion electrons. This same activity has been obtained by bombarding zinc with deuterons[13] and consequently must be assigned to Zn^{65}.

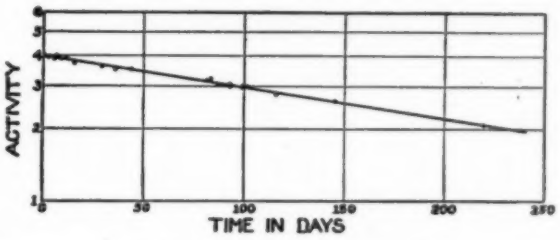

FIG. 8. Decay curve for Zn^{65}.

I wish to express my thanks to Professor L. A. DuBridge and Professor S. W. Barnes for advice given during the investigations, to Dr. J. H. Buck for help in bombarding samples and taking data, and to Mr. George Valley for the cloud-chamber photographs. The work has been supported in part by a grant from the Research Corporation.

[12] A preliminary report was made by S. W. Barnes and George Valley, Phys. Rev. **53**, 946 (1938). A more detailed report will be published soon.

[13] J. J. Livingood and G. T. Seaborg, Phys. Rev. **54**, 239 (1938).

DECEMBER 15, 1938 PHYSICAL REVIEW VOLUME 54

Proton Induced Radioactivities

III. Zinc and Selenium Targets

JOHN H. BUCK*
University of Rochester, Rochester, New York

(Received October 14, 1938)

Zinc bombarded with 6.5-Mev protons shows activities of half-lives 18.0±0.5 min., 72±4 min., 9.4±0.2 hr., and 84.4±2.0 hr., corresponding to the known periods of Ga^{70}, Ga^{68}, Ga^{66}, and Ga^{67}, respectively. In addition, a new period of 48±2-min. half-life is observed and assigned to Ga^{64}. Thick target excitation curves are given for Ga^{64}, Ga^{68}, and Ga.[70]. Selenium bombarded with 6.3-Mev protons shows activities of half-lives 6.3±0.2 min., 17.4±0.5 min., 4.4±0.3 hr., and 33±1 hr., corresponding to the known periods of Br^{78}, Br^{80} (2) and Br^{82}, respectively. The previously observed discrepancy between the thresholds for the two Br^{80} activities and their maximum β-ray energies has been confirmed. Thick and thin targets excitation curves were obtained. The cross section for the production of the Br^{80} isomers by the Se^{80} (p-n) reaction are 0.82 and 0.22×10^{-25} cm² for the short and long periods, respectively, at a proton energy of 6.3 Mev. The ratio of these two cross sections rises from 3.6 at 6.3 Mev to over 200 at 3.2 Mev.

INTRODUCTION

THIS work is a continuation of the studies[1] made in this laboratory of the nuclear reactions produced by high energy protons. The present paper concerns the results obtained when targets of zinc and selenium are bombarded by protons of energies up to 6.5 Mev. Results with these targets have already been reported[1] for proton energies up to 3.8 Mev. Much larger yields are obtained with the higher energy beam and additional periods are produced. Further studies of the excitation functions have therefore been made, particularly for the Br^{80} isomers produced from Se.

RADIOACTIVE Ga ISOTOPES FROM Zn

The complete decay curves for the radioactivity produced by 6.3-Mev protons in a pure

* Now at Massachusetts Institute of Technology, Cambridge, Massachusetts.

[1] DuBridge, Barnes, Buck and Strain, Phys. Rev. **53**, 447 (1938).

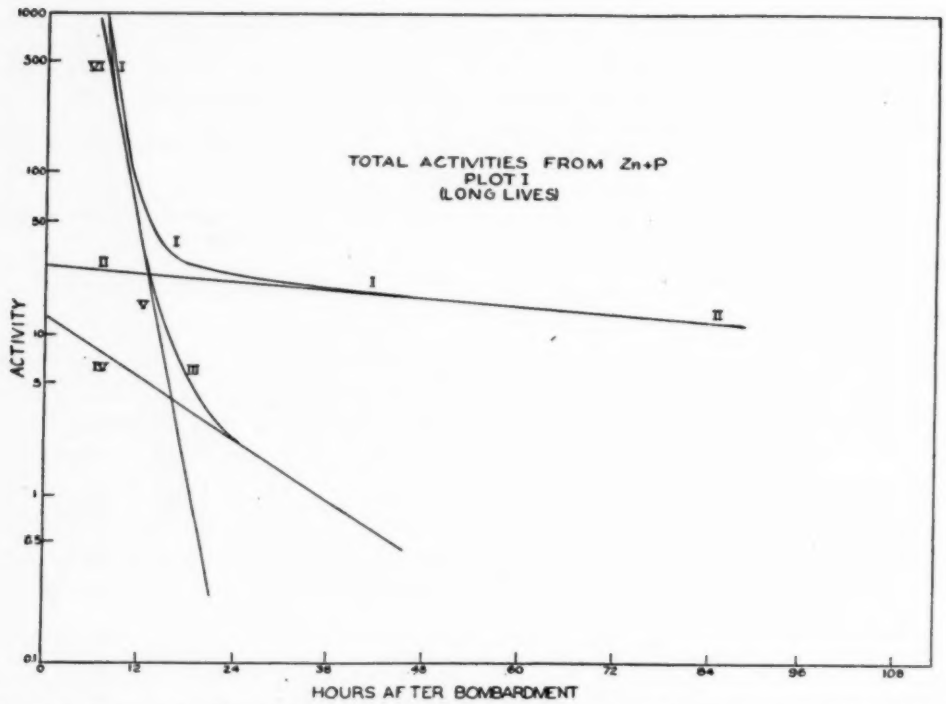

FIG. 1A. Decay of radioactivity of Zn target (long periods). I. Composite curve; II. 84.2-hr. activity; IV. 9.4-hr. activity; VI. 72-min. activity.

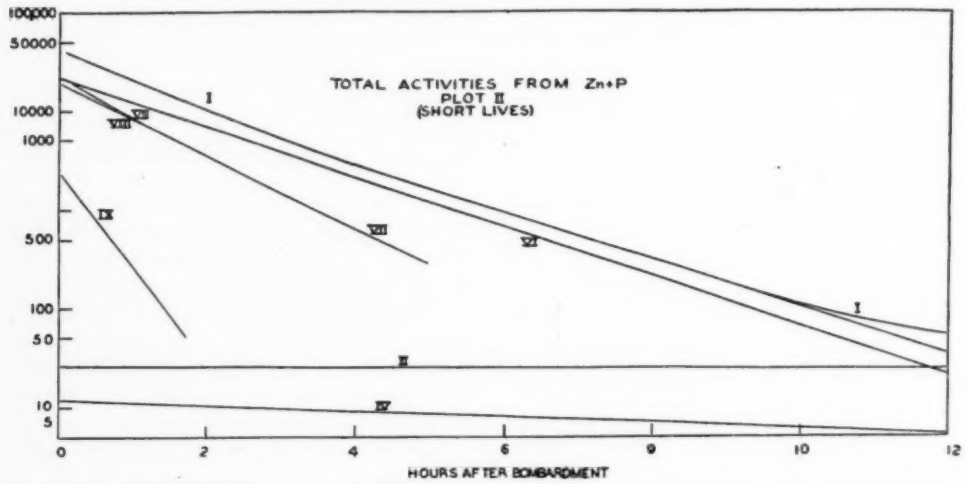

FIG. 1B. (Short periods.) VIII. 48-min. activity; IX. 18-min. activity.

Zn target are shown in Fig. 1. The curves are at once analyzed into five half-lives, all of which are found to occur only in Ga precipitates. The periods and the corresponding isotope assignments are listed in Table I.

The Ga^{68} and Ga^{70} periods were previously reported.[1, 2] The 84-hr. period was also reported but was too weak to be chemically identified. Later tests showed definitely that this was due to a Ga isotope. In the meantime Mann[3] found the same period in the Ga precipitate from Zn bombarded by alpha-particles, and assigned the activity to Ga^{67}. Alvarez[4] has shown this to be

[2] Livingston and Bethe, Rev. Mod. Phys. 9, 245 (1937).

[3] Mann, Phys. Rev. 53, 212 (1938).
[4] Alvarez, Phys. Rev. 53, 606 (1938).

an isotope which decays by capture of a K electron, the soft electrons emitted being K and L conversion electrons from a 100-kv gamma-ray emitted in the process. These results and the assignment to Ga^{67} are consistent with our observations.

The 48-min. and 9.4-hr. periods are not formed at energies below about 4 Mev. The latter has been identified as due to Ga^{66} by Ridenour and Henderson.[5] The former period is new. If it were isomeric with any of the others it should certainly have been observed in previous work. We therefore assign it to Ga^{64} produced from the abundant Zn^{64} by p-n reaction. This isotope cannot be formed by any other known type of process. If this assignment is correct then all of the five Zn isotopes have been converted to corresponding Ga isotopes by the proton beam. It is probable that the p-n reaction is responsible in each case since results in this laboratory show that p-γ reactions for elements in this range are improbable.

Thick target excitation curves for Ga^{64}, Ga^{68} and Ga^{70} are given in Fig. 2 showing thresholds of 4.1, 3.7 and 1.6 Mev, respectively. Excitation curves were not obtained for Ga^{66} or Ga^{67} because of the long bombardments required. However, the Ga^{67} activity (84.2 hr.) was detectable at energies below 3.5 Mev while the Ga^{66} activity was found only above 4.1 Mev.

Br Isotopes from Se

The complete decay curve for the activity of a Se target bombarded by protons is shown in Fig. 3. Chemical tests show all the activity to be due to Br isotopes. All the periods have been previously reported[1] and identified and are formed by the p-n reaction. The results are summarized in Table II.

TABLE I. *Radioactive* Ga *isotopes from* Zn.

Isotope	Period	Emitted Particle	Max. Energy Mev	Proton Threshold Mev	Yield* Rad. atoms per 10^6 protons
Ga^{64}	48±2 min.	+	(2.3)**	4.1	5.0
Ga^{66}	9.4±0.2 hr.	+	(>2.3)**	>4.1	1.1
Ga^{67}	84.4±2.0 hr.	−(K)		<3.5	—
Ga^{68}	72±4 min.	+	1.85	3.7	61.0
Ga^{70}	18±.5 min.	−		~1.6	64.0

* At 6.5 Mev for a thick target of the pure Zn isotope.
** Computed from the threshold.

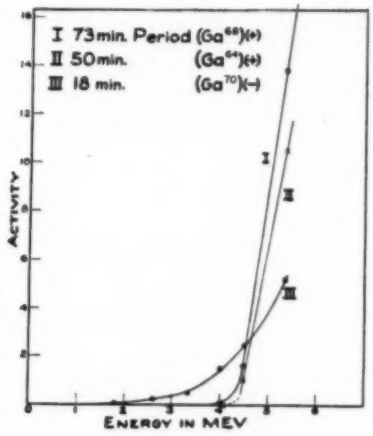

FIG. 2. Thick target excitation curves for zinc target.

The formation of the isomeric Br^{80} periods from Se^{80} is of particular interest. As was previously pointed out[1] Snell's[6] data on the β-ray energies for these two periods appear inconsistent with our threshold determinations. Thus Snell finds the 17.4-min. electron group to have a maximum energy of 2.2 Mev while for the 4.4-hr. group it is 2.0 Mev. In addition he found a soft gamma-ray (~0.4 Mev) accompanying the short period. This would indicate that the 17.4-min. isomer of the Br^{80} nucleus has an energy about 0.6 Mev above that of the 4.4-hr. isomer. Hence the long period would be expected to appear at lower proton energies. On the other hand, we found the threshold for the longer period to be *above* that of the shorter period by about 0.2 Mev.

More accurate and complete data on the excitation of all four Br activities have now been obtained and are plotted in Fig. 4. Curves I and II are for the two periods of Br^{80} and it is evident that the short period becomes observable at a proton energy of 2.9 Mev while the longer period first comes in at 3.1 Mev. The ratio of the observed activities (after 10 min. bombardments) is also plotted and rises from about 78 at 5.3 Mev to 2000 at 3.2 Mev. For an infinite bombardment the ratios would be 6.7 at 5.3 Mev and 182 at 3.2 Mev. A 5-hour bombardment at 3.0 Mev yielded no trace (i.e., < 1 mm) of the 4.4-hr. period but there was an initial

[5] Ridenour and Henderson, Phys. Rev. **52**, 869 (1937).

[6] Snell, Phys. Rev. **52**, 1007 (1937).

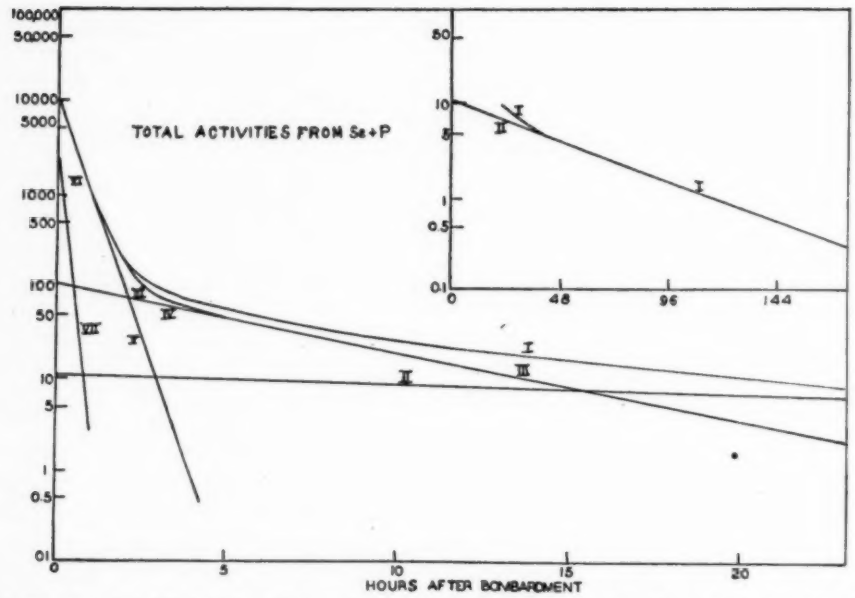

FIG. 3. Decay of radioactivity of Se target. I. Composite curve; II. 33-hr. activity; IV. 4.4-hr. activity; V. 17.4-min. activity; VII. 6.3-min. activity. (10-min. bombardment.)

activity of 20-cm deflection for the 17.4-min. period. There is thus no question but that the short period becomes observable at energies below those at which the long period can be detected.

The maximum β-ray energies of the isomeric activities have also been redetermined both by absorption in aluminum and from cloud chamber data. The absorption data gave 2.2 Mev and 2.0 Mev for these activities in exact agreement with Snell's values. The histograms for the distribution in curvature of cloud chamber tracks are shown in Fig. 5. The upper limits are at about 2.07 and 1.94 Mev for the short and long periods, respectively, in good agreement with the absorption data.

Snell has reported gamma-radiation with the 17.4-min. period but none with the 4.4-hr. period. In order to test this result a gamma-ray activity curve was taken for a sample of selenium bombarded for about 1 hour with 6.3-Mev protons. About 7 mm of Al was placed between the sample and ionization chamber to absorb all β-rays. The resulting decay curve for the gamma-rays only is shown in Fig. 6. It is evident that the 4.4-hr. period is represented so that penetrating radiation accompanies this activity. In view of Snell's work this radiation is certainly softer than the 17.4-min. gamma-rays, so that one is still forced to conclude that the short period level of Br^{80} lies 0.2 to 0.6 Mev above the long period. The threshold for the long period would be expected then to lie this much lower than for the short period.

A possible explanation for this apparent discrepancy has been suggested by Dr. M. Goldhaber.[7] It is necessary to assume in accounting

[7] Goldhaber, private communication.

TABLE II. Br *isotopes from* Se.

ISOTOPE	PERIOD	EMITTED PARTICLE	MAX. ENERGY MEV	PROTON THRESHOLD MEV	YIELD* (RAD. ATOMS PER 10^6 PROTONS)	CROSS SECTION AT 6.3 MEV $\times 10^{25}$ CM^2
Br^{78}	6.3±0.2 min.	+	2.3	4.1	1.4	
Br^{80}	17.4±0.5 min.	−	2.2	2.9	5.5	0.82
Br^{80}	4.4±0.3 hr.	−	2.0	3.1	0.82	0.23
Br^{82}	33±1 hr.	−	0.7	<3.5	2.6	

* At 5.3 Mev for a thick target of the pure isotope.

for nuclear isomers that the two states of the nucleus have a large spin difference which forbids gamma-ray transitions. If one assumes the long period isomer to have a spin of, say, six units, then neutrons of high angular momentum will have to be emitted in the $(p\text{-}n)$ reaction forming this isomer. This would make the reaction improbable near the threshold where the neutron energies are small and their wave-lengths large compared with nuclear dimensions. The formation of the long lived isomer will therefore not be probable until comparatively fast neutrons can be emitted. On the other hand, if the spin of the short lived isomer is zero, it will start being formed as soon as its threshold energy is reached. Thus the threshold of the 4.4-hr. activity may actually be lower than the 17.4-min. activity, but owing to the very low probability of formation no activity is detectable until the proton energy has been raised considerably above the threshold.

Cross Section for Br^{80} Reactions

To obtain data on the thin film excitation and the cross section of these reactions thin targets

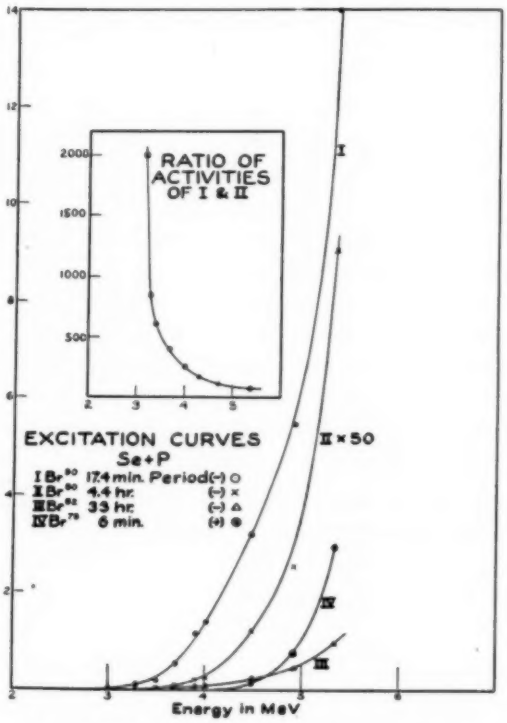
RATIO OF ACTIVITIES OF I & II
EXCITATION CURVES
Se+P
I Br80 17.4 min. Period(-) ○
II Br80 4.4 hr. (-) ×
III Br82 33 hr. (-) △
IV Br75 6 min. (+) ●
II×50
Energy in MeV

Fig. 4. Thick target excitation curves for Se (10-min. bombardment).

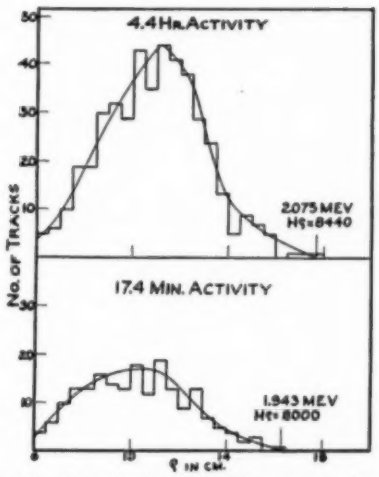

Fig. 5. Distribution of cloud chamber tracks for electrons from Br^{80}.

of Se were made by evaporating a film of selenium on 0.1-mil Al foil. From the center of the evaporated sheet ten small targets were cut and mounted. The thickness of the Se film was found by placing the ten targets in the proton beam and comparing the resulting reduction in range with that produced by Al foils alone. By this method the thickness of the Se film was computed to be 0.04 mil or 0.46 mg/cm².

During bombardment the ten foils were "stacked," and separated by sufficient Al foil to reduce the energy of the proton beam in steps of approximately 0.25 Mev.

A 3-minute bombardment at 0.12μa was sufficient to bring out the 17.4-min. period at energies down to 3.5 Mev and the 4.4-hr. period down to 4.5 Mev. Longer bombardments were prevented by heating of the front foils and evaporation of the selenium.

The activity of each Se film was followed for several hours and the initial activity due to each period determined from the decay curves. These activities, corrected to infinite bombardment, are plotted against the proton energy in Fig. 7. From the calibration of the ionization chamber and the measured thickness of the foils the cross section for the production of the 17.4-min. isomer for a 6.3-Mev proton beam was found to be 0.82×10^{-25} cm² and for the 4.4-hr. isomer 0.22×10^{-25} cm². The ratio of the two cross sections is 3.60. The ratio rises slowly with decreasing energy to 4.31 at 4.8 Mev. The above values might be in error by a factor of 2.

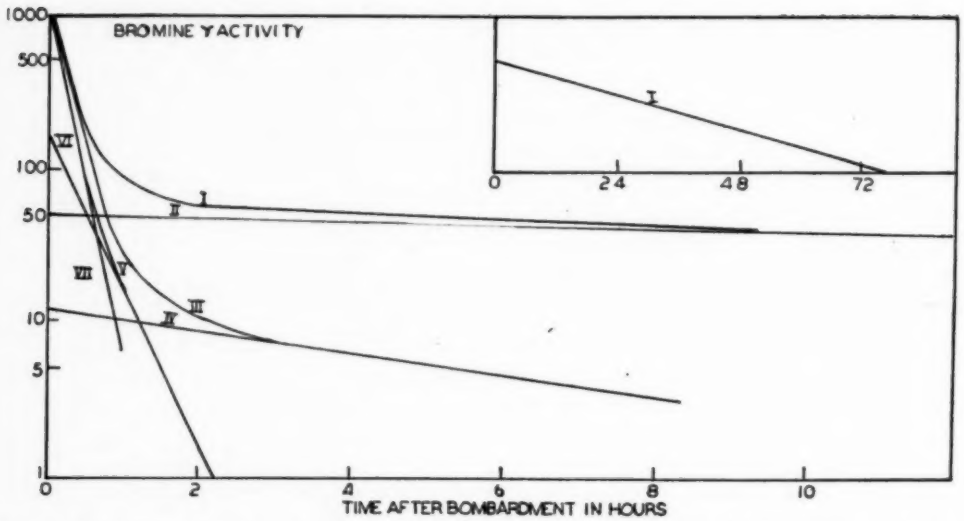

FIG. 6. Gamma-activity from Se+p. I. Composite curve; II. 33-hr. activity; IV. 4.4-hr. activity; V. 17.4-min. activity; VII. 6.3-min. activity.

This larger cross section for the short lived isomer also presents a problem if the above remarks on the spin values of two isomers are accepted. If the more stable isomer has a spin value six and the less stable isomer a spin zero, then the statistical weight of the former would exceed the latter in the ratio $(2I+1)$ or 13. The cross section for formation of the long period at high energies should then be greater than for the short period in this ratio. The evidence is, however, that as higher energies are reached the cross section ratio approaches the value of about 3 in favor of the *short* period. Obviously a simple statistical argument based on current nuclear models fails to account for these results.

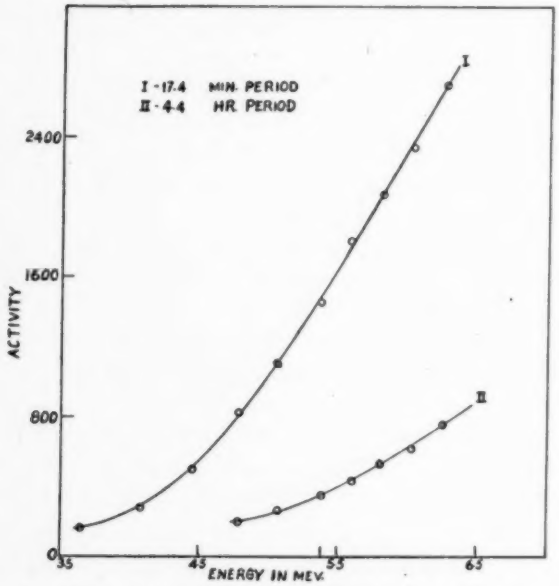

FIG. 7. Thin film excitation curves for Br^{80} periods (infinite bombardment).

In conclusion I wish to express appreciation to Professor L. A. DuBridge and Dr. S. W. Barnes for their continued interest and advice during the course of the work. I am also much indebted to Professor E. O. Wiig of the Chemistry Department who performed the chemical analyses necessary, to Dr. C. V. Strain and to Mr. George Valley for their assistance in taking the data. The work has been supported in part by a grant from the Research Corporation.

Internal Targets in the Cyclotron

ROBERT R. WILSON AND MARTIN D. KAMEN
Radiation Laboratory, Department of Physics, University of California, Berkeley, California
(Received October 3, 1938)

The large circulating ion current in the cyclotron which ordinarily does not reach the target chamber has been utilized in the preparation in high concentration of extremely active samples of radio-iron and radiophosphorus. By adapting as internal target the probes used in demonstrating the presence of the circulating current, it has been possible to enhance greatly the yields of radioactive materials as compared with those obtained in the usual manner at the target chamber. The construction of the probe, the nature of the circulating current and the manner in which the target material is applied to the probe are discussed. The general applications of the internal target technique are indicated.

INTRODUCTION

IT IS customary in atomic bombardments with the cyclotron to draw the ion currents into a target chamber by means of a suitable deflector arrangement. As recently shown,[1] the ion beams obtained in this manner represent only a small fraction of the ion currents circulating in the vacuum chamber proper. By the insertion of probes, it is possible to demonstrate the presence of many hundreds of microamperes of high energy ions whereas the ion beams emergent in the target chamber are smaller by an order of magnitude. Indeed, one may install several probes, used as internal targets, all of which are effective simultaneously in intercepting some of this large current without seriously altering the intensity of the beam in the target chamber. While the activations possible with the ion beams in the target chamber are sufficient for most purposes, there has arisen recently the need for extremely powerful samples of radioactive phosphorus and iron. Accordingly, we have investigated bombardment techniques based on the presence of the large circulating currents which ordinarily are not utilized. This investigation has disclosed a technique which has proven very successful in resolving many problems connected with the preparation of very active samples of radioactive phosphorus and iron and which should be quite general in application.

CONSTRUCTION OF PROBES

Although the details of construction of probes must necessarily vary from one cyclotron to another, a description of the particular probes used by us may be of some interest. At Berkeley the diametral edges of the accelerating electrodes, or dees, run from north to south, and probes can be introduced directly into the region between dees through windows located at the extreme north and south ends of the cyclotron vacuum chamber. Fig. 1 illustrates the south probe which consists essentially of a piece of copper tubing *aa* bent as shown. This provides support and water cooling for the end of the probe *b* which is subjected to the large ion bombardment. The end is covered by a copper jacket, hard-soldered in place, to which various target materials can be applied. It should be pointed out that it is necessary to use hard solder in any part of the probe exposed to the large ion beam or to the high radiofrequency field. Soft solder because of its poor heat and electrical conductivity as well as its low fusion temperature usually melts at exposed surfaces and causes arcing. The jog in the tubing *c* is so placed because otherwise the deflected beam which comes past this region would be intercepted.

A novel feature is the sliding vacuum seal *d* by means of which the probe is moved in and out. This consists of a piece of brass tubing *e* encasing the copper tubing. A hole of diameter about $\frac{3}{4}$ that of the brass tube is cut in the center of a circular piece of Duprene rubber. Upon being stretched around the brass tubing, the rubber is distorted near the tubing and is bent out as shown, *f*. This is then clamped between the two pieces of brass *g* so cut as to maintain the bend in the rubber outward from the vacuum. Thus

[1] Wilson, Phys. Rev. **54**, 240 (1938).

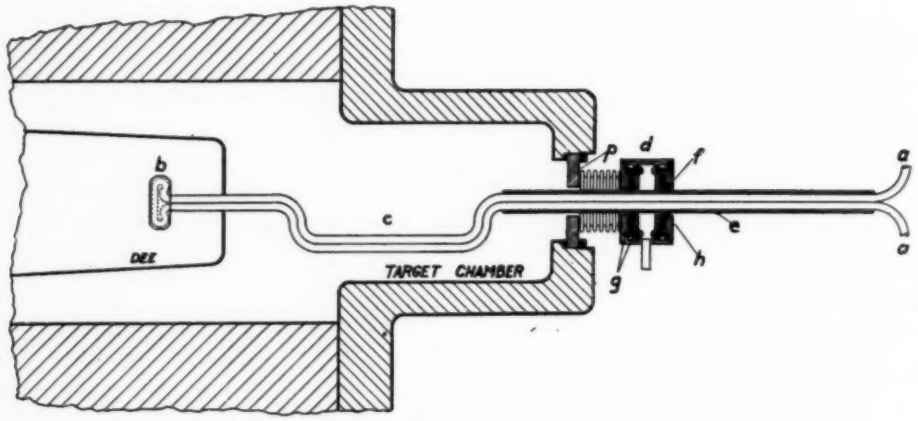

FIG. 1. The south probe.

the air forces the rubber against the tubing and so makes the seal. It is not necessary that the tubing be particularly straight, uniform, or scratch free for a good seal. A very small amount of stopcock grease on the tubing serves for lubrication. A second seal *h* is placed as shown behind the first seal and an airtight region left between the two. This provides for a means of evacuation behind the first seal in the event of a small leak. However, thus far this has proved unnecessary as the first seal acting alone holds even lower pressures than those used in the cyclotron. The probe can be moved in and out rapidly without disturbing the vacuum. Such a seal should find universal application wherever high speed pumping systems are employed, as it provides unlimited translational and rotational movements.

A sylphon connection between the sliding seal and the circular metal plate *p* which fits in place of a glass window provides for vertical motion of the end of the probe. The probe can be clamped at any position by means of a system of brass joints, clamps, and screw adjustments not shown in the diagram. The north probe is similar to the south probe, but there is no need for the jog in the copper tubing. A small spirit level is mounted on the outside of each probe in order to keep the target end vertical so as not to touch a dee.

At present, air must be let into the cyclotron chamber when a probe is installed. This could be avoided by an arrangement whereby the probe would first be installed in a small receptacle which could be roughly evacuated after installation and which could be connected to the cyclotron chamber by a vacuum gate. However, as the probe bombardments of the materials being activated at present extend over a period of several days each, no serious inconvenience is now caused by letting air into the cyclotron.

THE CIRCULATING CURRENT

There are several methods of estimating the current of high energy ions striking the probe. The current can be measured directly by insulating the probe and filtering off the large radio-frequency current also picked up; the heating of the cooling water can be measured; or a rough estimate can be obtained from the activity induced in a substance whose radioactive yield is known. The first method has the disadvantages that low energy ions can be picked up and secondary emission can occur. In the second and third methods one must assume a value of the average energy of the ions. All three ways have been used here with consistent results, but the second, of measuring the water heating, is found to be the most convenient, and probably the most reliable. If Δt is the temperature rise of the water, F is its rate of flow, and V is the average energy of the incident ions in megavolts, then the current to the probe in microamperes is given by:

$$i = 4.18(F\Delta t/V).$$

The correct value of V to be used in the equation is uncertain because the ions do not all originate at the same place and because of wandering of ion paths due to inhomogeneities in the magnetic

field. If for simplicity one assumes that the ions originate at the center and do not wander, the voltage will depend on the position of the probe as the square of the distance of the probe from the center. The values so assumed do not differ greatly from those obtained by dividing the product of V and i obtained from the heating measurement by the value of i obtained directly. Fig. 2 shows the current to the probe as measured by the heating plotted against the distance of the end of the probe from the center. As the probe is moved in from the edge of the dee, the current to it increases almost linearly with the distance for about the first ten centimeters, while the beam current decreases proportionally. When the beam current has been completely cut off, the current to the probe still increases, but not as rapidly as before. The manner in which the current increases as r becomes smaller can be ascribed to several causes: The ions do not originate at the same place; the ion paths wander because of magnetic field inhomogeneities; and ions are lost at lower energies by getting out of phase with the voltage.[2] Probably the most important of these is that the ions do not originate at the same place. This is so because of the length of the filament (about five cm) and because the electrons which form the ions can execute cycloidal motion in the crossed electric and magnetic field and wander several centimeters parallel to the gap between the dees—thus extending the region of ionization to about ten cm as the data indicate. Fig. 3 is also consistent with the occurrence of such a process. Here the current to two probes is shown; the north probe is fixed about five cm in from the north edge of the dee, and the current to each probe is plotted against the position of the south probe as the south probe is moved in. There is no shadow effect from the north probe, but as the south probe is moved in, it gradually robs the other probe of its current—taking most of it after being moved in ten or twelve centimeters.

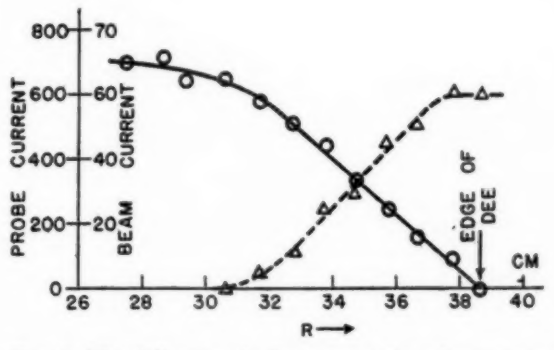

FIG. 2. The full curve is the current, in microamperes, to the south probe plotted against r, the distance of the end of the probe from the center of the cyclotron. The dotted curve represents the current, also in microamperes, that comes through the deflecting system to the target chamber plotted against r.

[2] Rose, Phys. Rev. 53, 392 (1938).

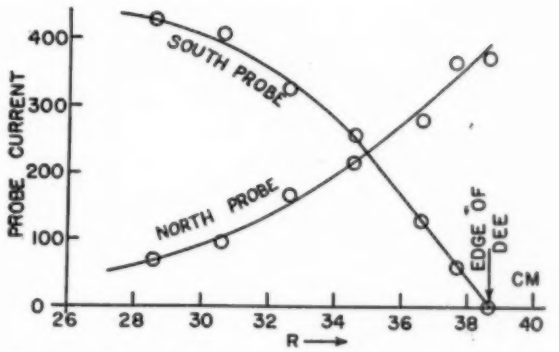

FIG. 3. The north probe is fixed in a position about 5 cm in from the periphery of a dee. The south probe is moved toward the center and the current in microamperes to each probe is plotted against the position of the end of the south probe.

The distribution of the beam falling upon the probe when it is located near the edge of a dee is shown in Figs. 4 and 5. These were obtained by passing the copper probe in front of a lead slit behind which was located an electroscope. Fig. 4 shows the vertical distribution, observed by placing the slit perpendicular to the leading edge of the probe. Because of the strong magnetic focusing most of the beam is confined within less than a centimeter. To obtain Fig. 5 which shows the horizontal distribution of ions on the probe, the slit was placed parallel to the edge. It is seen that the beam is spread over about one cm of the probe horizontally, whereas one would expect that it would spread over a distance corresponding to the change in radius of path an ion receives in being accelerated by twice the maximum voltage between dees. This turns out to be only about half of the observed spread, but numerical and graphical calculations show that the spreading out is just about what would be caused by the widening of successive paths because of the radially inhomogeneous magnetic field as sug-

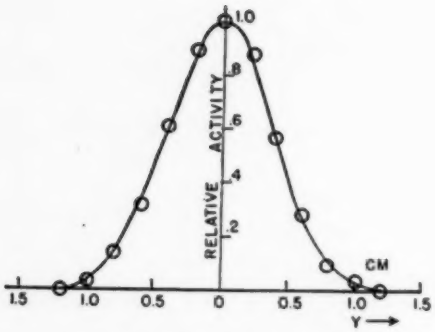

FIG. 4. The vertical distribution of the beam on the probe.

gested by Lawrence and Cooksey.[3] The maximum current to the probe as measured by the water-heating occurs at a slightly lower magnetic field strength than does the maximum of the beam current at the target chamber.

PRODUCTION OF RADIOACTIVE ISOTOPES BY PROBE BOMBARDMENT

The advantages inherent in probe bombardment when feasible are well exemplified in the two cases we have studied, radiophosphorus and radio-iron. These substances are produced by the deuteron bombardment of phosphorus and iron[4] according to the reactions

$$_{15}P^{31}+{}_{1}H^{2}={}_{15}P^{32}+{}_{1}H^{1},$$
$$_{26}Fe^{58}+{}_{1}H^{2}={}_{26}Fe^{59}+{}_{1}H^{1}.$$

A high energy beam (8 Mev) is necessary to produce the radio-iron (Fe^{59}) in appreciable quantities while the phosphorus reaction reaches good yields at 5.5 Mev. At present, the Berkeley cyclotron produces an 8-Mev beam, the intensity of which varies between 50 and 70 microamperes as measured at the target chamber. The activity required in phosphorus is of the order of 20 millicuries. To avoid serious limitations in therapeutic applications, the activity must be obtained with as little bulk of inactive material as possible (i.e., a high ratio of P^{32} to P^{31}).

To realize these yields with a 60-microampere beam at the target chamber, it is necessary to bombard the element itself as red phosphorus. An elaborate arrangement which has been found best consists of a knurled, water-cooled copper plate mounted with gaskets in an atmosphere of helium behind the thin aluminum window (5 cm in air equivalent stopping power) through which the beam emerges.[5] The phosphorus is pressed into the knurled grooves to a depth equal to the effective beam range in phosphorus and is then covered with thin gold-beaters foil (about 2 mm air equivalent stopping power). Thus, the phosphorus is in good thermal contact with a large, well-cooled surface. In this manner, it is found that thirty-five microampere-hours of bombardment at 8 Mev will yield one millicurie of activity. Hence 700 microampere-hours are required under these conditions to produce phosphorus samples strong enough for use in therapy. Moreover, since the effective portion of the beam is diffused over an area of approximately 10 cm^2, 1500–2000 milligrams of phosphorus are required to utilize the beam most effectively. Thus, one millicurie of activity is obtained for each 100 milligrams under the best conditions. For many purposes, it is desirable to obtain one millicurie per milligram of phosphorus. It can be appreciated readily that such a concentration of activity is far beyond the range of the target chamber bombardment.

In the case of iron, the problem is the production of enough activity even for "tracer" work. Because of the extreme rarity of Fe^{58}, the yield of Fe^{59} is extremely low, the best yields averaging one microcurie for 100 microampere-hours. Here again, a small bulk of material is required. It has been customary to bombard the iron simultaneously with the phosphorus by using an iron window (8 cm air equivalent stopping power) in place of the aluminum window. Unfortunately, it is quite difficult to prepare iron windows of this thinness completely hole-free, and those which are made do not last sufficiently long to produce strong iron samples. Moreover, the fact that only 8 cm of beam range is taken up in the iron reduces the activation by a factor of two.

All of these difficulties may be easily resolved by bombardment of ferrous phosphide on the probe. Ferrous phosphide as obtained from the City Chemical Corporation of New York is an easily-powdered, infusible mineral (melting point

[3] Lawrence and Cooksey, Phys. Rev. **50**, 1131 (1936).
[4] Newson, Phys. Rev. **51**, 624 (1937). Livingood, Fairbrother and Seaborg, Phys. Rev. **52**, 135 (1937). Livingood and Seaborg, Phys. Rev. **54**, 51 (1938).
[5] The final design of this chamber is due to Dr. F. N. D. Kurie, whose article is to appear shortly in the *Review of Scientific Instruments*.

about 1300°C) containing approximately 25 percent of phosphorus by weight. We have found that this material may be mounted satisfactorily in the following manner: A thin copper strip (2 cm ×1 cm) is tinned with "phos-copper," a hard solder alloy of copper and phosphorus. The copper is then placed on the part of the probe to be exposed and heated from below until the solder is molten. The ferrous phosphide powder is then sprinkled over the molten solder. On cooling, the mass is tamped free of excess phosphide. The residue on the surface represents about 100 milligrams of ferrous phosphide and is unusually hard and infusible. A surface of ferrous phosphide prepared in this way has withstood thousands of microampere-hours bombardment without the least deterioration. Tests have shown that the phosphide may be melted with an oxygen torch in air without noticeable decomposition. The presence of the phosphide in the vacuum chamber is not productive of gasiness and consequent unsteady operation.

The probe, having been prepared in this manner, is placed in position and adjusted. The adjustment is best described by reference to Fig. 2, an examination of which will indicate that 60–80 microamperes of current can be picked up on the probe without affecting the current at the target chamber. The final position of the probe will be governed both by the amount of current desired at the target chamber and the heating the target material on the probe can withstand safely. In the case of the phosphide, we have found that exposure to currents of 400 microamperes for several hours can be tolerated without serious deterioration. The procedure we consider best, however, is to insert the probe until it is taking out about 10 percent of the beam at the target chamber. Under these conditions the probe current as measured by the heating will vary between 150 and 200 microamperes. The length of time the probe is left in will vary from sample to sample depending on the half-life, yield desired, etc.

The chemical separation of iron and phosphorus from the other probe materials may be accomplished in a variety of ways depending on the final form in which the iron and phosphorus are desired. The following procedure may be recommended. The copper strip with its phosphide coating is dissolved in aqua regia with subsequent evaporation to dryness in excess HCl. The residue is then taken up in dilute HCl and the sulfides of copper and other heavy metals precipitated with H_2S. The filtrate is evaporated and the residue dissolved in a small amount of 6*N* HCl. The iron is extracted as iron chloride with ether saturated with 6*N* HCl.[6] The aqueous layer contains the phosphorus, cobalt and manganese as well as some nickel and zinc activities. The cobalt, manganese, nickel and zinc are present in microscopic quantities and it is advisable to add a minute amount of cobalt or manganese salts at this point to insure carriers for the cobalt and manganese activities. The solution should be evaporated, taken up in dilute nitric acid and the phosphorus precipitated several times as the phosphomolybdate. An alternative procedure consists in neutralizing the aqueous layer from the ether extraction with sodium hydroxide, the various "contaminants" such as cobalt and manganese then precipitating as phosphates. The amount of phosphorus lost in this way is negligible if the amount of cobalt added early in the procedure is very small. The phosphomolybdate precipitation is effective in recovering the phosphorus free of contaminants, but must be converted to sodium phosphate for use. This may best be accomplished by dissolving the phosphomolybdate in ammonia and precipitating the phosphorus as magnesium ammonium phosphate. The precipitate may be weighed and the calculated amount of NaOH added, the solution then being boiled until the ammonia no longer comes off. The solution is

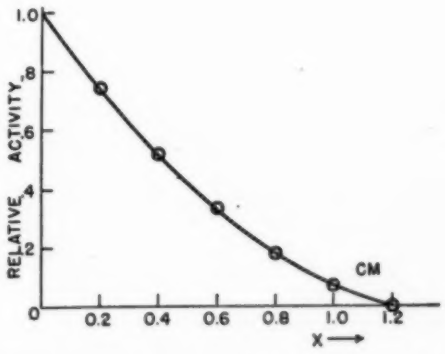

FIG. 5. The horizontal distribution of the beam on the probe.

[6] Noyes and Bray, *Qualitative Analysis for Rare Elements* (Macmillan, 1927), p. 160 *et seq.*

filtered from the magnesium hydroxide and contains the main portion of the phosphorus activity. The iron as extracted with ether must be washed with 6*N* HCl saturated with ether many times to ensure absence of contamination. It is advisable to have a small quantity of cobalt and phosphorus in the wash solution.

The yields obtained in this way show a remarkable enhancement compared to the yields observed in bombardments at the target chamber. In a day of operation, 10 millicuries of radio-phosphorus have been obtained in 40 milligrams of phosphorus. Exposures of several days should enable one easily to realize many times this activity, thus meeting the desideratum of one millicurie per milligram. This represents a concentration factor of 100 over target chamber yields with the same total activity. For iron, we obtain one microcurie per day per 40 milligrams of inert iron. The largest activities observed with target chamber bombardment are of the order of three microcuries distributed over 90 milligrams of iron. Hence, an exposure of a week or more should result in greatly increased iron yields. In fact, we have found that in a two-week exposure, it is possible to obtain 20 microcuries per 40 milligrams of iron. In this case, pure iron metal was used on the probe. The yield of iron from ferrous phosphide we find to be half of that observed from pure iron, a result which is to be expected from the fact that only half the target material is iron in the ferrous phosphide bombardment. As by-products, large copper, cobalt, manganese, nickel and zinc activities are produced which may be of some utility.[7] It must be emphasized that all of these activities are produced without interfering with bombardments proceeding simultaneously in the target chamber, so that one cyclotron may satisfy the needs of both biologist and physicist without extremely long periods of operation.

[7] Several hundreds of millicuries of the short lived isotopes of the above-mentioned elements can be made while for the long period activities yields ranging from a few microcuries to many millicuries can be obtained.

The method of probe bombardment is capable of extension to a wide variety of elements. Beryllium and molybdenum have been tried and found to exhibit greatly enhanced activities. The neutron yields from the beryllium-deuteron reaction render intense neutron activations possible in reasonable periods of bombardment; moreover, a possible extension in the application of neutrons to therapy is indicated. The investigations of Doctors Segrè and Seaborg[8] on the activities in element 43 produced by deuteron bombardment of molybdenum have been expedited greatly by the extremely powerful samples of molybdenum prepared on the probe. It is proposed shortly to bombard sulfur and tellurium as sulfides and tellurides.[9] In short, any infusible substance which can be joined in good thermal contact with the probe material can be adapted to probe bombardment. It should be possible to prepare most elements in the periodic system either pure or as compounds, in such fashion as to satisfy probe requirements. Obviously the method of internal targets should find its most important application in the preparation of radio-isotopes which are long lived and difficult of activation, as well as in the demonstration of the existence of many radio-isotopes as yet undiscovered.

We wish to acknowledge our special indebtedness to Professor E. O. Lawrence, whose suggestion of the existence of a large beam initiated this research. The work has been greatly facilitated by the unstinting cooperation of our colleagues in the Radiation Laboratory and by the assistance of the W.P.A. The continued financial support of the Research Corporation has rendered this research possible.

[8] E. Segrè and G. T. Seaborg, Phys. Rev. **54**, 772 (1938).

[9] *Note added in proof:*—Since this article was written, tellurium has been bombarded successfully on the probes. By fusing tellurium into thin copper strips, Dr. J. G. Hamilton has obtained satisfactory telluride targets which, on exposure to the internal beam, show enhancement of the yield of radio-iodine (period 8 days) by a factor of 3 to 5, as expected.

The Dissociation of Benzene (C_6H_6), Pyridine (C_5H_5N) and Cyclohexane (C_6H_{12}) by Electron Impact

A. HUSTRULID, P. KUSCH* AND JOHN T. TATE
Department of Physics, University of Minnesota, Minneapolis, Minnesota

(Received September 2, 1938)

The dissociation of C_6H_6, C_5H_5N, and C_6H_{12} by electron impact has been investigated with a mass spectrograph. Four doubly charged and thirty-one singly charged positive ions were observed in the dissociation of benzene. The relative abundance, for electrons of 72 volts energy, and the appearance potential are given for each ion. The first and second ionization potentials of benzene are 9.8 ± 0.1 and 17.2 ± 1.0 volts, respectively. The ionization potential of C_5H_5N is 9.8 ± 0.2 volt and of C_6H_{12}, 11.0 ± 0.2 volt. In each of the three vapors, certain of the ions resulting from the dissociation process have a doublet character. The components have a constant energy separation independent of magnetic field. The components also have different appearance potentials. The interpretation given is that these particular ions are formed by two different processes, one of which imparts a *definite* amount of kinetic energy to the ion.

INTRODUCTION

THE pioneer work of Smyth[1] and more recent studies[2–4] have shown that the identification with a mass spectrograph of the ions formed by electron impact in vapors is capable of giving valuable information about the molecular structure of these vapors. Directly observable are the nature (M/e value) of the ion formed, the minimum electronic energy which must be imparted to the molecule to produce this ion, and the relative probability, for any particular electron energy of impact, of forming ions of various kinds. In addition, a second experiment such as Lozier's[5] may determine the kinetic energy acquired by the ion in the dissociation process. As has been illustrated in previous work, observations of this kind may, when coupled with known thermochemical data, lead to new information about such things as heats of dissociation of the molecule, and of the molecular ion, ionization potentials of the molecule, of the molecular ion, and of the fragments into which the molecule may dissociate. Indirectly it is often possible to estimate bond energies of various kinds.

The purpose of the present paper is to describe the results obtained in an investigation of the dissociation of benzene (C_6H_6) and of related molecules under electron impact. The structure of the benzene molecule has been extensively studied by physical and chemical means. It was hoped that the appearance potentials and the probabilities of formation of the various ions produced in benzene might be interpreted in terms of the known structure of benzene and thus lead to some general guiding principle for the interpretation of the observed appearance potentials and probabilities of formation of ions produced from other complicated molecules under electron impact. In this hope we have been largely disappointed. The results, though interesting in themselves, have not been amenable to satisfactory interpretation in terms of known characteristics of the benzene molecule.

Previous studies of the dissociation of benzene by electron impact have been made by Linder,[6] and Friedlander and Kallman.[7] Conrad[8] studied the decomposition of benzene in a positive ray tube.

THE MASS SPECTROGRAPH

The apparatus is similar to that described by Nier.[9] The essential difference is that the filament is enclosed and has a separate pumping lead. The purpose of the housing around the filament is

* Now at Columbia University.

[1] For references to earlier work see Smyth, Rev. Mod. Phys. **3**, 347 (1931).
[2] Smith, Phys. Rev. **51**, 263 (1937).
[3] Kusch, Hustrulid and Tate, Phys. Rev. **52**, 843 (1937).
[4] Hipple, Phys. Rev. **53**, 530 (1938).
[5] Lozier, Phys. Rev. **46**, 268 (1934).
[6] Linder, Phys. Rev. **41**, 149 (1932).
[7] Friedlander and Kallman, Zeits. f. physik. Chemie **B17**, 265 (1932).
[8] Conrad, Trans. Faraday Soc. **30**, 215 (1934).
[9] Nier, Phys. Rev. **50**, 1041 (1936).

to prevent products of dissociation at the filament from diffusing back into the ionizing region. That the differential pumping system apparently fulfilled the purpose of preventing products of thermal dissociation from diffusing back into the ionizing region is evidenced by the fact that the character of the mass spectrum remained the same over rather wide ranges of pressure in the ionizing chamber. The metal parts of the apparatus were built entirely of Nichrome V with Pyrex tubing for supports and insulators.

Before assembly the metal parts were baked out in a vacuum quartz furnace. After assembly the whole apparatus was enclosed in an oven and baked out at 350°C for 36 hours. The residual pressure in the tube after this treatment, as determined by an ionization gauge, was less than 5×10^{-7} mm Hg.

A large water-cooled solenoid whose axis was parallel to the main tube, surrounded the entire apparatus and could give a magnetic field of 3000 gauss in the region of the analyzer. The resolving power was such that it was possible to detect the mercury isotopes separated by one atomic mass unit at 200. Although no careful observations were made, it was estimated that the background between the peaks was approximately one-half the average peak height when using the maximum available magnetic field.

TABLE I. *Ions formed in benzene by electron impact. Their appearance potentials and relative abundances are for electrons of 72 volts energy.*

M/e	Ion	Appearance Potential (volts)	Abundance
78	$C_6H_6^+$	9.8±0.1	100.0
77	$C_6H_5^+$	14.5±0.3	15.2
76	$C_6H_4^+$	15.0±0.3	4.6
75	$C_6H_3^+$	21.9±0.5	1.7
74	$C_6H_2^+$	23.9±0.5	4.0
73	C_6H^+	33.7±0.5	1.3
72	C_6^+	41.9±2.5	0.2
63	$C_5H_3^+$	16.8±0.3	2.6
62	$C_5H_2^+$	19.1±0.5	0.6
61	C_5H^+	27.4±1.0	0.5
60	C_5^+	44.0±2.5	0.2
52	$C_4H_4^+$	15.5±0.3	13.5
51	$C_4H_3^+$	18.5±0.3	15.7
50	$C_4H_2^+$	18.3±0.5	13.3
49	C_4H^+	27.6±1.0	2.1
48	C_4^+	40.4±2.5	0.3
39	$C_3H_3^+$	16.1±0.3	6.6
38	$C_3H_2^+$	23.0±0.5	3.6*
37	C_3H^+	27.4±1.0	2.5*
36	C_3^+	45.0±3.0	0.3
28	$C_2H_4^+$		0.2
27	$C_2H_3^+$	21.1±1.0	1.3
26	$C_2H_2^+$	17.9±1.0	1.1
25	C_2H^+	27.1±3.0	0.14
24	C_2^+		0.03
15	CH_3^+		0.01
14	CH_2^+		0.02
13	CH^+		0.03
12	C^+		0.05
2	H_2^+		0.15
1	H^+		0.2
39½	$C_6H_6^{++}$	27.0±1.0	1.8
38½	$C_6H_5^{++}$	30.4±2.5	0.18
37½	$C_6H_4^{++}$	39.8±2.5	0.42
30½	C_6H^{++}		0.015
39′	$C_3H_3^+ + KE$	>39	0.3
38′	$C_3H_2^+ + KE$	>39	0.4
37′	$C_3H^+ + KE$	>39	0.2
27′	$C_2H_3^+ + KE$	>39	0.09
26′	$C_2H_2^+ + KE$	>39	0.14
25′	$C_2H^+ + KE$	>39	0.03
15′	$CH_3^+ + KE$	29±3	0.1
14′	$CH_2^+ + KE$		0.003
13′	$CH^+ + KE$		0.002
12′	$C^+ + KE$		0.002

* Includes $C_6H_4^{++}$ and $C_6H_3^{++}$.

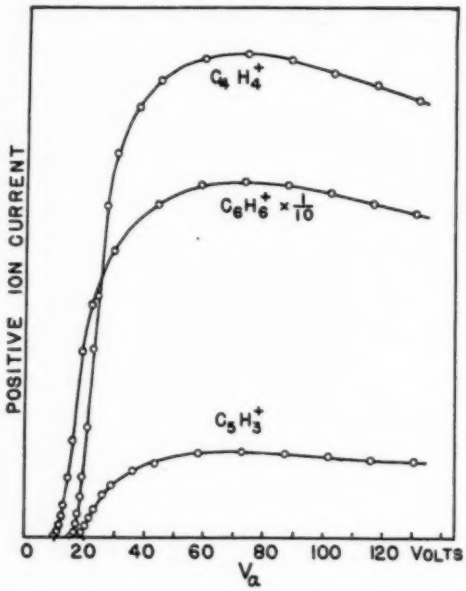

FIG. 1. Efficiency of formation of $C_6H_6^+$, $C_5H_3^+$ and $C_4H_4^+$ as a function of electron energy (V_a).

STUDY OF BENZENE

Mallinckrodt's thiophene-free benzene was fractionally crystallized five times. About one-half of the end product was then distilled off under reduced pressure and the remaining portion placed in a bulb connected to the ionizing region of the mass spectrograph by a fine capillary. The bulb could be maintained at any desired temperature. With the source at 0°C, the combined rate of leak and pumping speed was such as to give a pressure of about 10^{-4} mm Hg in the main tube. The only observed ions which could not reasonably be assumed to originate from dissociation of the benzene were those due to water. These peaks were at all times of *very low* intensity. A few of the peaks observed in this investigation had such M/e values that they might conceivably be due to CO, CO_2 or other vapors often observed as impurities in mass spectrographs. Since the intensity of any questionable peaks, for example, $M/e=28$, was the same function of pressure as that of peaks undoubtedly due to benzene, it is safe to say that these peaks arose from the dissociation of benzene

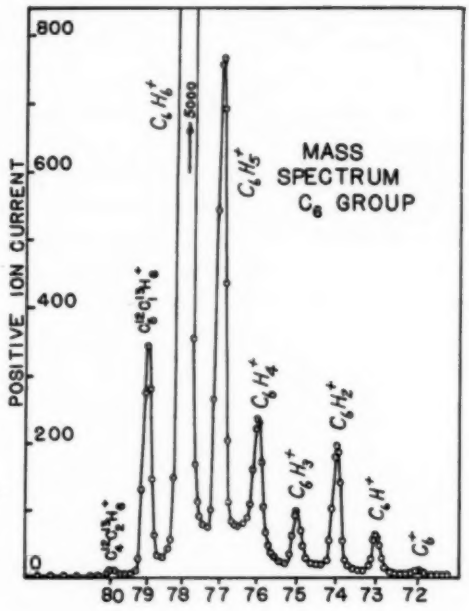

FIG. 2. Mass spectrum of ions with M/e values from 80 to 72.

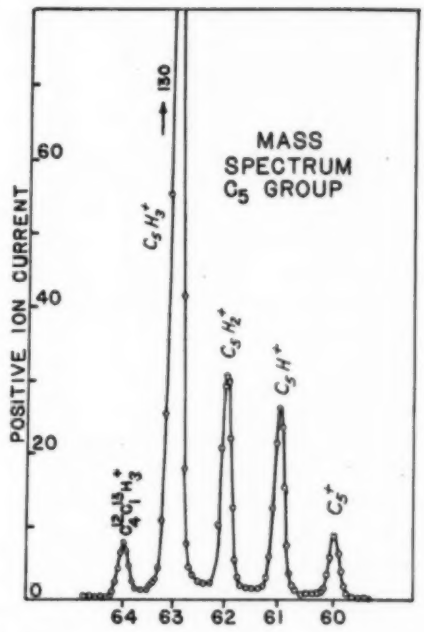

FIG. 3. Mass spectrum of ions with M/e values from 64 to 60.

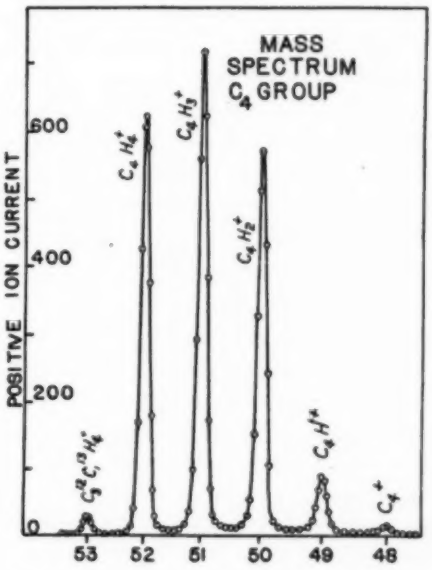

FIG. 4. Mass spectrum of ions with M/e values from 53 to 48.

and that impurities did not exist in important amounts.

Table I gives a summary of the results obtained for benzene. The nature of the ions, their appearance potentials, if determined, and their relative probabilities of formation for incident electrons of 72 volts energy are tabulated. The primed M/e values refer to rather sharp peaks on the high mass side of the corresponding peaks without primes. No integral M/e values could be assigned to these peaks by a simple comparison with the known M/e values of neighboring peaks. The evidence for associating these peaks with the M/e values assigned to them in Table I will be reviewed later. Suitable corrections to the abundances have been made for the presence of the carbon isotope of mass 13. It is possible that peaks caused by doubly charged ions of even mass (e.g. $C_4H_4^{++}$) coincide with some of the peaks of lower mass ($C_2H_2^+$), but this is unlikely since no doubly charged ions of odd mass (e.g. $C_4H_3^{++}$) were observed except for the C_6 group. In that case, the ions $C_6H_6^{++}$, $C_6H_5^{++}$, $C_6H_3^{++}$, C_6H^{++} were definitely observed but the ions $C_6H_4^{++}$ and $C_6H_2^{++}$, if they exist, coincide with $C_3H_2^+$ and C_6H^+. A search was made for negative ions, but none was found.

The ionization potential of benzene was found to be 9.8 ± 0.1 volt. Boucher[10] and Friedlander and Kallman[7] have obtained the values 9.6 ± 0.1 volt and 9.5 volts, respectively by direct measurement. Price and Wood[11] give the value 9.19

[10] Boucher, Phys. Rev. 19, 189 (1922).
[11] Price and Wood, J. Chem. Phys. 3, 439 (1935).

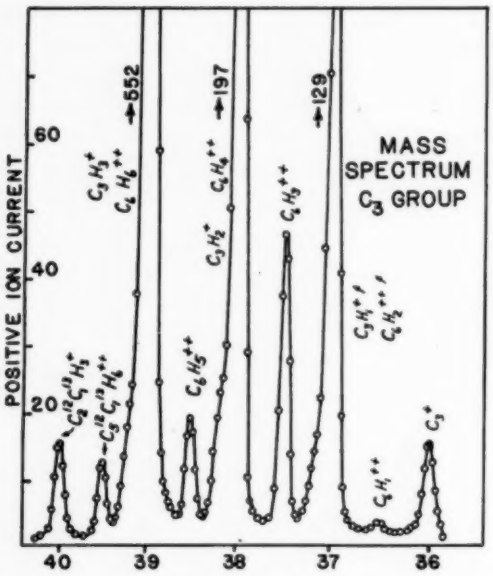

FIG. 5. Mass spectrum of ions with M/e values from 40 to 36.

± 0.005 volt obtained from spectroscopic evidence. The present determination of the ionization potential was made by admitting a mixture of benzene and mercury vapor to the mass spectrograph and observing the ion current as a function of electron energy near the threshold energy. The pressure was adjusted to give approximately the same slope to the curves for benzene and mercury. This method of estimating the ionization potential eliminates much of the uncertainty caused by contact potential and velocity distribution of electrons. The variation in the individual measurements of the ionization potential of benzene is much less than would seem to be the case from the probable error given here. The true ionization potential may differ from the observed one because of factors depending on the velocity distribution of electrons and the limiting sensitivity of the amplifier.

Price and Wood[11] also predict 11.7 ± 0.3 volt for the second ionization potential of benzene. The value obtained in the present work is 17.2 ± 1.0 volt. The value given by Price and Wood[11] is incompatible with the present observations.

The appearance potentials of ions other than $C_6H_6^+$ were determined by comparison with the ionization potential of benzene. The only appearance potentials found in the literature, other than the ionization potential, are those given by Friedlander and Kallman.[7] Their values in volts are as follows: $C_6H_4^+$, 18.5; $C_6H_2^+$, 25; and $C_2H_2^+$, 18. They give only upper or lower limits for the appearance potentials of the other ions which they identified.

Figure 1 gives sample curves for the relative efficiencies of formation of the more abundant ions as a function of the electron energy. It is observed that they are of the usual form. The curves for the other ions are similar.

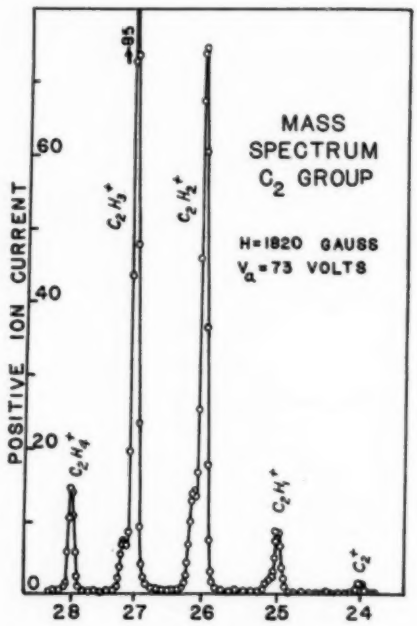

FIG. 6. Mass spectrum of ions with M/e values from 28 to 24.

Figures 2–7 inclusive show a typical mass spectrum for values of M/e from 80 to 12. These curves have not been corrected for small differences in electron current or gas pressure in going from one group to the next. The ions H_2^+ and H^+ were also found as given in Table I. A striking feature of the mass spectrum curves is that some of the peaks appear as doublets as shown in Figs. 6, 7 and 8. The component on the high mass side is the less intense one, except in the case of CH_3^+ where it is many times more intense than the component of apparently lower mass. The actual abundance of these "high mass" ions is considerably greater than the values given in Table I arrived at by measuring the peak heights, if they are ions with initial kinetic energy as interpreted in the following discussion, because

the solid angle from which these ions are collected is a small fraction of 4π steradians.

The difference in the accelerating potential required to focus an ion peak and the satellite of the peak on to the exit slit of the analyzer is constant regardless of the magnetic field which is used. Since the total accelerating potential which is required to focus is smaller at low than at high magnetic fields, the satellite is more nearly resolved from the main peak at low magnetic fields, even though the general resolution increases with the magnetic field. This effect is indicated for the peaks of $M/e=26$ and 27 in Figs. 6, 8(a) and 8(b) observed with magnetic fields of 1820, 1065 and 1320 gauss, respectively. The satellites of the peaks in the C_3 group, shown in Fig. 5, may, in the same way, be resolved from the main peak by suitably decreasing the magnetic field. No integral M/e

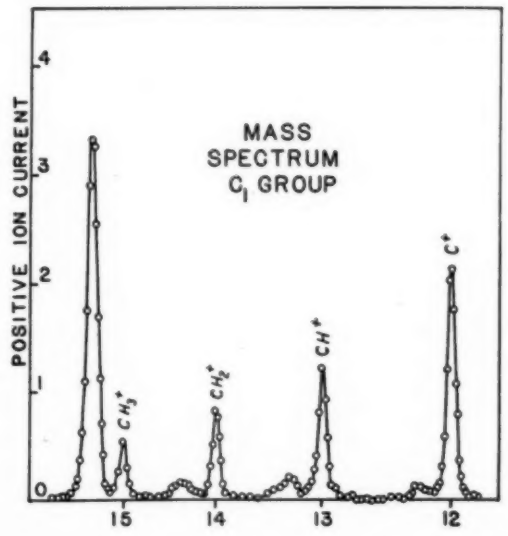

FIG. 7. Mass spectrum of ions with M/e values from 15 to 12.

value may then be assigned to the satellite peaks, but it is reasonable to assign the same M/e value to these peaks as to the main peaks from which they are separated by a constant energy difference.

The appearance potentials of the ions of the satellite peaks are, in general, higher than those of the ions of the main peaks. This is shown in Fig. 8(b) and 8(c) where the 26 and 27 peaks have been observed for different energies of the electrons producing the dissociation but for otherwise identical experimental conditions. No careful determination was made of the appearance potentials of the satellite peaks because of the low general resolution when the field was low enough to resolve the satellite peaks from the main peaks.

It seems reasonable to suppose that the satellite peaks are not ghosts produced by the mechanical and electrical arrangement of the mass spectrograph. The satellites of neighboring peaks bear no constant intensity relationship to the main peaks, and the peak caused by N_2^+ which appears in the same region as peaks which possess satellite, shows no trace of a satellite.

The satellite peaks are believed to be caused by ions to which the dissociation process has imparted a large kinetic energy lying within a *small* range. It can be shown that ions having kinetic energies in a small range will give a peak on the high mass side of the peak for ions of no kinetic energy. The momenta of the ions upon dissociation will be distributed over large angles, but only the momenta lying within the angle defined by the entrance slits of the analyzer will

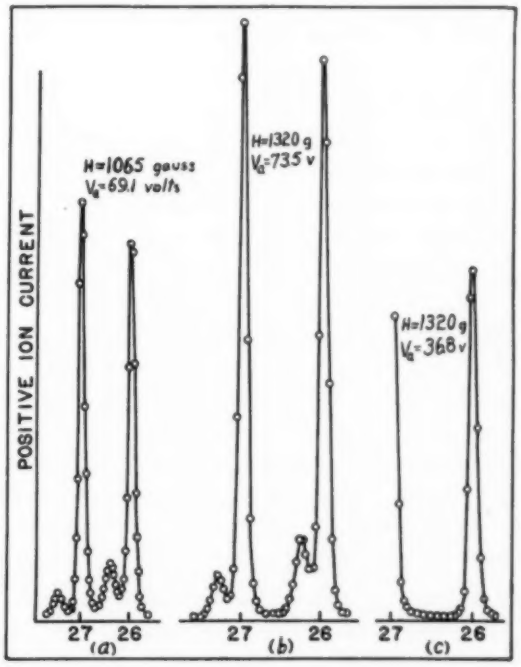

FIG. 8. Mass spectrum of ions with M/e values 26 and 27 for different values of magnetic field and different values of accelerating potentials (V_a) applied to electrons.

contribute to the observed peaks. If ions acquire a range of kinetic energy in the dissociation process, the peak caused by the ions will be broadened on the high mass side of the peak corresponding to no kinetic energy. If only a small proportion of the ions have an appreciable kinetic energy, they will appear as a foot on the high mass side of the peak. Such an effect has been observed by Tate, Smith and Vaughan,[12] and by Nier and Hanson[13] for H^+.

The most reasonable hypothesis which may be advanced for the occurrence of these peaks with their satellites is that the ion in question may be produced by at least two distinct dissociation processes. When the ions are produced by one of these processes, they acquire a large kinetic energy which is manifested by a displacement of the peak from its ideal position. The high appearance potentials which are associated with the ions corresponding to the satellite peaks suggest that these ions may be produced by the spontaneous dissociation into several parts of a large doubly charged ion which is extremely unstable. Such a spontaneous dissociation would require the conservation of momentum; this in turn requires that the lighter of two ions carry away more kinetic energy than the heavier of the two ions. A rough measurement of the kinetic energies showed that this condition is qualitatively obeyed.

While it is true that the appearance of the whole mass spectrum is rather surprising, certain features of the mass spectrum are of particular interest. For a group consisting of ions containing a constant number of carbon atoms (6, 5, 4 or 3) and a variable number of hydrogen atoms, the probability of formation of each ion decreases regularly with a decrease in the number of hydrogen atoms. Significant exceptions occur in the case $C_6H_3^+$ which is less abundant than both $C_6H_4^+$ and $C_6H_2^+$, and in the case of $C_4H_4^+$, $C_4H_2^+$ which have an approximately equal abundance. The group containing 5 carbon atoms is much weaker than the groups containing 6, 4, or 3 carbons and the ions $C_5H_5^+$ and $C_5H_4^+$ are entirely absent. The doubly charged ion $C_6H_3^{++}$ has, however, a relatively large intensity.

[12] Tate, Smith and Vaughan, Phys. Rev. **48**, 525 (1935).
[13] Nier and Hanson, Phys. Rev. **50**, 722 (1936).

Pyridine[14]

Because pyridine (C_5H_5N) is chemically similar to benzene, a brief study of the ions produced from it by electron impact was made. The mass spectrograph is unable to distinguish between the ions $C_nH_m^+$ and $C_{n-1}H_{m-2}N^+$ and, therefore, no careful study was made of the relative abundance of the ions and of their appearance potentials.

The mass spectrum of the ions produced by the dissociation of pyridine has the same general features as that of the ions produced from benzene. The ionization potential was found to be 9.8 ± 0.2 volt, the same as that of benzene within the limits of error. The abundance of the group of ions containing 5 carbons or 4 carbons and one nitrogen atom is extremely low. The low abundance of such ions is much more pronounced in the case of pyridine than in the case of benzene. It is not possible to determine whether ions containing 5 carbon atoms and 4 or 5 hydrogen atoms are produced, because the ions may not be identified uniquely.

As in the case of benzene, the ion $C_5H_3N^+$ is less abundant than either of the ions $C_5H_2N^+$ and $C_5H_4N^+$. The group of ions containing 4 carbons or 3 carbons and one nitrogen is relatively much more abundant than the corresponding group for benzene. The intensity of the peak caused by $(C_4H_4^+ + C_3H_2N^+)$ is about the same as that of the peak caused by $C_5H_5N^+$.

Peaks which possessed satellites were observed in the C_2 or CN group of peaks. Apparently the same conditions which give rise to ions of high kinetic energy in the dissociation of benzene exist for the dissociation of pyridine.

Cyclohexane

The ions observed as dissociation products of cyclohexane (C_6H_{12}) under electron impact and the relative abundances at an electron energy of 72 volts are tabulated in Table II. In addition to the ions tabulated there, the ions $C_6H_3^{++}$, $C_6H_5^{++}$, $C_6H_7^{++}$ and $C_6H_9^{++}$ were observed. Other doubly charged ions may be produced which are masked by singly charged ions of an

[14] Professor Lauer of the Chemistry Department kindly supplied us with samples of pyridine and cyclohexane.

TABLE II. *Nature and relative abundances of ions formed in cyclohexane by electrons with 72 volts energy.*

ION	$n=6$	5	4	3	2	1	0
$C_nH_{12}^+$	100.						
$C_nH_{11}^+$	5.9	1.2					
$C_nH_{10}^+$	0.4	1.2					
$C_nH_9^+$	0.6	46.4	3.8				
$C_nH_8^+$	0.2	3.6	223.				
$C_nH_7^+$	0.8	5.1	78.	42.			
$C_nH_6^+$	1.2	0.5	13.	77.	1.0		
$C_nH_5^+$	1.2	1.0	8.4	155.	15.6		
$C_nH_4^+$	0.1	0.1	2.4	11.7	13.3	0.2	
$C_nH_3^+$	0.1	0.6	5.3	50.2	27.6	3.0	
$C_nH_2^+$	0.3	0.3	3.9	4.2	3.4	0.3	
C_nH^+	0.1	0.2	0.5	2.2	0.2	0.1	—
C_n^+	0.2					0.1	—

equal M/e. The abundance values given in Table II have been corrected for the presence of the carbon isotope of mass 13.

The peak for $C_2H_4^+$ shows the presence of a satellite and thus indicates that the ion $C_2H_4^+$ may be produced by at least two different processes, in one of which the ion acquires a considerable kinetic energy.

The appearance potentials of only three ions were measured. The ionization potential of cyclohexane was found to be 11.0 ± 0.2 volt. The very abundant ions $C_4H_8^+$ and $C_3H_5^+$ were found to have appearance potentials of 11.7 ± 0.3 and 13.5 ± 0.3 volt, respectively.

A general appearance of the mass spectrum of the ions produced from cyclohexane differs markedly from that of the ions produced from benzene. The ions in the group containing 5 carbon atoms are less abundant than those in the groups containing 6, 4, and 3 carbon atoms, but the effect is less pronounced than in the case of benzene or pyridine. The ions $C_5H_5^+$ and $C_5H_4^+$, which were entirely absent in the case of benzene, do appear as dissociation products of cyclohexane. Their appearance in the present case precludes the possibility that they do not occur as dissociation products of benzene because of an inherent instability.

It is noteworthy that the ions $C_4H_8^+$ and $C_3H_5^+$ are much more abundant than the ion $C_6H_{12}^+$. This is contrary to the more usual case observed in electron impact experiments where the probability of ionization alone is greater than the probability of ionization plus dissociation. However, this agrees with the results of Hipple[4] in a study of ethane and Stewart and Olson[15] in a study of propane and butane.

[15] Stewart and Olson, J. Am. Chem. Soc. **53**, 1236 (1931).

DISCUSSION

Paucity of thermochemical and spectroscopic data and of work on simpler molecules prohibits the making of a satisfactory analysis of the processes by which the ions are formed. If one assumes, however, that the ring structure is maintained and that all free valences are taken care of by formation of double bonds or removal of a valence electron, something can be said about the possible processes. The sole test which is available to check the analysis will be the value obtained for the ionization potential of the new ion. The appearance potential of an ion which lacks one or more of the atoms of the parent molecule is the sum of three quantities: a dissociation energy, an ionization potential and the total minimum excitational and mutual kinetic energy with which the products can dissociate or $A=D+I'+E+K.E.$ The minimum excitational and kinetic energy with which the products dissociate is usually small and one may define a new quantity I, which is nearly equal to I', by $A-D=I$. This new I must have a value which is reasonable for the ionization potential of hydrocarbons and, therefore, should be in the range 9.0 to 15.0 volts.

For example:

$I'(C_6H_6) = 9.8$ volts
$I'(C_6H_{12}) = 11.0$ volts } Present work
$I'(C_5H_5N) = 9.8$ volts

$I'(CH_4) = 13.1$ volts—Smith[2]
$I'(C_2H_2) = 11.2$ volts—Tate, Smith and Vaughan[12]
$I'(C) = 11.2$ volts
$I'(H) = 13.5$ volts

Since A has been measured for many of the ions, a value of I may be obtained by calculating D. In making this calculation it will be assumed that the bond energies are additive.

Pauling and Sherman[16] and Dietz[17] have computed the bond energies as they occur in organic molecules. Such determinations for bonds involving carbon must always be made from thermochemical data, and these are in doubt by the uncertainty in the heat of sublimation of

[16] Pauling and Sherman, J. Chem. Phys. **1**, 606 (1933).
[17] Dietz, J. Chem. Phys. **3**, 58 (1935).

TABLE III. *Calculated values of the heats of dissociation, D, for various processes and the corresponding values of the ionization potentials for the organic radicals involved.*

PROCESS $C_6H_6\rightarrow$	DISSOCIATION ENERGY, D.	IONIZATION POTENTIAL OF RESULTING RADICAL
$C_6H_5^+ + H$	4.0 volts	10.5 volts
$C_6H_4^+ + 2H$	5.5 volts	9.5 volts
$C_6H_3^+ + 3H$	9.4 volts	12.5 volts
$C_6H_2^+ + 4H$	10.9 volts	13.0 volts
$C_6H^+ + 5H$	15.0 volts	18.7 volts
$C_6^+ + 6H$	16.5 volts	25.4 volts

carbon, $L(C)$. In considering the dissociation of benzene one is, however, interested only in the energy changes which occur when C_6H_6 is dissociated to a small extent into very similar forms. Such energy differences would not involve $L(C)$.

From the values given by Dietz for the bond energies, i.e., C−H bond = 3.97 volts, C−C bond = 3.17 volts and C=C bond = 5.65 volts,[18] D and I have been calculated for various dissociation processes of benzene and are given in Table III.

If it is assumed that the group of ions containing six carbons is produced by the removal of the hydrogen in atomic form and that the ion itself is ring-shaped with no free valences, reasonable values are obtained for the ionization potentials of C_6H_5, C_6H_4, C_6H_3 and C_6H_2 as is shown in Table III. The same reasoning gives values which are higher than might be expected for C_6H and C_6. These values cannot be reduced on the basis of the above picture, since as much energy as possible has been taken up as dissociation energy. Several possibilities occur as an explanation. The ionization potentials of C_6 and C_6H may actually be higher than the ionization potentials of stable hydrocarbons; the binding energies calculated from data on stable hydrocarbons may not be applicable to these hydrocarbons which are not chemically known; or the picture of the ion may be inaccurate.

If a dissociation process which will give reasonable values of the ionization potentials for the first members of the group is assumed for any other group, the same sort of discrepancy is observed. If the ions C_nH^+ and C_n^+ are to have reasonable ionization potentials, the neutral fragments which are produced must be much smaller than they are in the case of $C_nH_2^+$, $C_nH_3^+$. That this result is not entirely due to uncertainties in the calculation is manifested by the fact that an inspection of the appearance potentials in Table I indicates a sudden increase in the appearance potential for C_nH^+ and C_n^+.

It may be seen from an inspection of the experimental data and from a few simple calculations that when the ions $C_5H_3^+$, $C_5H_2^+$, $C_4H_4^+$, $C_4H_3^+$, $C_3C_3^+$ and $C_3H_2^+$ are formed the dissociation is not very extensive. The un-ionized portion of the molecule probably leaves as a single large fragment and as many hydrogen atoms as cannot be easily attached to the carbons of the fragment. This conclusion is not in accord with one which Smith[2] has made about the simpler hydrocarbon, methane, that of all the possible dissociation processes, those which require the greatest minimum energy actually occur.

In the same way as above one can make the calculations for the ions of cyclohexane for which the appearance potentials have been determined.

$$C_6H_{12}\rightarrow C_4H_8^+ + C_2H_4$$
$$D = 0.7 \text{ volt} \quad I(C_4H_8) = 11.0 \text{ volts}$$
$$C_6H_{12}\rightarrow C_3H_5^+ + C_3H_6 + H$$
$$D = 4.0 \text{ volts} \quad I(C_3H_5) = 9.7 \text{ volts}.$$

These processes seem very likely to be the correct ones because in either case the compounds involved are known and stable and the ionization potentials for the new radicals have reasonable values.

[18] The values 4.0, 3.2 and 5.7 have been used in the calculation.

Pressure Shifts of the High Terms of the Absorption Series of Na, Rb, and Cs Produced by Hydrogen and Nitrogen

NY TSI-ZÉ
Institute of Physics, National Academy of Peiping, China

AND

CH'EN SHANG-YI*
Norman Bridge Laboratory, California Institute of Technology, Pasadena, California

(Received August 23, 1938)

The pressure shifts of the high terms of the principal series of Na, Rb, and Cs produced by commercially pure hydrogen and nitrogen were studied. Measurements were made for different concentrations of the perturbing gases up to a pressure of about 12 atmospheres (617°K) for hydrogen and 7.5 atmospheres (548°K) for nitrogen. The former produced a strong while the latter a very slight violet shift and the effective cross sections as calculated by Fermi's equations were found to be 14.0 cm^3/cm^3, and 2.0 cm^3/cm^3, respectively. For axially symmetrical molecules the values of effective cross sections calculated from Fermi-Reinsberg equations do not agree with those obtained by a direct electrical method.

THE displacement of the high members of the principal series of Na and K produced by nitrogen and hydrogen has been measured by Amaldi and Segrè.[1] The highest concentration of hydrogen they used was 5.37×10^{19} cm^{-3}, and that of nitrogen was 3.84×10^{19} cm^{-3}. About the same time Füchtbauer, Schulz, and Brandt[2] determined the displacement of the sodium high series members produced by nitrogen with a higher concentration, *viz.* 6.62×10^{19} cm^{-3} ($t=440°C$, $p=6.40$ atmos.). The effective cross section of nitrogen obtained by the former was 0.93 cm^2/cm^3 and that obtained by the latter was 5 cm^2/cm^3. In the present research the displacement of the high members of the absorption series of Na, Rb, and Cs was studied under different pressures of the foreign gas (H_2 or N_2) up to a concentration of about 14.3×10^{19} cm^{-3} ($t=617°K$, $p=12.0$ atmos.) for hydrogen, and 9.8×10^{19} cm^{-3} for nitrogen ($t=548°K$, $p=7.47$ atmos.).

Because of the fact that the constant shift (in cm^{-1}) of the high members of the absorption series depends on the nature of the perturbing atoms and is independent of the nature of the absorbing vapor, as has been shown both theoretically[3] and experimentally,[1, 2, 4] data obtained from the three alkalis (Na, Rb, and Cs) were averaged, and the mean result was compared with those obtained by different authors.

OBSERVATIONS AND RESULTS

The experimental procedure and apparatus were the same as those employed previously.[4] Commercially pure hydrogen and nitrogen (the purity was about 99.5 percent) were used. A high intensity hydrogen discharge tube was used for the background of the absorption spectrum of sodium, while for rubidium and caesium the carbon arc was used. Because of the fact that water cooling was applied at both ends of the absorption tube, the following experimental difficulty was experienced.[5] The cold gas at the ends of the tube and the hot gas at the central part caused convection, resulting in a higher gas density at the lower part of the absorption column. Consequently, the light traveling through the absorption tube will be refracted downward. In fact, whenever more gas was added to the absorption tube, the optical system had to be

* Research Fellow of the China Foundation for the Promotion of Education and Culture.

[1] E. Amaldi and E. Segrè, N. Cimento **11**, 145 (1934).

[2] C. Füchtbauer, P. Schulz and A. F. Brandt, Zeits. f. Physik **90**, 403 (1934).

[3] E. Fermi, N. Cimento **11**, 157 (1934).

[4] Ny Tsi-Zé and Ch'en Shang-Yi, Phys. Rev. **51**, 567 (1937).

[5] Indeed, this trouble would be entirely removed if the whole absorption tube were uniformly heated and MgO windows developed by R. T. Brice and J. Strong (J. Opt. Soc. Am. **25**, 207 (1935)) were used. One of the authors is doing this.

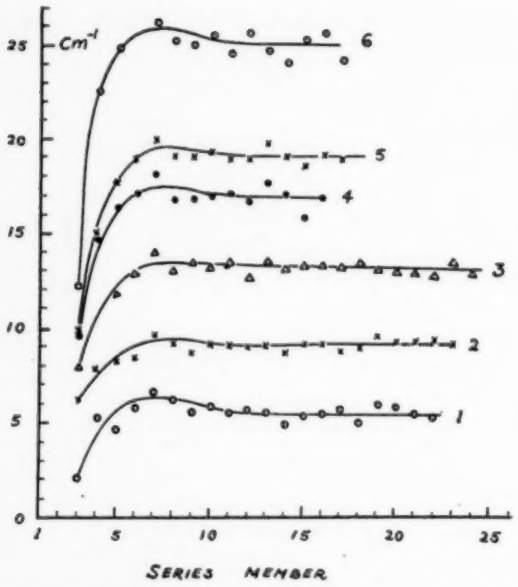

FIG. 1. The displacement of the Cs principal series perturbed by hydrogen. (Violet shift in cm^{-1} against series members.) Curve 1. $t=545°K$, $p=2.22$ atmos.; curve 2. $t=580°K$, $p=4.17$ atmos.; curve 3. $t=621°K$, $p=5.70$ atmos.; curve 4. $t=594°K$, $p=7.60$ atmos.; curve 5. $t=620°K$, $p=9.2$ atmos.; curve 6. $t=595°K$, $p=11.3$ atmos.

readjusted in order to allow the transmitted light to enter the slit of the spectrograph normally. This phenomenon was found to be negligibly small for helium and hydrogen, slight for neon, appreciable for argon, and most pronounced for nitrogen, in accordance with the above explanation that the light will be deviated more for heavier and more refractive gases.

Both for hydrogen and for nitrogen the shift first increases with the ordinal number of the lines in the series, then attains a weak maximum around the 7th member, and finally approaches a constant value at about the 14th.

Hydrogen produces a strong violet shift. Measurements were made for pressures up to 12.0 atmospheres ($t=617°K$) from the third member of the principal series up to about the 23rd. When the concentration of hydrogen was high, say a relative density greater than 3.5, the lines were rather diffused; hence for high concentrations the values were given only for members up to the 17th. Fig. 1 shows the results obtained when caesium was used as the absorbing atom.

Considerable trouble was met in the experiments with nitrogen. The refraction, as mentioned above, began to cause trouble when the pressure was increased to three atmospheres. When the pressure was as high as 7.5 atmospheres, the refraction of light and the increasing opacity of the alkali cloud rendered the transmitted light too weak to photograph.

Nitrogen made the high series lines of the alkalis much more diffuse than hydrogen, so for high concentrations of nitrogen the precision of

TABLE I. *The mean shifts of the high terms of the principal series of* Na, Rb *and* Cs *produced by hydrogen.* (∇_ϵ *and* ∇_σ *are the values calculated from Fermi's equations.*)

PRESSURE (ATMOS.)	TEMPERATURE	RELATIVE DENSITY	∇ (cm^{-1}) (VIOLET)	∇_ϵ (cm^{-1}) (RED)	∇_σ (cm^{-1}) (VIOLET)	SERIES MEMBERS	ALKALI
1.63	718°K	0.62	3.24	0.39	3.63	13–24	Na
2.25	609	1.01	5.01	0.74	5.75	13–22	Rb
2.22	545	1.12	5.47	0.85	6.32	13–22	Cs
3.21	720	1.22	6.26	0.95	7.21	13–20	Na
4.17	580	1.96	9.11	1.79	10.90	13–23	Cs
4.40	609	1.97	9.85	1.80	11.65	14–22	Rb
5.70	621	2.50	13.10	2.48	15.58	13–24	Cs
6.58	713	2.52	12.48	2.50	14.98	13–18	Na
8.55	725	3.22	15.45	3.47	18.92	13–18	Na
7.77	614	3.43	16.44	3.78	20.22	14–17	Rb
7.60	594	3.48	16.81	3.85	20.66	13–16	Cs
9.2	620	4.04	19.04	4.70	23.74	13–17	Cs
11.41	722	4.31	20.46	5.12	25.58	13–16	Na
11.3	595	5.18	24.8	6.54	31.3	13–17	Cs
12.0	617	5.31	24.4	6.77	31.2	13–17	Rb

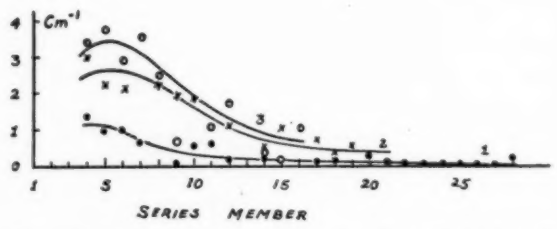

FIG. 2. The displacement of the Cs principal series perturbed by nitrogen. (Violet shift in cm^{-1} against series members.) Curve 1. $t=569°K$, $p=2.48$ atmos.; curve 2. $t=555°K$, $p=4.23$ atmos.; curve 3. $t=548°K$, $p=7.47$ atmos.

TABLE II. *The mean shifts of the high terms of the principal series of* Na, Rb *and* Cs *produced by nitrogen.* (∇_ϵ *and* ∇_σ *are the values calculated from Fermi's equations.*)

PRESSURE (ATMOS.)	TEMPERATURE	RELATIVE DENSITY	∇ (cm^{-1}) (VIOLET)	∇_ϵ (cm^{-1}) (RED)	∇_σ (cm^{-1}) (VIOLET)	SERIES MEMBERS	ALKALI
2.17	728°K	0.81	0.04	1.27	1.31	14–18	Na
2.27	591	1.05	0.18	1.80	1.98	14–22	Rb
2.48	569	1.19	0.03	2.11	2.1	14–26	Cs
3.92	726	1.47	0.13	2.80	2.9	14–18	Na
4.22	580	1.98	0.2	4.16	4.4	14–19	Rb
4.23	555	2.08	0.3	4.45	4.7	14–21	Cs
6.61	723	2.50	0.2	5.69	5.9	14–17	Na
8.73	727	3.28	0.2	8.17	8.4	14–15	Na
7.28	580	3.42	0.3	8.64	8.9	14–16	Rb
7.47	548	3.72	0.4	9.66	10.1	14–16	Cs

measurement was greatly lowered, and determinations were made only for lines up to about the 17th member of the principal series. It produced a slight violet shift for about the first ten terms, then the shift decreased to very small values approaching the magnitude of the experimental error. Results obtained when caesium was used as the absorbing atom are shown in Fig. 2.

According to Fermi's theory the effective cross sections for the single atoms of perturbing gases can be deduced from the observation of the constant shifts of the high series lines of the alkalis.[6] Tables I and II summarize the results obtained from different determinations, where ∇ means the constant shifts of the high terms observed, ∇_r the shift due to the polarization of the foreign atoms in the field of the core of the alkali atom, and ∇_v the shift caused by the perturbation of the valence electron by the foreign atoms. Fig. 3 shows the relationship between the constant shifts of the high terms and the concentrations of the perturbing gases. From the slopes of these curves, which are 5.85 cm^{-1} (violet) per unit relative density and 2.2 cm^{-1} (violet) per unit relative density for hydrogen and nitrogen, respectively, the effective cross section for all the atoms in one cm^3 at one mm pressure and 0°C can at once be calculated. The results obtained in the present experiment were compared with those by different authors as shown in Table III.

Although Fermi's equations were derived for spherically symmetrical molecules; nevertheless, an extension of his treatment to axially symmetrical molecules as given by Reinsberg[7] shows that Fermi's equations can also be applied to them without any appreciable correction. But a comparison of the values of effective cross sections as found in this way with those extrapolated from Ramsauer and Kollath's curves[8] to very low electron velocity indicates that for spherically symmetrical molecules, the values obtained from spectroscopic observations agree fairly well with those obtained by the direct electrical method, while for axially symmetrical ones the values are apparently discrepant. This fact suggests that the theoretical treatment of the problem needs some further consideration.

TABLE III. *The effective cross sections in* cm^2/cm^3 *of hydrogen and nitrogen for electrons of very low velocity as measured by different authors.*

GAS	AMALDI AND SEGRÈ	FÜCHTBAUER ETC.	WAHLIN	NY AND CH'EN
H_2	12.3	—	24.4	14.0
N_2	0.93	5	10	2.0

[6] The detailed method of calculation can be found elsewhere, such as the references cited in this paper.

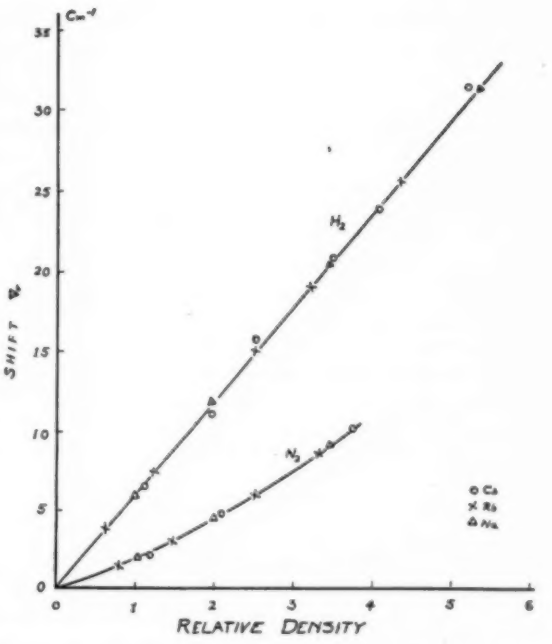

FIG. 3. Shift ∇_v *vs.* the relative density of perturbing gas.

The authors wish to thank Professor W. V. Houston for his valuable help in writing the paper.

[7] C. Reinsberg, Zeits. f. Physik **93**, 416 (1935).
[8] C. Ramsauer and R. Kollath, Ann. d. Physik **3**, 536 (1929); **4**, 91 (1930). Also H. B. Wahlin, Phys. Rev. **37**, 260 (1931).

The Binding Energy of O^{16}

W. J. KROEGER
University of Pittsburgh, Pittsburgh, Pennsylvania

(Received July 25, 1938)

A perturbation calculation has been made to determine the binding energy of the O^{16} nucleus. Zero-order eigenfunctions constructed from harmonic oscillator functions in a central field were used in conjunction with a symmetrical form of the Hamiltonian involving space exchange, space-spin exchange, nonexchange and spin exchange terms and only one range function of Gaussian form. The coefficients of the interactions were selected to give agreement with the scattering results and the observed energies of H^3 and He^4, and to satisfy the requirement of the upper limit of nuclear masses. The interaction so selected leads to a very small first-order binding energy, 19 mc^2. Second-order contributions to the energy were calculated from the interaction of excited states with the ground state. The energy is thus estimated to be about 79 mc^2 in second order. The third-order contributions were found to be disturbingly large, amounting to perhaps half of the second-order contributions, but of opposite sign. The procedure does, however, appear to converge and it is believed that the end result is indicated sufficiently well to show that the assumed interactions are inadequate to produce the required binding energy of O^{16}.

IN THE manner described by Inglis,[1] the spherically symmetric central-field representation is introduced into the wave equation of N particles with their center of gravity at rest

$$(E-H)\psi=\left\{\frac{1}{2}\left(1-\frac{1}{N}\right)\sum_{a=1}^{N}\nabla_a^2 - \frac{1}{N}\sum_{a>b=1}^{N}\nabla_a\cdot\nabla_b - U+E\right\}\psi=0 \quad (1)$$

by the addition and subtraction of the fictitious harmonic oscillator potential $\frac{1}{2}\sum_1^N(\sigma\alpha)^2r_a^2$. The perturbation term of the Hamiltonian is then

$$H'=H-H^0=\frac{1}{2N}\sum_{a=1}^{N}\nabla_a^2-\frac{1}{2}\sum_{a=1}^{N}(\sigma\alpha)^2r_a^2 + \frac{1}{N}\sum_{a>b=1}^{N}\nabla_a\cdot\nabla_b+U, \quad (2)$$

where U is the interaction between the particles, σ is an arbitrary parameter to be varied, and α is the inverse squared breadth introduced by the analytic form of the potential well, $\exp(-\alpha r_{ij}^2)$.

Zero-order states are constructed from the products of the one-particle harmonic oscillator eigenfunctions in Cartesian coordinates given by H^0, suitably antisymmetrized in each of the two kinds of particles because of their equivalence degeneracy. The zero-order state corresponding to the set of spin and directional quantum numbers,

$$0_\pi{}^+0_\pi{}^-1_\pi{}^+1_\pi{}^-(01)_\pi{}^+(01)_\pi{}^-(001)_\pi{}^+(001)_\pi{}^-;$$
$$0_\nu{}^+0_\nu{}^-1_\nu{}^+1_\nu{}^-(01)_\nu{}^+(01)_\nu{}^-(001)_\nu{}^+(001)_\nu{}^-,$$

where π and ν refer to proton and neutron, respectively, is the only one associated with the lowest energy of the O^{16} nucleus and is the proper zeroth order eigenfunction of the ground state.

In the calculation of the matrix elements of the interactions, one obtains integrals of the form

$$\int_{-\infty}^{+\infty}\int_{-\infty}^{+\infty}\psi_a(x_1)\cdot\psi_b(x_2)\cdot\exp\left[-\alpha(x_1-x_2)^2\right]\cdot\psi_c(x_1)\cdot\psi_d(x_2)\cdot dx_1\cdot dx_2=(\sigma/\tau)^{\frac{1}{2}}f_{abcd} \quad (3)$$

where the ψ's are the normalized harmonic oscillator functions belonging to the potential $\frac{1}{2}(\sigma\alpha)^2x^2$ and $\tau=\sigma+2$. The list of such integrals f_{abcd} given by Inglis[2] is extended as follows:[3]

$$\begin{aligned}
f_{5010}&=(15/8)^{\frac{1}{2}}\cdot[1/\tau^2-1/\tau^3],\\
f_{4020}&=3^{\frac{1}{2}}\cdot[-1/\tau+2/\tau^2-(5/4)/\tau^3],\\
f_{2121}&=[1-3/\tau+(15/2)/\tau^2-(15/2)/\tau^3],\\
f_{2220}&=(1/2)^{\frac{1}{2}}\cdot[-1/\tau+6/\tau^2-(15/2)/\tau^3],\\
f_{5111}&=(15/8)^{\frac{1}{2}}\cdot[1/\tau^2-6/\tau^3+7/\tau^4],\\
f_{4211}&=3^{\frac{1}{2}}\cdot2\cdot[-1/\tau^2+(15/4)/\tau^3-(35/8)/\tau^4],\\
f_{3311}&=(9/2)[1/\tau^2-(10/3)/\tau^3+(105/27)/\tau^4],\\
f_{2222}&=[1-4/\tau+15/\tau^2-30/\tau^3+(105/4)/\tau^4].
\end{aligned} \quad (4)$$

[1] Inglis, Phys. Rev. **53**, 880 (1938); **51**, 531 (1937).

[2] Inglis, Phys. Rev. **51**, 531 (1937), Eq. (10).

[3] The value of f_{2220}, included for the purpose of record, has been supplied by Dr. D. R. Inglis.

TABLE I. *Doubly and quadruply excited states differing from the ground state by one set of quantum numbers (Class 1).*

QUANTUM NUMBERS	No.	H_{20}'
$0_\pi{}^+\ldots$ $1_\pi{}^+\ldots$		ground state
$2_\pi{}^+\ldots$ $\ldots$	12	$-\frac{17}{32}\frac{\sigma\alpha}{\sqrt{2}}+B(\sigma/\tau)^{\frac{1}{2}}\cdot[(5-2g_0-\lambda)(f_{2000}+f_{2110}+2f_{2000}f_{1100})+(-2-g_0+\lambda)(f_{2000}+f_{2101}+2f_{2000}f_{1010})]$
$\ldots$ $3_\pi{}^+\ldots$	12	$-\frac{15}{32}\left(\frac{3}{2}\right)^{\frac{1}{2}}(\sigma\alpha)+B(\sigma/\tau)^{\frac{1}{2}}\cdot[(5-2g_0-\lambda)(f_{3100}+f_{3111}+2f_{3100}f_{1100})+(-2-g_0+\lambda)(f_{3010}+f_{3111}+2f_{3010}f_{1010})]$
$\ldots$ $12_\pi{}^+\ldots$	24	$-\frac{15}{32}\frac{\sigma\alpha}{\sqrt{2}}+B(\sigma/\tau)^{\frac{1}{2}}\cdot[(5-2g_0-\lambda)(f_{2000}(f_{1111}+f_{1100}+f_{1100}{}^2)+f_{2110}f_{1100})+(-2-g_0+\lambda)(f_{2000}(f_{1111}+f_{1010}+f_{1010}{}^2)+f_{2101}f_{1010})]$
$4_\pi{}^+\ldots$	12	$B(\sigma/\tau)^{\frac{1}{2}}\cdot[(5-2g_0-\lambda)(f_{4110}+f_{4000}(1+2f_{1100}))+(-2-g_0+\lambda)(f_{4101}+f_{4000}(1+2f_{1010}))]$
$22_\pi{}^+\ldots$	12	$B(\sigma/\tau)^{\frac{1}{2}}\cdot[(5-2g_0-\lambda)(f_{2000}(f_{2000}+2f_{2110}+f_{2000}f_{1100}))+(-2-g_0+\lambda)(f_{2000}(f_{2000}+2f_{2101}+f_{2000}f_{1010})]$
$\ldots$ $5_\pi{}^+\ldots$	12	$B(\sigma/\tau)^{\frac{1}{2}}\cdot[(5-2g_0-\lambda)(f_{5111}+f_{5100}(1+2f_{1100}))+(-2-g_0+\lambda)(f_{5111}+f_{5010}(1+2f_{1010})]$
$\ldots$ $14_\pi{}^+\ldots$	24	$B(\sigma/\tau)^{\frac{1}{2}}\cdot[(5-2g_0-\lambda)(f_{4110}f_{1100}+f_{4000}(f_{1100}+f_{1111}+f_{1100}{}^2))+(-2-g_0+\lambda)(f_{4101}f_{1010}+f_{4000}(f_{1010}+f_{1111}+f_{1010}{}^2))]$
$\ldots$ $32_\pi{}^+\ldots$	22	$B(\sigma/\tau)^{\frac{1}{2}}\cdot[(5-2g_0-\lambda)(f_{3100}f_{2110}+f_{2000}(f_{3111}+f_{3100}[1+f_{1100}]))+(-2-g_0+\lambda)(f_{3101}f_{2101}+f_{2000}(f_{3111}+f_{3010}[1+f_{1010}]))]$
$\ldots$ $122_\pi{}^+\ldots$	12	$B(\sigma/\tau)^{\frac{1}{2}}\cdot[(5-2g_0-\lambda)(f_{2000}{}^2(f_{1111}+f_{1100})+2f_{2000}f_{1100}f_{2110})+(-2-g_0+\lambda)(f_{2000}{}^2(f_{1111}+f_{1010})+2f_{2000}f_{1010}f_{2101})]$

These have been obtained by direct integration or by expansion of the expression[4]

$$\sum_{a,\,b,\,c,\,d} f_{abcd}\cdot 2^{\frac{1}{2}(a+b+c+d)}\cdot(a\,!b\,!c\,!d\,!)^{-\frac{1}{2}}\cdot p^a q^b r^c s^d$$

$$=\exp\{-1/\tau[p^2+q^2+r^2+s^2-2(pq+ps+qr+qs)-2(\tau-1)(pr+qs)]\} \quad (5)$$

and equating coefficients.

INTERACTIONS

The general symmetric form of interaction

$$U=\sum_{\text{all pairs}} J(r_{ij})0_{ij}$$

with

$$0_{ij}=[(1-g-g_1-g_\sigma)P_{ij}{}^{(q)}+gP_{ij}+g_1 1_{ij}+g_\sigma P_{ij}{}^{(\sigma)}] \quad (6)$$

is used, where $P_{ij}{}^{(q)}$ is the space interchange operator, P_{ij} the space-spin operator, 1_{ij} the ordinary operator, and $P_{ij}{}^{(\sigma)}$ the spin operator. $J(r_{ij})$ has the form $J(r_{ij})=B\exp(-\alpha r_{ij}{}^2)$. The Coulomb operator has been omitted from the interaction Hamiltonian.

The values of the parameters proposed by Inglis[2]

$$B=-92,\quad \alpha=22,\quad g_0=g+g_\sigma=0.22,\quad \lambda=1+5g_1+4g_\sigma=1.25 \quad (7)$$

are used. These satisfy the requirements of scattering[5] and the observed energies of H^2 and He^4 as well as the limitation upon the g's proposed by Breit and Feenberg.[6] In some parts of the calculation it is required that g_1 and g_σ be known separately. For this purpose the values $g_1=0.03$ and $g_\sigma=0.025$ have been used. The effect of this detailed specification is not very great, since most of the contributions depend only upon the parameters g_0 and λ.

These conditions upon the g's have the important result for O^{16} of eliminating the prospect of any large contribution to the energy from the first-order calculation. One may obtain much greater binding in the first order by using an interaction not satisfying these conditions.

BINDING ENERGY

Using the interaction of Eq. (6), one obtains for the first order energy of O^{16}

$$E^{(0)}+E^{(1)}=69/4\sigma\alpha+24B(\sigma/\tau)^{\frac{1}{2}}[(-1+2g_0+\lambda)+2/\tau\cdot(2+g_0-\lambda)+(15/4)(1-g_0)/\tau^2] \quad (8)$$

[4] Obtained by an integration involving the generating function of the Hermite polynomials as described in *Introduction to Quantum Mechanics*, Pauling and Wilson (McGraw-Hill, 1935), particularly page 80.

[5] Breit, Condon and Present, Phys. Rev. **50**, 824 (1936).

[6] Breit and Feenberg, Phys. Rev. **50**, 850 (1936).

TABLE II. *Pairs of sets of ground state quantum numbers.*

TYPE	LIKE-PARTICLE LIKE-SPIN SETS	LIKE-PARTICLE UNLIKE-SPIN SETS	UNLIKE-PARTICLE LIKE-SPIN SETS	UNLIKE-PARTICLE UNLIKE-SPIN SETS
I		0_π^+ 0_ν^- 0_ν^+ 0_π^-	0_π^+ 0_ν^+ 0_π^- 0_ν^-	0_π^+ 0_ν^- 0_π^- 0_ν^+
II	0_π^+ 1_π^+ 0_ν^+ 1_ν^+ 0_π^- 1_π^- 0_ν^- 1_ν^- 0_π^+ 01_π^+ 0_ν^+ 01_ν^+ 0_π^- 01_π^- 0_ν^- 01_ν^- 0_π^+ 001_π^+ 0_ν^+ 001_ν^+ 0_π^- 001_ν^- 0_ν^- 001_ν^-	0_π^+ 1_π^- 0_ν^+ 1_ν^- 0_π^- 1_π^+ 0_ν^- 1_ν^+ 0_π^+ 01_π^- 0_ν^+ 01_ν^- 0_π^- 01_π^+ 0_ν^- 01_ν^+ 0_π^+ 001_π^- 0_ν^+ 001_ν^- 0_π^- 001_π^+ 0_ν^- 001_ν^+	0_π^+ 1_ν^+ 0_ν^+ 1_π^+ 0_π^- 1_ν^- 0_ν^- 1_π^- 0_π^+ 01_ν^+ 0_ν^+ 01_π^+ 0_π^- 01_ν^- 0_ν^- 01_π^- 0_π^+ 001_ν^+ 0_ν^+ 001_π^+ 0_π^- 001_ν^- 0_ν^- 001_π^-	0_π^+ 1_ν^- 0_ν^+ 1_π^- 0_π^- 1_ν^+ 0_ν^- 1_π^+ 0_π^+ 01_ν^- 0_ν^+ 01_π^- 0_π^- 01_ν^+ 0_ν^- 01_π^+ 0_π^+ 001_ν^- 0_ν^+ 001_π^- 0_π^- 001_ν^+ 0_ν^- 001_π^+
III		1_π^+ 1_π^- 1_ν^+ 1_ν^- 01_π^+ 01_π^- 01_ν^+ 01_ν^- 001_π^+ 001_π^- 001_ν^+ 001_ν^-	1_π^+ 1_ν^+ 1_π^- 1_ν^- 01_π^+ 01_ν^+ 01_π^- 01_ν^- 001_π^+ 001_ν^+ 001_π^- 001_ν^-	1_π^+ 1_ν^- 1_ν^+ 1_π^- 01_π^+ 01_ν^- 01_ν^+ 01_π^- 001_π^+ 001_ν^- 001_ν^+ 001_π^-
IV	1_π^+ 01_π^+ 1_π^- 01_π^- 1_ν^+ 01_ν^+ 1_ν^- 01_ν^- 1_π^+ 001_π^+ 1_π^- 001_π^- 1_ν^+ 001_ν^+ 1_ν^- 001_ν^- 01_π^+ 001_π^+ 01_π^- 001_π^- 01_ν^+ 001_ν^+ 01_ν^- 001_ν^-	1_π^+ 01_π^- 1_π^- 01_π^+ 1_ν^+ 01_ν^- 1_ν^- 01_ν^+ 1_π^+ 001_π^- 1_π^- 001_π^+ 1_ν^+ 001_ν^- 1_ν^- 001_ν^+ 01_π^+ 001_π^- 01_π^- 001_π^+ 01_ν^+ 001_ν^- 01_ν^- 001_ν^+	1_π^+ 01_ν^+ 1_π^- 01_ν^- 1_ν^+ 01_π^+ 1_ν^- 01_π^- 1_π^+ 001_ν^+ 1_π^- 001_ν^- 1_ν^+ 001_π^+ 1_ν^- 001_π^- 01_π^+ 001_ν^+ 01_π^- 001_ν^- 01_ν^+ 001_π^+ 01_ν^- 001_π^-	1_π^+ 01_ν^- 1_π^- 01_ν^+ 1_ν^+ 01_π^- 1_ν^- 01_π^+ 1_π^+ 001_ν^- 1_π^- 001_ν^+ 1_ν^+ 001_π^- 1_ν^- 001_π^+ 01_π^+ 001_ν^- 01_π^- 001_ν^+ 01_ν^+ 001_π^- 01_ν^- 001_π^+
Typical matrix element	$[1-2(g_1+g_\sigma)]\cdot f_{ABba}$ $+[-1+2(g_1+g_\sigma)]\cdot f_{ABab}$	$[1-g_0-(g_1+g_\sigma)]\cdot f_{ABba}$ $+[-g_0+(g_1+g_\sigma)]\cdot f_{ABab}$	$[1-(g_1+g_\sigma)]\cdot f_{ABba}$ $+[(g_1+g_\sigma)]\cdot f_{ABab}$	$[1-g_0-g_1]\cdot f_{ABba}$ $+[g_1]\cdot f_{ABab}$

where the term $69/4\sigma\alpha$ consists of the zeroth order energy $E_0^0=36\sigma\alpha$ plus contributions $-153\sigma\alpha/8$ and $3\sigma\alpha/8$ from the terms

$$(1/2N)\sum_a \nabla_a^2 - \tfrac{1}{2}\sum_a (\sigma\alpha)^2 r_a^2 \quad \text{and} \quad (1/N)\sum_{a>b}\nabla_a\cdot\nabla_b,$$

respectively, of the perturbation Hamiltonian. The minimum of this expression for the parameters given is $E^{(0)}+E^{(1)}=-19\ mc^2$ at $\sigma=0.5$.

The second-order contributions (which were calculated for a range of values of σ) have a variation with σ that makes the minimum of the second-order energy $E^{(0)}+E^{(1)}+E^{(2)}$ occur at $\sigma=0.7$. At this place the first-order energy becomes $E^{(0)}+E^{(1)}=-6\ mc^2$.[7]

The second-order energy $E^{(0)}+E^{(1)}+E^{(2)}$ is obtained by evaluating the expression

$$E^{(2)}=\sum_a (H_{a0}')^2/(E_0^0-E_a^0) \qquad (9)$$

containing the interactions H_{a0}' of excited states a in the zero-order representation with the ground state. Only states of even excitation may give a nonzero result, so that the procedure can be divided into a consideration of the contributions of the doubly excited states $E_D^{(2)}$, those of the

[7] The small magnitude of the first-order energy is caused by the influence of the spin dependent parameter g_0 and the limitation upon λ, as may be seen by employing an operator consisting of Majorana force plus ordinary force in the following proportions:

$$g_1=0.20,\quad g=0,\quad g_\sigma=0,\quad \lambda=2.00(\lambda>1.25,\ g_0=0),$$

which gives a first-order energy in the neighborhood of $-200\ mc^2$.

TABLE III. *Doubly and quadruply excited states differing from the ground state in two sets of quantum numbers.*

TYPE	QUANTUM NOS.	NO.	H_{20}'
I*	$2\pi^+$ $2\pi^-$	6	$+B(\sigma/\tau)^{\frac{1}{2}}[1-2g_0][f_{2200}]$
	$2\pi^+$ $02\pi^-$	12	$+B(\sigma/\tau)^{\frac{1}{2}}[1-2g_0][f^2_{2000}]$
	$11\pi^+$ $11\pi^-$	6	$B(\sigma/\tau)^{\frac{1}{2}}[1-2g_0][f^2_{1100}]$
II†	$3\pi^+$ $2\pi^+$	12	$B(\sigma/\tau)^{\frac{1}{2}}[1-2g_0][f_{3110}-f_{3201}]$
	$3\pi^+$ $02\pi^+$	24	$B(\sigma/\tau)^{\frac{1}{2}}[1-2g_0][f_{3010}-f_{3100}]$
	$12\pi^+$ $2\pi^+$	24	$B(\sigma/\tau)^{\frac{1}{2}}[1-2g_0][f_{2101}f_{2000}-f_{2110}f_{2000}]$
	$12\pi^+$ $02\pi^+$	24	$B(\sigma/\tau)^{\frac{1}{2}}[1-2g_0][f_{2100}f_{1010}-f_{2000}f_{1100}]$
	$12\pi^+$ $002\pi^+$	24	$B(\sigma/\tau)^{\frac{1}{2}}[1-2g_0][f^2_{2000}f_{1010}-f^2_{2000}f_{1100}]$
	$21\pi^+$ $11\pi^+$	24	$B(\sigma/\tau)^{\frac{1}{2}}[1-2g_0][f_{2110}f_{1100}-f_{2101}f_{1100}]$
	$111\pi^+$ $011\pi^+$	12	$B(\sigma/\tau)^{\frac{1}{2}}[1-2g_0][f^2_{1100}f_{1010}-f^2_{1100}]$
	$03\pi^+$ $11\pi^+$	24	$B(\sigma/\tau)^{\frac{1}{2}}[1-2g_0][f_{3100}f_{1100}-f_{3100}f_{1010}]$
	$021\pi^+$ $101\pi^+$	24	$B(\sigma/\tau)^{\frac{1}{2}}[1-2g_0][f_{2000}f^2_{1100}-f_{2000}f_{1100}f_{1010}]$
III	$2\pi^+$ $2\pi^-$	6	$\frac{1}{12}\sigma\alpha+B\cdot(\sigma/\tau)^{\frac{1}{2}}[1-2g_0][f_{2211}]$
	$11\pi^+$ $11\pi^-$	12	$\frac{1}{12}\sigma\alpha+B\cdot(\sigma/\tau)^{\frac{1}{2}}[1-2g_0][f_{1111}f_{1100}]$
	$02\pi^+$ $02\pi^-$	12	$B\cdot(\sigma/\tau)^{\frac{1}{2}}[1-2g_0][f_{2200}f_{1100}]$
	$011\pi^+$ $011\pi^-$	6	$B\cdot(\sigma/\tau)^{\frac{1}{2}}[1-2g_0][f^2_{1100}]$
	$2\pi^+$ $02\pi^-$	12	$B\cdot(\sigma/\tau)^{\frac{1}{2}}[1-2g_0][f_{2011}f_{2000}]$
	$02\pi^+$ $2\pi^-$	12	$B\cdot(\sigma/\tau)^{\frac{1}{2}}[1-2g_0][f_{2011}f_{2000}]$
	$02\pi^+$ $002\pi^-$	12	$B\cdot(\sigma/\tau)^{\frac{1}{2}}[1-2g_0][f^2_{2000}f_{1100}]$
	$3\pi^+$ $3\pi^-$	6	$B\cdot(\sigma/\tau)^{\frac{1}{2}}[1-2g_0][f_{3211}]$
	$03\pi^+$ $03\pi^-$	12	$B\cdot(\sigma/\tau)^{\frac{1}{2}}[1-2g_0][f_{3200}f_{1100}]$
	$12\pi^+$ $12\pi^-$	12	$B\cdot(\sigma/\tau)^{\frac{1}{2}}[1-2g_0][f_{2200}f_{1111}]$
	$012\pi^+$ $012\pi^-$	12	$B\cdot(\sigma/\tau)^{\frac{1}{2}}[1-2g_0][f_{2200}f^2_{1100}]$
	$21\pi^+$ $21\pi^-$	12	$B\cdot(\sigma/\tau)^{\frac{1}{2}}[1-2g_0][f_{2211}f_{1100}]$
III	$111\pi^+$ $111\pi^-$	6	$B(\sigma/\tau)^{\frac{1}{2}}[1-2g_0][f_{1111}f^2_{1100}]$
	$4\pi^+$ $2\pi^-$	6	$B(\sigma/\tau)^{\frac{1}{2}}[1-2g_0][f_{4211}]$
	$04\pi^+$ $02\pi^-$	12	$B(\sigma/\tau)^{\frac{1}{2}}[1-2g_0][f_{4200}f_{1100}]$
	$04\pi^+$ $002\pi^-$	12	$B(\sigma/\tau)^{\frac{1}{2}}[1-2g_0][f_{4000}f_{2000}f_{1100}]$
	$04\pi^+$ $2\pi^-$	12	$B(\sigma/\tau)^{\frac{1}{2}}[1-2g_0][f_{4000}f_{2011}]$
	$4\pi^+$ $02\pi^-$	12	$B(\sigma/\tau)^{\frac{1}{2}}[1-2g_0][f_{4011}f_{2000}]$
	$31\pi^+$ $11\pi^-$	12	$B(\sigma/\tau)^{\frac{1}{2}}[1-2g_0][f_{3111}f_{1100}]$
	$13\pi^+$ $11\pi^-$	12	$B(\sigma/\tau)^{\frac{1}{2}}[1-2g_0][f_{3100}f_{1111}]$
	$013\pi^+$ $011\pi^-$	12	$B(\sigma/\tau)^{\frac{1}{2}}[1-2g_0][f_{3100}f^2_{1100}]$
	$22\pi^+$ $2\pi^-$	12	$B(\sigma/\tau)^{\frac{1}{2}}[1-2g_0][f_{2211}f_{2000}]$
	$22\pi^+$ $02\pi^-$	12	$B(\sigma/\tau)^{\frac{1}{2}}[1-2g_0][f_{2011}f_{2200}]$
	$22\pi^+$ $002\pi^-$	12	$B(\sigma/\tau)^{\frac{1}{2}}[1-2g_0][f_{2011}f^2_{2000}]$
	$022\pi^+$ $2\pi^-$	6	$B(\sigma/\tau)^{\frac{1}{2}}[1-2g_0][f_{2011}f^2_{2000}]$
	$022\pi^+$ $02\pi^-$	12	$B(\sigma/\tau)^{\frac{1}{2}}[1-2g_0][f_{2200}f_{2000}f_{1100}]$
	$211\pi^+$ $011\pi^-$	6	$B(\sigma/\tau)^{\frac{1}{2}}[1-2g_0][f_{2011}f^2_{1100}]$
	$121\pi^+$ $101\pi^-$	12	$B(\sigma/\tau)^{\frac{1}{2}}[1-2g_0][f_{20}f_{1111}f_{1100}]$
	$3\pi^+$ $12\pi^-$	12	$B(\sigma/\tau)^{\frac{1}{2}}[1-2g_0][f_{3111}f_{2000}]$
	$03\pi^+$ $21\pi^-$	12	$B(\sigma/\tau)^{\frac{1}{2}}[1-2g_0][f_{3011}f_{2100}]$
	$03\pi^+$ $012\pi^-$	12	$B(\sigma/\tau)^{\frac{1}{2}}[1-2g_0][f_{3100}f_{2000}f_{1100}]$
	$12\pi^+$ $102\pi^-$	6	$B(\sigma/\tau)^{\frac{1}{2}}[1-2g_0][f^2_{2000}f_{1111}]$
IV**	$2\pi^+$ $11\pi^+$	12	$\sigma\alpha/16\sqrt{2}+B(\sigma/\tau)^{\frac{1}{2}}[1-2g_0]\times[f_{2101}f_{1100}-f_{2110}f_{1010}]$
	$11\pi^+$ $02\pi^+$	12	$\sigma\alpha/16\sqrt{2}+B(\sigma/\tau)^{\frac{1}{2}}[1-2g_0]\times[f_{2101}f_{1100}-f_{2110}f_{1010}]$
	$101\pi^+$ $011\pi^+$	12	$\frac{1}{12}\cdot(\sigma\alpha)+B(\sigma/\tau)^{\frac{1}{2}}[1-2g_0]\times[f^2_{1100}-f_{1100}f_{1010}]$
	$002\pi^+$ $11\pi^+$	12	$+B(\sigma/\tau)^{\frac{1}{2}}[1-2g_0]\times[f_{2000}f_{1010}f_{1100}-f_{2000}f_{1100}f_{1010}]$

* No doubly excited states of class 2 in this category because of the exclusion principle.
† Doubly excited states of class 2 are excluded by Pauli principle or lead to a duplication of states of class 1 already given in Table I.
** Quadruply excited states of this type have been omitted because of the lengthiness of the list.

TABLE IV. *Group of states associated with a given selection of directional quantum numbers (type IV).*

QUANTUM NUMBERS	NO.	H_{20}'
$\ldots 1_\pi{}^+\ldots 01_\pi{}^+\ldots 01_\pi{}^-\ldots 01_\nu{}^+\ldots 01_\nu{}^-\ldots$		ground state
$\ldots 2_\pi{}^+\ldots 11_\pi{}^+\ldots\ldots$	12	$\frac{\sigma\alpha}{16\sqrt{2}}+B(\sigma/\tau)^{\frac{1}{2}}\cdot[(1-2g_0)f_{2101}f_{1100}+(-1+2g_0)f_{2110}f_{1010}]$
$\ldots 2_\pi{}^+\ldots\ldots 11_\pi{}^-\ldots\ldots$	12	$\frac{\sigma\alpha}{16\sqrt{2}}+B(\sigma/\tau)^{\frac{1}{2}}\cdot[(1-g_0-(g_1+g_\sigma))f_{2101}f_{1100}+(-g_0+(g_1+g_\sigma))f_{2110}f_{1010}]$
$\ldots 2_\pi{}^+\ldots\ldots\ldots 11_\nu{}^+\ldots\ldots$	12	$\frac{\sigma\alpha}{16\sqrt{2}}+B(\sigma/\tau)^{\frac{1}{2}}\cdot[(1-(g_1+g_\sigma))f_{2101}f_{1100}+(g_1+g_\sigma)f_{2110}f_{1010}]$
$\ldots 2_\pi{}^+\ldots\ldots\ldots\ldots 11_\nu{}^-\ldots$	12	$\frac{\sigma\alpha}{16\sqrt{2}}+B(\sigma/\tau)^{\frac{1}{2}}\cdot[(1-g_0-g_1)f_{2101}f_{1100}+(g_1)f_{2110}f_{1010}]$
$\ldots 11_\pi{}^+\ldots\ldots\ldots 2_\pi{}^-\ldots\ldots\ldots$	12	$B(\sigma/\tau)^{\frac{1}{2}}\cdot[(-g_0+(g_1+g_\sigma))f_{2101}f_{1100}+(1-g_0-(g_1+g_\sigma))f_{2110}f_{1010}]$
$\ldots 11_\pi{}^+\ldots\ldots\ldots\ldots\ldots 2_\nu{}^+\ldots\ldots$	12	$B(\sigma/\tau)^{\frac{1}{2}}\cdot[(g_1+g_\sigma)f_{2101}f_{1100}+(1-(g_1+g_\sigma))f_{2110}f_{1010}]$
$\ldots 11_\pi{}^+\ldots\ldots\ldots\ldots\ldots\ldots 2_\nu{}^-\ldots$	12	$B(\sigma/\tau)^{\frac{1}{2}}\cdot[(g_1)f_{2101}f_{1100}+(1-g_0-g_1)f_{2110}f_{1010}]$
*$\ldots 2_\pi{}^-\ldots\ldots\ldots\ldots\ldots\ldots 11_\nu{}^+\ldots$	12	$B(\sigma/\tau)^{\frac{1}{2}}\cdot[(g)f_{2101}f_{1100}+(g_\sigma)f_{2110}f_{1010}]$
*$\ldots 11_\pi{}^-\ldots\ldots\ldots\ldots\ldots\ldots 2_\nu{}^+\ldots$	12	$B(\sigma/\tau)^{\frac{1}{2}}\cdot[(g_\sigma)f_{2101}f_{1100}+(g)f_{2110}f_{1010}]$

* These are excited states with $\Sigma m_{s\sigma}=0$, but where $\sum_\pi m_{s\pi}=\pm 1$ and $\sum_\nu m_{s\nu}=\mp 1$.

quadruply excited states $E_Q{}^{(2)}$, of the sextuply $E_S{}^{(2)}$, and so forth, where

$$E^{(2)}=E_P{}^{(2)}+E_Q{}^{(2)}+E_S{}^{(2)}+\cdots.$$

It is a further convenience to classify the excited states according to the manner in which their sets of one-particle quantum numbers differ from those of the ground state. Two classes need be considered. Those which differ from the ground state by only one set are listed in Table I together with their matrix elements $H_{0\alpha}'$.

Class 2 contains those differing from the ground state by two sets of quantum numbers. In the list of excited states of class 2 given in Table III, one state α will represent an entire group. The scheme is described in the following note.

TABLE V. *Numerical results* $\sigma=0.7$.*

TYPE OF EXC. STATE	FIRST-ORDER ENERGY $E^{(0)}+E^{(1)}$	SECOND-ORDER CONTRIBUTIONS TO $E^{(2)}$			3D.-ORDER CONT. OF DIAGONAL TERMS TO $E^{(3)}$	
		DOUBLY EXC. $E_D^{(2)}$	QUAD. EXC. $E_Q^{(2)}$	SEXT. EXC. $E_S^{(2)}$	DBLY. $E_D^{(3)}$	QPLY. $E_Q^{(3)}$
1 set differs from ground state		− 4. (−37.)	− 3.5	0.		
2 sets differ:						
Type I			− 5.8	− 2.		
Type II			− 9.3	− 4.		
Type III		− 8. (−14.)	− 7.7	0.		
Type IV		−14. (− 9.)	− 7.9	− 7.		
Totals	−6. (−271)	−26 (−60.)	−34.	−13.	+36	

$E^{(0)}+E^{(1)}=-6.\quad E^{(0)}+E^{(1)}+E^{(2)}\approx-79\quad E^{(0)}+E^{(1)}+E^{(2)}+E^{(3)}\approx-43$

* The terms in parentheses represent the part of the perturbation energy coming from the interaction alone.

The second class of states is best handled with the aid of Table II. Table II lists all pairs of ground state one-particle quantum number sets, grouped in a certain arrangement. Since each state of the second class may differ from the ground in two sets of quantum numbers, it can be classified by referring to the scheme in Table II according to which the two analogous sets of the ground state are grouped. Therefore, in what follows, such excited states will be said to belong to type I, II, III, or IV according to the corresponding classification of the differing sets of the ground state in Table II.

For every state α differing from the ground state by two sets: α: $\cdots(A_xA_yA_zm_s^a)\cdots(B_xB_yB_zm_s^b)\cdots$, ground state: $\cdots(a_xa_ya_zm_s^a)\cdots(b_xb_yb_zm_s^b)\cdots$, and hence belonging to type I, II, III, or IV according to the classification of the sets $(a_xa_ya_zm_s^a)(b_xb_yb_zm_s^b)$ in Table II, one obtains a matrix element containing the two integrals[8]

$$f_{ABab}=f_{(x)ABab}\cdot f_{(y)ABab}\cdot f_{(z)ABab}$$

and

$$f_{ABba}=f_{(x)ABba}\cdot f_{(y)ABba}\cdot f_{(z)ABba}. \tag{10}$$

Associated with α, there is a group of states α', α'', $\alpha'''\cdots$, all of the same type and each differing from α by a permutation of the numbers A, B, $m_s^am_s^b$ among the particles, space directions, and plus or minus directions of spin; each producing, however, the same integrals in its matrix element as α. The members α, α', α'', $\alpha'''\cdots$ of such a group correspond to the grouping of ground state quantum sets given in Table II for the type of state in question. By this correspondence, the number of states of a given type in a group can be counted and their net contribution to the second-order energy calculated in one operation, since it depends only upon the integrals f_{ABab} and f_{ABba}. (In the case of the doubly excited states, the operation is more complicated because of the presence, in the matrix elements, of terms coming from the fictitious oscillator potential.)

A subclassification exists within the group $(\alpha'\alpha''\cdots\alpha^r\cdots)$ according to whether a state α^r of the group differs from the ground state by a like-particle like-spin, like-particle unlike-spin, unlike-particle like-spin, or an unlike-particle unlike-spin pair of quantum number sets. Each state α^r corresponding to such a subclassification has a common matrix element. Such typical matrix elements are given at the bottom of Table II. Also, excited states with Σm_s (over-all particles) $=0$ but with $\Sigma_x m_{s_x}=\pm1$ and $\Sigma_y m_{s_y}=\mp1$ must be considered. The above remarks are illustrated by a complete example given in Table IV.

The second-order contributions to the energy have been computed for several values of the parameter σ. The value $\sigma=0.7$ gives the lowest second-order energy. For this value of σ, $E_D^{(2)}$ and $E_Q^{(2)}$ have been calculated and the respective contributions listed in Table V according to the types of states from which they come. The contribution of sextuply excited states of type I also was calculated. The $E_S^{(2)}$ of other types of states was estimated.[9] The figures in parentheses in Table V are the contributions from the interaction part of the perturbation term. Following the trend of these for the doubly, quadruply, and sextuply excited states, it appears that the octuply excited states may be neglected. To this degree of approximation, the second-order energy is $E^{(0)}+E^{(1)}+E^{(2)}\approx-79\,mc$.

The third-order energy $E^{(0)}+E^{(1)}+E^{(2)}+E^{(3)}$

[8] Here $f_{(x)ABab}=f_{\alpha\beta\gamma\delta}$ and $f_{(x)ABba}=f_{\alpha\beta\gamma\delta}$, where $\alpha=A_x$, $\beta=B_x$, $\gamma=a_x$, and $\delta=b_x$. The integrals containing quantum numbers assigned to the y and z directions have similar definitions except that y and z appear in place of x.

[9] This may be done as follows. On writing down the states in question, by inspection certain ones are found to be the most important. By evaluating these and using an average value for the states of small weight, a fair approach to the correct contribution may be found.

is obtained by computing

$$E^{(3)}=\sum_{a,b}\frac{H_{0a}'(H_{ab}'-\delta_{ab}H_{00}')H_{0b}'}{(E_0^0-E_a^0)(E_0^0-E_b^0)}. \quad (11)$$

Previous experience with this sum[1] indicates that the contributions of the diagonal elements

$$\sum_a\frac{(H_{0a}')^2(H_{aa}'-H_{00}')}{(E_0^0-E_a^0)^2}$$

are the most important, since the nondiagonal ones are smaller by a factor of the order of g_0 and, moreover, are apt to cancel. In those cases,[1] the third order was found to be small compared to the second-order results, hence a very critical determination was not necessary to obtain a good approximation.

For O^{16}, the third order appears to be fairly large and this method of approximation will not be so satisfactory. However, such an estimate of the size of the third-order elements was made by computing the average value of $H_{aa}'-H_{00}'$ for several of the most important groups of the doubly and quadruply excited states. The results showed $E_D^{(3)}$ and $E_Q^{(3)}$ to be positive and to range in magnitude from about one-third to one times the corresponding $E_D^{(2)}$ and $E_Q^{(2)}$, with the average factor about one-half. States of type II have important contributions to the third order in this approximation. Convergence appears to be slow, a result also shown by the calculation of Nakabayasi.[10]

From the value of $+36\,mc^2$ given by the third-order approximation, the third-order energy is $E^{(0)}+E^{(1)}+E^{(2)}+E^{(3)}\backsimeq -43\,mc$. If the contributions of successive orders follow this pattern, i.e., to alternate in sign with diminishing amplitude, the final energy will lie in this region (-43 to $-79\,mc^2$). If such is the case, the assumed interactions are unable to account for the observed binding energy of O^{16}.

I am very grateful to Dr. D. R. Inglis for suggesting the calculation and for much advice and assistance during its progress.

[10] Nakabayasi, Sci. Rep. Tohoku Imp. Univ. **25**, 1141 (1937).

DECEMBER 15, 1938 PHYSICAL REVIEW VOLUME 54

Nuclear Two-Body Variational Problem

WILLIAM RARITA, *Brooklyn College, Brooklyn, New York*

AND

ZAKA I. SLAWSKY, *University of Michigan, Ann Arbor, Michigan*

(Received October 3, 1938)

To test the reliability of variational calculations in nuclear problems the energy and wave function for the ground state of H^2 is first computed variationally and then compared to the results obtained from the exact solution. For an exponential potential and for a wave function in the form of an exponential times a power series, we find that the variational method is accurate and rapidly convergent.

THE final conclusions of a recent paper[1] on the light nuclei depend on the reliability of the variational calculation for the binding energy of H^3. The validity of the energy convergence involved has been doubted by G. Breit.[2] To ascertain the dependability of the variational method for nuclei and in particular for H^3, we propose to treat the analogous problem for the binding energy of H^2. The exact solution, well known for exponential potentials, will serve as a final check on the accuracy of the work.

For an exponential potential[3] $-Be^{-2r/b}$, the Schrödinger equation[4] is

[1] Rarita and Present, Phys. Rev. **51**, 788 (1937).
[2] G. Breit, Rev. Sci. Inst. **9**, 63 (1938).

[3] B is the depth and b is the range of the interaction. E is the energy of the ground state of H^2.
[4] Nuclear units are used in this paper, mc^2 for energy and $(\hbar^2/Mmc^2)^{\frac{1}{2}}$ for length.

TABLE I. *Variational method.*

n	0	5	8	9	∞
E	−4.064	−4.249	−4.326	−4.3277	−4.329

TABLE II. *Coefficients c_n.*

	$n=0$		
	c_0		$(2)^{-\frac{1}{2}}$
	$n=8$		
c_0	0.610,931,7	c_4	−0.14,211,334
c_1	0.275,063,75	c_5	0.001,466,599,7
c_2	−0.227,200,17	c_6	−0.000,085,291,88
c_3	0.078,688,57	c_7	0.000,002,582,657,4
		c_8	−0.000,000,031,314,096

$$-\left\{\frac{d^2}{dr^2}+\frac{2}{r}\frac{d}{dr}+Be^{-2r/b}\right\}\psi(r)=E\psi(r). \quad (1)$$

We first use the trial function $\psi(r)=c_0e^{-kr}$. The parameter k is fixed by minimizing the energy in (1). The arbitrary constant c_0 may be determined by the normalization of $\psi(r)$.

Transforming to $s=2kr$, we get from (1)

$$-\left\{4k^2\left[\frac{d^2}{ds^2}+\frac{2}{s}\frac{d}{ds}\right]+Be^{-\alpha s}\right\}\psi(s)=E\psi(s), \quad (2)$$

where $\alpha=1/bk$.

We now choose a general expansion for $\psi(s)$, consisting of a complete set of functions $u_n(s)$ with arbitrary coefficients c_n.

$$\psi(s)=\sum_{n=0}^{\infty}c_nu_n(s)=e^{-s/2}\sum_{n=0}^{\infty}c_ns^n. \quad (3)$$

The minimization of the energy leads to the usual secular determinant.[5]

Taking $B=241.8$, $k=4.3$ and $\alpha=1.205$ we get the results shown in Table I, in which n is the subscript of the last function $u_n(s)$ used in the expansion (4). The value for $n=\infty$ is obtained from the exact solution of the problem. As seen from the smallness and rapid diminution of the successive energy contributions, convergence has definitely set in for $n\geq 8$. We estimate the limiting energy to be $E=-4.329\pm0.001$ in excellent agreement with the value given by the exact solution.[6]

[5] Present, Phys. Rev. **50**, 635 (1936).

TABLE III. *Comparison of the wave function obtained variationally with that given by the exact solution.*

		$(2k)^{\frac{1}{2}}s\psi(s)$	
r/b	$NJ_p(\beta e^{-r/b})$	$n=8$	$n=0$
0.00	0	0	0
0.25	0.685,27	0.683,46	0.699,22
0.50	1.161,99	1.159,58	1.136,43
0.75	1.414,99	1.416,42	1.385,26
1.00	1.504,21	1.507,73	1.500,95
1.50	1.425,21	1.424,00	1.486,80
2.00	1.227,88	1.224,14	1.309,14
3.00	0.843,12	0.846,88	0.856,38
4.00	0.566,22	0.565,33	0.497,96
8.00	0.113,669	0.114,148	0.036,023
12.00	0.022,807	0.025,675	0.001,954
16.00	0.004,576	0.002,446	0.000,094,3
20.00	0.000,918	−0.006,533	0.000,004,26
24.00	0.000,184	−0.003,222	0.000,000,185

The wave function obtained variationally was computed for $n=0$ and $n=8$. $\psi(s)$ is normalized so that $\int_0^\infty\psi^2(s)s^2ds=1$. The values of the coefficients c_n are given in Table II.

It is valuable to compare the wave function obtained variationally with that given by the exact solution,[7] $NJ_p(\beta e^{-r/b})$. If $N^2\int_0^\infty J_p^2(\beta e^{-r/b})dr=1$, then $NJ_p(\beta e^{-r/b})=(2k)^{\frac{1}{2}}s\psi(s)$. The values of these functions for various values of r are entered in Table III. The agreement for the wave function is satisfying.

We wish to thank Professor G. Breit for suggesting and encouraging this work during his stay at the last summer symposium at the University of Michigan, where this paper was begun.

[6] For a Gaussian potential and for a wave function expandable in terms of Hermitian functions, the convergence is rather slow. Cf. Warren and Margenau, Phys. Rev. **52**, 1027 (1937).

[7] N is a constant of normalization. For its evaluation see Motz and Rarita, Phys. Rev. **52**, 271 (1937). $\beta=b(B)^{\frac{1}{2}}$. $J_p(x)$ is the Bessel function of the order p.

The Spacing of Energy Levels in Light Nuclei*

LLOYD MOTZ
Columbia University, New York, New York

AND

EUGENE FEENBERG
New York University, Washington Square College, New York, New York

(Received August 29, 1938)

The single particle model supplemented by a semi-empirical determination of the dependence of potential energy on symmetry character is used to obtain statistical information about the distribution of energy levels in light nuclei ($A \leq 16$). Table II shows the analysis of the low-lying configurations for $A=16$ into states with definite values of the orbital angular momentum and the symmetry character. Similar tables which we have prepared for values of $A<16$ have been omitted because of their length. Tables III to VI give the spin multiplet structure as a function of the symmetry type and the isotopic number $|N-Z|$. Finally, Tables VII and VIII show the dependence of the level spacing on total angular momentum and on $|N-Z|$ in the several isobaric series with $A=10$, 11, 12, and 13.

The most frequently occurring value of the orbital angular momentum is $L=2$ (D states). Levels with total angular momentum $F=2$ (even nuclei) and $F=5/2$ (odd nuclei) are most closely spaced. The level spacing is not a monotonic decreasing function of A; for example, in the series $A=4n$ and $|N-Z|=0$, Be^8 has 87 levels, C^{12} 192 and O^{16} has 60 in the energy range 0–23 Mev. In the series $A=4n$ the level density is considerably greater for $|N-Z|=2$ than for $|N-Z|=0$; the reverse is true in the series $A=4n+2$. For odd nuclei the level density is practically independent of $|N-Z|$ up to an excitation energy of 20 Mev, but for higher excitation energies it increases with $|N-Z|$.

INTRODUCTION

BARDEEN and Feenberg[1] have calculated the level spacing in intermediate nuclei using the statistical model supplemented by Wigner's[2] semi-empirical theory of the dependence of potential energy on symmetry character. The results are not immediately applicable to light nuclei ($A \leq 16$) because the statistical model does not provide a suitable set of single particle levels in this case. In place of the statistical model we utilize here the closely related model of single particle orbits determined by the motion of the individual particles in a spherically symmetrical potential well. The state of a particle is specified by the quantum numbers n, l, m_l, m_s. Protons and neutrons are treated on exactly the same footing.

The arrangement of the energy levels for the single particle model has been worked out by Elsasser[3] for an infinite well and by Margenau[4] for a finite well. In both cases the order of the levels is the same; the effect of the finite potential is to lower and compress all the levels which fall below the top of the well.[5]

The equations which determine the distribution of single particle levels in a finite potential well are given in reference 4. In the present calculations R, the radius, and V, the depth of the well, are chosen so that V is at least as large as the maximum kinetic energy in a completely degenerate neutron gas of 146 particles. This maximum kinetic energy can be computed from the relation

$$N=32\pi^2(RP)^3/9h^3, \tag{1}$$

where N is the number of neutrons and P is the maximum momentum. Placing $R=BA^{\frac{1}{3}}e^2/mc^2$, we obtain

$$\frac{1}{2M}P^2=\frac{18.7}{B^2}(N/A)^{\frac{1}{3}}mc^2. \tag{2}$$

With $A=238$ and $N=146$ (uranium), the maximum kinetic energy becomes $(13.5/B^2)\,mc^2$. If we choose $R=1.7\times10^{-13}A^{\frac{1}{3}}$ cm, B takes on the value 0.61, so that we have

$$\text{Maximum kinetic energy}=36.4\,mc^2 = 18.5 \text{ Mev}. \tag{3}$$

* Publication assisted by the Ernest Kempton Adams Fund for Physical Research of Columbia University.

[1] J. Bardeen and E. Feenberg, Phys. Rev. **54**, 809 (1938).
[2] E. Wigner, Phys. Rev. **51**, 947 (1937).
[3] W. M. Elsasser, J. de phys. et rad. **4**, 549 (1933).
[4] H. Margenau, Phys. Rev. **46**, 613 (1934).
[5] H. A. Bethe and R. F. Bacher, Rev. Mod. Phys. **8**, 173 (1936), Fig. 8.

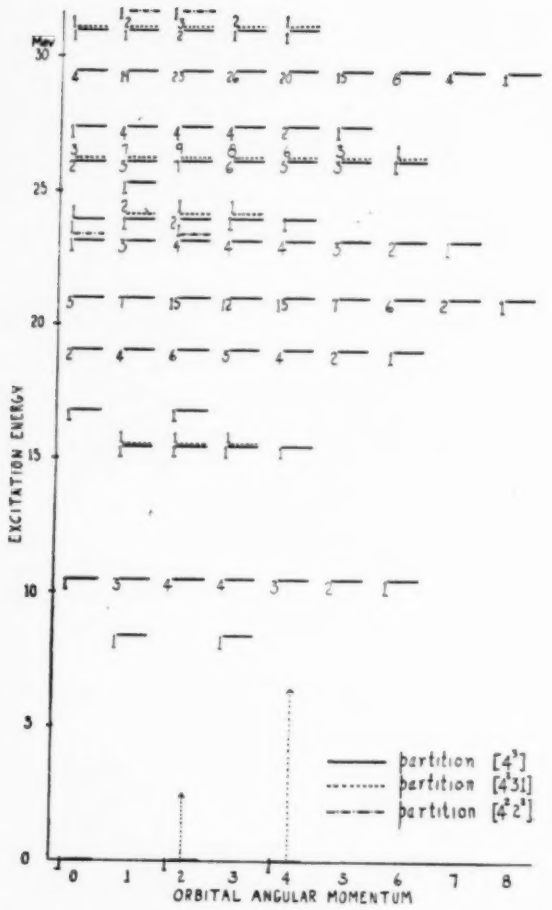

FIG. 1. The energy level diagram for C^{13}. The number to the left of each level is the multiplicity of the level in the configuration of space orbits. The dotted arrows indicate the splitting which occurs within the normal state configuration and the partition $[4^3]$ in the Hartree approximation (references 7, 8).

If we adopt this value for V, we find that the separation between the $1s$ and $2p$ levels in N^{15} is of the order of magnitude found experimentally for the lowest excitation energy of N^{15}, *viz:* six Mev, so that this procedure seems to be reasonable. To find the positions of all the levels for each nucleus, we should have to solve the equations given by Margenau.[4] Since we are not interested in the details of the single particle model, however, but rather in the rough statistical features, an approximate solution will suffice.

The influence of the finite depth of the well on the positions of the levels can be represented fairly well by a change of scale, i.e., by multiplying the levels found by Elsasser for a well of finite depth by a factor $C(A)$. This factor can be computed from the numerical results for the levels $(1s)$ and $(2p)$.

With $V=18.6$ Mev and $A=15$, we find

$$C(15)=0.621 \quad (1s \text{ level})$$
$$C(15)=0.595 \quad (2p \text{ level}).$$

If the variation of $C(A)$ for different levels is neglected, the dependence on A is given with sufficient accuracy in Table I. For the finite well the spacing between single particle levels is proportional to the factor $C(A)/A^{\frac{1}{3}}$ which varies less rapidly with A than $A^{-\frac{1}{3}}$.

THE SYMMETRY PROPERTIES OF NUCLEAR CONFIGURATIONS

The linear manifold in function space generated by the complete set of configurations containing a particles in the $1s$ shell, b particles in the $2p$ shell, etc. is transformed into itself by rotations and permutations of coordinates. Consequently, this manifold can be expressed as a sum of invariant subspaces which are associated with definite values of the total angular momentum and with definite symmetry types. Methods for determining the angular momentum values and the symmetry types contained in a configuration have been described and applied in several recent papers.[6, 7]

We have prepared tables of the multiplet structure (angular momentum values and symmetry types) associated with a number of low lying configurations for all the nuclei from $A=4$ to $A=16$. These tables include all the excited configurations up to about 30 Mev excitation energy for the heavier nuclei and considerably higher excitation energies for the lighter nuclei. Following the convention of atomic

[6] E. Wigner, Phys. Rev. **51**, 106 (1937).
[7] F. Hund, Zeits. f. Physik **105**, 220 (1937).

TABLE I. *Values of $C(A)$ for various values of A.*

A	4	5	6	7	8	9	10	11	12	13	14	15	16
$C(A)$	0.453	0.487	0.514	0.538	0.555	0.568	0.580	0.591	0.601	0.609	0.615	0.621	0.625

spectra, we use the symbols S, P, D, F, G, H, I, J, K for the angular momentum values 0, 1, 2, 3, 4, 5, 6, 7, 8, respectively. The various (irreducible) symmetry types are denoted in the usual manner by the partition symbols $[\lambda_1\lambda_2\cdots\lambda_i]$.

An example of an energy level diagram constructed from the tables is shown in Fig. 1. All levels associated with a given configuration and symmetry type are plotted with the same excitation energy. In making such diagrams one must take into account the total excitation energy of the configuration, which is equal to the sum of the kinetic energy excitations (denoted in the upper left-hand corners of Table II as Kinetic Excitation Energy), and the potential energy, which depends in a simple manner on the symmetry character. The latter term, which is indicated in Table II as Symmetry Displacement, can be computed from the formula

$$U=\tfrac{1}{2}A(A-1)\left\{\frac{\chi(P)}{\chi(1)}-\left(\frac{\chi(P)}{\chi(1)}\right)_0\right\}\mathfrak{L}(A) \quad (4)$$

found by Wigner[2] for the symmetry dependent part of the potential energy. Here $\chi(P)$ and $\chi(1)$ are the characters associated with an interchange and with the identity, respectively. The subscript 0 indicates the state of greatest symmetry permitted by the exclusion principle. The matrix element $\mathfrak{L}(A)$ must be determined empirically. To obtain numerical values for $\mathfrak{L}(A)$, we use the Li^8-Be^8 and $B^{12}-C^{12}$ mass differences in the relations

$$U(8)=4\mathfrak{L}(8)=(Li^8-Be^8)+(H^1-n^1)+\text{the Coulomb Energy Difference } (Be^8-Li^8), \quad (5)$$

$$U(12)=4\mathfrak{L}(12)=(B^{12}-C^{12})+(H^1-n^1)+\text{the Coulomb Energy Difference } (C^{12}-B^{12}). \quad (6)$$

With estimated Coulomb energy differences[8] of 1.5 Mev in Eq. (5) and 2.5 Mev in Eq. (6), the results are

$$\mathfrak{L}(8)\sim 4.2 \text{ Mev}, \qquad \mathfrak{L}(12)\sim 3.9 \text{ Mev}. \quad (7)$$

The value of $\mathfrak{L}(12)$ is uncertain by ± 0.2 Mev because the B^{12} mass value has not been definitely established. We have used the mean of the upper and lower bounds given by Livingston and Bethe.[9] Although $\mathfrak{L}(A)$ must fall off asymptotically as $1/A$, a much smaller variation for small values of A is not unreasonable.[2]

An estimate of the level density can be obtained from diagrams such as Fig. 1 if one knows the spin multiplicity associated with each symmetry type. Tables III, IV, V, and VI, computed by the methods described in references 1 and 6 give the structure of the spin multiplet as a function of $|N-Z|$ and the symmetry character. All partitions which differ only in the number of four groups have the same spin multiplet structure; also interchange of the numbers of three groups and unit groups leaves the spin multiplet structure unchanged. Thus, for example, the irreducible representations [44331], [331], and [311] are all associated with the same spin values.

[8] E. Feenberg and M. Phillips, Phys. Rev. **51**, 597 (1937).
[9] M. S. Livingston and H. A. Bethe, Rev. Mod. Phys. **9**, 373 (1937).

TABLE II. *The multiplet structure for $A=16$.*

Kinetic Excitation Energy in Mev	Configuration	Symmetry Displacement 0	$4\mathfrak{L}$	$6\mathfrak{L}$	$8\mathfrak{L}$	$10\mathfrak{L}$
		Partition [4⁴]	[4³31]	[4²22]	[4²21²] [4²3²]	[4²3²1²]
0	$(1s)^4(2p)^{12}$	S				
9.02	$(1s)^4(2p)^{11}(3d)$	FDP	FDP			
13.32	$(1s)^4(2p)^{11}(2s)$	P	P			
16.24	$(1s)^3(2p)^{12}(3d)$	D	D			
18.04	$(1s)^4(2p)^{10}(3d)^2$	$IHG^4F^3D^4P^2S^3$	$IH^2G^4F^3D^3P^2S^3$	$IHG^3F^3D^4PS^3$	$H^2G^2F^3D^3P^3$	GFD^3PS
19.85	$(1s)^4(2p)^{11}(4f)$	GFD	GFD			
20.54	$(1s)^3(2p)^{12}(2s)$	S	S			
22.34	$(1s)^4(2p)^{10}(3d)(2s)$	$GF^3D^3P^2S$	$G^2F^4D^2P^4S^2$	GFD^3PS	$GF^2D^3P^2S$	FDP
25.26	$(1s)^3(2p)^{11}(3d)^2$	$HG^2F^3D^3P^2S$	$H^2G^4F^3D^2P^2S^2$	HGF^3DP^2	$HG^2F^2D^3P^2S$	GFD^3PS
26.65	$(1s)^4(2p)^{10}(2s)^2$	DPS	$D^3P^2S^2$	DS	DPS	P

TABLE III. *The spin multiplet structure for* $|N-Z|=0$.

SYMMETRY TYPE [PARTITION]	SPIN 0	1	2	3	4
$[2]$	1	1			
$[1^2]$	1	1			
$[31]$	1	2			
$[2^2]$	2	1	1		
$[21^2]$	1	3	1		
$[1^4]$	1	1	1		
$[321]$	2	4	2		
$[31^3]$	1	3	2		
$[2^3]$	2	2	1	1	
$[2^21^2]$	2	4	3	1	
$[21^4]$	1	3	3	1	
$[3^21^2]$	2	3	3		
$[32^21]$	3	6	4	2	
$[321^3]$	2	6	6	2	
$[2^4]$	3	2	2	1	1
$[2^31^2]$	2	6	4	3	1
$[2^21^4]$	2	4	6	3	1

TABLE IV. *The spin multiplet structure for* $|N-Z|=2$.

SYMMETRY TYPE [PARTITION]	SPIN 0	1	2	3	4
$[2]$	1				
$[1^2]$		1			
$[31]$	1	1			
$[2^2]$	1	1			
$[21^3]$	1	2	1		
$[1^4]$		1	1		
$[321]$	2	3	1		
$[31^3]$	1	2	2		
$[2^3]$	2	1	1		
$[2^31^2]$	1	4	2	1	
$[21^4]$	1	2	3	1	
$[3^21^2]$	1	3	2		
$[32^21]$	3	5	3	1	
$[321^3]$	2	5	5	2	
$[2^4]$	2	2	1	1	
$[2^31^2]$	2	5	4	2	1
$[2^21^4]$	1	4	5	3	1

DISCUSSION OF THE TABLES

The multiplet structure for $A=16$ is shown in Table II. Similar tables which we prepared for $A<16$ are omitted because of their great length. An examination of these tables reveals that the number of levels with given orbital angular momentum attains a maximum at $L=2$ (D states) for almost all the configuration and partitions. A closely related dependence on the total angular momentum is found when the spin multiplicities (Tables III–VI) are taken into account. For even values of A the number of levels with given total angular momentum ($\mathbf{F}=\mathbf{S}+\mathbf{L}$) has a maximum at $F=2$; for odd values of A the maximum occurs at $F=5/2$. This is shown in Tables VII and VIII.

The tables indicate a general increase of level density with n in each nuclear series $A=4n$, $4n\pm1$, $4n+2$, up to about $A=12$ and then a sharp decrease. An estimate of this effect in the $4n$ series can be obtained by counting all the levels up to 23 Mev excitation energy for Be^8, C^{12}, and O^{16}. In making the count, the multiplicity of levels with definite values of the total angular momentum is determined from the orbital angular momentum and spin multiplicities in the usual manner. The numbers found are 87, 192 and 60, respectively, standing in the ratios 5 : 11 : 3.4. In the $4n+2$ series the maximum occurs at $A=10$, and in the $4n\pm1$ series at $A=11$. The reason for the decrease in the number of levels for A larger than 12 is to be found in the operation of the exclusion principle, which becomes very effective in cutting down the number of levels associated with the low lying configurations when the p shell is

TABLE V. *The spin multiplet structure for* $|N-Z|=1$.

SYMMETRY TYPE [PARTITION]	SPIN 1/2	3/2	5/2	7/2	9/2
$[1]$	1				
$[21]$	2	1			
$[1^3]$	1	1			
$[31^2]$	2	2			
$[2^21]$	3	2	1		
$[21^3]$	2	3	1		
$[321^2]$	4	5	2		
$[31^4]$	2	3	2		
$[2^31]$	4	3	2	1	
$[2^21^3]$	3	5	3	1	
$[3^21^3]$	3	4	3		
$[32^21^2]$	6	8	5	2	
$[321^4]$	4	7	6	2	
$[2^41]$	5	4	3	2	1
$[2^31^3]$	4	7	5	3	1

TABLE VI. *The spin multiplet structure for* $|N-Z|=3$.

SYMMETRY TYPE [PARTITION]	SPIN 1/2	3/2	5/2	7/2	9/2
$[21]$	1				
$[1^3]$		1			
$[31^2]$	1	1			
$[2^21]$	2	1			
$[21^3]$	1	2	1		
$[321^2]$	3	3	1		
$[31^4]$	1	2	2		
$[2^21]$	3	2	1		
$[2^21^3]$	2	4	2	1	
$[3^21^3]$	2	3	2		
$[32^21^2]$	5	6	3	1	
$[321^4]$	3	5	5	2	
$[2^41]$	4	3	2	1	
$[2^31^3]$	3	6	4	2	1

nearly or completely filled. It is clear that beyond O^{16} the level density should again rise rapidly with increasing A. Thus both C^{12} and Ne^{20} should have more levels in a given energy interval than O^{16}.

Tables VII and VIII show the dependence of level density on total angular momentum and $|N-Z|$ in the isobaric series with $A=10$, 11, 12 and 13. The results for the dependence on $|N-Z|$ are very similar to those found in reference 1 for nuclei of intermediate mass. One sees, for example, that the energy levels of B^{10} and B^{12} should be more closely spaced than those of Be^{10} and C^{12}, respectively. For odd nuclei the level density should increase with increasing $|N-Z|$ for sufficiently high excitation energies. This effect does not appear in Table VIII, where the dependence of level density on $|N-Z|$ is shown to be almost constant, because we have stopped at 23 Mev excitation energy. In the range 23–31 Mev the level density for $|N-Z|=3$ is double that for $|N-Z|=1$. In Tables VII and VIII the total number of energy levels obtained by counting all the levels for all values of the total angular momentum is included.

TABLE VII. *The dependence of the level spacing on total angular momentum and on $|N-Z|$ for the 4n and 4n+2 isobaric series. Total number of levels in the range 0–23 Mev excitation energy.*

F	$A=10$ $\|N-Z\|=0$	$\|N-Z\|=2$	$A=12$ $\|N-Z\|=0$	$\|N-Z\|=2$
0	76	34	17	95
1	201	78	32	250
2	261	108	48	318
3	245	89	37	287
4	177	66	30	205
5	101	31	14	132
6	46	14	10	73
7	16	3	3	29
8	4	1	1	8
9	1			1
Total	1128	424	192	1398

TABLE VIII. *The dependence of the level spacing on total angular momentum and on $|N-Z|$ for the $4n\pm1$ isobaric series. Total number of levels in the range 0–23 Mev excitation energy.*

F	$A=11$ $\|N-Z\|=1$	$\|N-Z\|=3$	$A=13$ $\|N-Z\|=1$	$\|N-Z\|=3$
1/2	96	92	84	79
3/2	156	158	136	119
5/2	175	168	140	122
7/2	143	135	113	104
9/2	92	87	73	66
11/2	48	45	41	33
13/2	19	18	18	13
15/2	5	5	6	4
17/2	1	1	1	1
Total	735	709	612	541

A different total number of levels is obtained if one first counts all the levels belonging to the various L values in a partition and then multiplies this number by the spin multiplicity of the partition being considered. The numbers obtained in this way are in all cases slightly larger than those given in the tables.

Recently an alpha-particle molecular model has been used by Wheeler[10] to construct energy level diagrams for C^{12} and O^{16}. The molecular model and the single particle model agree in predicting that the angular momentum value which occurs most frequently is $L=2$. However the former model gives O^{16} a level density double that of C^{12}, whereas with the latter model the same ratio of level densities is less than one-third. The two models also disagree in the magnitude of the level density for C^{12}, the molecular model yielding the greater density by a factor between two and three; agreement can be obtained by a reasonable adjustment of the parameters (nuclear radius, elastic force constants) available in the two methods of calculation.

[10] J. A. Wheeler, Phys. Rev. **52**, 1083 (1937).

The Dissociation of $C_2H_2D_2$ by Electron Impact

J. DELFOSSE* AND JOHN A. HIPPLE, JR.**
Palmer Physical Laboratory, Princeton University, Princeton, New Jersey
(Received October 29, 1938)

The dissociation of $C_2H_2D_2$ by electron impact has been investigated. In order to obtain a consistent interpretation of the distribution of intensities of the different ions produced, it is necessary to assume that there is a selective process favoring the splitting of the C−H bond over the splitting of C−D. The probability p introduced to take this effect into account has been calculated. From that value of p, an estimate of the intensity of the ion C_2HD has been made, which agrees with the measured one. In addition to that, it has been shown that the formation of CH_2 in C_2H_4 is a splitting of the double bond between the carbons alone, and that in the formation of H_2^+ in C_2H_4, the hydrogen atoms come from the same radical.

THE mass spectrometer has been used recently to a considerable extent to study the manner in which polyatomic molecules are dissociated by a single electron impact. This study has revealed many interesting facts, and in numerous instances it has been possible to correlate the results obtained with thermochemical data. In all this work, although the resultant charged fragments are readily identified, there is no means of telling how the bonds are broken when there are several atoms of the same kind in a molecule as, for example, in the hydrocarbons. The authors have been fortunate in obtaining a pure sample of di-deutero-ethylene, *cis* and *trans*, prepared by Jungers of the University of Louvain.[1] From the study of the Raman spectra, it was known that the sample was practically pure cis- and transdeutero-ethylene—the amount of asymmetric form present being less than 1.0 percent. A mass-spectrometer analysis of this gas was made[2] and the results compared with those obtained in C_2H_4 by Kusch, Hustrulid and Tate.[3] In this comparison, some striking differences were noted. An analysis of these differences leads to a better insight into the manner in which the ethylene molecule is dissociated.

The discussion in this paper is concerned with the relative intensities of the product ions, rather than their appearance potentials. The analysis was made with a mass spectrometer previously described in the literature.[4] To show how intensities measured on this instrument check with those of K, H and T, the analysis of C_2H_4 has been repeated and the results are given in Table I along with those of K, H and T. The results obtained in different runs with the same apparatus show considerably better agreement than would be indicated by the table where two different instruments are compared.

In Table II is shown the distribution of intensities obtained with $C_2H_2D_2$.

If we assume that the ions containing the same number of carbon and hydrogen atoms are equally probable, we can write:

$$\text{(a) } (C_2HD_2)=(C_2H_2D);\quad \text{(b) } (C_2H_2)=(C_2D_2);\quad \text{(c) } (C_2H)=(C_2D),$$

where the expression (C_2X_n) represents the intensity of the ion C_2X_n on the scale used in the table. But then, the relations (a) and (c) together with the data of Table II give:

$$(C_2D_2)=35-34=1;\quad (C_2H_2)=11-2.7=8.3;$$

and the relation (b) is not satisfied. Evidently, the assumption that it is equally as probable to

TABLE I. *Relative intensities of ions produced in C_2H_4 by 75-volt electrons. Comparison of our results with those of Kusch, Hustrulid and Tate.*

ION	K, H, T	AUTHORS	ION	K, H, T	AUTHORS
C_2H_4	100	100	CH_2	0.6	0.5
C_2H_3	57.2	60	CH_2	5.2	4.8
C_2H_2	51.3	57	CH	2.5	2.65
C_2H	8.8	9.6	C	1.7	1.4
C_2	2.7	3.1			

* C. R. B. Fellow.
** Now at Westinghouse Research Laboratories, East Pittsburgh, Pennsylvania.
[1] DeHemptinne, Jungers and Delfosse, J. Chem. Phys. 6, 319–324 (1938).
[2] Delfosse and Hipple, Phys. Rev. 53, 683 (*A*) (1938).
[3] Kusch, Hustrulid and Tate, Phys. Rev. 52, 843 (1937).
[4] Bleakney and Hipple, Phys. Rev. 53, 521 (1938).

TABLE II. *Relative intensities of ions produced in* $C_2H_2D_2$ *by 75-volt electrons.*

Ion	Mass	Int.	Ion	Mass	Int.
$C_2H_2D_2$	30	100	C_2	24	2.7
C_2HD_2	29	34	CHD	15	4.8
C_2H_2D, C_2D_2	28	35	CD	14	2.15
C_2HD	27	32.5	CH	13	1.08
C_2H_2, C_2D	26	11	C	12	1.65
C_2H	25	2.7			

knock off a hydrogen as a deuterium atom is not justified.

The solution to the problem appears to be indicated by the lower mass region. At mass 13, there is a peak which can be attributed only to CH. The peak at mass 14 could conceivably be attributed to CD or CH_2. However, in view of the structure of this molecule, it would appear to be more likely to form CD than CH_2. The absence of a corresponding CD_2 peak is a confirmation of this view. It, therefore, seems legitimate to attribute all of mass 14 to CD. Now it is interesting to note that the intensity of mass 14 is twice that of mass 13 (within the experimental error). That is to say:

$$(CD)/(CH)=2.15/1.08=2.$$

This indicates that in the breakup of the parent molecule, it is twice as probable for the carbon atom to retain a deuterium atom as it is for it to retain a hydrogen atom when there is a choice.

It is now of interest to investigate whether the distribution of intensities in the upper mass region can be explained on the same basis. It is immediately evident that the difficulties mentioned earlier will be helped considerably by again assuming that the relative probability is the same as in the lower region. However, it is possible to use the intensity distribution to determine the relative probability. Let the probability of forming an ion by removing a deuterium and a hydrogen atom be p and 1, respectively. Then from Table II, the following relations are obtained:

(1) $(C_2HD_2)=34$,
(2) $(C_2H_2D)+(C_2D_2)=35$,
(3) $(C_2H_2)+(C_2D)=11$,
(4) $(C_2H)=2.7$,
(5) $p(C_2HD_2)=(C_2H_2D)$,
(6) $p^2(C_2D_2)=(C_2H_2)$,
(7) $p(C_2D)=(C_2H)$,

which gives for p the value $p=0.33$, and for the intensities of the different ions, the following values:

$$(C_2HD_2)=34, \quad (C_2H_2)=2.6,$$
$$(C_2H_2D)=11, \quad (C_2H)=2.7,$$
$$(C_2D_2)=24, \quad (C_2D)=8.2.$$

Furthermore, from these data an estimate of the intensity (C_2HD) can be made. Although the formation of C_2HD is four times as probable as that of C_2D_2, the factor p has to be taken into account in correcting for the intrinsic probabilities of D and H, which gives

$$(C_2HD)=4p(C_2D_2) \quad \text{or} \quad (C_2HD)=32,$$

in good agreement with the experimental value given in Table II. Finally, it is interesting to compare the relative abundances of the ions C_2H_n in C_2H_4 with the sum of the relative abundances of the corresponding ions in $C_2H_2D_2$.

TABLE III. *Comparison of relative abundances of corresponding ions in* C_2H_4 *and* $C_2H_2D_2$.

(C_2H_4)	100	$(C_2H_2D_2)$	100
(C_2H_3)	60	$(C_2H_2D)+(C_2HD_2)$	45
(C_2H_2)	57	$(C_2H_2)+(C_2D_2)+(C_2HD)$	59
(C_2H)	9.6	$(C_2H)+(C_2D)$	10.9
(C_2)	3.1	(C_2)	2.7
(CH_2)	4.8	(CHD)	4.81
(CH)	2.65	$(CH)+(CD)$	3.22
(C)	1.4	(C)	1.65

This table shows that except for C_2H_3, the relative abundances are nearly the same in both C_2H_4 and $C_2H_2D_2$.

From the preceding remarks, it is evident that with the introduction of a constant, p, a consistent interpretation of the intensity distribution is obtained. Whether the probability p is 0.5 or 0.3 or some intermediate value (or not the same in the upper mass region as in the lower one) this evidence does show that there is a selective process favoring the splitting of the C−H bond over the splitting of C−D.

Another remark has to be made with regard to Table III. The fact that the relative abundance of the ions CH_2 in C_2H_4, and CHD in $C_2H_2D_2$ is the same, together with the absence of any ion CD_2 is evidence that the formation of CH_2 from C_2H_4 by electron impact is a splitting of the double bond between the carbons alone. The

study of molecular hydrogen ions produced from the ethylene $C_2H_2D_2$ is also of interest. It is possible to tell whether the molecular hydrogen ions formed come from two atoms belonging to the same radical, or whether all the combinations of hydrogen atoms are possible. In the first case the ratio DD/HD would be 0, and in the second case it would be $\frac{1}{4}$. Using first a hot tungsten filament as electron source, the ratio obtained was $\frac{1}{4}$. But because of a possible thermal decomposition of the ethylene against the filament, the same experiment was repeated with an oxide coated filament, and gave the result 1/15. The comparison between the two results shows clearly that in the first experiment the most important role was played by the molecular hydrogen ion coming from thermodissociation. With the oxide coated filament, this effect is far less important. In view of this, we can assume the true ratio to be less than 1/15. This is strongly in favor of the first assumption mentioned before.

The authors take this opportunity to thank Professor Walker Bleakney for many helpful discussions.

DECEMBER 15, 1938 PHYSICAL REVIEW VOLUME 54

An Atomic Distribution Function for Liquid Sodium

C. N. WALL*
North Central College, Naperville, Illinois
(Received October 6, 1938)

An atomic distribution function for liquid sodium is developed. A simple liquid model of the quasi-solid type is assumed in which each atom is trapped by its immediate neighbors in a small spherical cell within which it is free to move about. The resulting distribution function contains three parameters which are evaluated by fitting the function to the experimental distribution curves for liquid sodium given by Trimble and Gingrich. An approximate value of the free volume of the liquid as a function of the absolute temperature is obtained. By means of the free energy equation the entropies and latent heats of fusion and vaporization for liquid sodium are calculated and compared with the observed values.

INTRODUCTION

IN a recent article, Trimble and Gingrich[1] have given atomic distribution curves for liquid sodium at temperatures of 100°C and 400°C. These curves, which are derived by an analysis of the x-ray diffraction patterns of the liquid,[2] give the radial atomic configuration in the liquid. Presumably they should yield important information about the liquid state of sodium.

For a profitable use of atomic or molecular distribution curves, it is of considerable value to represent them by an analytical function. Prins[3] has proposed a series of error functions for the general liquid distribution function. This representation is based upon a "smeared out" model of the corresponding crystalline solid. Bernal[4] has generalized the treatment to some extent. For the case of monatomic or quasi-monatomic liquids, assumed to possess molecular homogeneity,[5] he has shown that the distribution function of a liquid can be derived from a knowledge of its intermolecular potential function. Unfortunately this potential function is not known in many cases, or, if known, is expressed in a form so complex as to destroy its utility.

The purpose of this paper is to develop a distribution function for liquid sodium somewhat different in form from that proposed by Prins. A direct consequence of this development is the determination of the so-called free volume of liquid sodium.

FREE ENERGY EQUATION AND FREE VOLUME

The concept of free volume has been very fruitful in the study of liquids and gases. Guggen-

* On leave of absence at M. I. T. during 1937–38.

[1] Trimble and Gingrich, Phys. Rev. **53**, 278 (1938); also, Tarasov and Warren, J. Chem. Phys. **4**, 236 (1937).

[2] Zernike and Prins, Zeits. f. Physik **41**, 184 (1927).

[3] Prins, Physica **3**, 147 (1936).

[4] Bernal, Trans. Faraday Soc. **33**, 27 (1937); also, Kirkwood, J. Chem. Phys. **3**, 300 (1935).

[5] All interior molecules of the liquid have statistically equivalent molecular environments.

heim[6] has shown that its use effects an essential simplification in the expression for the free energy (Helmholtz) of a simple liquid. It is assumed that the potential energy of a simple liquid has a pronounced minimum for a certain set of molecular configurations, and is effectively infinite for all others. This particular set of configurations is characterized by assigning to each molecule in the liquid a small volume v within which it is more or less free to move independently of the other molecules without appreciably altering the condition of minimum potential energy for the entire assembly. This volume may be called the free volume of the molecule. On this assumption the free energy of a simple liquid is given approximately by the equation,[7]

$$F=-NkT[\ln J(T)+\ln v]+\Phi. \qquad (1)$$

In Eq. (1) Φ is the minimum potential energy of the molecular assembly and $J(T)$ is the ordinary partition function for the molecules. The other symbols have their usual significance. For a monatomic liquid at moderate temperatures $J(T)$ may be assumed to take its classical value, $(2\pi mkT/h^2)^{\frac{3}{2}}$.

According to Guggenheim Eq. (1) is valid either for a quasi-solid model of a liquid in which the molecules are not allowed to change places, or for an imperfect gas model in which the molecules are allowed to change places. Eyring and his associates,[8] who have made material contributions to the theory of the liquid state, appear to hold a slightly different point of view on this matter.[9]

Lennard-Jones and Devonshire[10] have been very successful in accounting for the main features of the liquid and gaseous states of those molecular aggregates whose molecular potential may be satisfactorily represented by the well-known function, $\lambda/r^{12}-\mu/r^6$. They consider each molecule in the liquid or dense gas as being temporarily trapped in a cell by its immediate neighbors. The effective volume of the cell constitutes the free volume for the molecule. Thus Φ in Eq. (1) may be determined as a function of the specific volume and v as a function of the specific volume and temperature of the liquid. Hence the free energy is known.

Eventually it may be possible to apply some such method as that of L.-J. and D. to liquid sodium. A fairly good approximation for Φ (in the solid state) appears to be available.[11] A corresponding expression for v is needed. It will be shown that an analysis of the atomic distribution curves for liquid sodium apparently yields good values of v at 100°C and 400°C and, in addition, gives the approximate variation of v with the absolute temperature.

Development of Atomic Distribution Function

In developing the atomic distribution function for liquid sodium a quasi-solid model for the liquid is adopted. This model is essentially equivalent to that proposed by L.-J. and D., i.e., each atom in the liquid is assumed to be trapped

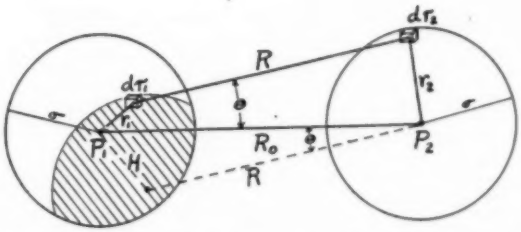

FIG. 1. Atomic cells of two neighboring atoms. The shaded portion of the left sphere represents the volume integral in Eq. (6). It is generated by the motion of $d\tau_1$ when the line R of fixed length and direction is moved parallel to itself through all positions consonant with the condition that $d\tau_1$ and $d\tau_2$ remain in their respective spheres.

(at least temporarily) in a small spherical cell by its immediate neighbors. In order to proceed it is necessary to make some assumption concerning the form of the potential energy function within the cell. The papers of L.-J. and D. suggest two general types of functions. One is the ordinary parabolic type used extensively in the theory of

[6] Guggenheim, Proc. Roy. Soc. **A135**, 181 (1932); also, Fowler, *Statistical Mechanics* (second edition), p. 522 *et seq.*

[7] Not valid for helium and hydrogen.

[8] Eyring and Hirschfelder, J. Phys. Chem. **41**, 249 (1937); Kincaid and Eyring, J. Chem. Phys. **5**, 587 (1937); Hirschfelder, Stevenson and Eyring, J. Chem. Phys. **5**, 897 (1937).

[9] According to Eyring *et al.* the communal sharing of free volume by the molecules in a liquid contributes a term, $-NkT$, to its free energy. Cf. Gurney and Mott, J. Chem. Phys. **6**, 222 (1938); Fowler, *Statistical Mechanics* (second edition), pp. 191–192.

[10] Lennard-Jones and Devonshire, Proc. Roy. Soc. **A163**, 53 (1937); **A165**, 1 (1938). Lennard-Jones, Physica **4**, 941 (1937). Wheeler, Ind. Acad. Sc. Proc. **4**, 291 (1936).

[11] Fröhlich, Proc. Roy. Soc. **A158**, 97 (1937); also, Bardeen, Phys. Rev. **53**, 683 (1938).

solids. The other is the discontinuous box type in which the potential is practically constant throughout the cell except at the cell boundary where it becomes infinite. Since this latter form appears to give a better correspondence with the experimental data, it will be assumed in the following development.[12]

Let the distance between the cell centers P_1 and P_2 of two nearest neighboring atoms in the liquid be R_0 as shown in Fig. 1. About each center let us describe a sphere of radius σ. Let the volume v of each sphere represent the free volume for the atom trapped within it. The probability that atom 1, i.e., its center, lies in the volume element $d\tau_1$ having coordinates x_1, y_1, z_1 with respect to P_1 may be written in the form,

$$p(x_1, y_1, z_1)d\tau_1/v, \tag{2}$$

where $p=\begin{cases}1 \text{ if } r_1=(x_1^2+y_1^2+z_1^2)^{\frac{1}{2}}<\sigma\\ 0 \text{ if } r_1>\sigma\end{cases}$.

A corresponding expression may be written for atom 2.

The probability of atom 1 lying in $d\tau_1$ and atom 2 lying in $d\tau_2$ will be[13]

$$p(1)p(2)d\tau_1 d\tau_2/v^2. \tag{3}$$

Let us replace the coordinates x_2, y_2, z_2 by a new set X, Y, Z defined by the linear relations,

$$\begin{aligned}x_2&=x_1+X-X_0,\\ y_2&=y_1+Y-Y_0,\\ z_2&=z_1+Z-Z_0,\end{aligned} \tag{4}$$

where X_0, Y_0, Z_0 are the relative coordinates of the cell centers, and X, Y, Z are the relative coordinates of the two atoms at $d\tau_1$ and $d\tau_2$. Making these transformations in expression (3), we get,

$$(1/v^2)p(x_1, \cdots)p(x_1+X-X_0, \cdots)\times dx_1dy_1dz_1dXdYdZ. \tag{5}$$

The probability of relative coordinates X, Y, Z occurring between the two atoms may be obtained from (5) by integrating over all x_1, y_1, z_1 with fixed X, Y, Z, *viz.*,

$$(1/v^2)dXdYdZ\int\int\int p(x_1, \cdots)\times p(x_1+X-X_0, \cdots)dx_1dy_1dz_1. \tag{6}$$

If we bear in mind the conditions to which the p function is subjected in (2), it is clear that the volume integral in expression (6) is equal to the volume common to two intersecting spheres, each of radius σ, whose centers are separated by the distance,

$$\begin{aligned}H&=[(X-X_0)^2+(Y-Y_0)^2+(Z-Z_0)^2]^{\frac{1}{2}}\\ &=[R^2+R_0^2-2RR_0\cos\theta]^{\frac{1}{2}},\end{aligned}$$

where θ is the angle between R and R_0 as shown in Fig. 1. The volume common to the two intersecting spheres is

$$v\left[1-\frac{3H}{4\sigma}+\frac{H^3}{16\sigma^3}\right].$$

Substituting this quantity in expression (6) and writing dX, dY, dZ in spherical coordinates, we get,

$$1/v\left[1-\frac{3H}{4\sigma}+\frac{H^3}{16\sigma^3}\right]R^2\sin\theta dRd\theta d\phi. \tag{7}$$

Expression (7) is the probability that the two atoms will have relative spherical coordinates of R, θ, ϕ, the line joining the cell centers giving the direction of the polar axis. A direct integration of this expression over θ and ϕ gives the probability of finding the two atoms within a distance R to $R+dR$ of each other. The integration limits for ϕ and θ are, respectively, 0 to 2π and

$$0 \text{ to } \theta_0=\cos^{-1}\left[\frac{R^2+R_0^2-4\sigma^2}{2RR_0}\right].$$

The integration gives[14]

$$\frac{2\pi R^2dR}{v}\left[\frac{4\sigma^2-(R_0-R)^2}{2RR_0}+\frac{|R_0-R|^3-(2\sigma)^3}{4\sigma RR_0}-\frac{|R_0-R|^5-(2\sigma)^5}{80\sigma^3RR_0}\right]. \tag{8}$$

[12] The development given is based upon classical principles. It is unlikely that the use of the quantum theory would lead to very different results except for light atoms or low temperatures. *Vide*, e.g., Slater, Phys. Rev. **38**, 237 (1931); also, Uhlenbeck and Beth, Physica **3**, 729 (1936).

[13] The events are assumed to be independent.

[14] It is clear from the development that (8) is only valid for the interval, $R_0-2\sigma\leqq R\leqq R_0+2\sigma$. Outside this interval the probability in question is zero.

A rearrangement of terms in this expression and the substitution, $v=4\pi\sigma^3/3$, give

$$\frac{3RdR}{5R_0\sigma}\left[1-\frac{5(R_0-R)^2}{4\sigma^2}\times\left\{1-\frac{|R_0-R|}{2\sigma}+\frac{|R_0-R|^3}{40\sigma^3}\right\}\right]. \quad (9)$$

Let N_0 be the average number of nearest neighbors surrounding an atom in the liquid, and let $\rho_0(R)$ be the density of these atoms at distance R from the given atom. Then the probability of finding a neighboring atom at distance R from this given atom is $(4\pi R^2\rho_0(R)dR)/N_0$. This quantity must equal that given in (9), hence,

$$4\pi R\rho_0(R)=\frac{3N_0}{5\sigma R_0}\left[1-\frac{5(R_0-R)^2}{4\sigma^2}\times\left\{1-\frac{|R_0-R|}{2\sigma}+\frac{|R_0-R|^3}{40\sigma^3}\right\}\right], \quad (10)$$

for $R_0-2\sigma\leqq R\leqq R_0+2\sigma$.

$4\pi R\rho_0(R)=0$, for all other R.

In Eq. (10) $\rho_0(R)$ represents the density of the nearest neighbors of any atom, i.e., the density of those atoms whose cell centers lie on the first coordination sphere of radius R_0. It is assumed that this density is practically the total density of atoms for the interval, $0\leqq R\leqq R_0$. Thus in this interval Eq. (10) gives the atomic distribution function of the liquid.

In order to extend the range of the distribution function it is necessary to consider density contributions from atoms whose cell centers lie on coordination spheres of order higher than the first. If ρ_i is the density contribution of the N_i atoms lying on the $i+1$ coordination sphere of radius R_i, then the total density $\rho(R)$ is given by the equation,

$$4\pi R\rho(R)=4\pi R\sum_{i=0}\rho_i(R), \quad (11)$$

where $\rho_i(R)$ is given by an equation of the same form as Eq. (10) with N_0 and R_0 replaced by N_i and R_i.

On the assumption of molecular homogeneity in a liquid it seems clear that N_i and R_i should be functions of N_0 and R_0. Bernal[4] has pointed this out and has given rough estimates of N_i and R_i for the second and third coordination spheres in terms of those of the first. So far as the author is aware, the general problem has not been solved. Assuming the existence of such relationships there remain in Eqs. (10) and (11) the three parameters σ, N_0 and R_0, to be determined. In the next section of this paper it will be shown that approximate values of these parameters for liquid sodium may be obtained by an analysis of its atomic distribution curves.

Determination of Parameters

The method of determining the parameters σ, N_0 and R_0 for liquid sodium is simply that of fitting the distribution function given in Eq. (10) to the experimental values given by T. and G. Because of the difficulty of obtaining reliable values of N_i and R_i in terms of N_0 and R_0, Eq. (10) is used, and hence, only that part of the experimental curve for which $R\leqq R_0$.[15, 16]

Let us rewrite Eq. (10) in the form,

$$\sigma^2=\frac{y_0}{y_0-y}\frac{5(R_0-R)^2}{4}\times\left[1-\frac{|R_0-R|}{2\sigma}+\frac{|R_0-R|^3}{40\sigma^3}\right], \quad (12)$$

where $y=4\pi R\rho_0(R)$ and $y_0=(3N_0)/(5\sigma R_0)$. It is clear that y_0 is the maximum value of y. By constructing a table of $y\sim R$ values obtained from the $4\pi R^2\rho(R)$ curve given by T. and G., it is an easy matter to determine values of y_0 and R_0. By substitution of these values of y_0 and R_0 in Eq. (12) and use of successive pairs of experimental values of y and R, the equation may be solved for σ by iteration. The constancy of σ for different $y\sim R$ values is an indication that Eq. (10) is approximately correct, at least. The results of the calculation are shown in Table I.

An examination of Table I shows that the variation in the values of σ for each distribution curve is small. There is very little change in

[15] Unfortunately this portion of the curve is influenced considerably by the large angle part of the experimental scattering curve; thus its exact shape is not as reliable as would be desirable.

[16] It is assumed that the overlap from the second coordination sphere of atoms is negligible up to this point.

TABLE I. *Calculated values of σ.*

	R in A	y(exp.)	σ in A
	A. Temperature 100°C		
max.	3.79	2.45	
1	3.00	0.39	0.62
2	3.20	0.88	0.60
3	3.40	1.57	0.60
4	3.60	2.17	0.58
			Ave. 0.60
$R_0=3.79$A		$y_0=3N_0/5\sigma R_0=2.45$	
$\sigma=0.60$A		$\sigma/T^{\frac{1}{2}}=0.0311$	
$N_0=9.28$ atoms			

	R in A	y(exp.)	σ in A
	B. Temperature 400°C		
max.	3.80	1.84	
1	3.00	0.56	0.76
2	3.20	0.99	0.78
3	3.40	1.37	0.76
			Ave. 0.77
$R_0=3.80$A		$y_0=1.84$	
$\sigma=0.77$A		$\sigma/T^{\frac{1}{2}}=0.0297$	
$N_0=8.95$ atoms			

the values of N_0 and R_0 in going from 100°C to 400°C for liquid sodium, but there appears to be a considerable increase in the value of σ, and hence, in the free volume of the liquid. It is found that $\sigma/T^{\frac{1}{2}}$, T being the absolute temperature of the liquid, has practically the same value at 100°C and 400°C. Consequently it seems safe to assume that $\sigma/T^{\frac{1}{2}}$ is constant over the indicated temperature range.

It is of interest to compare the values of $y=4\pi R\rho(R)$ as calculated by Eqs. (10) and (11), from the parameter values given in Table I-A, with those values given by the experimental curve of T. and G. for 100°C. In the interval, $0\leqq R\leqq R_0$, Eq. (10) is used. In order to extend the range beyond $R=R_0$, Eq. (11) is used along with the approximate values of N_1, N_2, R_1 and R_2 as given by Bernal.[4] The results are shown in Table II and Fig. 2.

APPLICATIONS

It is now possible to make use of the free energy equation (1) in order to determine some of the properties of liquid sodium. The free volume per atom of liquid sodium may be written in the form, $v=4\pi\sigma^3/3=bT^{\frac{1}{2}}$, since σ is approximately proportional to $T^{\frac{1}{2}}$. The value of b is 126×10^{-30} cm^3 degrees$^{-\frac{1}{2}}$ from Table I-A. $J(T)$ is assumed to take its classical value, $[2\pi mkT/h^2]^{\frac{1}{2}}$. Making these substitutions in Eq. (1), we obtain for the free energy of liquid sodium

$$F=-NkT\left[\ln\left(\frac{2\pi mkT}{h^2}\right)^{\frac{1}{2}}+\ln(bT^{\frac{1}{2}})\right]+\Phi. \quad (13)$$

In Eq. (13) both b and Φ are unknown functions of the specific volume of the liquid. Hence it is not possible to obtain the equation of state. It is, however, quite feasible to determine the entropy of liquid sodium by means of the relation, $S=-(\partial F/\partial T)_V$. Using this relation, the entropy is given by the equation,[17]

$$S=-\left(\frac{\partial F}{\partial T}\right)_V=Nk\left[\ln\left(\frac{2\pi mkT}{h^2}\right)^{\frac{1}{2}}+\ln(bT^{\frac{1}{2}})+3\right]. \quad (14)$$

TABLE II. *Comparison of values of $y=4\pi R\rho(R)$ as calculated by Eqs. (10) and (11) from the parameter values given in Table I-A with the values given by the experimental curve of Trimble and Gingrich. Temp. 100°C; $\sigma=0.60$A; $N_0=9.28$; $R_0=3.79$A.*

R in A	$4\pi R^2\rho$(exp.)	$4\pi R\rho$(exp.)	$4\pi R\rho$(calc.)
2.6	0	0	0
2.8	0.40	0.14	0.06
3.0	1.16	0.39	0.34
3.2	2.83	0.88	0.87
3.4	5.32	1.57	1.57
3.6	7.81	2.17	2.19
3.8	9.31	2.45	2.45
$R>R_0$	$N_1=6$ $R_1=5.1$	$N_2=13$ $R_2=6.2$	
4.0	8.31	2.08	2.23
4.2	6.32	1.51	1.66
4.4	5.49	1.25	1.13
4.6	5.15	1.12	0.90
4.8	5.15	1.07	0.96
5.0	5.32	1.06	1.15
5.2	5.82	1.12	1.21
5.4	6.57	1.22	1.17
5.6	7.32	1.31	1.27
5.8	8.73	1.51	1.56
6.0	10.15	1.69	1.94
6.2	12.32	1.99	2.14

[17] $\partial\Phi/\partial T$ is assumed to be negligible. Φ is presumably a function of the temperature through the Fermi energy of the electrons, a factor which becomes important at high temperatures. $Nk/J=1.986$ cal. degree^{-1} mol^{-1}; $mk/h^2=1.215\times10^{14}$ c.g.s. units; $b=126\times10^{-30}$ c.g.s. units.

The value of the entropy of liquid sodium at its melting point (370.5°K) as calculated by Eq. (14) with conversion from ergs to calories is 15.7 cal./degree/mol. The corresponding entropy of solid sodium at this temperature, as taken from the work of Simon and Zeidler,[18] is 13.9 cal./degree/mol. The difference of these two values, 1.8 calories degree^{-1} mol^{-1}, is the entropy of fusion of sodium. The latent heat of fusion corresponding to this entropy change is 2.8 kilojoules per mol. This may be compared with the observed value of 2.65 kilojoules per mol as given in the *International Critical Tables*. No doubt the good agreement is fortuitous to some extent since the entropy of fusion of sodium is small compared with the entropies of the solid and the liquid at the melting point. Also there is some variation in the value of S for the solid as given by different authors.

The specific heat at constant volume for liquid sodium may be obtained from Eq. (14) by means of the relation, $C_V = T(\partial S/\partial T)_V$. The calculation yields the classical value $3Nk$ which is approximately correct. The values of C_V for the alkali metals appear to rise somewhat above the classical value.[18]

At the boiling point of sodium under atmospheric pressure (1153°K) the entropy of the liquid as determined by Eq. (14) is 22.4 cal. degree^{-1} mol^{-1}.[19] The approximate entropy of the vapor at this temperature may be calculated by the equation,[20]

$$S_{\text{vapor}} = Nk[\ln(2\pi mkT/h^2)^{\frac{1}{2}} + \ln(V/N) + 5/2 + \ln 2], \quad (15)$$

where V is the volume of a mol of the vapor at the boiling point. The calculation gives $S_{\text{vapor}} = 43.4$ cal. degree^{-1} mol^{-1}. The entropy of vaporization is thus 21.0 cal. degree^{-1} mol^{-1} at the boiling point and the corresponding latent heat of vaporization 102 kilojoules per mol. The observed value is 105 kilojoules per mol. This excellent agreement is partially explained by the fact that V/N for the vapor is about 10^5 times as large as is v for the liquid at the boiling point.[21] Hence a relatively large error in v would not greatly affect the value of the entropy of vaporization. This fact coupled with the observation that V/N is practically the same for all vapors under like conditions of temperature and pressure seems to form the basis of Trouton's rule[22] as modified by Hildebrand, namely, that the entropies of vaporization of all pure liquids are the same at temperatures where the vapor concentrations are the same.[23]

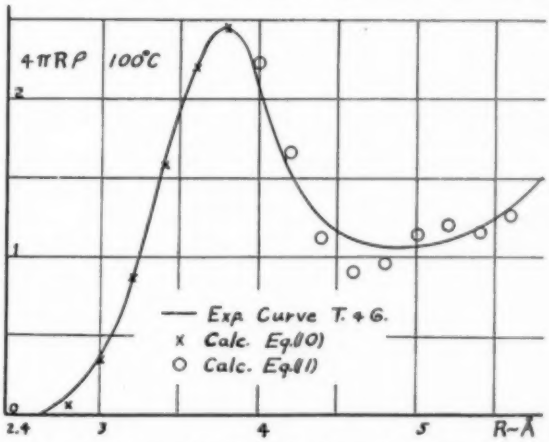

FIG. 2. Values of $4\pi R\rho$ plotted as a function of R.

It is a pleasure to acknowledge the writer's indebtedness to Professor J. C. Slater for his stimulating aid in the inception and solution of this problem, and to Professors N. S. Gingrich and B. E. Warren for their very helpful suggestions and information.

[18] Simon and Zeidler, Zeits. f. physik. Chemie **A123**, 383 (1926); Rodebush and Rodebush, *International Critical Tables*, Vol. 5, p. 88.

[19] The extrapolation to such high temperatures may not be justifiable.

[20] The vapor is assumed to be a perfect gas except for the multiplicity of the ground state of the sodium atom which introduces the term $Nk \ln 2$. The appreciable number of Na_2 molecules present at this temperature is neglected. *Vide.*, e.g., Loomis and Nusbaum, Phys. Rev. **40**, 380 (1932).

[21] At the b.p. of sodium V/N for the vapor is 1.56×10^{-19} cc per atom while v for the liquid is 4.90×10^{-24} cc per atom.

[22] Trouton, Phil. Mag. [5] **18**, 54 (1884).

[23] Hildebrand, J. Am. Chem. Soc. **37**, 970 (1915); see also reference 10.

The Spectrum of Lead Hydride

W. W. WATSON
Sloane Physics Laboratory, Yale University, New Haven, Connecticut
(Received September 29, 1938)

From a lead arc in a hydrogen atmosphere at four to five atmospheres pressure, a "many-lined" spectrum in the region 5000–7000A due to PbH has been produced. Practically all of the lines have been assigned to ten bands constituting a $^2\Sigma \rightarrow {}^2\Sigma$ transition between an upper state of low stability and a stable ground state ($\omega_e = 1565.2$, $B_e = 4.972$). Strong interaction with other states is evidenced by a very large spin-doubling ($\gamma = 6.17$) in the lower state and in the upper state by an unorthodox variation of B_v* with v, irregular spin doubling, a prominent failure of the Mecke rule and a sharp cut-off of levels at about ½ volt above $K' = 0$, $v' = 0$.

THE source ordinarily used in obtaining the emission spectra of metallic hydrides is an arc between electrodes of the metal burning in a hydrogen atmosphere at a pressure of but a few centimeters of Hg. A lead arc under these conditions, however, displays no characteristic hydride spectrum. But since the elements Tl and Bi which flank Pb in the periodic table both have interesting hydride spectra,[1,2] it was thought that with some different experimental source a spectrum of PbH could be produced. Grundström and Valberg found that Tl too showed no hydride spectra in low pressure sources, but they were successful in producing TlH bands either in thermal emission in an electric furnace or in a high pressure arc providing the hydrogen pressure was above 50 cm of Hg. Of these two sources the arc in hydrogen at four atmospheres pressure was much more intense.

With a similar lead arc in hydrogen at four to five atmospheres pressure, I have found a band spectrum of the many-lined type in the region from 5000 to 7000A which from all indications is to be assigned to the PbH molecule. The analysis of this spectrum shows that the upper of the two electronic states involved is of low stability and has its equilibrium point at a considerably larger internuclear distance than that of the lower state. Now Farkas[3] and Olsson[4] have shown that the emission from an arc at high gas pressure is principally thermal radiation. At low pressure, the excitation being by electron impacts, this higher electronic state is not populated, since during electron impact excitation the internuclear distance in the molecule cannot change. But if at the high pressures approximate thermodynamic equilibrium exists, with much interchange between this upper electronic state and other repulsion states, the population of molecules in this state is built up to such an extent that the transitions to the lower ground state, even though improbable according to the Franck-Condon principle, give rise to a band system of fair intensity.

EXPERIMENTAL

A vertical arc was maintained between a fixed water-cooled copper cathode and an adjustable anode made of a thin-walled iron cup filled with "test lead." The source of potential was a 1000-volt d.c. generator delivering a current of 0.8 ampere. At hydrogen pressures of four to five atmospheres the PbH spectrum was emitted with fair intensity and the band lines were not too much pressure-broadened. Higher pressures were not used because of the diminution of the effective resolution on the spectrograms caused by this broadening of the lines, as well as the increased difficulty in making the arc run steadily. The PbH spectrum extends from 5000A on into the infra-red, but good spectrograms were obtained only of the range 5000–6800A with Eastman F-I plates. The second order of the 21-foot grating in a stigmatic mounting was used; the average dispersion was 2.24A per mm. Exposure times of about eight hours were necessary.

[1] TlH: B. Grundström and P. Valberg, Zeits. f. Physik **108**, 326 (1938).
[2] BiH: A. Heimer, Zeits. f. Physik **95**, 328 (1935).
[3] L. Farkas, Zeits. f. Physik **70**, 733 (1931).
[4] E. Olsson, Zeits. f. Physik **104**, 402 (1937).

In the whole of the visible spectrum the only atomic lines other than those of Pb I and Pb II produced by this source are those of H, Na and faintly the Tl resonance line at 5350A. Since NaH and TlH may be ruled out, PbH is the indicated emitter of this spectrum. Also the quantum analysis given below yields very reasonable lower state values of the constants B_e and ω_e in comparison with those known for TlH and BiH. About one thousand PbH band lines of measurable intensity were recorded between 5000A and 6800A. The considerable overlapping of the bands, the lack of band heads, and the large spin doubling all contributed to make the spectrum of the "many-lined" type. A very large majority of these lines has been assigned to the ten bands tabulated below; the whole constitutes a single electronic transition of the $^2\Sigma \rightarrow {}^2\Sigma$ type. Since the line breadths decrease somewhat the accuracy of measurement, wave numbers are given to only one decimal place.

Analysis of the Spectrum

There are four branches in each band, strongly degraded to the red and with large second differences (~ 5 cm^{-1}) between successive rotational lines. This at once indicates a multiplicity of two, which is to be expected for the neutral PbH molecule, and an upper electronic state with a much lower vibrational frequency and much larger moment of inertia than for the lower state. From the rough equality in intensity of the four branches in some of the bands which are free of any partial fusions of branches, from the number of missing lines at the origin and the lack of any apparent spin-orbit doubling, $^2\Sigma \rightarrow {}^2\Sigma$ would seem to be the best choice of electronic transition involved. Quantum assignments based on the usual combination differences are presented in Table I.

Although the four branches are of approximately equal intensity in those bands with $v''=1$ and 2, throughout the spectrum, and especially in the bands of the $v''=0$ progression, the R_1 and P_2 branches seem to be somewhat more intense than the R_2 and P_1 branches. Transitions such as $^2\Pi$ (case a)$\leftrightarrows{}^2\Pi$ (case b) should have sub-bands with two strong and two weaker satellite branches, but this spectrum cannot be of this type since there is no evidence for another set of sub-bands and no internal combinations such as ${}^sR_{21}(J-1)-{}^qP_{21}(J+1) = R_1(J-1)-P_1(J+1)$ exist. I therefore assume that the eye estimates of intensities are rather inaccurate (for they are considerably influenced by the many partial fusions of the pressure-broadened lines which occur particularly in the 2,0 and 3,0 bands), and that the equality in intensity of the branches for the higher K values characteristic of $^2\Sigma \rightarrow {}^2\Sigma$ bands is nearly enough established.

From the combination differences the rotational energy term constants have been computed in the customary semi-graphical manner. These constants are assembled in Table II. The value $B_e''=4.972$ is to be compared with the values 4.806 and 5.136 for TlH and BiH, respectively. In the upper electronic state the B_v's do not decrease in the usual manner regularly with increasing v. The B_v' values first increase and then decrease as v' increases, this despite the fact that the values of $\Delta G(v'+\frac{1}{2})$ decrease steadily with increase in v' (cf. Table III). By way of possible explanation of this abnormality it should be pointed out that these experimental B's are really B^*'s which may differ very appreciably from the true B_v values[5] if there is strong quantum mechanical interaction with near-lying $^2\Pi$ states. As further evidence for the existence of other electronic states of PbH close to this upper $^2\Sigma$ state there may be mentioned the large and irregularly varying values of γ in this state, the existence of perturbations in several of its rotational levels, the marked failure of the Mecke rule for this $^2\Sigma$ state, and the sharp cut-off of all its energy levels at a height of about $\frac{1}{3}$ volt above $K'=0$, $v'=0$. Each of these facts merits a brief discussion.

In the lower electronic state the constant γ of the spin doubling relation $\Delta\nu_{12}(K)=\gamma(K+\frac{1}{2})$ is of record size, 6.17 for $v''=0$, but there is no departure from the normal linear variation of the doubling with $K+\frac{1}{2}$ except for some decrease at the highest K values. In the upper $^2\Sigma$ state, however, the γ's are smaller—3.05, 2.65, 2.28 and 1.49 for $v'=0,1,2$ and 3, respectively, at $K'=14$—vary irregularly at certain rotational

[5] R. S. Mulliken and A. Christy, Phys. Rev. **38**, 87 (1931).

TABLE I. *Assignments of lines in the* $^2\Sigma - {}^2\Sigma$ *system of* PbH. cm^{-1} *units. d denotes fused lines.*

K''	0,0				1,0				2,0				3,0				4,0			
	P_1	R_1	P_2	R_2	P_1	R_1	P_2	R_2	P_1	R_1	P_2	R_2	P_1	R_1	P_2	R_2	P_1	R_1	P_2	R_2
0										18874.1				19305.3						
1										873.1				303.3						
2										867.5				297.0						
3			17962.7*d*			18433.6*d*			18814.8	857.5	18836.2			285.9	19266.7*d*					
4		17970.8*d*	946.6			428.8	18412.3		791.2*d*	843.5	815.9		19220.8*d*	270.2	246.1					
5	17875.4*d*	955.5	925.6			419.1	396.4		762.2*d*	824.5	791.2*d*		190.4*d*	250.0	220.8*d*					
6	841.6	936.2	899.9			405.2	376.0		728.9*d*	801.3	762.2*d*		155.7*d*	225.0	190.4*d*					
7	803.2	912.3	869.6		18291.3	387.0	351.5	18391.4	691.1*d*	773.6	728.9*d*		116.2*d*	195.1	155.7*d*	19231.3				
8	759.8	883.8	834.8		253.9	364.3	322.5	367.6*d*	648.6*d*	741.4	691.1*d*		072.0*d*	160.6	116.2*d*		19544.4	19551.8		
9	712.2	850.8	795.4		211.8	337.2	289.2	340.9	601.8*d*	704.6*d*	648.6*d*		0.230*d*	121.1	072.0*d*	166.9	500.3	509.6		
10	659.8	812.9	751.3	17846.5	165.4	305.6	251.2*d*	308.9*d*	550.4*d*	663.3	601.8*d*	18711.0	18969.3*d*	076.7	023.0*d*		450.7	462.1		
11	602.6	770.1	702.4	807.1	114.7	269.4	209.2	271.5	494.3*d*	617.1	550.4*d*	668.8	910.8*d*	027.2	18969.3*d*	082.6	395.3	409.3		
12	541.0	722.5*d*	648.9	762.7	059.3	228.5	162.3	229.8*d*	433.3*d*	566.1	494.3*d*	622.2	18972.6	912.8	910.8*d*	032.8	333.9	351.2		
13	474.8	670.0	590.6	713.8	17999.4	182.8*d*	111.0	182.8*d*	367.6*d*	510.0	433.3*d*	570.2		847.4*d*	847.4	18977.5	266.7*d*	287.6		
14	403.4	612.5	527.5	659.8*d*	934.9	076.9	17994.1	131.1	299.3	449.1	367.6*d*	512.8	706.1	776.7	704.6*d*	850.5	192.7	218.6		
15	326.8*d*	550.0	459.3	599.8	865.7*d*	016.4	928.4	073.8	224.8	382.6	297.1	450.1*d*	627.7	716.7	625.3	778.4*d*	112.3	143.6		
16	246.1	482.6	386.2		791.5	17950.9	857.9	011.5	144.9*d*	310.9	221.4	382.6*d*	543.8	699.9	540.7	669.9*d*	024.5	062.6		
17		409.9	308.2		712.7	880.1	782.4	17944.1	060.8	233.7	140.6	308.9*d*	454.6	617.1	450.1	615.4	18929.3	18975.6		
18		332.3	225.2			804.0	701.8	871.1	17970.8	150.8	054.6*d*	229.8*d*	359.5	527.9	353.7	523.8	825.6	882.0		
19		249.6	137.1		539.6	722.5*d*	615.8	792.8	875.4	060.8	17962.7*d*	144.9*d*	258.8	431.9	251.2*d*	425.4	714.3	781.6		
20			044.3		445.6		524.9	708.8	774.5	17966.9	865.7*d*	054.6*d*	151.5	328.8	141.9	319.5		673.7		
21			16946.1		346.2	542.9	428.6		667.0	865.7*d*	762.7*d*	17955.5*d*	038.0	218.1	025.9	206.0		557.9		
22					241.6	444.5	326.8*d*		555.5	758.1	653.9*d*		17917.4	099.1						
23					131.6	340.4	219.6	423.1	437.3	643.8	539.1	741.3	789.4	17970.8	17902.6					
24					015.6*d*	230.5	107.1		312.4*d*	522.4	417.8		653.9*d*	832.1	771.7					
25						114.9	16988.9		181.2	393.6	290.3	499.4	508.4							
26						16993.3			043.3	257.0*d*	156.3*d*									
27						865.3					015.6									
28											16867.9*d*									
29											712.0									

K''	0,1				1,1				2,1				0,2				1,2			
	P_1	R_1	P_2	R_2	P_1	R_1	P_2	R_2	P_1	R_1	P_2	R_2	P_1	R_1	P_2	R_2	P_1	R_1	P_2	R_2
0													15038.5*d*							
1													038.5*d*							
2	16448.8	16483.4											15005.4	034.1*d*	15016.4	15038.5*d*				
3	429.1*d*	478.4*d*			16931.5*d*								14986.5	026.0*d*	001.2	034.1*d*				
4	405.7	469.1	16445.3		926.8	16910.5*d*							963.8	013.9*d*	14982.1	026.0*d*				
5	377.8	455.9	425.0		918.2	894.7							937.3	14997.8*d*	959.2	013.9*d*				
6	345.5	438.0*d*	400.7		905.6	875.5							906.8	977.6	932.0*d*	14997.8*d*	15386.3	356.6		
7	308.9	416.1	372.1	16438.0*d*	888.6*d*	852.2							872.4*d*	953.4	901.1	976.9	448.5	429.5	15432.2*d*	
8	268.2	389.8	339.2	414.9	867.9	824.9			17264.5	17343.6			834.2	925.1	866.0*d*	951.7	410.6	384.9	410.6	15468.9
9	223.1	359.1	301.9	387.8*d*	843.1	793.4	16872.5		197.3	326.8*d*			791.9	892.5	827.0	922.2	355.4	323.3	355.4	453.6
10	174.0	323.8*d*	260.3	355.5	813.8	757.9*d*	847.3*d*		157.3	279.4			745.5	855.8	783.7	888.5	322.0	286.1	322.0	434.6
11	120.1	284.1	214.3	319.1	780.3	718.1	817.5		113.0*d*	249.6				814.8	736.4	850.2	379.8	245.1	379.8	411.5
12	061.9	239.8	163.8	277.8	628.6	674.1	783.6		064.4	215.5	17156.3	17312.4		769.5		807.7	349.0	200.4	349.0	384.2	284.8
13	15999.4*d*	190.9	108.7	231.9	576.5	700.1	744.5		012.3*d*	177.1	113.0*d*	257.0				760.8	314.1	151.6	243.6	352.7	243.6
14	932.2	137.3	049.2	181.2	520.1	652.9*d*	701.0	652.9*d*	16955.1*d*	134.2	065.1	183.6				709.1	314.1	098.8	198.3	317.0	198.3
15	860.6	078.8	15983.1	125.6	459.7	601.5	515.9	599.6	828.0	086.7	012.3*d*	140.1					275.0	042.0	148.9	276.8	148.9
16	784.1*d*	15947.8*d*	842.8	15999.4*d*	394.4	545.2	454.2	541.6	757.9*d*	034.6	16955.1*d*	091.8						184.0	095.5		095.5
17	703.5*d*	873.2	764.7	929.7	324.8	484.0	387.8*d*	478.4*d*	682.9	915.7	826.9*d*	16980.5						131.9	037.7	183.2	037.7
18	617.8*d*	796.3	681.5	854.5	250.6	418.0	316.8	410.4	848.6	826.9*d*	755.8	917.0						075.2	14975.5	129.4	975.5
19	527.8	714.0	593.8	775.0	171.7	346.9	240.9	337.0	776.5	755.8	679.8	847.3*d*						915.9	909.0	070.8	909.0
20	431.6	626.3	501.5	688.0	087.9	270.7	160.2	258.4	698.9	679.8	598.6	774.1						846.4	837.9	007.4	837.9
21	332.1	533.7	404.7	598.3	15999.4*d*	189.3	074.5	174.4	614.6	429.1*d*	512.3	694.2						772.8	762.3	14939.1	762.3
22	227.6	436.0	300.7	503.1	905.9	102.4	15983.8	085.0	526.4	334.2	420.7	608.5								866.0*d*	
23	118.3	333.3	194.1	402.8	807.4		888.0	087.1	431.4	232.7	323.8*d*	516.9								787.6	
24	004.1	225.6	082.4	297.5	703.5*d*	15912.7	787.1	15990.2	330.2	127.7	221.2									704.1	
25	14885.0	112.7	14965.7	187.2	594.8	809.5	680.9	889.8	222.6		112.7	315.0									
26		14995.0	844.2		480.8	700.7	569.5	784.1*d*	108.2	15698.4	15998.4	204.5									
27		872.4*d*			361.4	586.2	452.8	672.3	774.4	15986.6	877.9	087.0									
28		744.6			236.5	466.4	330.6*d*	555.1	643.9	857.8	751.2	15962.6									
29					106.2	339.1	203.1	432.2*d*	506.7	721.2	617.8*d*	830.8									
30					14970.7		070.4	304.0	362.2	575.8	477.8	691.2									
31					828.2		788.6		210.1*d*	420.6	330.6*d*	543.5									
									049.8		175.7										
											012.5										

TABLE II. *Constants of the energy terms for* PbH. *cm⁻¹ units.*

CONSTANT	$^2\Sigma'$	$^2\Sigma''$
B_0^*	2.660	4.899
B_1^*	2.766	4.754
B_2^*	2.770	4.609
B_3^*	2.646	
B_e^*		4.972
α		0.145
r_0	2.507*A*	1.848*A*
D_0	-4.07×10^{-4}	-2.01×10^{-4}
ω_e	455.6	1565.2
$\chi\omega$	4.0	30.3
ν_e	18530.3	

TABLE III. PbH *band origins.*

v'	$v''=0$		1		2
0	17982.0	*1505.3*	16476.7	*1444.3*	15032.4
	445.9		*448.2*		*448.4*
1	18427.9	*1503.0*	16924.9	*1444.1*	15480.8
	439.8		*437.0*		
2	18867.7	*1505.8*	17361.9		
	431.2				
3	19298.9				
	(*401*)				
4	19700				

levels and tend to maximum values at intermediate K values. For $v'=2$, for example, the spin doubling drops to zero and reverses sign at $K=29$. Peculiar variations in the spin doubling such as these have been noted before for upper $^2\Sigma$ levels of CaH, CdH, and HgH, for each of which interaction with near-lying $^2\Pi$ levels is known to be responsible.

Perturbations occur in $v'=0$ at $J=19\frac{1}{2}$ for the T_1 terms and at $J=20\frac{1}{2}$ for the T_2 terms, in $v'=1$ at $J=28\frac{1}{2}$ and in $v'=2$ at $J'=20\frac{1}{2}$. The perturbations are not large, but the fact that there are several indicates the presence of one or more Σ or Π states at about this same energy interval above the ground state.

The array of band origins is given in Table III. If the Mecke rule that the ratio of the ω values in the two electronic states should be about the same as that of the B values held, one would expect upper state vibrational intervals of about 800 cm^{-1}. There are several arguments against placing just alternate v' levels in any one electronic state or considering each v' level as a different electronic state. This upper $^2\Sigma$ state must then represent a strong violation of the Mecke rule. A similar failure of this rule occurs in the $D\,^2\Sigma$ state of CaH.

There is a rather sharp cut-off in the rotational series in the 4,0 band at $K'=20$ and no 5,0 band seems to exist. This $K'=20$ level lies about 2700 cm^{-1} above $K=0$ of the $v'=0$ level. In the 2,1 and 3,0 bands the branches drop sharply to zero intensity at $K'=30$ and 24, respectively. These levels lie about 2850 to 2900 cm^{-1} above $K=0$, $v'=0$. There is thus an instability of the levels of this state above about $\frac{1}{3}$ of a volt. Apparently no tendency exists for the stabilization by the high pressure of still higher levels as happens in certain CaH and AlH states. There is also evidence from the course of the $\Delta_2F'(J)$ difference at the higher J levels for the setting in of a considerable centrifugal expansion of the molecule, for these differences actually reach a maximum and begin to decrease with increasing K in the $v'=2$ and 3 levels.

DISCUSSION

Probably both of these PbH states are formed from a Pb atom in its lowest $6p^2$ configuration plus the H electron promoted to a seven-quantum orbit. They could, for example, be $6p\sigma^2 7s\sigma$ and $6p\pi^2 7s\sigma$. The lower of these two $^2\Sigma$ states may well be the ground state of PbH. Configuration theory would predict a number of Σ, Π, Δ and Φ states, both doublets and quartets, from these same electrons, and it would indeed be surprising if the stable states investigated here did not show signs of strong interaction with other near-lying electronic states. The large size of the spin doubling in the ground $^2\Sigma$ state would indicate the possible existence of a low $^2\Pi$ state with the same configuration as for this $^2\Sigma$ state except that one $6p\sigma$ electron has become $6p\pi$. Search of the photographic infra-red might reveal bands involving such a state as well as furnish data on higher levels of the ground state which has an unusually large anharmonic term in its vibrational level scheme.

The arc in gases under high pressure would seem to be a source that should be further exploited. Data on a large number of new molecular energy states perhaps may thus be easily produced.

Rotational Structure of the $^3\Sigma \rightarrow {}^3\Pi$ Bands of BF

F. W. PAUL AND H. P. KNAUSS
Mendenhall Laboratory of Physics, Ohio State University, Columbus, Ohio

(Received September 19, 1938)

The rotational analysis has been made of the (0,0), (0,1), (0,2) and (1,0) bands of the A system of BF. The bands are interpreted in terms of a $^3\Sigma \rightarrow {}^3\Pi$ transition with coupling intermediate between case a and case b. The triplet separation of the upper ($^3\Sigma$) state is too small to be observed; that of the lower ($^3\Pi$) state is $-12.7B''$. The Λ-type splitting of the $^3\Pi$ states is less than 0.2 cm^{-1}. Other constants evaluated are: $B'_0=1.6235$, $B'_1=1.6030$, $D'_0=-4.2\times10^{-6}$, $D'_1=-9.7\times10^{-6}$, $B''_0=1.4030$, $B''_1=1.3851$, $B''_2=1.3672$, all in cm^{-1} units; $I'_e=16.93\times10^{-40}$ g cm^2, $I''_e=19.56\times10^{-40}$ g cm^2, and $r''_e=1.312\times10^{-8}$ cm.

THE band spectrum of BF is of interest because of its predicted similarity to the well-known spectra of CO and N_2. An earlier paper[1] from this laboratory reported on the spectrum of BF excited by means of an electrodeless discharge maintained in BF_3 gas. Sixteen of the bands obtained were assigned to two systems with a common lower electronic level. The present paper presents the rotational analysis of four bands of the A system, based on plates made in the same manner as the earlier ones, but with improved experimental conditions.

Experimental

The BF_3 gas used was obtained in a Pyrex flask from Booth and Willson of the Western Reserve University at the time of the earlier experiments. We transferred it to a carefully evacuated and baked out discharge tube by distillation at liquid-air temperatures. The discharge tube was provided with a quartz window, attached by means of a quartz to Pyrex graded seal. It was sealed off from the vacuum system while the BF_3 gas was solidified in a side arm by means of liquid air. The refrigeration of the side arm was then controlled to bring the pressure to a value suitable for producing an electrodeless discharge.

The oscillator used for exciting the discharge consisted of two 75-watt tubes, type 852, working in push-pull at a frequency of 20 megacycles. Plate current was obtained from a 2000-volt d.c. motor-driven generator. The power input was maintained at about 250 watts. The improved results obtained in the present experiments must be ascribed mainly to the superiority of this oscillator to the one used before, as the other conditions were substantially unchanged. The visible spectrum was examined frequently during the run, and it was found that the highest pressure at which the discharge could be maintained was most satisfactory for getting the BF bands. At low pressures, when the side arm became too cold, the Balmer lines of hydrogen showed up as an impurity.

An exposure of 30 hours was made with the 30,000-line, 21-foot grating of this laboratory. During the first 20 hours, the plates were half covered by metal shields supported independently of the plate-holder to provide both a 10-hour and a 30-hour exposure on each plate. An iron arc spectrum for wave-length comparisons was superimposed on part of the long exposure.

The dispersion in the first order is about 1.2A/mm at 3000A. A Geneva Society measuring engine was used in measuring the plates. The experimental error may be estimated as about 0.05 cm^{-1}. Measurements were made in both first and second order. The (0,0) band was measured in the third order also, but the resolution was no better than that obtained in the second order.

Results

The appearance of the bands of this system is illustrated by Fig. 1, a reproduction of the (0,0) band, in which the assignments of the lines to branches are indicated. An anticipated similarity with bands of the CO molecule which was supported by the appearance of the bands suggested

[1] H. M. Strong and H. P. Knauss, Phys. Rev. **49**, 740 (1936).

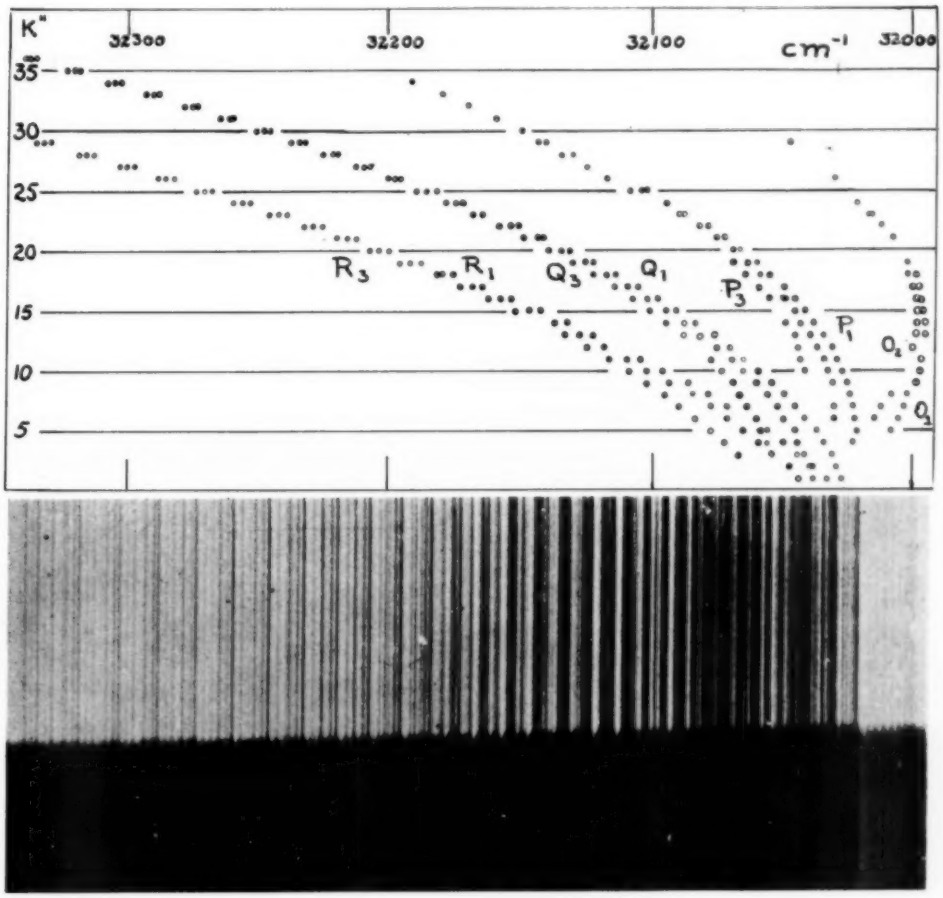

FIG. 1. Fortrat diagram and an enlargement of a part of the (0,0) band of the $^3\Sigma \rightarrow {}^3\Pi$ system of BF. The points are the identified members of the branches and are placed directly above the line so identified.

that the *A* system bands were, like the third positive system of CO, produced by a $^3\Sigma \rightarrow {}^3\Pi$ transition. Our analysis shows that this interpretation is correct.

A diagram showing the 27 branches of a $^3\Pi \rightarrow {}^3\Sigma$ transition allowed by the selection rules is given by Jevons.[2] In the third positive $^3\Sigma \rightarrow {}^3\Pi$ bands of CO, Dieke and Mauchly[3] found that the triplet separation of the $^3\Sigma$ state is so small that it can be neglected, thereby reducing the number of expected branches to 15, all of which they observed. The bands considered here have the same kind of structure, but show none of the strong perturbations which are present in CO. With the intensities present on our plates, we observed 11 branches of the possible 15. A schematic term diagram, Fig. 2, shows the observed transitions and indicates how the various branches are designated. The upper levels are drawn as triplets, although the triplet separation actually is too small to appear in our data. The subscripts 1, 2 and 3, are assigned in the order of increasing frequency. Lines are designated by means of K'' rather than J''.

In Table I are listed the band lines observed with visual estimates of the intensities, and assignments. Unassigned lines, present because of isotopic or other overlapping bands, have been omitted to save space. The assignments of J values were made graphically. In the tails of the bands, lines could be grouped into branches by inspection, and tentative assignments of J

[2] W. Jevons, *Report on Band Spectra of Diatomic Molecules* (London, 1932), Fig. 45, p. 186.
[3] G. H. Dieke and J. W. Mauchly, Phys. Rev. **43**, 12 (1933).

values were made. These were adjusted to be consistent in the four bands studied. Rotational spacings in the upper ($^3\Sigma$) levels obtained from the various bands were found by listing $R_i(K) - Q_i(K)$ and $Q_i(K+1) - P_i(K+1)$, and similarly wave number differences characteristic of the lower ($^3\Pi$) levels were obtained as $R_i(K) - Q_i(K+1)$. The agreement of these values obtained from the different bands is typically within 0.1 cm^{-1}, which supports the validity of the assignments. No allowance has been made for the Λ-type doubling of the $^3\Pi$ levels, as we have been unable to evaluate it from our data, except to estimate an upper limit of 0.2 cm^{-1} for the Λ separation. If the Λ-type splitting were absent, $R_i(K) - Q_i(K)$ should equal $Q_i(K+1) - P_i(K+1)$. These two quantities show no consistent difference in our data.

The differences $R_i(K) - Q_i(K)$ for the different bands show rather large variations from each other in the region of low values of K. These variations are attributed to inaccuracy in the evaluation of the wave numbers of the lines, due to lack of resolution.

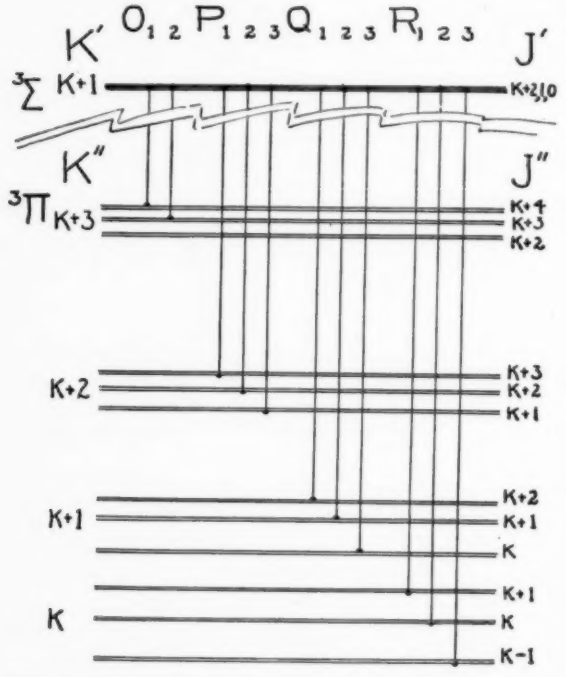

FIG. 2. Schematic diagram of the observed transitions between $^3\Sigma$ upper states and $^3\Pi$ lower states in BF. The designations of the various branches are shown at the top of the diagram. The multiplet splitting of the upper state and the Λ-type splitting of the lower state are indicated although they are too small in magnitude to be evaluated.

In order to evaluate the molecular constants B and D it is necessary to apply the theory of Gilbert[4] for the case of coupling intermediate between case a and case b. This has been done approximately, by ignoring Λ-type doubling, and neglecting possible terms in $J^3(J+1)^3$. The Q and R branches have been used to determine the constants of the $^3\Pi$ state, since the P branches are not well developed in this system of bands. If we write

$$\Delta_2 W_i(J) = R_i(J) - Q_i(J+1) + R_i(J-1) - Q_i(J),$$

the sum of these quantities can be used as an approximation to $\Sigma\Delta_2 W_i(J)$ in Gilbert's equation. The molecular constants obtained by this method are given in Table II.

The value of $\lambda = A/B$ for the bands has been obtained graphically from the experimental data by the method described by Challacombe and Almy.[5] The best value for this constant was found to be $\lambda = -12.7$. With this value and the values of B'' previously obtained, the constant A was found to be -17.81 for (0,0); -17.59 for (0,1), and -17.36 for (0,2). This gives the multiplet splitting in cm^{-1} for the $^3\Pi$ states. The minus sign indicates that the multiplet structure is inverted. This result is corroborated by the rotational analysis, as it is found that the rotational levels designated as F_3 go over into the $^3\Pi_0$ levels at low K values, and the F_1 levels go over into the $^3\Pi_2$ levels.

The data for the (0,0), (0,1) and (1,0) bands permitted an unambiguous extrapolation to determine B_v''. The slopes of the straight lines used for these bands were all negative and of the order of 10^{-6} cm^{-1}. They do not seem to us to be significant because an approximation was used in determining $\Delta_2 W_i(J)$. In the case of the (0,2) band, a plot of $\Sigma\Delta_2 W_i(J)/6(2J+1)$ against $J(J+1)$ gives a curved instead of a straight line, which indicates either that the Λ-type doubling has a larger effect in this band than in the others, or that a term in $J^3(J+1)^3$ is present in the rotational energy. Extrapolation of the curve which best fits the experimental points gives $B_2'' = 1.3472$. Extrapolation of a straight

[4] Cecil Gilbert, Phys. Rev. **49**, 619 (1936).
[5] C. N. Challacombe and G. M. Almy, Phys. Rev. **51**, 930 (1937).

TABLE I. *Rotational structure of (0,0), (0,1), (0,2) and (1,0) bands of* BF. *D = diffuse and db = double.*

INT. (EST.)	ν OBS. CM^{-1}	ASSIGNMENT
	(0,0) Band	
5	31994.96	O_{13}, 14
1	95.87	O_{11}, 15
2	96.98	O_{10}, 16
2	97.46	O_{17}
2	98.40	O_9; O_{14}, 15
3	99.06	O_{18}; O_{13}, 16
3*db*	32000.05	O_{12}, 17
3*db*	01.25	O_8, 19; O_{28}
4	02.46	O_{17}
2	04.16	O_{120}
3	04.81	O_{16}
2	06.72	O_{121}
3	07.65	O_{15}; O_{28}
4	10.54	O_{122}; O_{27}
3	13.63	O_{26}
0	14.84	O_{123}
2	16.27	O_{223}
10	20.49	O_{224}; P_{15}
3	21.15	P_{16}
4	21.90	O_{24}; P_{17}
5	23.07	P_{18}
6	24.44	P_{19}
10	26.23	P_{110}; Q_{11}
3	28.32	Q_{12}; P_{111}
20*db*	29.34	O_{126}; P_{16}, 7
10	30.76	Q_{13}; P_{112}; P_{29}
3	32.05	R_{11}; P_{210}
20*db*	33.67	Q_{14}; P_{113}; P_{211}
4	35.92	Q_{15}; P_{212}
5	37.01	R_{12}; P_{114}; Q_{31}
20*db*	38.65	Q_{32}; P_{213}
5	40.67	P_{210}; Q_{16}; P_{115}; Q_{33}
1	41.62	P_{311}; P_{214}
2	42.29	R_{31}
1	43.11	P_{312}; R_{13}; Q_{34}
20	44.89	P_{213}; Q_{17}; P_{116}; Q_{35}; P_{215}
3	47.12	O_{129}; R_{32}
1?	48.38	P_{314}; Q_{36}
15	49.20	R_{14}; Q_{18}; P_{117}; P_{216}
4	51.71	Q_{37}
10	53.78	Q_{33}; Q_{19}; R_{33}
8	54.29	P_{316}; P_{118}
5	55.38	Q_{34}; R_{15}; Q_{28}
5	57.40	Q_{35}; P_{318}
10	58.66	P_{317}; Q_{110}; R_{34}
8	59.65	Q_{36}; P_{119}; Q_{29}
5	62.44	Q_{37}; P_{319}
2*db*?	63.38	P_{218}; R_{16}
5	64.15	Q_{111}; R_{35}; Q_{210}
8	65.40	Q_{38}; P_{120}
2	66.29	R_{33}
2	68.55	Q_{39}; P_{319}; P_{220}
5	69.20	Q_{211}
2	69.86	Q_{112}
1	70.50	R_{17}; R_{36}
3*db*	77.49	R_{34}; P_{121}
5	72.46	Q_{310}
5	74.59	Q_{312}; P_{221}
5	76.04	Q_{113}
5	76.90	R_{35}; Q_{311}; R_{37}
20*tr*	78.54	R_{18}; P_{122}
5	80.42	Q_{313}; P_{222}
8	81.74	Q_{312}
8	82.45	R_{36}; Q_{114}
1	83.71	R_{38}
4*db*	85.32	R_{19}
8*D*	86.94	Q_{313}; P_{123}; Q_{314}
2	87.77	R_{37}; P_{223}
5	89.55	Q_{115}
2	92.30	R_{39}
20*db*	93.22	Q_{314}; P_{124}; Q_{215}
1	93.93	R_{38}
2	94.52	R_{110}
5	96.89	Q_{116}
5	99.36	Q_{315}
15*db*	32100.49	R_{39}; R_{310}; Q_{316}
1	01.51	P_{125}
2	03.15	R_{111}; P_{225}
4	04.67	Q_{117}
3	06.20	Q_{316}
1	07.62	R_{310}; P_{225}
5*tr*	08.24	R_{311}; Q_{317}
4	12.82	Q_{118}
5	13.46	Q_{317}
5	15.30	R_{311}
5	16.21	P_{226}; Q_{318}
5	17.22	R_{312}
20	32121.35	Q_{318}; R_{313}; Q_{119}
3	23.51	R_{312}
2	24.02	P_{227}
4	24.68	Q_{319}
2	26.27	R_{313}
4	29.47	Q_{319}; P_{228}
5	30.49	Q_{120}
1	31.15	R_{314}
3	32.13	R_{313}
8	33.55	P_{228}; Q_{220}
2	35.82	R_{314}
5	38.17	Q_{320}
1	39.21	P_{229}
4	40.09	Q_{121}
5	41.38	R_{315}
5	42.90	P_{329}; Q_{321}
3	45.77	R_{315}
5	47.36	Q_{321}
1	48.51	P_{330}
4	49.98	Q_{322}
2	50.94	R_{315}
1	51.96	R_{316}
5	52.69	Q_{322}
2	56.21	R_{316}
5	56.95	Q_{322}
3	58.23	P_{331}
4	60.25	Q_{323}
4	61.01	R_{316}
5	63.00	R_{317}; Q_{223}
5	66.99	Q_{323}; R_{317}
2	68.46	P_{232}
4	71.06	Q_{124}
4	71.60	R_{317}
3	73.58	Q_{324}
3	74.44	R_{318}
4	77.50	Q_{324}
2	78.30	R_{318}
1	79.09	P_{333}
10	82.41	R_{318}; Q_{125}
5	84.66	Q_{325}
3	86.33	R_{319}
5	88.46	Q_{325}
3	90.12	R_{319}; P_{334}
10	93.96	R_{319}; Q_{126}
3	96.21	Q_{326}
3	98.52	R_{320}
4	99.85	Q_{326}
5	32202.13	R_{320}
8	06.01	R_{320}; Q_{127}
5*D*	08.18	Q_{327}
5	11.69	Q_{327}; R_{321}
3	14.74	R_{321}
8	18.40	R_{321}; Q_{328}
4	20.51	Q_{328}
8*D*	24.17	Q_{328}; R_{322}
2	27.75	R_{322}
5	31.33	R_{322}; Q_{329}
4	33.51	Q_{329}
4	36.75	Q_{329}
2	37.90	R_{323}
3	41.12	R_{323}
10	44.64	R_{323}; Q_{330}
3	46.69	Q_{330}
3	49.99	Q_{330}
2	51.90	R_{324}
3	55.07	R_{324}
5	58.41	R_{324}; Q_{331}
2	60.44	Q_{331}
2	63.59	Q_{331}
2	66.28	R_{325}
3	69.33	R_{325}
8*db*	72.62	R_{325}; Q_{132}
2	74.65	Q_{332}
4	77.68	Q_{332}
2	81.04	R_{326}
3	84.07	R_{326}
3	87.39	R_{326}; Q_{133}
3	89.21	Q_{333}
3	92.27	Q_{333}
1	96.37	R_{327}
2	99.22	R_{327}
2	32302.54	R_{327}; Q_{134}
3*db*?	04.32	Q_{334}
1	07.25	Q_{334}
2	12.11	R_{328}
2	15.00	R_{328}
2	18.17	R_{328}; Q_{135}
4	19.93	Q_{335}
2	22.72	Q_{335}
5	28.24	R_{329}
2	31.04	R_{329}
2	32334.22	R_{329}; Q_{136}
2	35.82	Q_{336}
3	38.70	Q_{336}
	(0,1) Band	
4	30716.28	P_{15}, 6
3	17.24	P_{17}
5	18.63	P_{18}
8	20.23	P_{19}
2	22.81	P_{110}
5*db*	24.89	P_{111}; P_{16}, 7
5*D*	26.39	P_{18}, 9
20*D*	27.96	P_{112}; P_{210}
3	30.15	P_{311}
3	30.98	P_{113}
1	31.88	Q_{15}
5	32.76	P_{312}
15*db*?	34.38	P_{16}, 7
10	35.83	P_{15}, 8; Q_{16}; P_{114}; P_{313}
0	37.95	P_{311}
10	39.13	P_{14}; P_{115}; P_{214}
4	40.28	P_{13}, 12; Q_{17}; Q_{35}
10	43.56	P_{116}; Q_{26}
6	44.77	R_{14}; Q_{18}
3	45.41	P_{314}
3	47.08	Q_{37}; P_{216}
8	48.71	Q_{32}; P_{315}; P_{117}
5	49.80	Q_{33}; Q_{19}
2	51.08	Q_{34}; R_{15}; Q_{28}
2	51.73	Q_{35}; P_{217}
2	53.39	P_{316}
3	54.28	Q_{36}; P_{118}
8*db*	55.28	Q_{110}; Q_{29}
4	56.88	Q_{37}; P_{218}
10*D*, *db*	58.05	R_{32}; P_{317}; R_{16}
15*db*	60.50	Q_{38}; Q_{111}; P_{119}; Q_{210}
2	62.27	R_{33}
8*db*	64.08	Q_{39}
3	65.70	R_{36}; Q_{311}
5	66.76	R_{34}; R_{17}; Q_{112}; P_{120}
4	68.51	Q_{310}; P_{319}
1	69.59	P_{320}
5	71.48	R_{35}; Q_{312}
4	72.10	R_{37}
10	73.37	Q_{311}; Q_{113}
5	73.85	P_{321}
1	74.39	P_{320}; R_{18}
1	75.82	P_{321}
8	77.09	R_{36}
5	77.75	Q_{313}
5	78.55	Q_{312}
20*db*?	80.72	P_{321}; Q_{114}; P_{122}
2	82.08	R_{37}; R_{19}
4	83.04	P_{322}
15	84.42	Q_{313}; Q_{214}
8	87.75	Q_{115}; R_{39}
1	88.66	P_{322}; P_{123}
3	89.35	R_{38}
5	90.69	Q_{314}; R_{110}; P_{223}
5*db*	91.80	Q_{315}
5	95.67	P_{323}; Q_{116}
5	96.35	R_{39}; R_{310}
5	97.47	Q_{315}; P_{124}
8	99.40	R_{311}; Q_{216}; P_{224}
5	30803.90	R_{310}; P_{324}; Q_{117}
5	04.89	Q_{316}; R_{311}
2	05.95	P_{125}
4	07.43	Q_{317}; P_{325}
3	08.92	R_{112}
4	11.82	R_{311}
8	12.75	Q_{317}; Q_{118}
3	14.08	P_{126}; R_{312}
4	16.00	Q_{218}
1	16.52	P_{326}
2	18.80	R_{113}
3	20.32	R_{312}
5	20.96	Q_{318}; P_{226}
4	21.96	Q_{119}
4	23.62	R_{313}
6	25.05	P_{127}; Q_{319}
2?	29.18	R_{114}
4	29.79	R_{313}; Q_{319}
1	30.53	P_{327}
8	31.68	Q_{120}
2	33.61	R_{314}
8	34.74	P_{128}; Q_{320}
1	37.10	P_{328}
5	39.07	Q_{320}
3	30839.55	R_{314}; R_{115}
2	40.48	P_{328}
4	41.77	Q_{121}
2*db*?	43.92	R_{315}
4	44.61	Q_{321}
2	45.60	P_{129}
2	46.95	P_{329}
6	49.02	R_{315}; Q_{321}
3	50.83	R_{116}
1	51.68	P_{329}
4	52.37	Q_{322}
6	55.01	R_{316}; Q_{322}
1	56.73	P_{130}
10	59.42	R_{316}; Q_{322}
4	62.10	P_{330}; R_{117}
4	63.43	Q_{323}
6	66.13	R_{317}; Q_{323}
0	68.33	P_{131}
5	70.05	Q_{323}
5	70.79	R_{317}
1	73.35	P_{331}
2	74.25	R_{118}
4	74.98	Q_{124}
4	77.44	Q_{324}
2	78.09	R_{318}
1	80.57	P_{132}
4	81.32	Q_{324}
2	82.36	R_{318}
2	85.33	P_{332}
8	86.88	R_{119}; Q_{125}
5	89.32	Q_{325}
2	90.40	R_{319}
5	93.04	Q_{325}; P_{133}
4	94.39	R_{319}
2	97.77	P_{333}
5	99.53	R_{320}; Q_{126}
3	30901.72	Q_{326}
3	03.22	R_{320}
4	05.32	Q_{326}
3	06.97	R_{320}
2	10.68	P_{334}
4	12.35	Q_{127}
4	13.01	R_{321}
4	14.57	Q_{327}
3	16.45	R_{321}
5	18.06	Q_{327}
5	19.99	R_{321}
1	24.09	P_{335}
4	25.77	Q_{128}
2	26.84	R_{322}
4	27.85	Q_{328}
3	30.12	R_{322}
4	31.27	Q_{328}
4	33.55	R_{322}
3	38.08	P_{336}
4	39.66	Q_{329}
3	41.10	R_{323}
3	41.62	Q_{329}
2	44.31	R_{323}
3	44.92	Q_{329}
4	47.62	R_{323}
4	53.99	Q_{330}
5	55.92	R_{324}; Q_{330}
5	59.05	Q_{330}; R_{324}
2	62.10	R_{324}
1	67.05	P_{338}
3	68.78	Q_{331}
10*D*	70.85	R_{325}; Q_{331}
10	73.90	Q_{331}; R_{325}
2	77.10	R_{325}
1	82.33	P_{339}
4	84.03	Q_{132}
3	85.90	Q_{332}
3	86.70	R_{326}
3	88.86	Q_{332}
3	89.64	R_{326}
4	92.59	R_{326}
2	99.74	Q_{133}
2	31001.55	Q_{333}
2	02.86	R_{327}
3	04.53	Q_{333}
2	05.74	R_{327}
2	08.48	R_{327}
2	15.99	Q_{134}
2	17.67	Q_{334}
2	19.42	R_{328}
3	20.53	Q_{334}
2	22.22	R_{328}
3	24.91	R_{328}
3	32.76	Q_{135}
3	34.30	Q_{335}

TABLE I. (*Continued*).

INT. (EST.)	ν OBS. CM^{-1}	ASSIGNMENT
	(0,1) Band	
2	31036.55	$R_{12}9$
3*db*?	37.10	$Q_{23}5$
3	39.29	$R_{23}9$
4	41.84	$R_{23}9$
	(0,2) Band	
3*D*	29409.18	$O_12$10, 11, 12, 13
3*D*	10.57	$O_12$14, 9
1	11.63	$O_12$8, 15
3	13.12	$O_12$7, 16; $O_12$11, 12, 13
2	13.75	$O_23$14
1?	14.49	$O_23$10, 15
2	16.01	$O_23$6; $O_23$16
3	17.32	O_29
5	17.65	$O_23$17
5*db*?	20.24	O_25
2	23.82	O_219
2	25.26	O_220
3	29.70	O_221
4*db*	31.56	O_221; P_16
3	32.55	P_17
4*db*?	33.98	P_18
5*db*?	36.14	O_222; P_19
2	38.40	P_110
4*db*?	39.58	P_25, 6
2	40.51	P_27
3	41.16	P_28; P_111
2	42.01	P_29
2	42.73	P_210; Q_131
5*db*	44.18	P_112
1	45.28	Q_14
4	46.49	P_211
4	48.14	P_113; Q_15
5	49.29	Q_22; P_212
3	50.81	P_27, 8; Q_23
2	51.15	P_29; Q_16
4	52.29	P_210; P_213; P_114
4	52.97	Q_24
2	53.52	P_211
6*db*	55.19	Q_25; R_13; Q_17
3	56.78	P_212; P_214; P_115
5	58.25	R_22; Q_25
3	59.97	P_215; Q_18
2	61.10	R_14
5	61.92	Q_27; P_116
1?	62.96	P_214; R_23
2	65.18	Q_23; P_216; Q_19
5	66.10	Q_24; Q_28
3	67.50	Q_25; P_117; R_15
1	68.44	R_24
2	69.59	Q_26
5	70.72	Q_29; P_217; Q_110
1?	71.37	P_216
3	72.25	Q_27
3	73.81	R_25; P_118; R_16
6	75.74	Q_28; Q_210
2	76.71	P_218; Q_111
4	77.60	R_23
3	79.53	Q_29
2	80.10	R_26; P_119
1	81.04	R_17
5	81.61	R_24; Q_211
3	83.22	Q_112
5	83.93	Q_210
2	86.22	R_25
2	87.12	R_27; P_120
5*db*?	87.80	P_219; Q_212
3	89.08	Q_211; R_18
2	90.18	Q_113
2	91.56	R_26
10	94.56	Q_212; P_220; R_28; Q_213; P_121
5	97.53	R_27; R_19; Q_114
3	29500.91	Q_213
5	01.58	Q_214
2	02.75	P_122
3	03.52	R_19
3	04.10	R_28
3	05.41	Q_115
2	06.19	R_110
3	07.67	Q_214
4	09.26	Q_215
3	11.37	R_29; R_210; P_123
2	13.77	Q_116
2	14.93	Q_215
1	29515.46	R_111
5*db*?	17.42	Q_216
2	19.11	R_210
2	20.38	R_211; P_124
8	22.71	Q_216; Q_117
1	25.28	R_112
3	25.99	Q_217
4	27.53	R_211
5*db*	30.10	R_212; P_125
3	31.18	Q_217
3	31.92	Q_218
8*db*	35.20	Q_218; R_113
2	36.41	R_212; P_225
5	40.07	Q_218; R_213; P_126
3	41.73	Q_219
2	44.78	Q_219
3	45.90	R_213; P_226; R_114
4	49.50	Q_219
4	50.55	R_214
3	52.04	Q_220
3	54.97	Q_220
3	56.00	R_214; P_227
1	57.23	R_115
3	59.48	Q_220
2	61.62	R_215
3	62.84	Q_221
3	65.64	Q_221
2	66.54	R_215
1	66.98	P_228
2	68.87	R_216
4	69.94	Q_221
4	73.06	R_216
4	74.18	Q_222
2	76.85	Q_222
2	77.65	R_216
1	78.53	P_229
4	80.98	Q_222; R_117
3*D*	84.96	R_217
4	85.95	Q_223
4	88.54	Q_223
3	89.27	R_217
1	90.37	P_230
4	92.50	Q_223
2	93.52	R_218
3	97.32	R_218
4	98.26	Q_224
4	29600.69	Q_224
2	01.45	R_218
1*db*	02.89	P_231
4	04.55	Q_224
2	06.56	R_119
3	10.21	R_219
4	11.08	Q_225
4	13.44	Q_225
3	14.17	R_219
1	15.74	P_232
4	17.12	Q_225
2	20.13	R_220
2	23.59	R_220
3	24.43	Q_226
3	26.58	Q_226
2	27.36	R_220
1	29.30	P_233
3	30.17	Q_226
2	34.17	R_221
3	37.58	R_221
3	38.17	Q_227
4	40.35	Q_227
4	41.10	R_221
2	43.25	P_234
4	43.81	Q_227
2	48.68	R_222
2	52.01	R_222
3	52.43	Q_228
2	54.54	Q_228
3*db*	55.40	R_222
3	57.86	Q_228
3	63.71	R_223
8*db*	67.06	R_223; Q_229
3	69.20	Q_229
2	70.05	R_223
5	72.47	Q_229
1	79.14	R_224
5	82.38	R_224; Q_230
3*db*	84.33	Q_230
2	85.38	R_224
2	87.56	Q_230
2	29695.12	R_225
4	98.15	R_225; Q_131
4	29700.05	Q_231
2	01.03	R_225
3	03.11	Q_231
3	11.57	R_226
4	14.47	R_226; Q_132
3*db*	16.34	Q_232
2	17.31	R_226
4	19.20	Q_232
3	28.59	R_227
5	31.30	R_227; Q_133
3	32.97	Q_233
3	34.08	R_227
4	35.92	Q_233
5	48.73	R_228; Q_134
4	50.10	Q_234
4	51.48	R_228
5*db*	53.28	Q_234
	(1,0) Band	
2	33576.72	O_113
1	79.10	O_118, 19; O_215, 16
2	80.65	O_111; O_214, 17, 18
2*D*	82.64	O_19; O_212
2*db*	84.53	O_18, 21
1	86.04	O_122; O_210, 21
2	87.02	O_17
1	88.41	O_222
2	89.63	O_123; O_29
1	91.00	O_16; O_223
2	92.57	O_124; O_28
1	94.20	O_224
2	95.70	O_27
1	97.38	O_125; O_225
2	98.99	O_26
2	33601.19	O_126; O_25
10	05.50	O_127; P_16
2?	06.14	O_24, 27; P_17
2	07.01	P_18
3	08.10	P_19
3	09.50	P_110
3	11.16	P_111
5*db*	13.60	P_112; P_26
2	14.20	P_25, 7, 8
4	15.39	Q_13; P_113; P_24, 10
3	16.51	P_23, 11
5	18.26	Q_14; P_212
2	20.40	Q_15; P_213
3	21.41	P_115
5	22.73	P_214
8*db*	24.80	Q_16; Q_22; P_116; P_215; P_311
5*db*	26.16	Q_23
10	28.75	Q_17; Q_24; P_117; P_214; P_216
1	30.12	Q_25
4	32.79	Q_18; Q_26
1*db*?	34.09	R_14; R_22; P_216
1	35.80	Q_27
4	37.15	Q_19; P_217
2	39.10	R_23; Q_28
3*db*	41.27	Q_110; P_218
3	42.41	Q_24
3	43.00	Q_29; Q_25
1	44.52	R_24; Q_26
1	45.16	P_220
4	46.46	Q_111; Q_210; Q_27; P_219
2	47.70	R_16
3	49.00	R_25
3	49.76	Q_28
10	51.66	Q_112; Q_211; Q_19
1	53.54	R_23
1?	54.14	R_17; R_26
3	55.22	Q_210; P_221
2	56.47	Q_212
3	57.33	Q_113; R_24
4	59.33	Q_211
1	60.36	R_27; P_222
5	61.67	R_18; Q_213; R_25
8	63.41	Q_114; Q_212
3	66.24	R_26; P_223
2	67.36	R_28; Q_214
3	68.33	R_19; Q_213
3	69.43	Q_115
2	71.49	R_27
1	33672.58	P_224
5*db*	73.59	Q_215; Q_214
1	75.15	R_29
2	76.14	R_110; Q_116; R_28
3	79.31	Q_215
2	79.72	Q_216; P_225
1	82.56	R_210; R_29
5	83.22	Q_217
3	85.37	R_211; Q_216
3	86.57	Q_217; P_226
10*D*	90.46	Q_118; R_211; R_210
2	91.94	Q_217
3	93.83	R_212; Q_218
2	94.31	P_227
2	97.13	R_211
4	98.26	Q_219; R_212
4	98.88	Q_218
5*db*	33701.63	R_213; Q_219
2	04.72	R_212
5	06.46	Q_220; R_213; Q_219
4	09.60	Q_220
2	11.01	R_214
2	12.74	R_213
3	14.08	Q_220
2	15.08	Q_221
2	16.18	R_214
3	17.81	Q_221
2	21.13	R_215; R_214
3	22.39	Q_221
2	23.92	Q_222
3*D*	25.25	R_215
2	26.67	Q_222
2	30.21	R_215
2	30.79	R_216; Q_222
2	33.25	Q_223
1	34.48	R_216
3	35.79	Q_223
4*db*	39.62	R_216; Q_223
2	40.68	R_217
3	42.92	Q_224
3	45.42	R_217; Q_224
3	49.20	R_217; Q_224
1	51.12	R_218
3	52.96	Q_225
5	55.34	R_218; Q_225
3	59.22	R_218; Q_225
1	62.05	R_219
2	63.42	Q_226
4	65.87	R_219; Q_226
5*db*	69.69	R_219; Q_226
3	73.49	R_220
3	74.08	Q_227
5*db*	76.82	R_220; Q_227
3	80.04	Q_227
3	80.85	R_220
5	85.32	R_221; Q_128
2	87.65	Q_228
2*db*	88.63	R_221
3	91.11	Q_228
3	92.37	R_221
3	97.19	R_122; Q_129
2	99.19	Q_229
2	33800.61	R_221
2	02.56	Q_229
2	04.00	R_222
3*D*	09.37	R_123; Q_130
2*D*	11.13	Q_230
2	13.04	R_223
2	14.33	Q_230
2	16.24	R_223
2	21.56	Q_231
1	22.49	R_224
2	23.46	Q_231
2	25.68	R_224
3	26.59	Q_231
2	28.87	R_224
2	34.35	Q_232
3	36.04	R_225; Q_232
3	39.07	R_225; Q_232
2*D*	42.32	R_225
3*D*	47.85	Q_233
3	49.41	R_226; Q_233
4	52.41	R_226; Q_233
1	55.28	R_226

TABLE II. *Molecular constants of the upper* ($^3\Sigma$) *and lower* ($^3\Pi$) *electronic states of the* BF *A-system bands.*

	B_v (cm^{-1})	D_v (cm^{-1})	α (cm^{-1})	I_e (g cm^2 $\times 10^{40}$)	r_e cm $\times 10^8$
$v'=0$	1.6235	-4.2×10^{-6}	0.025	16.93	1.220
1	1.6030	-9.7×10^{-6}			
$v''=0$	1.4030		0.0179	19.56	1.312
1	1.3851				
2	1.3672*				

* Extrapolated.

line fitted to the data gives $B_2''=1.3770$. The former value seems too low and the latter too high. The value 1.3672 included in Table II is that obtained from the equation $B_v=B_e+\alpha(v+\frac{1}{2})$ where α is determined from $B_0''-B_1''$.

The constants for the $^3\Sigma$ state have been obtained graphically in the following manner. If $T(K)$ represents the total energy of the rotational energy level, then

$$\Delta_1F_i(K+\tfrac{1}{2})=T_i(K+1)-T_i(K)$$
$$=R_i(K)-Q_i(K)\pm\delta_{AB}$$

where δ_{AB} represents the Λ-type splitting. Since the $^3\Sigma$ states may be represented by the equations of Hund's case b, we have

$$\Delta_1F_i(K+\tfrac{1}{2})=2B'(K+1)+4D'(K+1)^3+\cdots.$$

Averaging over the three sub-states gives:

$$[\Sigma_i\Delta_1F_i(K+\tfrac{1}{2})]/[6(K+1)]$$
$$=B'+2D'(K+1)^2+\cdots.$$

Neglecting the Λ-type splitting we have

$$\Sigma_i[R_i(K)-Q_i(K)]/6(K+1)$$
$$=B'+2D'(K+1)^2+\cdots.$$

The left side of this equation, evaluated experimentally, has been plotted against $(K+1)^2$. The intercept of the straight line obtained has been taken as the value of B' and the slope as $2D'$. The value of B' for $v'=0$ is the average of the values obtained from the (0,0), (0,1) and (0,2) bands. The value for $v'=1$ is obtained from the (1,0) band. These values are given in Table II.

ACKNOWLEDGMENTS

The authors are grateful to Professor H. S. Booth and Mr. Karl S. Willson who prepared the pure sample of BF_3, and to Mr. George E. Hansche, who assisted in obtaining the spectrum photographs.

The Mechanism of the Negative Point to Plane Corona Near Onset*

G. W. TRICHEL
Department of Physics, University of California, Berkeley, California

(Received October 4, 1938)

Oscillographic studies have been made of the currents in negative point to plane coronas in air. The oscillograms obtained indicate that the negative corona current is composed of discrete pulses whose magnitude and frequency have a definite relationship to the corona current, point size and gas pressure. The frequency of the current pulses appears to be independent of gap length under the experimental conditions studied. The frequency of the oscillations does not appear to be affected by changes in the electrical constants of the discharge circuit outside the gap. The periodic character of the discharge seems to derive logically from space charge formation in the gap and subsequent clearing under the action of the electrostatic field.

INTRODUCTION

OSCILLOGRAPHIC studies have been made of the corona currents in negative point to plane coronas in air. The circuit arrangement used is shown schematically in Fig. 1.

Direct current at any desired voltage up to 25 kv is obtained from a half-wave Kenetron rectifier which keeps a $\frac{1}{4}$-mf condenser charged. The voltage is regulated by a Variac transformer in the primary circuit of the high voltage transformer. The voltage across the gap is read by means of one section of a White potentiometer across a part of a calibrated resistance tower connected in parallel with the gap. With the galvanometer used a voltage sensitivity of three volts per mm deflection was obtained. The gap consisted of points of several types opposed to a brass plate six inches in diameter. A radio receiver was used to pick up current variations in the gap. This receiver consisted of a 6J7 biased detector and two stages of resistance coupled amplification with 6F6 tubes. The receiver and gap were completely enclosed in a grounded sheet metal box 27×27×30 inches. The output of the radio receiver was condenser-coupled through a shielded cable to the vertical plates of a nine-inch Dumont cathode-ray oscillograph. This oscillograph was equipped with a single sweep device so that photographs could be readily made of a single transit of the electron beam. A Leica camera was used to photograph at a lens aperture of f2 the single sweeps on Agfa ultra-speed panchromatic film. The films were projected to give an oscillogram approximately the full size of the trace on the oscillograph screen and measurements were made on these enlargements. With a sweeping time of 5/10,000 sec. the highest frequency photographed and resolved was 208,000 c.p.s. The time scale of the oscillograms was established by taking oscillograms of the output of a calibrated oscillator with the same sweep setting that was used for the corona oscillograms. Repeated photographs of a constant frequency wave indicate that the sweeping time of the single sweep may vary as much as 10 percent. This must be considered in the evaluation of the oscillograms of negative corona obtained with this instrument.

In earlier experiments a tuned input to the detector was used in order to obtain a maximum sensitivity. This was abandoned to avoid the

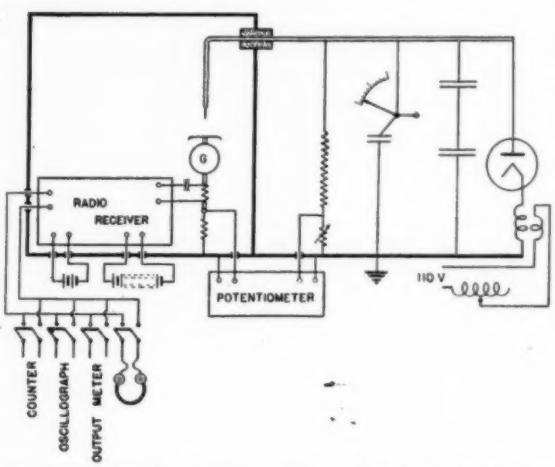

FIG. 1. Schematic diagram of the electrical circuits employed for negative point corona measurements.

* This work was done in partial fulfillment for the degree of Ph.D. in Electrical Engineering at the University of California.

parasitic oscillations set up in the tuned circuit by shock excitation from the corona pulses. In the present experiments the detector was coupled to the corona circuit through a condenser and a 10,000-ohm noninductive grid return. The voltage applied to the set was taken across a 1000-ohm restistor in the ground lead from the plate electrode of the gap. The average current was read by measuring the voltage across this 1000-ohm resistor with the other half of the White potentiometer. Changes in current of the order of 10^{-9} ampere could be detected with this arrangement. A check was made with different values of grid resistor, coupling condenser and ground resistor to determine the effect of these values on the recorded frequency when corona current and gap were constant. These elements appeared to have no effect on the frequency of the recorded impulses but did change the magnitude of the recorded signals.

Four types of points were used as negative electrodes. Points I and II were of platinum wire of 0.5 and 1.5 mm diameter, respectively, having a hemispherical end of the same radius as the body. Point III was of brass, similar in shape, having a diameter of 4.73 mm and point IV was a steel sewing needle having an included angle of approximately 30° at the point.

Oscillograms were made of the transient characteristics of the corona current for different values of corona current, point and gap distance being kept constant. Fig. 2 shows a typical series obtained with point I at a gap distance of 3 cm. The current fluctuations are seen to consist of a succession of very regular impulses similar to those produced by a relaxation oscillator. The frequency varies linearly with the corona current over the range of currents observed. The shape of the impulses remains constant except that the decay curve is interrupted at higher and higher values as the impulses become closer together with increasing current.

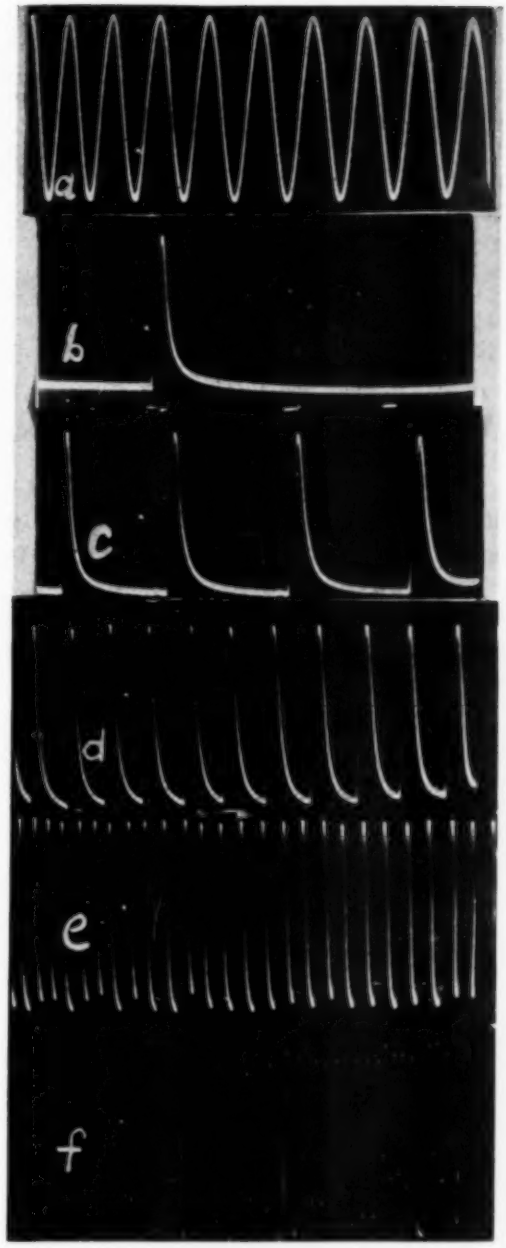

FIG. 2. Typical oscillograms of negative point corona for a 0.5-mm diameter point and 3-cm gap. (a) 8000 cycles calibrating wave; (b) single pulse 0.1μA; (c) 0.7μA; (d) 2.0μA; (e) 5.0μA; (f) 12.0μA.

Figure 3 gives the results of measurements made upon a series of four different points. It appears that frequency is a function of point diameter varying as a complicated and somewhat irregular inverse function of the radius at the point for the same corona current.

Figure 4 gives the results obtained when the same point (point I) was used with different gap distances.

Figure 5 illustrates the behavior of the frequency of the negative impulses when air pressure is varied. To obtain the effect of changes in pressure the electrodes were enclosed in a glass chamber having a grounded screen around the

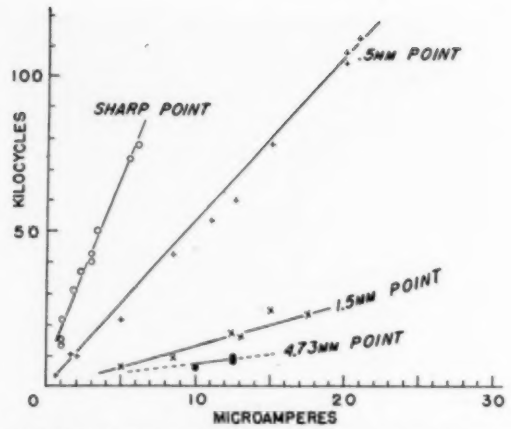

FIG. 3. Plot of the variation of frequency as a function of point size.

inside to prevent the accumulation of charge on the glass. The effects of small changes in pressure are not well resolved but some information can be gained as to the general trend of change in frequency with pressure.

DISCUSSION

Negative point corona phenomena appear to depend almost entirely upon the surface of the

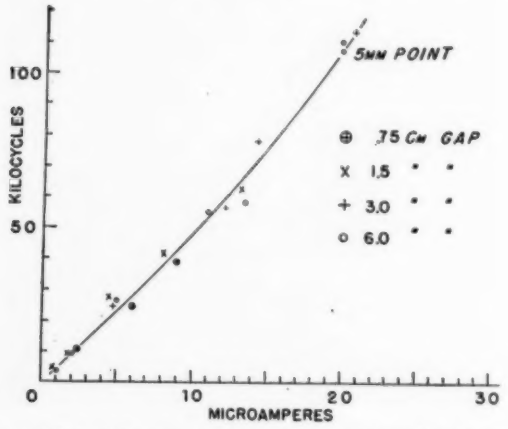

FIG. 4. Plot of the variation of frequency with change in gap distance for a 0.5-mm point.

point and the conditions which exist in the immediate vicinity of the point. The corona starts when a field exists near the point sufficient for a positive ion (produced in the field by some outside agency) to gain enough energy in its last free path to produce at least one secondary electron. The value of this energy depends on the work function of the surface for secondary electron emission on positive ion bombardment. This is described by Townsend's coefficient γ and γ is high when the work function is low. The coefficient γ is dependent on the state of the surface and is altered materially by adsorbed gas films.

The new electron proceeds away from the cathode in a field strong enough for it to form new ions by inelastic collisions with neutral molecules, and the electrons so ejected may continue the process of ionization. The number of ions *per impact* of electrons with molecules decreases as the electrons recede from the electrode to weaker field regions. The electrons, however, initially increase nearly exponentially in number with distance from the electrode until the fields become too weak to cause ionization. In air the electrons, after being slowed down, eventually attach to O_2 molecules to form negative ions. In the region where the electrons attach the accumulation of negative ions builds up a strong negative space charge. After a series of such cumulative electron avalanches, the process has left behind a cloud of positive ions of more or less spindle-shaped density contour with its apex towards the cathode. This process occurs in about 10^{-7} second. The positive ion space charge then moves towards the cathode under the influence of the field in the gap. The presence of this cloud of positive ions in the gap at first causes a greatly increased field near the negative point with increasing ionization by collision in this region and increasing secondary emission of electrons from the cathode. At the same time, the field beyond this space charge in the gap is decreased so that almost no ionization can take place beyond some tens of electron free paths. When this cloud of positive ions has reached a point very close to the cathode, ionization by collision practically ceases, and shortly thereafter the current begins to decrease. This comes about because the distance between the cathode surface and the positive space charge is zero or else too short to permit successive ionizing impacts in this region and through the shielding effect of the positive space charge which reduces the field beyond it to a point below that at which ionization by collision can occur. The current thus declines as the latter part of the dense portion of the ion cloud is drawn into the cathode. As

the last individuals of the positive ion cloud reach the cathode, giving a weak current, the field again rises to high values beyond the first few free paths. The few remaining positive ions approach with sufficient energy to release at least one more electron causing the process of multiple ion production to repeat itself. The oscillatory nature of the current therefore depends upon the fact that the great mass of positive ions are produced by ionizing impacts by electrons at some distance from the cathode, in a position where they must ultimately choke off the discharge. This causes the stopping of electron ionization beyond the cathode space charge and results in a marked decrease or cessation of corona current until the normal gradients are restored.

In support of this explanation of the process we have already noted that the frequency is not a function of gap length for a given point, but varies linearly with current independent of gap length. The current however increases as the potential applied to the point increases. Hence the sweeping rate must increase as the fields increase. The added field also enables ionization to begin before as much of the space charge has been dissipated as is the case for lower fields. Thus as the potential increases the new discharge starts at a higher value of the decreasing current, and the discharges are more frequent. The sharply defined frequency and the fact that the current increases *nearly* in proportion to the frequency implies a marked constancy in other factors affecting the current such as area of discharge, etc. This inference indicates that further discussion requires more data concerning the discharge than that given by the oscillograms.

The quantitative studies were accordingly supplemented by a visual observation of the corona with a telemicroscope of some ten cm focal length such as is used with electroscopes. Observations with the dark-adapted eye yielded the following data, some of which may be new. The discharge for sharp needles always localized at the point, in the region of highest field strength and was confined to that region. With larger points the glow extended over limited but greater areas than with sharp points. While the glow was *near* the region of highest field intensity, it was *not always* to be found at that point. The glow, however, always started at the same spot on a given point and always *remained about constant in size* irrespective of current until there appeared a new or second spot. The sizes observed varied but lay between 0.15 mm and 0.20 mm in diameter for the point used. Plural spots were confined only to more extended surfaces at higher fields. This action of the active area contrasts sharply

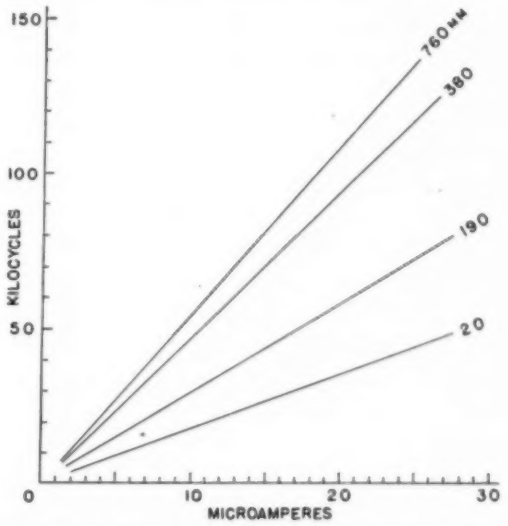

FIG. 5. Plot of the variation of frequency as a function of air pressure.

with the positive point where the glow spread progressively over the point as current and field increased.

Perhaps the most striking observation was that the intense zone of bluish light always appeared slightly detached from the cathode surface, indicating the existence of an exceedingly minute dark space next the cathode, analogous to the Crookes dark space. Beyond this the luminosity gradually faded off to be followed in general by another dark space, analogous to the Faraday dark space, beyond which there was a distinct but faint and very diffuse violet glow. This is shown in the sketch of Fig. 6. As fields and currents increased or pressure decreased this faint glow, analogous to the positive column, spread further into the gap, eventually covering quite a region about the point.

When the field had increased sufficiently with the larger points, a second luminous discharge spot appeared on the point. Frequently the appearance of the second spot caused the first

spot to extinguish temporarily and thereafter the discharge alternated from one spot to the other. At still higher currents a third spot was observed, etc. While the regularity of the discharges shown in Fig. 2 at high frequencies is in part disturbed by the limit of resolution of the oscillograph, the indications were that the periodic discharge went over to an irregular discharge at currents and potentials at which the second spot appeared. The discharges always appeared at the same localities and at about the same currents and potentials for a given point.

The discussion of the observed quantitative data indicated that it was necessary to consider the area of the discharge, for the whole previous discussion was confined to electrode areas involving a few electron avalanches which are infinitesimal. However, as was seen, except for the finest points the regular discharge as usually observed covers an area far from infinitesimal, $\sim$0.1 mm. This requires explanation. From what is known of the mechanism, it is clear that the discharge must always start from that region at which we have the lowest work function for secondary electron emission by positive ion bombardment, i.e., the highest γ, and the highest field strength available. This means that for any extended surface spots which have an especially high γ may initiate a discharge even though they are *not* at the point of highest field intensity. Once the discharge initiates at one spot by positive ion impact, the intense photoelectric ionization about the active zone will spread positive ions laterally so that the *area* of the spot will *spread as far as the region of low work function and high field localization* will permit. This lateral spread of ionization over the electrode surface must be very rapid; otherwise the current rise could not be as sharp as observed. Thus the maximum ionization and the positive ion flow must be achieved over the spot in less than 10^{-6} second. If regions of very variable γ exist, a spot will be confined only to a region where the highest γ obtains with the requisite field. Spots will be larger for points of large radius than for small points as the larger high field regions give a greater opportunity for fully utilizing sensitive areas of high γ. Different electrodes may show spots of differing size. For a given electrode material the frequency for a given current should

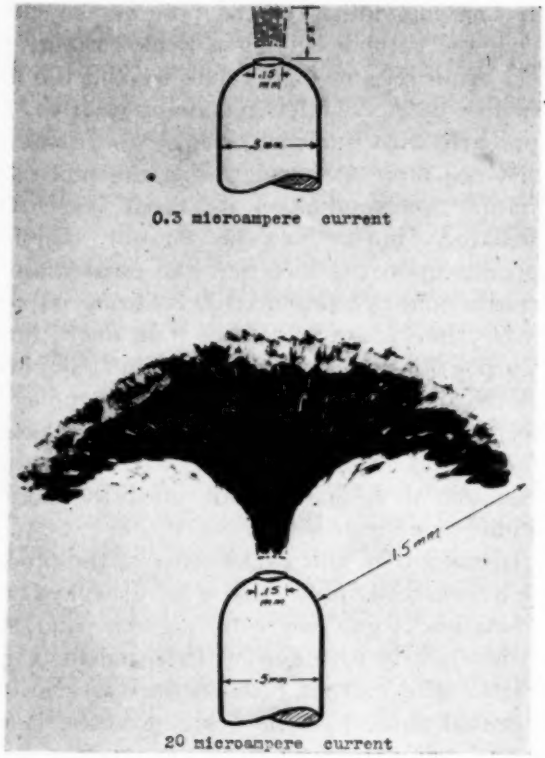

FIG. 6. Visual appearance of negative point corona.

increase at first rapidly as the point becomes larger eventually for large points reaching a constant value characteristic of the particular electrode. As γ does not change *continuously* over the surface, small increases in field strength and current cannot increase the spot area markedly. The current for a given spot will thus be able to increase only by a more rapid sweeping rate and accordingly more rapid discharge rate, as indicated by the results. Hence the frequency is nearly a linear function of the current. Non-linearity would be accounted for by slight changes in spot area as have been observed. With sharp points the fields are higher for the same current on account of the limited region and surface area available for discharge and consequently the frequency is higher for a given current.

The limit of frequency at which the periodic discharge disappears and gives place to the irregular noisy corona has not as yet been observed. It must occur at currents and potentials where more than one spot appears, as coherence of phase then ceases. The movement of the discharge from one spot to the next and

back again can be explained on a classical basis. Positive ion bombardment denudes the surface of its gas film. This decreases γ and the discharge shifts to a spot of higher γ and appropriate field strength. After some time the first spot regains its sensitivity and the discharge returns.

Decreasing the pressure increases the mean free path of the electrons and the mobility of the ions. Thus the potential difference required to give a certain current might be expected to decrease in proportion to the pressure. The potential difference between the electrodes required to produce a given corona current, however, decreases by a factor less than the ratio of pressures. This follows since the reduction of pressure reduces the number of molecules in the high field region. The scarcity of molecules and correspondingly increased mean free path increase the distance between inelastic collisions. Hence if the same number of ions are produced, Townsend's α must have an appreciable value at *greater* and *greater* distances from the electrode as the pressure is decreased which in turn means an increased field. That is, the space charge is produced at a distance from the cathode and increases as pressure decreases thus requiring higher point potentials. This is borne out by the visual observation that the whole discharge appears to extend farther out into the gap at low pressure than for the same current at atmospheric pressure.

The frequency of the negative corona process must depend upon (1) the rate of ion production and (2) the rate of clearing of the space charge by the field. Since the ionizing electrons travel at high speeds the current will rise at a high rate; perhaps the slowest element is the time taken in lateral spread of the spot. The decline of the current depends on the cessation of ionization because of space charge accumulation and the time for a finite travel of the newly created positive ions to the electrode to remove the space charge. This time will vary with the field gradient. The decline of current follows the cessation of ionization and the sweeping out of the positive ion cloud. The decline will thus at first be rapid, becoming slower as the less dense and most distant portions of the positive ion cloud are drawn in. This accounts for the shape of the current pulses shown in Fig. 2. As the fields increase in intensity the positive ions are swept from the critical region in shorter time intervals, and the degree to which the ions are swept out for the next discharge does not need to be nearly as complete. Ionization will therefore begin again at a higher point on the discharge curve exactly as is shown by a comparison of the shapes of the oscillograms made under different discharge current conditions.

Mr. M. Sitney working in this laboratory has made a graphic study of the ionization produced in the vicinity of parabolic points. For these points the field before onset is capable of mathematical solution as a function of the total potential across the gap and the distance from the point. His plots of the ionization produced by a single electron ejected from the point obtained by numerical integration based on Sanders' values[1] of Townsend's α give a space distribution of ions in substantial agreement with the hypothesis of the writer. In this calculation, however, the very important effect of the positive space charge on the character of the curve had to be omitted.

The calculated distance of the *peak* of the positive ion space charge distribution from the electrodes for points of 0.25 and 0.5 mm radius at values of X/p at the surface of 105 and 108 is 0.05 mm and 0.2 mm at 760 mm pressure. In actual practice the effect of the space charge will be to shift the maximum very much nearer the electrode and to steepen the front. Except for various distorting factors in the detector and in current measurement the shape of the *current impulse* due to positive ions may not be far from the actual contour of positive space charge density. Thus one may well expect the distances to the electrode to be *materially less than those calculated*, in agreement with observation; for the thickness of the Crookes dark space was too small to resolve in the telemicroscope. The intensity of ionization at the maxima will cause the maximum luminosity of the spot to be in a very thin region about this point. At the *electrode surface*, despite the high fields and high values of α, however, there will be a relatively dark region akin to the Crookes dark space due to the relatively few ions formed. The exceptionally

[1] F. B. Sanders, Phys. Rev. **41**, 667 (1932); **44**, 1020 (1933).

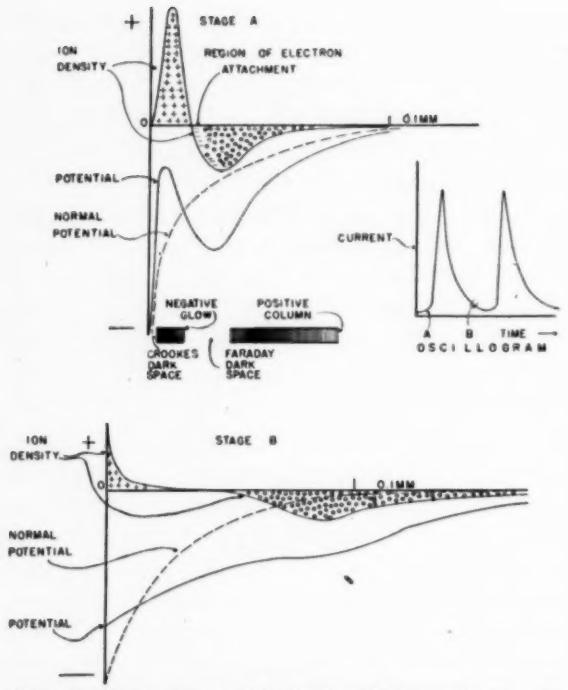

FIG. 7. Space charge distribution before and after the electron avalanches. Stages *A* and *B* probably correspond to points *A* and *B* on current oscillograms.

high fields between positive space charge and electrode, together with the values of the probability of excitation and ionization, will cause the appearance of the highest states of excitation in the luminous portion or negative glow. Here spark lines should be quite prominent. This is indicated by the color and spectra of the discharge. The progress of the electrons away from the point and their relatively rapid attachment to make slow ions when their energy is reduced at some distance from the point will build up a considerable negative space charge well beyond the luminous region of positive ions. With the weak field over the main length of the gap, the space charge can build up to considerable magnitudes where electrons attach. Hence a marked field distortion can take place. In this region of negative space charge, gradients of sufficient magnitude again might occur to cause ionization and excitation. These fields will be low compared with those at the point but may produce enough ionization and excitation to give a faint luminosity. In the region between the far side of the positive space charge and the negative space charge there appears to be little ionization. The "positive" column observed is probably the region of distortion due to the negative space charge concentration and the Faraday dark space corresponds to the region between this and the positive space charge. At high current densities the extent and intensity of these regions become much increased. The conditions which appear to exist are indicated schematically in Fig. 7, which is self-explanatory. From this it is clear that ultimate breakdown to a spark will occur as a result of the negative space charge accumulation at high current densities.

In conclusion the writer desires to express his gratitude to Professor L. B. Loeb, under whose direction the work was undertaken, for his continual guidance and for his considerable contribution towards the interpretation of the results. The writer also wishes to acknowledge his thanks to Mr. A. F. Kip, Research Corporation Fellow, for his hearty cooperation in many of the measurements and in their interpretation. The writer's thanks are due to Mr. M. Sitney, voluntary research worker, for his assistance in calculations. The writer must also acknowledge his indebtedness to the assistance of Mr. Edward Nunes and Mr. Roy Melton, workers on W.P.A. for their kindness in building up many of the electrical circuits required in this and in the positive corona study.

An Experimental Investigation of de Broglie's Equation

J. G. TAPPERT
Randal Morgan Laboratory of Physics, University of Pennsylvania, Philadelphia, Pennsylvania
(Received May 9, 1938)

The validity of de Broglie's equation is checked experimentally for electrons of 24 to 64 electron-kilovolts energy. The experiment consists essentially of deflecting a beam of cathode rays by an electrostatic field and, keeping the deflection constant, determining the relation between the intensity of the deflecting field, V, and the de Broglie wave-length, λ, of the deflected electrons. On the assumption that the motion of the electrons is in accordance with the laws of relativistic mechanics, and that the de Broglie wave-length is inversely proportional to the momentum, it is shown theoretically that the expression $\lambda^2 V(1+h^2/m_0^2c^2\lambda^2)^{\frac{1}{2}}$ should be independent of λ. Within the limits of experimental error this expression is found to be independent of λ, thereby demonstrating that the de Broglie equation, $\lambda=h/mv$, combined with the relativity expression for m, is adequate to describe the facts.

I

SINCE the discovery in 1927 of the phenomenon of electron diffraction, many experimenters have been attracted to this field. The great usefulness of electron diffraction as a *method* of research soon became apparent and, as a consequence, electron diffraction, itself, as a *subject* of research was somewhat neglected. In particular, few experiments[1-9] have been performed to check the fundamental relation given by de Broglie's equation,

$$\lambda=(h/m_0v)(1-v^2/c^2)^{\frac{1}{2}}.$$

The present research was undertaken in order to obtain an increase of precision in checking the theory by experiment. The method used avoids the necessity of measuring high voltages or determining the geometry and absolute intensity of deflecting fields of force, and thus eliminates the principal sources of error encountered by earlier experimenters.

II

The diffraction apparatus used to investigate the validity of the de Broglie relation is shown schematically in Fig. 1.

The beam of electrons produced in the cold cathode discharge tube is collimated by two diaphragms placed 8.9 cm apart. The circular openings in these diaphragms are 0.01 cm in diameter. The collimated beam passes between two mutually insulated plates which constitute a velocity selector. These plates are about 11.4 cm long, 1.9 cm wide and separated from each other by 0.475 cm. A final diaphragm, located 2.5 cm beyond the deflecting plates, is provided with a hole 0.01 cm in diameter. The specimen holder is securely fastened to this diaphragm. Another diaphragm, provided with a 0.041-cm slit, is located 1.9 cm in front of the final diaphragm. This diaphragm serves to prevent secondary electrons, produced in the velocity selector, from passing through the final hole.

A sheet of lead foil separates the diffraction and camera chamber from the velocity selector chamber, thus assuring a field-free space in the former. The total distance from the specimen holder to the photographic plate is 29.46 cm. A baffle, located approximately midway between the specimen holder and the photographic plate prevents reflections from the walls of the tube.

A pair of Helmholtz coils, of 12-inch radius, is mounted around the diffraction apparatus in such a position as to neutralize effectively the earth's magnetic field in the region between the anticathode and the specimen holder.

Two stages of mercury diffusion pumps, backed by a Cenco vacuum pump, serve to evacuate the velocity selector and camera

[1] G. P. Thomson, Proc. Roy. Soc. **117**, 600 (1928); **119**, 651 (1928); **125**, 352 (1929).
[2] A. Reid, Proc. Roy. Soc. **119**, 663 (1928).
[3] R. Ironside, Proc. Roy. Soc. **119**, 668 (1928).
[4] M. Ponte, Ann. de physique **13**, 395 (1930).
[5] E. Rupp, Ann. d. Physik **9**, 458 (1931); **10**, 927 (1931).
[6] F. Kirchner, Ann. d. Physik **11**, 741 (1931).
[7] R. v. Meibom and E. Rupp, Ann. d. Physik **13**, 725 (1932); **17**, 221 (1933).
[8] J. Gnan, Ann. d. Physik **20**, 361 (1934).
[9] J. V. Hughes, Phil. Mag. **19**, 129 (1935).

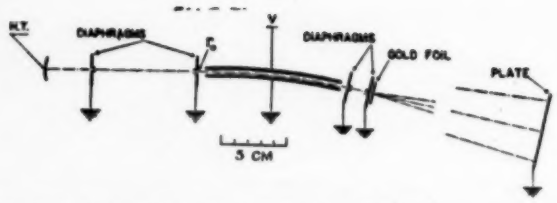

FIG. 1. Schematic diagram of electron diffraction apparatus.

chambers. The pressure in these parts is kept below 10^{-6} mm of Hg, during operation. A separate diffusion pump, operating into the same fore-vacuum, is used for the discharge tube. The pressure in the discharge tube is regulated to give the correct current flow by means of an adjustable leak from the fore-vacuum.

The high tension for the discharge tube is obtained from a 70,000-volt transformer. A commutator type rectifier provides full-wave rectification. An autotransformer in the primary circuit permits the desired control of the voltage. Two large Leyden jars, across the high tension lines, serve to by-pass the high frequency components introduced by the commutator.

The deflecting voltage, used by the velocity selector, is obtained from a power pack of conventional design. The filter circuit of this power supply includes six microfarads capacity. Since the maximum current drawn from this power pack is only 300 microamperes, the 60-cycle ripple is negligible. Line fluctuations in the primary power lines are reduced to a minimum by means of a saturated iron type voltage regulator. A high resistance potentiometer permits the necessary voltage adjustment. The maximum voltage available is about 850 volts.

A 300-volt, megohm Weston voltmeter, provided with a suitable precision wire-wound multiplier, serves for the determination of the deflecting voltage. The voltmeter was carefully calibrated against a Weston laboratory standard voltmeter (0.1 percent accuracy).

A comparator was used to measure the diameters of the diffraction rings registered on the photographic plates.

III

In this section there will be developed certain theoretical relationships which serve as the basis of the experimental work.

Consider an electron traveling through a potential field, $V\phi(\mathbf{r})$, where V is a scalar parameter independent of $\mathbf{r}$. If the accelerating field $\nabla(V\phi)$ is not great, the motion of the electron is "quasi-stationary," and in accordance with the equation

$$e\nabla(V\phi)=m_0 d/dt\{(1-v^2/c^2)^{-\frac{1}{2}}d\mathbf{r}/dt\}. \quad (1)$$

This may be transformed into

$$Ve\nabla\phi=m_0\left(1-\frac{v^2}{c^2}\right)^{-\frac{1}{2}}\frac{d^2\mathbf{r}}{ds^2}+m_0\frac{dv}{ds}\left\{\left(1-\frac{v^2}{c^2}\right)^{-\frac{1}{2}}v+\left(1-\frac{v^2}{c^2}\right)^{-\frac{1}{2}}\frac{v^3}{c^2}\right\}\frac{d\mathbf{r}}{ds}. \quad (2)$$

Recalling that the vectors $d\mathbf{r}/ds$ and $d^2\mathbf{r}/ds^2$ are at any point mutually perpendicular, and that $d\mathbf{r}/ds$ is a unit vector, we get by scalar multiplication,

$$Ve\nabla\phi\cdot\frac{d^2\mathbf{r}}{ds^2}=m_0\left(1-\frac{v^2}{c^2}\right)^{-\frac{1}{2}}v^2\left(\frac{d^2\mathbf{r}}{ds^2}\right)^2, \quad (3)$$

and

$$Ve\nabla\phi\cdot\frac{d\mathbf{r}}{ds}=m_0\frac{dv}{ds}\left\{\left(1-\frac{v^2}{c^2}\right)^{-\frac{1}{2}}v+\left(1-\frac{v^2}{c^2}\right)^{-\frac{1}{2}}\frac{v^3}{c^2}\right\}. \quad (4)$$

At points where the curvature of the trajectory does not vanish, Eq. (3) gives

$$\frac{e}{m_0c^2}\frac{\nabla\phi\cdot d^2\mathbf{r}/ds^2}{(d^2\mathbf{r}/ds^2)^2}=R=V^{-1}\left(1-\frac{v^2}{c^2}\right)^{-\frac{1}{2}}\frac{v^2}{c^2}. \quad (5)$$

By integration, Eq. (4) gives

$$\left(1-\frac{v^2}{c^2}\right)^{-\frac{1}{2}}=\left(1-\frac{v_0^2}{c^2}\right)^{-\frac{1}{2}}+\frac{Ve(\phi-\phi_0)}{m_0c^2}, \quad (6)$$

in which v_0 is the velocity of the electron at a point where the potential is $V\phi_0$.

Equation (5) may now be written,

$$R=\frac{\left\{\left(1-\frac{v_0^2}{c^2}\right)^{-\frac{1}{2}}+\frac{Ve(\phi-\phi_0)}{m_0c^2}\right\}^2-1}{V\left\{\left(1-\frac{v_0^2}{c^2}\right)^{-\frac{1}{2}}+\frac{Ve(\phi-\phi_0)}{m_0c^2}\right\}}. \quad (7)$$

If we now impose the condition that $d^2\mathbf{r}/ds^2$ (at a point where $\phi=\phi_0$) be independent of the energy of the electron, we get

$$V^{-1}(1-v_0^2/c^2)^{-\frac{1}{2}}(v_0^2/c^2)=R_0\neq f(v_0). \quad (8)$$

Substitution of Eq. (8) in Eq. (7) results in

$$R=R_0+2\frac{e(\phi-\phi_0)}{m_0c^2}-\frac{e(\phi-\phi_0)}{m_0c^2}\cdot\frac{v_0^2}{c^2}$$

$$+\text{higher powers of } e(\phi-\phi_0)/m_0c^2. \quad (9)$$

The first two terms on the right of this expression are independent of the energy of the electron. Under the conditions of the experiment to be described the remaining terms are less than 0.07 percent of R_0.[10] Thus, if Eq. (8) is satisfied, $d^2\mathbf{r}/ds^2$ is, within the limits of experimental error,[11] independent of the energy of the electron. That is, the differential equation of the trajectory,

$$d^2\mathbf{r}/ds^2=F(d\mathbf{r}/ds,\mathbf{r}), \quad (10)$$

is independent of the electron's energy. If the point of entry of the electron into the field, $V\phi$, and the direction of the electron's velocity[12] at that point are also independent of the energy, the whole trajectory will be independent of the electron's energy. The construction of the apparatus insures that these boundary conditions are satisfied. From the de Broglie relation

$$\lambda=(h/m_0v)(1-v^2/c^2)^{\frac{1}{2}}, \quad (11)$$

the third condition, Eq. (8), may be written

$$\lambda^2V(1+h^2/m_0^2c^2\lambda^2)^{\frac{1}{2}}=h^2/m_0^2c^2R_0=\text{const.} \quad (12)$$

The fact that this equation represents the condition that the path of the electron is independent of λ (or the energy) constitutes a verification of de Broglie's relation, (11).

It will be noted that the development given above makes no assumptions concerning the form of the electric field other than that $e(\phi-\phi_0)/m_0c^2$ is small compared to R (Eq. (9)). This greatly simplifies the experimental application of the developed relations.

IV

From Fig. 1 it is clear that at the point, $\mathbf{r}_0$, the cathode rays travel in a direction fixed by the two collimating diaphragms, and that in the space between the two plates the electric field at any point is directly proportional to the voltage applied between the plates. It is also evident from the unidirectional character of the electric field that a single point, beyond the deflecting field, will serve to determine uniquely the whole trajectory of the beam passing through that point. Thus, the beam that passes through the final diaphragm hole satisfies the conditions which were shown, in Part III, to lead to the expression $\lambda^2V(1+h^2/m_0^2c^2\lambda^2)^{\frac{1}{2}}=\text{constant}$.

Eighteen photographs were taken to check the validity of this equation. The energies of the cathode rays were between 24 and 64 electron-kilovolts. Gold was used as the diffracting material.

In the analysis of these plates the following sources of error must be considered:

(1) *The measurement of the deflecting voltage.*—Because of the calibration of the voltmeter against the Weston laboratory standard voltmeter, the voltage readings are reliable to about 0.1 percent of their full scale reading. (Full scale reading with multiplier—850 volts.) An error in the value of the multiplier resistance would have no significant effect on the results, since it would

TABLE I. *Experimental results.*

PLATE	V (e.m.u.)	λ (cm)	λ^2V (e.m.u.)	$\lambda^2V(1+h^2/m_0^2c^2\lambda^2)^{\frac{1}{2}}$ (e.m.u.)
11–2	8.080×10^{10}	4.713×10^{-10}	1.795×10^{-8}	2.019×10^{-8}
18–5	8.000	4.730	1.790	2.012
18–2	7.789	4.812	1.804	2.020
8–2	7.469	4.907	1.799	2.007
18–4	7.200	5.013	1.810	2.011
16–5	6.920	5.127	1.819	2.013
16–2	6.754	5.188	1.818	2.007
8–4	6.451	5.321	1.827	2.008
11–3	6.051	5.510	1.837	2.008
18–3	5.703	5.694	1.849	2.009
8–1	5.509	5.808	1.858	2.014
16–3	5.440	5.841	1.856	2.010
16–4	4.926	6.183	1.883	2.023
11–5	4.469	6.490	1.882	2.009
11–1	3.989	6.919	1.909	2.024
16–1	3.520	7.366	1.910	2.011
18–1	3.217	7.711	1.913	2.006
11–4	3.046	7.881	1.892	1.979

[10] The approximate values of the quantities involved are: $R_0=3\times10^{-12}$ e.m.u., $e(\phi-\phi_0)/m_0c^2(\text{max.})=1\times10^{-14}$ e.m.u., $v_0^2/c^2(\text{max.})=0.2$.

[11] An error of 0.07 percent in the experimental determination of V would result in an error of 0.07 percent in the curvature along the *whole* electron path. Since the precision of the measurement of V is not sufficient to detect such an error, the uncertainty due to variation of curvature with electron energy is, *a fortiori*, less than the accidental errors of measurement.

[12] These are the boundary conditions for the differential equation (10).

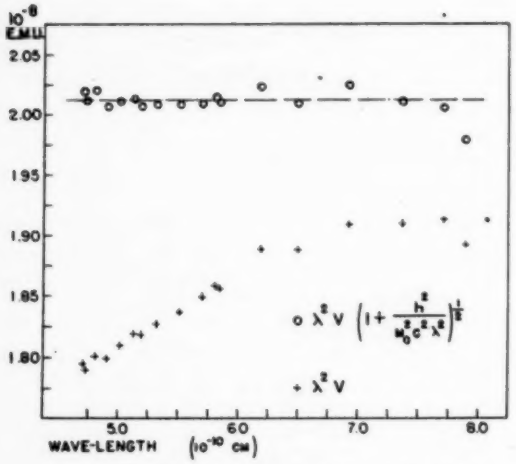

FIG. 2. Results of the experimental test of de Broglie's equation.

merely change the value of the constant determined.

(2) *Determination of the wave-length.*—The only appreciable errors in the determination of the wave-length are due to the measurement of the diffraction ring diameters. Small errors in the plate distance or in the assumed lattice constant of gold, since they have nearly equal effects for all plates, merely change the value of the experimentally determined constant. The probable error in the determination of λ, calculated from the statistical deviations of various diameter measurements, is considerably less than 0.1 percent for most of the plates.

The experimental results are tabulated in Table I and shown graphically in Fig. 2. It is evident that the function

$$\lambda^2 V(1+h^2/m_0^2c^2\lambda^2)^{\frac{1}{2}}$$

is actually found to be a constant for electrons in the range of energies from 24 to 64 electron-kilovolts.[13]

The average value of the quantity

$$\lambda^2 V(1+h^2/m_0^2c^2\lambda^2)^{\frac{1}{2}},$$

as measured on seventeen plates, is 2.0124×10^{-8} e.m.u. with a mean deviation of 0.0045×10^{-8}. The average value of the first eight plates, taken in order of increasing λ, is 2.0121×10^{-8} with a mean deviation of 0.0039×10^{-8}. The average of the last eight plates is 2.0132×10^{-8} with a mean deviation of 0.0052×10^{-8}.

We note that the precision of the experiment, statistically determined, is in fair agreement with the anticipated errors of measurement—the constant is reliably determined to within about 0.2 percent. Since the constant is approximately proportional to λ^2, we may conclude from this experiment that the de Broglie wave-length of an electron, in the energy range of 24 to 64 electron-kilovolts, is inversely proportional to the momentum to within about 0.1 percent. This is, then, a close confirmation of the de Broglie relation.

For the sake of comparison, Table I and Fig. 2 also include the values of the product $\lambda^2 V$. *Without* relativity this quantity would be constant.

V

The constant of proportionality in de Broglie's equation was not determined in the present experiment. The method used, however, might be extended in the following manner to obtain the value of this important constant.

If electrons of moderate energy were employed, it would be possible to measure with precision both the discharge tube voltage and the voltage impressed on the deflecting plates. A Faraday collector would serve to indicate when the electron beam actually passed through all the diaphragms. (No diffracting material would be used.) The constant, R_0, of the apparatus could then be calculated from Eq. (8) since the energy of the electrons as well as the necessary deflecting voltage would be known. The constant of Eq. (12), as determined by the present experiment, would then be a definite function of universal constants. The determination of this combination of universal constants would depend, then, only upon the measurement of moderate voltages and the measurement of wave-lengths by a diffraction experiment.

The writer wishes to acknowledge his indebtedness to Professor C. B. Bazzoni, under whose direction this investigation was undertaken, for kindly encouragement and advice.

[13] Plate 11–4 is obviously discordant and is not included in the summary. The deviation of this plate from the average is more than seven times the average deviation of the remaining plates. This plate was considerably fainter than the others.

Note on the External Photoelectric Effect of Semi-Conductors

E. U. CONDON
Westinghouse Research Laboratories, East Pittsburgh, Pennsylvania
(Received October 10, 1938)

An analysis of the effect of contact potentials on photoelectric measurements with semi-conductors is made, which indicates a new method of determining the width of the forbidden energy interval for electrons in a semi-conductor. A possible application to precision determination of h/e by the photoelectric effect is indicated.

THE usual textbook and lecture account of Einstein's photoelectric equation does not state the case very carefully in regard to the effect of contact potentials on the actual experimental arrangements. The situation is correctly presented in Hughes and DuBridge, *Photoelectric Phenomena*, p. 22, where attention is called to some anomalous results obtained with copper oxide in Millikan's early work, which Millikan described as "spurious" contact potential differences. The point of this note is to show that these "spurious" contact potential differences have a natural explanation in terms of current theories of semi-conductors and that accurate measurement of them can give information of importance for our knowledge of semi-conductors.

For the reader's convenience, the argument concerning the stopping potentials for photoelectrons will be repeated here in its usual form. Fig. 1 shows the experimental setup with light of frequency ν falling on the photoelectrically sensitive plate A, and potential V adjustable until none of the electrons emitted from A are able to reach the collector C. Then V is said to be the stopping potential for this combination of electrodes and this frequency of light. Of course, as is well known from the recent careful researches of DuBridge, Houston, and others,[1] there is no sharply defined value of V at which the current abruptly cuts off, but rather it tails off as an exponential function of Ve/kT. This is as good as a sharp cut-off if we ignore quantities of the order kT (1/40 electron volt at room temperature) which will be done in the first part of the discussion.

Figure 2 is a schematic energy level diagram showing the potential energy of an electron when in A, in C, and in the space between. The curve, potential energy, labeled U, rises abruptly by 10 or 20 electron volts in a distance of 10^{-8} cm or so at the surface of each conductor and is approximately constant over the macroscopic distance of separation of the two conductors. For each conductor there is drawn in Fig. 2 a horizontal line at the level corresponding to the thermodynamic potential per electron, $u-Ts+pv$, of the electrons in that conductor. If the two conductors are allowed to come into thermodynamic equilibrium by mutual exchange of charges, they will take up total charges that will set up a field such that the thermodynamic potential of the electrons in each metal is the same. However, if they only exchange charges rapidly through the agency of an external source of electromotive force located between them as at V in Fig. 1, then a quasi-equilibrium state is set up in which the thermodynamic potentials of the electrons in the two conductors are related as in Fig. 2.

In the theory of thermionic emission, it is shown that the thermionic work function is equal to the difference between potential energy of an electron just outside the emitter and the thermodynamic potential per electron of an electron inside the emitter, so K_A and K_C are the respective work functions in Fig. 2. In considering the

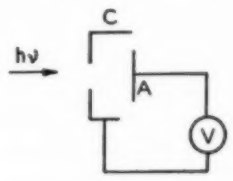

FIG. 1. Experimental arrangement.

[1] DuBridge, *New Theories of the Photo-electric Effect*, Actualités scientifiques et industrielles, 268 (Herman et Cie., Paris, 1935): Houston, Phys. Rev. **52**, 1047 (1937).

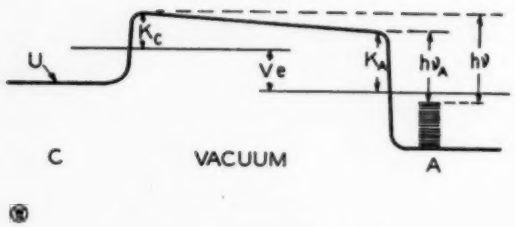

FIG. 2. Schematic energy level diagram.

photoelectric emission of electrons from A, the usual Einstein relation is used, which says that in the direct act of absorption of a quantum of light, all the energy $h\nu$ of that quantum is directly given to the single electron, which makes a transition in the absorption act. This means that the most energetic electrons emitted have an energy $h\nu$ greater than that of the most energetic electrons in the emitter that are able to absorb light. Ignoring quantities of the order kT we may say that the most energetic electrons in A are those whose energy is $h\nu_A$ less than the potential energy of a free electron at rest just outside of A. Then if V has been so adjusted that it just stops the fastest electrons from reaching the collector C, we shall have a situation in which the level that is $h\nu$ above the limiting energy of electrons in A will be equal to the energy of an electron at rest just outside of C, that is, calling this stopping potential V_A,

$$eV_A+K_C=(K_A-h\nu_A)+h\nu. \quad (1)$$

If arrangements are made to substitute an emitter B in place of A without disturbing the properties of C, then for its stopping potential V_B, the analogous equation holds

$$eV_B+K_C=(K_B-h\nu_B)+h\nu. \quad (2)$$

Suppose we measure V_A and V_B for the same light frequency. Subtracting the two equations, we have

$$e(V_A-V_B)=(K_A-h\nu_A)-(K_B-h\nu_B), \quad (3)$$

which gives, on the right, the theoretical interpretation of the experimentally observed quantity on the left.

The experiments[2] of Millikan and also of Kadesch and Hennings show that when various metals are used for the different emitters A, B, the quantity V_A-V_B is zero. From this we conclude that the difference $(K_A-h\nu_A)$ is the same for all metals tested which is quite in accord with modern theory of metals. In the modern theory[3] the thermodynamic potential appears in the Fermi distribution function factor

$$(e^{(E-K_A)/kT}+1)^{-1},$$

which gives the probability of occupation of an allowed state by an electron if the allowed state is of energy E. This factor changes rapidly from unity down to zero over a region of the width kT at the place where $E=K_A$. Hence the theory predicts that $(K_A-h\nu_A)$ is the same for all metals and is actually equal to zero. The stopping potential measurements verify the first part of this statement and are consistent with the second.

However, the experiments of Millikan showed that when one of the pair of emitters was a metal, say B, and the other, say A, is copper oxide, a semi-conductor, then V_A-V_B is not zero, but is of the order of one volt. This effect was described by Millikan by saying that copper oxide showed a *spurious* contact potential difference as contrasted with the *true* contact potential difference shown by metals. Attempts have been made to find an origin of the spurious contact potential difference in terms of grease films, etc.

It is clear that the origin of the so-called spurious potential difference is an intrinsic property of the semi-conductor itself. If B is a metal, then $K_B-h\nu_B$ is actually zero and the experimentally measured quantity (V_A-V_B) is a direct measure of the quantity $(K_A-h\nu_A)$ for the semi-conductor. This interpretation is also in accord with the modern theories of semi-conductors as developed principally by A. H. Wilson[4] and presented in Fowler's *Statistical Mechanics*. In a semi-conductor, it will be recalled, we have a band of allowed energy states which at absolute zero is completely filled. Above it is a forbidden range of energy, then one or more bands of allowed levels which are normally not occupied. In the case of an im-

[2] Millikan, Phys. Rev. **7**, 18, 355 (1916); **18**, 236 (1921); Kadesch and Hennings, Phys. Rev. **8**, 221 (1916).

[3] See for example, Sommerfeld and Bethe, *Handbuch der Physik*, Vol. 24/2 (Springer, Berlin, 1933), p. 342, or Fowler, *Statistical Mechanics* (Cambridge University Press, 1936), Chap. XI.

[4] A. H. Wilson, Proc. Roy. Soc. **A133**, 458 (1931); **A134**, 277 (1932).

purity semi-conductor, there are some extra levels associated with wave functions localized around the impurities or lattice imperfections in a manner that has often been discussed in the literature of semi-conduction. At any finite temperature there will be a very few electrons thermally excited into the upper band with a corresponding small deficiency of electrons from the otherwise filled band. The thermodynamic potential K_A has to take up such a value that the number of electrons thermally excited to the "empty" band is equal to the number missing from the "filled" band. Under simple, plausible assumptions, this makes K_A have a value at the center of the interval between the "filled" and "empty" bands. (See Fig. 3.) This neglects impurity levels and supposes the effective mass of electrons in each band to be the same. If these conditions are not fulfilled, then K_A will not be exactly in the middle of the forbidden interval, but in any case its location can be calculated in terms of basic features of the band structure and the location and number of impurity levels.

As to photoemission from the semi-conductor, the electrons of highest energy will result from the absorption of a quantum $h\nu$ by the very few electrons in the "empty" band. But these will be so few in number that it may be expected that they will have escaped detection in experiments where no special effort was made to find them. Then the highest energy electrons which appear in abundance will be those which come from the top of the "filled" band. Hence $(K_A - h\nu_A)$ will theoretically be not zero, and will in fact, be equal to one-half the width of the forbidden energy range in the simpler cases. This is the interpretation which is offered for Millikan's observations on copper oxide.

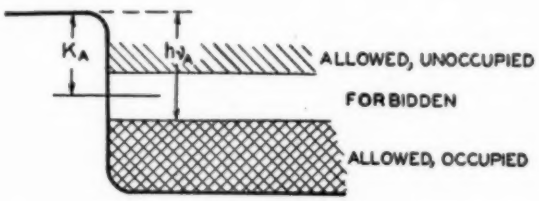

FIG. 3. Energy level diagram for semi-conductor.

The width of the forbidden energy range also plays a role in the temperature dependence of the bulk conductivity of the semi-conductor on Wilson's theory. While the existing data do not permit of any precision test of whether the photoelectric effect and the temperature dependence of conductivity give the same results, still both methods are in agreement for copper oxide in giving about two volts for the width of the forbidden range.[5]

Another interesting consequence of these ideas was pointed out to me by Dr. W. H. Wells, in a conversation at these Laboratories. He notes that the sharpness of cut-off of the photoelectron current with gradual increase of the retarding potential V ought to be much sharper in the case of a semi-conductor than in the case of a metal. This fact is of considerable interest in itself in view of the large amount of work that has gone into studying the details of the cut-off for metals.[1] It also seems to have an important bearing on experiments such as those of Houston and his associates[6] who are making precision determinations of h/e by measuring the change of stopping potential with change of light frequency. Difficulty of exact definition of what is meant by stopping potential is one of the most troublesome features of such experiments, and it seems that the difficulty would be obviated by using a semi-conductor instead of a metal as the photoemitter.

It appears, therefore, that the ideas here presented should provide a useful new approach to the study of semi-conductors and afford a means of unraveling the hitherto chaotic field of photoemission by compounds. They also suggest an improved way of determining h/e from the photoelectric effect. Experiments from the point of view of application to semi-conductors are being planned in these Laboratories.

[5] Gudden, Ergebn. d. exakt. Naturwiss. **13**, 223 (1934).
[6] Overhage, Phys. Rev. **52**, 1039 (1937). Also unpublished work reported by Houston at a colloquium during the Physics of Metals summer session of the University of Pittsburgh, 1938.

The Magnetization of Ferromagnetic Colloids

W. C. ELMORE*
Massachusetts Institute of Technology, Cambridge, Massachusetts
(Received October 12, 1938)

The magnetization curves of colloidal magnetite (Fe_3O_4) and colloidal siderac ($\gamma-Fe_2O_3$) have been determined by a null method for fields from 0 to 400 gauss. The measured curves have been found to agree with a theoretical curve based on the following assumptions: (1) Each colloid particle is a permanent magnet. This assumption is in accord with a prediction of the theory of ferromagnetism that small ferromagnetic particles be single magnetic domains. (2) There exists a distribution in the size of the particle moments similar to the weight distributions which have been found for other colloids. (3) The particles behave as the molecules of a classical paramagnetic gas. On this basis the average particle moment is found to be $5.2(10)^{-16}$ for the magnetite sol and $7.4(10)^{-16}$ for the siderac sol. Several other quantities related to the colloids are briefly discussed.

IN a recent note[1] the writer described the preparation of a colloidal magnetite suitable for studying magnetic structures by the magnetic powder method.[2] For various reasons it appeared interesting to investigate the magnetization curve of such a colloid, particularly since the magnetic properties of ferromagnetic colloids for the most part have escaped the attention of other workers. Knowledge of the magnetization curve should be useful for estimating the intensity of the stray fields responsible for the powder patterns. As a first step towards such an estimation the present study has been devoted to determining and analyzing the magnetization curves of two different ferromagnetic colloids which have been used in powder pattern investigations.

A number of years ago Frenkel and Dorfman[3] predicted from energy considerations that sufficiently small ferromagnetic particles (diameter 100 mμ or smaller) should be single ferromagnetic domains. An attempt by Montgomery[4] to verify this prediction for nickel colloids was unsuccessful, probably because the nickel oxidized before measurements could be made. As pointed out by Montgomery,[3] if the colloid particles be small permanent magnets, they should behave as the molecules of a classical paramagnetic gas obeying the Langevin equation

$$I=I_s\,(\coth a-1/a)=I_sL(a) \qquad (1)$$

where $a=\mu H/kT$. Since the magnetic moment per particle μ would have a value much larger than that of a single atom, saturation effects in weak fields ($a\geq 1$) should be easily observed. It will be shown that the magnetization curves for two different iron oxide colloids are actually similar to the Langevin curve, but that before a quantitative agreement can be made, it is necessary to modify the Langevin curve by assuming a distribution in the size of the particle moments. In addition, values of I_s must be taken smaller than those expected from the amount of iron present as determined by chemical analysis.

Method of Measurement and Specimens

Measurements were made by a null method. In a circuit containing a sensitive ballistic galvanometer the additional flux linkage produced by the sample was balanced by setting a calibrated mutual inductance. The arrangement used, shown by diagram in Fig. 1, was designed by Professor F. Bitter for the measurement of susceptibilities of the order of 10^{-3}. M_1 and M_2 were two mutual inductances made as nearly identical as possible and connected in opposition. The secondary coils, 5 cm long, contained 10,000 turns of fine wire. The primary coils, 25 cm long, had a mean diameter of 2.3 cm and produced a nearly uniform magnetizing field $H=41.9i$ over the length of the inner coil. M_3 was a Leeds &

* Now at Swarthmore College, Swarthmore, Pennsylvania.
[1] W. C. Elmore, Phys. Rev. **54**, 309 (1938).
[2] F. Bitter, *Introducion to Ferromagnetism* (McGraw-Hill Book Co., 1937), pp. 55–66.
[3] J. Frenkel and J. Dorfman, Nature **126**, 274 (1930). See also C. G. Montgomery, Phys. Rev. **38**, 1782 (1931).
[4] C. G. Montgomery, Phys. Rev. **39**, 163 (1932).

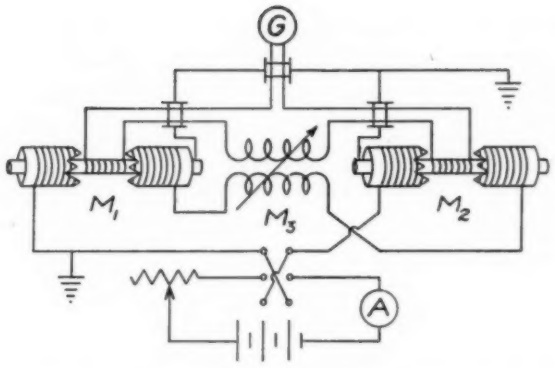

FIG. 1. Diagram illustrating the method used for measurements.

Northrup variable mutual inductance having a range +0.06 to −0.06 millihenry and safely passing 10 amperes. To prevent galvanometer drift, all secondary leads were shielded. The shields, the brass tubes on which M_1 and M_2 were wound, and one point of the primary circuit were all grounded.

For measurement, the colloid sample was drawn into the inner tube of M_1 which was mounted with its axis vertical. The zero balance was easily checked after allowing the sample to drain out. For large currents M_3 could be set for no galvanometer deflection directly to $(10)^{-7}$ henry by momentarily closing the primary circuit several times. For smaller currents, where the heating of the magnetizing coils was negligible and where the galvanometer deflections were smaller, a number of deflections each side of the balance point were taken by reversing the primary current. The balance point was then determined graphically to almost the same precision as for the larger currents. The measurements made by this method were good to a few percent.

By a simple analysis, the equations for the susceptibility k and the intensity of magnetization I of the colloid are the following:

$$k=\frac{(\Delta M)i(10)^8}{4\pi ANH}=54.3(\Delta M), \qquad (2)$$

$$I=\frac{(\Delta M)i(10)^8}{4\pi AN}=0.227(\Delta M)i, \qquad (3)$$

where ΔM = change in setting of M_3 (in henries) required for balance when the sample is introduced; i = magnetizing current in amperes; A = cross-sectional area of sample = 0.350 cm²; N = number of turns in secondary of M_1 = 10,000; H = magnetizing field = 41.9i gauss. The greatest current used was about 10 amperes; the values for ΔM ranged between the limits $2.7(10)^{-6}$ and $17(10)^{-6}$ henry.

Two different specimens were investigated: one, the magnetite sol prepared as already described;[1] the other, a sample of colloidal gamma-ferric oxide (siderac) prepared several years ago by means of a colloid mill by Sharp and Dohme of Philadelphia, Pennsylvania. The sample measured had remained undisturbed in a corked bottle for more than a year so that all coarse particles had settled out. Chemical analyses for total iron content[5] indicated that the two specimens contained iron equivalent to a

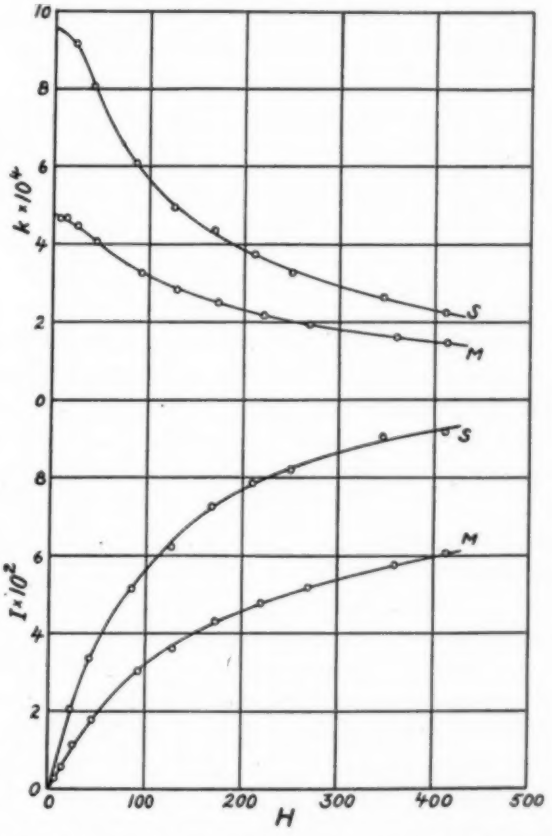

FIG. 2. Curves showing the dependence on field strength of the susceptibility and the intensity of magnetization for the magnetite colloid (curves M) and the siderac colloid (curves S).

[5] Kindly made by A. Klemka, Department of Chemistry, Massachusetts Institute of Technology.

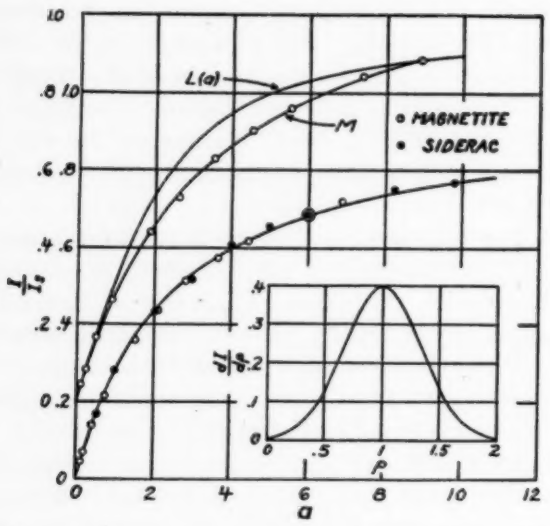

FIG. 3. Upper curves illustrate the poor agreement between the Langevin curve and the experimental curve for magnetite. Lower curve is the modified Langevin curve obtained by assuming the particle moment distribution shown in the insert. The experimental points for both colloids fit the modified curve within the experimental error.

concentration 0.00206 g/cm³ of Fe_3O_4 and 0.00420 g/cm³ of Fe_2O_3, respectively. All measurements were made at a room temperature of 27°C.

RESULTS AND DISCUSSION

The experimental curves for k and I *versus* H are shown in Fig. 2 for both the magnetite sol (curves M) and the siderac sol (curves S). In Fig. 3 (upper curves) the magnetization curve M has been fitted to the Langevin curve so that the two curves coincide at their extremities and have the same slope at the origin. This procedure amounts to choosing values for I_s and μ in Eq. (1). The agreement is by no means satisfactory and is no better for the siderac sol.

To improve matters, several possibilities have been considered. In particular it is suggested that a distribution in the size of the particle moments may be responsible for the discrepancy between the experimental and Langevin curve. The measurements of particle size distributions in colloids have been few in number and of fairly recent date. Using an ultracentrifuge, Nichols, Kraemer and Bailey[6] determined the (optical) weight distribution as a function of particle diameter r for certain iron oxide colloids. They found fairly broad distributions approximately Gaussian in shape. If the magnetic moment per particle is assumed proportional to the volume of the particle ($\mu = \text{const.}\ r^3$) then distribution in magnetic moments should be similar to the weight distributions. The expression

$$dI/d\rho = (B/\pi^{\frac{1}{2}}) \exp[-B^2(1-\rho)^2], \qquad (4)$$

where $\rho = r/r_0$ and B is a constant, is a Gaussian distribution about the particle diameter r_0. When $B \doteqdot 3/\sqrt{2}$ it is very similar to the weight distributions which have been found for other colloids. A smaller value of B leading to a broader distribution is not possible since an appreciable area under the distribution curve would then lie to the left of the origin $\rho = 0$. Hence if the distribution (4) with $B \geq 3/\sqrt{2}$ does not happen to lead to an agreement between experiment and theory it will be necessary to assume a non-Gaussian distribution or to invoke a different mechanism to account for the shape of the magnetization curves. Fortunately this has not been found necessary.

The magnetization curve appropriate to the distribution (4) with $B = 3/\sqrt{2}$ can be calculated from the integral

$$I = I_s \frac{3}{(2\pi)^{\frac{1}{2}}} \int_0^\infty \exp[-9(1-\rho)^2/2] L(a_0\rho^3) d\rho, \qquad (5)$$

where $a_0 = \mu_0 H/kT$ and μ_0 is the moment of a particle having the diameter r_0. The integral (5) has been evaluated numerically for a number of values of a_0, giving the lower curve in Fig. 3. The curve has been plotted by taking $a = 4a_0/3$ so that its initial slope is the same as that of $L(a)$. The experimental points for both colloids have been fitted to this curve by the method previously used for the Langevin curve, giving an agreement which is now within the experimental error for both colloids. In Table I the constants needed to produce this fit have been collected, together with other related quantities. As an insert in Fig. 3 is shown the distribution (4) with $B = 3/\sqrt{2}$.

In the table μ_0 is not the most frequently occurring particle moment but the moment which corresponds to the peak in the distribution (4). The saturation moment per unit volume I_s is

[6] J. B. Nichols, E. O. Kraemer and E. D. Bailey, J. Phys. Chem. 36, 326 (1932).

that occurring in Eq. (5). Its values are to be compared with those of I_s' which have been computed from the chemically determined colloid concentrations and the specific intensities of magnetization for the two oxides as reported in the literature.[7] The estimated diameter r_0 of a particle of moment μ_0 has been calculated from the expression

$$\mu_0=(\pi/6)(I_s/I_s')I_0r_0^3, \tag{6}$$

where I_0 is the bulk saturation intensity of magnetization for magnetite or siderac,[8] and where the particle has been assumed spherical.

Several possible explanations can be offered to account for the difference between the values of I_s and I_s'. The most likely explanation is that a considerable portion of the iron determined by chemical analysis (good to four percent) was not present as magnetite or siderac but as some other nonferromagnetic oxide of iron. For instance, it was observed that prolonged shaking in a test tube oxidized the reddish-black magnetite sol into one which was deep red in color and nonferromagnetic.

Other factors which could reduce the observed values of I_s have to do with the nature of the colloid particles. Only if the particles be single crystals free from serious imperfections does it seem likely that they would be single magnetic domains, i.e., domains in which all the elementary magnets are in a parallel alignment throughout the particle. In addition the values of I_s may be reduced by the relatively large number of atoms present on the surface of the particles. For instance, if a particle contains $(10)^6$ atoms, about 13 percent of the atoms will not be completely surrounded by neighbors. Although it is not possible at present to estimate the importance of the various factors which have just been discussed, it is a fair conclusion that small ferromagnetic particles are not demagnetized in the macroscopic sense of the word, in agreement with the prediction of Frenkel and Dorfman.[3] Certainly no macroscopic magnets of spherical shape exhibit a remanence comparable with that observed for the colloid particles.

The author is greatly indebted to Professor F. Bitter, Department of Metallurgy, for the loan of the apparatus with which measurements were made, and for interesting discussions about the ferromagnetism of small particles.

TABLE I. *Constants chosen for best fit of experimental points to Eq. (5).*

	μ_0	I_s	I_s'	I_s/I_s'	r_0
magnetite	$5.2(10)^{-16}$	0.084	0.192	0.44	17 mμ
siderac	$7.4(10)^{-16}$	0.120	0.319	0.38	21 mμ

[7] P. Weiss and R. Forrer, Ann. de physique **12**, 279 (1929).

[8] In obtaining I_0 the densities of the two oxides have been taken as 5.2 and 5.1 g/cm³, respectively.

Electronic Conduction In Insulating Crystals Under Very High Field Strength

A. VON HIPPEL
Electrical Engineering Department, Massachusetts Institute of Technology, Cambridge, Massachusetts
(Received September 19, 1938)

After a short discussion of electronic conduction in insulators with the main emphasis placed on the electrostatic coupling between electron and lattice, new experimental results are given: Current-voltage characteristics and photoelectric response have been measured in single crystals up to the breakdown point. Ten million volts per centimeter have been reached in mica, and phenomena have been observed acoustically, making a crystalline type of light-counter feasible. The dark-currents and photocurrents observed give information about the mechanism of electric conduction under very high field strength.

1. The Behavior of Electrons and Holes in Insulating Crystals

SINCE the development of Bloch's theory of electronic conduction in metals and its very successful application, many authors have believed that the only difference between metals and insulators lies in the zone structure of the electronic levels. In a good conductor the lowest band is half-filled or the allowed bands overlap; in a good insulator the lowest band is completely filled and the next higher allowed zone is empty and distinctly separated.[1] According to this conception, to convert the insulator into a conductor, it is only necessary to transfer electrons from the lower into the upper band. The electrons transferred and the positive holes left in the lower zone will be free to move through the lattice and to establish metallic conduction.

For a number of years the author, studying the behavior of insulating crystals under very high field strengths, has stressed the point that this zone picture for insulators does not contain the whole story. It has to be supplemented by a consideration of the decisive influence of the electric forces coupling the movement of the electrons to the heavy building stones of the lattice. In ionic crystals this coupling is so strong that the moving electrons can be treated rather as charged particles than as electron waves. As shown in previous papers the most important consequences of this situation are the following:

The lower filled band in such crystals as the alkali-halides consists of electrons *locally* bound to the lattice points. Excitation to the next higher states does not bring the electrons into a conduction band but into *locally bound* excited states, which can be seen in two groups of double bands in the absorption spectrum of the crystals.[2] During the lifetime of such excited states the lattice rearranges itself, and dissipates a part of the excitation energy into lattice vibrations.[2,3] This distortion of the crystal has not only the consequence of shifting the frequency of the light emitted compared with that of the light absorbed, but it can even prevent re-emission, because the electron in the reverse process has to pay for the lattice distortion.[4] Heat vibration and light absorption can transfer an electron from an excited state into a conducting state, but its behavior is also then very different from that of a metal electron: The electron acts like a space charge, distorting the lattice as it moves along; that is it emits and also absorbs phonons in its migration.[5] These conducting electrons travel in preferential lattice directions;[6] if their velocity becomes too low, they are trapped by the lattice disturbance created by their presence.[7,8] This

[1] Cf. for instance, F. Seitz and R. P. Johnson, J. App. Phys. **8**, 84, 186, 246 (1937).

[2] A. von Hippel, Zeits. f. Physik **93**, 86 (1934).

[3] A. von Hippel, Zeits. f. Physik **101**, 680 (1936).

[4] The two-dimensional potential diagram Fig. 1 may elucidate this situation in a clearer way than the picture given originally by the author: An electron has been raised by light absorption from A to B. In the condensed system the oscillation energy becomes rapidly dissipated and lowers the excited state to C. Now a temperature vibration must lift the state to D, before it can fall back to the original state A by again dissipating the oscillation energy. More likely in the case illustrated is the direct transfer B-D-A dissipating the total light quantum absorbed in one act into heat. This accounts apparently for the experimental observation, that at low temperatures light can be absorbed in ionic crystals without any visual effect. The author has given a detailed discussion elsewhere (reference 3).

[5] A. von Hippel, Zeits. f. Physik **75**, 145 (1932).

[6] A. von Hippel, Zeits. f. Physik **68**, 309 (1931).

[7] A. von Hippel, Ergebn. d. Exakt. Naturwiss. **14**, 113 (1935).

[8] L. Landau had already proposed a quantum mechanical trapping mechanism for electrons (Physik. Zeits.

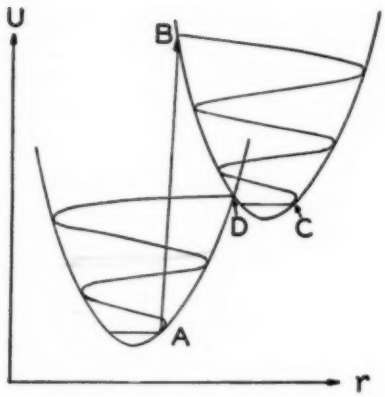

FIG. 1.

trapping makes phosphorescence possible.[3] Under the influence of very high field strength, on the other hand, the electrons can reach velocities which make the excitation of lattice vibrations unlikely; acceleration, impact ionization, and electric breakdown result.[5]

According to this conception the assumption that the holes left in the lower filled levels of the insulator can be treated like free conducting positrons also does not seem completely justified. These holes correspond in the alkali-halides to neutral halogen atoms; they can be trapped like the surplus electrons, but the lattice distortion created will be different. Therefore light absorption of different position and probability will bring the electron and the hole back from the fixed state into the mobile state.[3] Moreover, the migration process differs appreciably: the surplus electron may travel relatively smoothly over larger distances; the hole has to move over much rougher potential hills corresponding to the classical picture of an electron exchange from neighbor to neighbor (Fig. 2).

The viewpoints summarized above have been gained by the author in discussing his own experimental results and those of R. W. Pohl and his co-workers. Some recent theoretical papers have reached confirming conclusions:

Frenkel[9] postulated independently and at about the same time as the author the existence of trapped excited states called excitons and of trapped electrons and holes. Wannier,[10] Seitz,[11] and Mott[12] find excitation states below the ionization states in the alkali-halide crystals. Seitz[11] calculated the phosphorescence of the alkali-halide-thallium crystals by using the mechanism of lattice distortion. Seeger and Teller,[13] computing the interaction between conducting electrons and the ionic lattice, find the high friction for the electrons and the right order of magnitude for the breakdown strength.[14]

In the present paper the author presents some new experimental results about the electric conduction of insulating crystals in the range of very high field strength. It seems that the phenomena observed fit into the picture[15] given above.

2. Experimental Arrangement

The goal of the experiments was to measure the current-voltage characteristic in single crystals, especially in the alkali-halides, up to the breakdown point. Some preliminary curves have already been published by the author[7] rejecting a statement of Inge and Walther[16] that the electronic currents before breakdown could reach

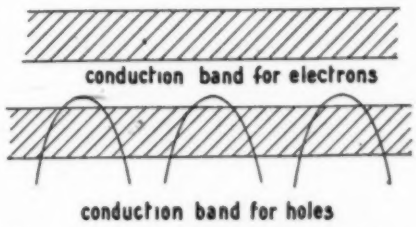

FIG. 2. Difference in the conduction bands of electrons and of holes.

Sowjetunion **3**, 664 (1933)), as the author has now found out, but our ideas are different. According to Landau, slow electrons cannot be trapped because their position is badly defined on account of their long wave-length. They have to be speeded up by an activation energy before they can be caught locally. The author on the other hand, feels that such an activation energy is not needed; on the contrary, the slow electrons are most liable to become trapped on account of the coupling mechanism outlined above. (In a private communication Dr. Teller stated more accurately: the potential energy $u=-e^2/r$ of the electron decays as $1/r$ but its kinetic energy $(h/\lambda)^2\cdot 1/2m$ decays as $1/r^2$ and is therefore smaller than u for slow electrons).

[9] J. Frenkel, Physik. Zeits. Sowjetunion **9**, 158 (1936).
[10] G. H. Wannier, Phys. Rev. **52**, 191 (1937).
[11] F. Seitz, J. Chem. Phys. **6**, 150 (1938).
[12] N. F. Mott, Trans. Faraday Soc. **34**, 500 (1938).
[13] R. J. Seeger and E. Teller, Program Washington Meeting, 1938, No. 47; Phys. Rev. **54**, 515 (1938).
[14] The interesting theory of H. Fröhlich, Proc. Royal Soc. London **160**, 230 (1937), realizes the important electrostatic coupling mechanism between electrons and lattice, but does not take the dielectric constant into account.
[15] Cf. also A. von Hippel, J. App. Phys. **8**, 815 (1937).
[16] L. Inge and A. Walther, Archiv f. Elektrot. **28**, 729 (1934).

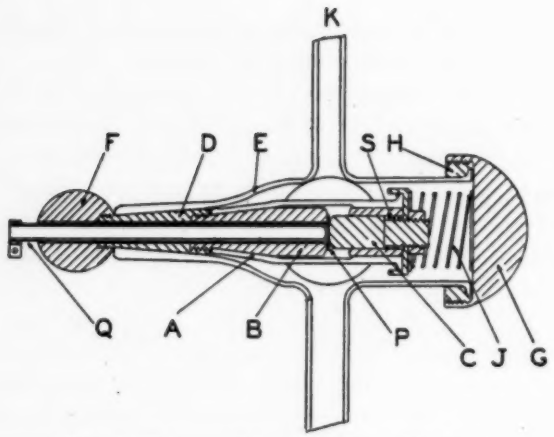

FIG. 3. Cross section of the crystal holder.

the magnitude of many amperes and would destroy the insulator by heat. The currents actually found directly before breakdown were of the order of 10^{-9} to 10^{-8} ampere, but they showed besides a tendency to decrease in time, and other peculiarities, which made the reconstruction of the apparatus and additional photoelectric measurements advisable.

A cross section of the crystal holder is given in Fig. 3. An interior glass tube *A* contains the two electrodes *B* and *C* holding the crystal plate *P* between themselves by the soft spring action of the spiral *S*. One of the highly polished steel electrodes (*B*) has at its center a longitudinal hole fitting a quartz tube *Q* polished on the end to the curvature of the metal surface. The quartz is covered by a semi-transparent Pt layer and is insulated over its length from the electrode by a very thin layer of glypthal lacquer. A conical piece *D* fixes *B* in *A* and fits into a second glass tube *E*; a sphere *F* catches *D* from the outside. The other end of *E* is closed by a hemispherical brass piece *G* which screws over the ring *H* and presses the cone *D* into place by a spring *J*. Longitudinal illumination of the crystal under high voltage is possible through the quartz tube, transverse illumination through two opposite quartz windows on *E* lined up with holes in the inside tube *A*. The vessel *E* can be evacuated through the glass tube *K* and can then be filled with an insulating liquid (oil or pyranol).

The electrode *G* was connected to the high voltage side of a power pack; the rectified voltage of the pack (range 5 kv and 20 kv) was smoothed by large condensers. The electrode *F* was connected to ground; hence the electrode *B* was the shield connected to the outside of a concentric cable, which protected the measuring electrode, the metal layer of the quartz tube *Q*, against disturbances. From the contact *L*, the shielded lead connected to the grid of a *P* 54 tube used in a Barth circuit[17] arrangement. The total insulation was sufficient for measuring safely between 10^{-12} and 10^{-5} ampere by switching to different grid resistors. The voltage across the sample was measured with high resistances (order 10^8 ohm) and a Rubicon galvanometer. Resistances and a glow discharge tube protected the circuit against excess currents after breakdown.

For the photoelectric measurements a double monochromator was constructed with motor-drive and wave-length control. A General Electric tungsten band lamp and a mercury lamp of the Hippel type[18] served as light-sources. The intensity of the monochromatic radiation was measured by a vacuum thermopile of the Cartwright type and a Cs-vacuum-photo-cell.

3. RESULTS

Figures 4 to 7 give a characteristic picture of the phenomena observed when a KCl crystal plate of 120μ thickness is used.

In the dark the current begins to rise rapidly

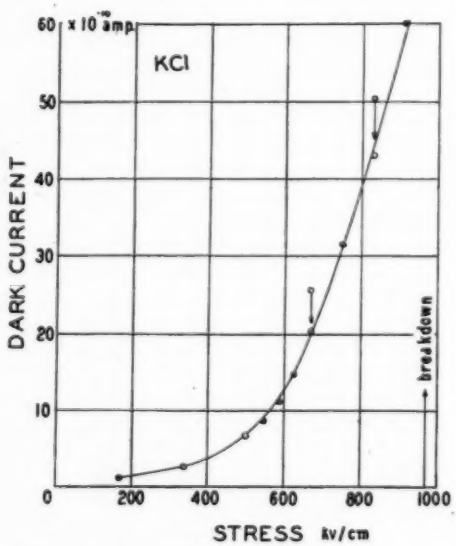

FIG. 4. Current-field-strength characteristic of the dark-current in KCl up to the breakdown point.

[17] Cf. D. B. Penick, Rev. Sci. Inst. **6**, 115 (1935).
[18] W. Harries and A. von Hippel, Physik. Zeits. **33**, 81 (1932).

under the influence of higher field strengths, but even at the breakdown point it is not higher than about $8 \cdot 10^{-9}$ ampere. The breakdown appears suddenly as an abrupt instability, but the approach of the breakdown point often announces itself quite clearly through the time dependence of the dark-current. Normally after shifting to a higher voltage the current decays in time, as indicated on two points of the curve (Fig. 4) by arrows. Shortly before breakdown the current value often fluctuates unsteadily and may even increase with time.

Illuminated with visible or ultraviolet light down to 2500A, the clear untreated crystal does not show any photoelectric reaction. But if the crystal has been colored with *F* centers by migration of electrons, the situation changes completely. Fig. 5 gives the transmission curve of the colored crystal plate measured by the recording color-analyzer of Professor Hardy. Besides the well-known *F* band, an absorption in the violet appears which belongs to a surface coloration by electrons. Such surface bands can be observed in many crystals and glasses, and they can be understood by viewpoints given elsewhere.[15]

Figure 6 shows the photoelectric response of the colored crystal for constant light intensity and constant field strength; the electric curve matches the absorption curve almost perfectly. In addition, Fig. 7 gives the photoelectric current-voltage characteristic for constant illumination with the green mercury line. The light-current becomes about saturated where the dark-current

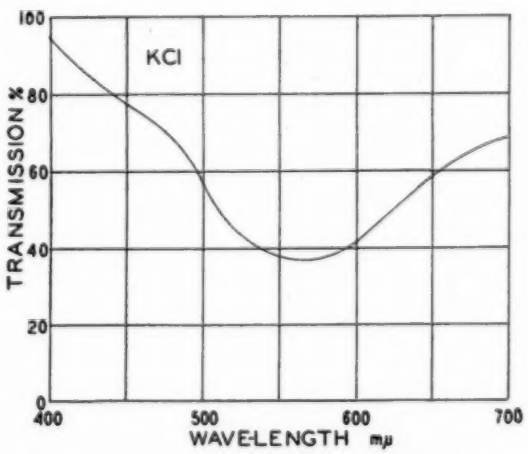

FIG. 5. The transmission curve of the KCl crystal.

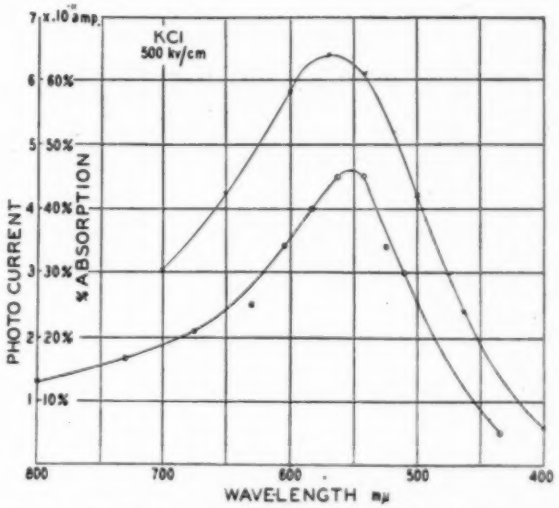

FIG. 6. The photoelectric response o of the KCl crystal compared with the curve of light absorption x. (The percent values of the absorption correspond to a larger crystal from which the sample was split, and have therefore only relative meaning.)

rises steeply.[19] The light-current is proportional to the light intensity, so far as has been measured.

The photoelectric response can be used to explain why the dark-current depends upon time: In going backwards with the voltage, a point is reached where the photocurrent becomes zero; for lower voltages it becomes negative. Hence a space charge has been built up, measured in magnitude by the voltage of zero response. In this crystal the polarization voltage amounted to 700 volts corresponding to 58 kv/cm, if the field strength is assumed to be equally distributed across the crystal.

As a second example, the curves of a KBr crystal are given, which had not been quenched after coloring. Accordingly, its transmission curve (Fig. 8) shows a very broad absorption (formation of colloidal particles), but the photoelectric response indicates clearly the position of the *F* band (Fig. 9). The quantum yield of the *F* centers seems to be higher than that of colloidal particles, as one may expect. The photoelectric sensitivity of the KBr crystal at 600 mμ was about three times as high as that of the Cs-photo-cell[20] for the same wave-length, if the filter action of the platinized quartz tube was

[19] The last points of the photocurrent curve are not very accurate on account of the large and fluctuating dark-current; it may be that the photocurrent even decreases for the highest field strength.

[20] Pressler photo-cell, Cs-vacuum type.

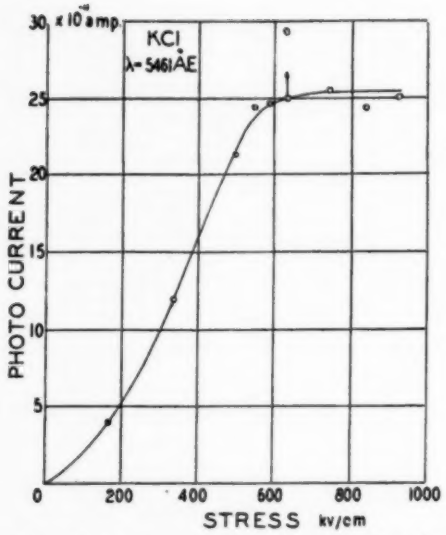

FIG. 7. Photoelectric current as function of field strength in KCl for the green mercury line.

taken into account. The Pt layer proved to be a neutral filter for the spectral range used. An interesting time effect could be observed on the KBr photocurrent: Red illumination gave a response decaying in time; toward shorter wave-length this after-effect became less and less pronounced, disappeared at about 540 mμ, and changed sign towards an increase with time in the bluer spectral range.[21]

Coloring of a KBr crystal with Cu atoms by the author's electric method[22, 23] did not produce any marked photosensitivity. This is to be expected when one considers the great tendency of copper ions to recapture electrons.[15]

4. Control Measurements with Another Apparatus

On account of the fact that for the first time current-voltage characteristics have been obtained in the range of highest field strength, it seemed desirable to check the results in a quite

[21] This phenomenon apparently corresponds to the Herschel effect: The light absorption of the colloidal particles creates smaller centers absorbing farther towards the blue, hence the absorption in the red decreases in time. The bands of the different centers partly overlap, for light of shorter wave-length, therefore, the increase of *F* centers compensates and overcompensates the decrease in the number of bigger colloidal particles.

[22] A. von Hippel, Zeits. f. Physik **98**, 580 (1936).

[23] The author has been kindly advised by Professor Pohl that already in 1933 Miss Marietta Blau produced and measured for spectroscopic reasons the Cu coloration in NaCl and KCl (Nachr. Göttinger Gesellschaft d. Wissenschaften II, No. 51, 1933).

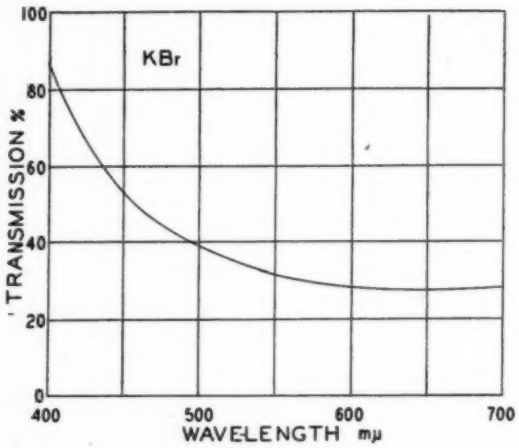

FIG. 8. Transmission curve of a KBr crystal, slowly cooled.

different experimental arrangement. Therefore the crystal-holder shown in Fig. 10 had been constructed. The crystal-plate is again placed between two metal electrodes *B* and *C*; the insulated metal core of *B* acts as measuring electrode. But the main change is that this holder can be screwed into a steel pipe which can be evacuated or can be connected to a nitrogen tank. Hence the high voltage measurements can be made under a pressure of 100 atmospheres of N_2, which together with a dielectric guard ring[7] forms a very effective shield against edge effects.

The dark-currents measured with this arrangement check the results obtained above perfectly. Fig. 11 presents the currents through three different alkali-halides, NaCl, KBr and RbI, on

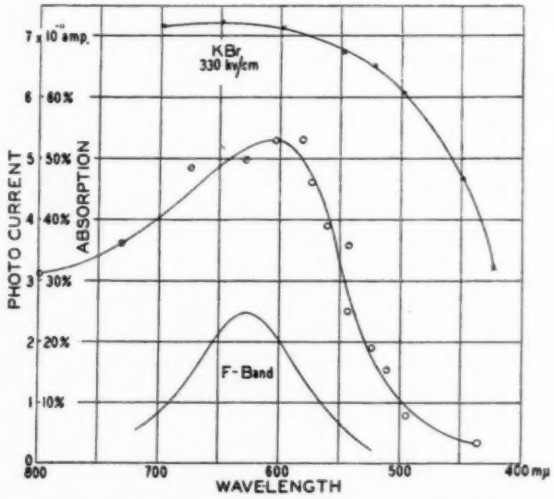

FIG. 9. Photoelectric response o and relative absorption × of the KBr crystal compared with position of the *F* band.

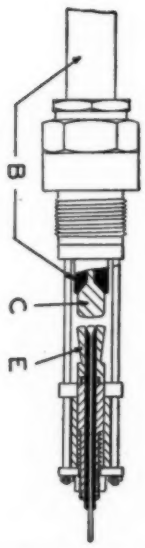

FIG. 10. Cross section of the second crystal holder. (The black insulation is amber.)

a reduced voltage scale. The ratio of field strength to breakdown field strength has been plotted; this shift makes the curves practically coincide.

A much larger current range is covered by measurements on a clear mica sheet of about 6.5μ thickness, shown in Fig. 12. Here about $3 \cdot 10^{-8}$ ampere have been reached with the amazing field strength of about ten million volts per centimeter.[24] Even in this case the character of the phenomenon is not altered; the breakdown appears as an abrupt discontinuity; below this point the current can be drawn for considerable time without apparent harm.

A simple exponential relation between current and voltage as proposed by Poole[25] does not hold in this high field strength range.

5. Acoustical Observations

If the measuring electrode is connected not to an electrometer tube but to a high gain amplifier with loudspeaker, some interesting observations can be made: A rattling noise resembling that of a fast-counting Geiger counter can be heard, increasing very much in intensity with voltage, and dying out in time to fewer and fewer impulses, if the dark-current decreases with time. A similar statistical counting effect is produced by illumination, constant apparently in time, very much increasing in intensity with voltage. If the crystal was illuminated with a flashlight through the quartz window of the holder (Fig. 4) a noise resembling machine-gun fire could be produced at the highest field strength.

The possibility exists that here single electronic avalanches have been heard, and that a crystal-photon-counter can be constructed.

6. Discussion

It seems unlikely that the dark-current corresponds to electrolytic conduction; its steep rise with voltage, its rapid fluctuations, and its noisiness point towards an electronic phenomenon. Assuming this, the observations form a consistent picture:

Electrons pulled from the cathode into the crystal by the high field strength applied, are transported over the rows of the cations (Fig. 13) towards the anode. A part of them comes through, others after progressing an average displacement distance w in field direction become trapped. Correspondingly a space charge forms decreasing the field strength at the cathode, the current

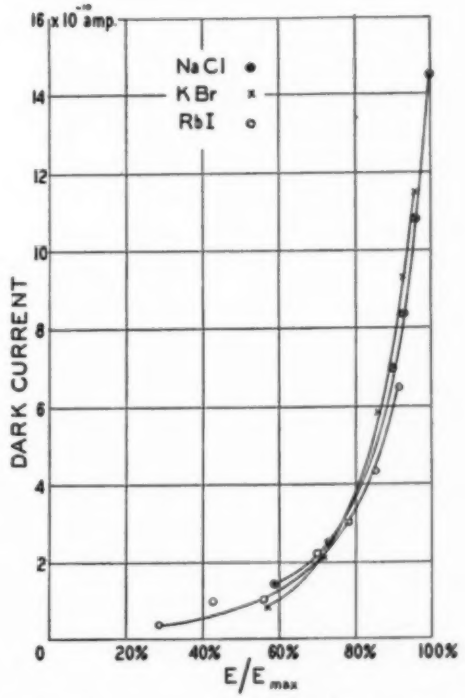

FIG. 11. The dark-current in NaCl, KBr and RbI compared on a reduced-voltage scale.

[24] The thickness of the mica has been measured with an optical micrometer of Zeiss; the value may have an error of 10 percent.

[25] H. Poole, Phil. Mag. **42**, 488 (1921).

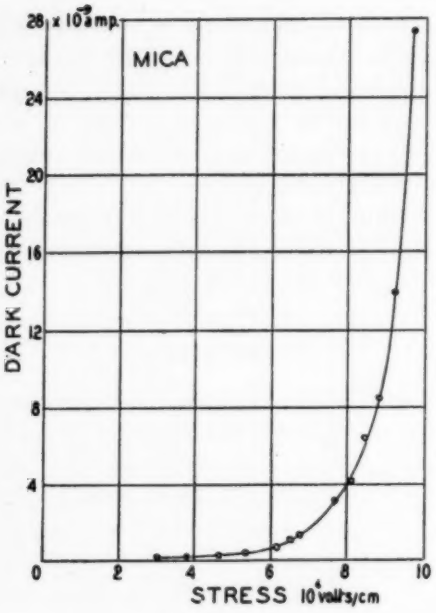

FIG. 12. Dark-current in mica.

decays in time. The negative space charge increases the field strength towards the anode and the displacement distance w increases proportional to the field strength,[26] hence electrons liberated from their trapped position by a heat vibration of the lattice will reach the anode. Besides the field distribution favors a second kind of electron migration (Fig. 13), a pulling *in* of electrons from halogen ions into the anode and transfer of the neutral halogen atoms by electron exchange through the rows of the anions to the cathode or to the space charge zone, where they recapture their electron (hole-migration).

The result is a dark-current steeply increasing with field strength on account of the field emission of the electrodes and decaying in time asymptotically towards an equilibrium value on account of the space charge formed (Figs. 4, 11 and 12). The number of trapped electrons is normally too small to be detected photoelectrically against the background of the dark-current. But a primary discolored crystal with its large number of F centers demonstrates the capture of electrons directly in its saturation curve (Fig. 7). The photocurrent as a function of voltage should approach a saturation value of $\frac{1}{2}$ electron per quantum absorbed, if w becomes

[26] K. Hecht, Zeits. f. Physik **77**, 240 (1932).

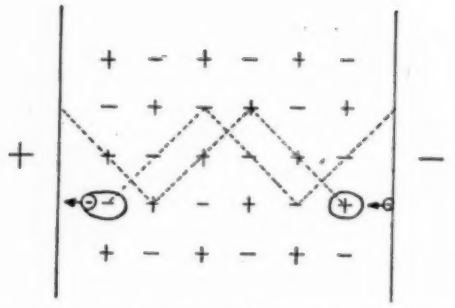

FIG. 13. Schematic diagram of the two types of electronic conduction.

comparable to the electrode distance d.[27] In Fig. 7 this seems the case at 600 kv/cm for $d=120\mu$, a value not inconsistent with those measured by Pohl and his co-workers at lower field strength.[28] An accurate comparison cannot be made, because the concentration of color centers in our case is not known.[4]

According to this conception the steep rise of the current-voltage characteristic is mainly due to field emission, not to ionization processes. The probability of speeding up surplus electrons to ionizing velocities does not become appreciable before the breakdown voltage, and then breakdown starts immediately, because the large number of impacts across the crystal creates very high avalanches and a field distortion accelerates the process.[15] But at local inhomogenities of the lattice short avalanches may be produced earlier and thus account for a part of the noise observed. Some noise may originate from surface charges and some from a transport of charges by jerks.

Before discussing further details, the experimental material has to be improved. A greater variety of crystals treated in different ways should be measured, the current-voltage-time characteristics should be recorded, and the temperature dependence of the phenomena should be studied. Besides a clear picture has to be gained about the influence of the lattice structure on the electronic conduction linking our field to that of the semi-conductors. Adequate experimental methods are under development.

Some of the KCl and KBr crystals used were furnished by Professor D. C. Stockbarger, to whom the author wishes to express his thanks.

[27] R. Hilsch and R. W. Pohl, Zeits. f. Physik **108**, 60 (1938).
[28] R. W. Pohl, Physik. Zeits. **39**, 45 (1938).

The Heat Capacity of Rochelle Salt Between −30° and +30°C

ARTHUR J. C. WILSON
Massachusetts Institute of Technology, Cambridge, Massachusetts

(Received September 12, 1938)

The heat capacity of Rochelle salt has been measured in the temperature range −30° to +30°C by the method of adiabatic electric heating. Two samples of the salt have been investigated, one consisting of eleven single crystals of total weight about 123 grams, the other of small crystals, almost a powder, of total weight about 58 grams. The heat capacities of the two samples are nearly the same. They are well represented (mean deviation of individual points 0.3 percent) by the straight lines:

$$C_p = 1.290 + 0.0031t \quad \text{(crystals)}$$
$$C_p = 1.289 + 0.0034t \quad \text{(powder)}.$$

The heat capacity is in joule/g·°C; t is in °C. There are indications of anomalies at approximately −18° and possibly +24°C, but the maximum departure from the straight lines is less than 1 percent. The direction of the indicated anomalies and their order of magnitude is in agreement with theory. The small amplitude of the anomaly at +24° is not in agreement with the measurements of previous observers.

INTRODUCTION

THE temperature variation of the heat capacity of Rochelle salt (sodium potassium dextro-tartrate tetrahydrate, $KNaC_4H_4O_6 \cdot 4H_2O$) is of considerable interest since it is connected with the spontaneous polarization[1] of the crystals. By an argument similar to that applied to the analogous magnetic phenomenon[2] it may be shown that the anomalous heat capacity associated with the potential energy of the spontaneous polarization is

$$\Delta C = -\tfrac{1}{2} f \partial P^2/\partial t \quad \text{erg/cm}^3\cdot\text{°C} \qquad (1)$$

where f is a constant ("Lorentz factor;" "coefficient of the inner field") for which various values ranging from about 2 to $4\pi/3$ have been suggested and P is the spontaneous polarization in electrostatic units. To get the anomalous heat capacity in joule/g·°C Eq. (1) must be divided by the density of Rochelle salt and 10^7:

$$\Delta C = -\frac{f}{2\rho 10^7}\frac{\partial P^2}{\partial t} \sim -10^{-7}\frac{\partial P^2}{\partial t} \text{ joule/g}\cdot\text{°C}. \qquad (2)$$

P has recently been measured by Tarnopol[3] and Bradford[4] by different methods. From neither set of measurements is it possible to account for an anomaly of much more than +0.003 joule/g·°C at the upper Curie point (∼+24°C) or −0.005 joule/g·°C at the lower Curie point (∼−18°C).

Measurements near the upper Curie point have been made by Kobeko and Nelidow[5] and by Rusterholz.[6] The writer is unaware of any previous measurements near the lower Curie point. Kobeko and Nelidow found a heat capacity of about 92.6 cal./mole·°C and a break of about 7 cal./mole·°C (0.1 joule/g·°C) at 26°. Rusterholz found a heat capacity of 104 cal./mole·°C at 24° and a break of about 6 cal./mole·°C (0.09 joule/g·°C) at 25.8°C.

From measurements of many electrical properties of Rochelle salt made by Mueller[7] one would expect the break to come at about 24° rather than at 26°. The difference in absolute value (∼11 percent) between the values of Kobeko and Nelidow and of Rusterholz is hardly satisfactory. It was therefore decided to measure the heat capacity of Rochelle salt with three main

[1] An account of this and other peculiarities of Rochelle salt may be found in reference (7).
[2] See, for example, Pierre Weiss and P. N. Beck, J. de Phys. 7, 249 (1908).
[3] Lester Tarnopol, M. S. Thesis, Massachusetts Institute of Technology, 1934. Fig. 17, reference (7), is based on Tarnopol's work.
[4] Eliot Bradford, B. S. Thesis, Massachusetts Institute of Technology, 1934. As far as the writer knows this has not been published.
[5] P. P. Kobeko and J. G. Nelidow, Physik. Zeits. Sowjetunion 1, 382 (1932).
[6] A. A. Rusterholz, Helv. Phys. Acta 7, 643–644 (1934); 8, 39–54 (1935).
[7] Hans Mueller, Phys. Rev. 47, 175–191 (1935).

intentions: (1) to investigate the variation in the neighborhood of the lower Curie point, (2) to decrease the uncertainty in the absolute value of the heat capacity and (3) to attempt to reconcile the discrepancy between the electric Curie point (~24°) and the thermal Curie point (~26°).

Method

A modification of the method of adiabatic electric heating developed by Bronson and his students[8–11] was used. The salt was enclosed in a copper calorimeter fitted with a heating coil. The calorimeter was suspended inside a jacket immersed in a stirred oil bath. A differential thermocouple ran between the calorimeter and the jacket. The temperature of the oil bath was regulated so that the temperature difference indicated by the thermocouple was kept small. The temperature of the oil bath was measured by a platinum thermometer.

To obtain the heat capacity of the salt the following procedure was used. The temperature of the calorimeter was measured by measuring that of the bath when the differential thermocouple indicated zero. The calorimeter was then heated a suitable amount (0.2° to 5° depending on circumstances), the energy supplied being measured carefully. The temperature of the calorimeter was again determined. Dividing the energy supplied by the change in temperature gave the heat capacity of the calorimeter plus salt. The (previously measured) heat capacity of the empty calorimeter was subtracted and the difference divided by the mass of the salt to give its heat capacity in joule/g·°C.

Apparatus

(a) Calorimeters and thermocouples

Two calorimeters were used in the course of this work. The first is shown inside the jacket in Fig. 1. It consisted of an outer cup of copper about 3 mm thick with a cover which screwed firmly into place. Into this fitted an inner cup of ½ mm brass on the outside of which the heating coil was wound and into which the salt was put. The calorimeter was suspended in the jacket by three wire hooks.

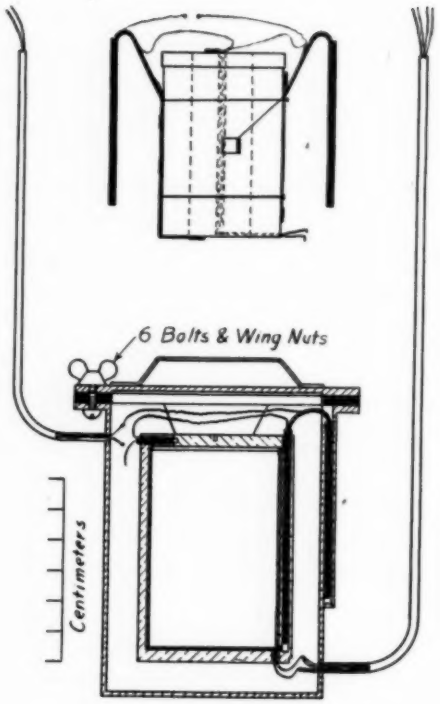

FIG. 1. The calorimeters and jacket.

An eight-junction copper-constantan thermocouple was used. The calorimeter junctions were distributed over the surface of the calorimeter in an attempt to get a good average of its surface temperature. There was one junction which fitted into the bottom of the calorimeter, one (shown in Fig. 1) in the top and two groups of three each in the side of the calorimeter. One side group is shown in Fig. 1; the other is omitted in order to show other details. The six side junctions were distributed approximately uniformly along the length of the calorimeter. The jacket junctions were in two groups of four which fitted into tubes soldered on opposite sides of the jacket. The thermocouple was connected by an all-copper circuit to a Leeds & Northrup galvanometer of sensitivity such that one cm deflection corresponded to about 0.001° difference in temperature between calorimeter and jacket. The heat capacity of this calorimeter plus the part of the thermocouple heated by it was about 180 joule/°C.

[8] H. L. Bronson, H. M. Chisholm and S. M. Dockerty, Can. J. Research **8**, 282–303 (1933).
[9] S. M. Dockerty, Can. J. Research **9**, 84–93 (1933).
[10] H. L. Bronson and A. J. C. Wilson, Can. J. Research, **A14**, 181–193 (1936).
[11] S. M. Dockerty, Can. J. Research **A15**, 59–66 (1937).

The second calorimeter (inset, Fig. 1) was of much lighter construction, being a single cup of 0.005″ copper foil. Its interior was divided into six sections by radial fins of copper foil. The heating coil was wound longitudinally in the notches between opposite pairs of fins. The eight thermocouple junctions were cemented permanently into small foil pockets soldered to its outer surface. The distribution of the junctions is fairly clear from the figure. The heat capacity of this calorimeter was about 11 joule/°C.

(b) Oil bath

The oil (kerosene was used in most of the measurements) was contained in an earthenware crock of about four gallons capacity. The crock was insulated on bottom and sides by rock wool. The top could be covered to a great extent with cushions filled with hair felt. Inside the crock there was a brass framework which supported the calorimeter jacket, heating coils, platinum thermometer and stirring motors.

The bath was stirred by two "Economy" stirrers whose original propellers had been replaced by others of larger size. The stirrers were mounted on opposite sides of the bath. There were two heating coils, also on opposite sides of the bath. They had a resistance of about 40 ohms each and were made of bare wire to decrease heating lag. They could be connected in series or in parallel with one another and in series with a variable resistance, ammeter and the 110-volt line.

Cooling the bath was at first accomplished by a rather complicated apparatus which pumped cold oil into the bath. This was reasonably satisfactory at the higher temperatures, but the rapid variations in temperature caused by the injection of the large quantities of cold oil required to maintain, say, $-20°$ made it almost impossible to obtain accurate measurements near the lower Curie point. After some experimenting, the method adopted was to place solid carbon dioxide in direct contact with the crock, the amount used being determined by the temperature desired. The method was not ideal as it produced larger temperature gradients than were desirable but it was fairly satisfactory at all temperatures.[12]

[12] An oil bath was used instead of a more convenient copper adiabatic jacket of the type described in references (9, 10 and 11) because of two considerations which seemed convincing when the work was started. (1) It was thought that temperature uniformity in the oil bath would be better than in a copper jacket. On testing with a differential thermocouple it was found to be somewhat better than the jacket of reference (10), but not as much better as had been anticipated. (2) The surface of the calorimeter heats up faster than the interior of the salt so that when the heating current is turned off the temperature of the calorimeter falls rather rapidly. The fall was not as fast as had been expected and it now seems likely that a copper jacket would have sufficed.

(c) Jacket

The jacket is shown in Fig. 1. It was made of brass; the details of its construction are fairly clear from the drawing. At first there was considerable trouble in making the cover oil-tight. Gaskets of ordinary rubber were tight for a short time but deteriorated rapidly in the oil. A gasket of "Thiokol" was not attacked by the oil but did not make an oil-tight joint. The oil crept in between the brass flanges and the gasket. The method finally adopted was to coat both the flanges and the gasket with rubber cement and allow it to dry before screwing down the cover.

(d) Other apparatus

The rest of the apparatus was of standard construction and requires no description. The platinum thermometer was calibrated at the melting point of mercury, the melting point of ice, sodium sulphate decahydrate transition point and the boiling point of water. Its fundamental interval was found to be 10.010_0 ohms; δ was found to be 1.48 from the mercury point, 1.47 from the sodium sulphate point. The difference is within the limits of error. Each point, except the mercury point, was repeated at intervals.

Measurements

The procedure followed in making the measurements has been described. The first measurements were those of the first calorimeter as a function of temperature. Then, to check the ability of the apparatus to give reliable values of the absolute magnitude of heat capacity, the heat capacity of copper was measured. The copper was in the form of small shot intended for analytical work and was stated to contain less than 0.04 percent impurities. The values found were slightly over 0.1 percent greater than those

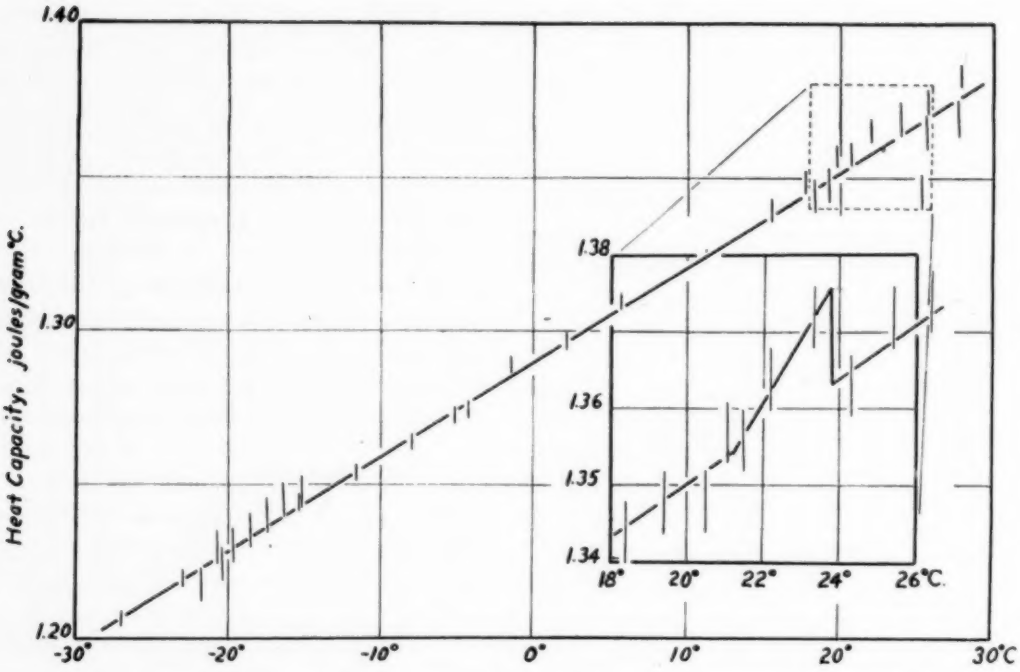

FIG. 2. Heat capacity of the large crystals of Rochelle salt in the range −30 to +30°C.

of Dockerty.[9, 11] The agreement is satisfactory.[13]

The calorimeter was then filled with small crystals of Rochelle salt (Merck). It was found to require about an hour for the calorimeter to reach thermal equilibrium with the result that the measurements scattered badly. More concordant measurements on the same material were obtained later so it does not seem necessary to discuss these.

Eleven single crystals, specially cut by the Brush Development Company to pile into a roughly cylindrical shape which fitted loosely into the calorimeter, were each wrapped in copper foil and put in the calorimeter. The foil served the double purpose of preventing charges produced by the pyroelectric effect from interfering with the normal change of polarization with temperature, and of decreasing the time required to reach thermal equilibrium. Measurements were made over the range −30° to +30°C (Fig. 2). Near the lower Curie point no anomaly was found. At the upper Curie point there were some indications of an anomaly of ½ or 1 percent, but they were not very convincing. The set of measurements showing the effect most clearly is inset in Fig. 2. It must be emphasized that if all points were shown, no one would draw an anomaly if it were not expected. The straight line $C_p = 1.290 + 0.0031t$ represents the 48 experimental points with a mean deviation of about 0.3 percent.

The measurements with the first calorimeter showed that to obtain greater "resolving power" two things were necessary: The time required to reach thermal equilibrium should be decreased and the heat capacity of the calorimeter should be reduced to a small fraction of that of the salt. These ends were attained with the second calorimeter. A measurement with it with a temperature interval of 0.3° was apparently as reliable as one with an interval of 1° made with the first calorimeter.

After the determination of the heat capacity of the second calorimeter it was filled with small crystals of Rochelle salt and about 120 measurements made. They are plotted in Fig. 3. Space does not permit publishing tables of the measurements. Except in the neighborhood of −18° they are well represented by the straight line $C_p = 1.289 + 0.0034t$. The mean deviation of points

[13] The values in reference (9) are about 0.2 percent low. After it was published it was found that the Leeds & Northrup volt box used had a ratio of about 25.047 : 1 instead of 25.000 : 1 as it should have had. The correction, but not the reason for it, is mentioned in reference (10).

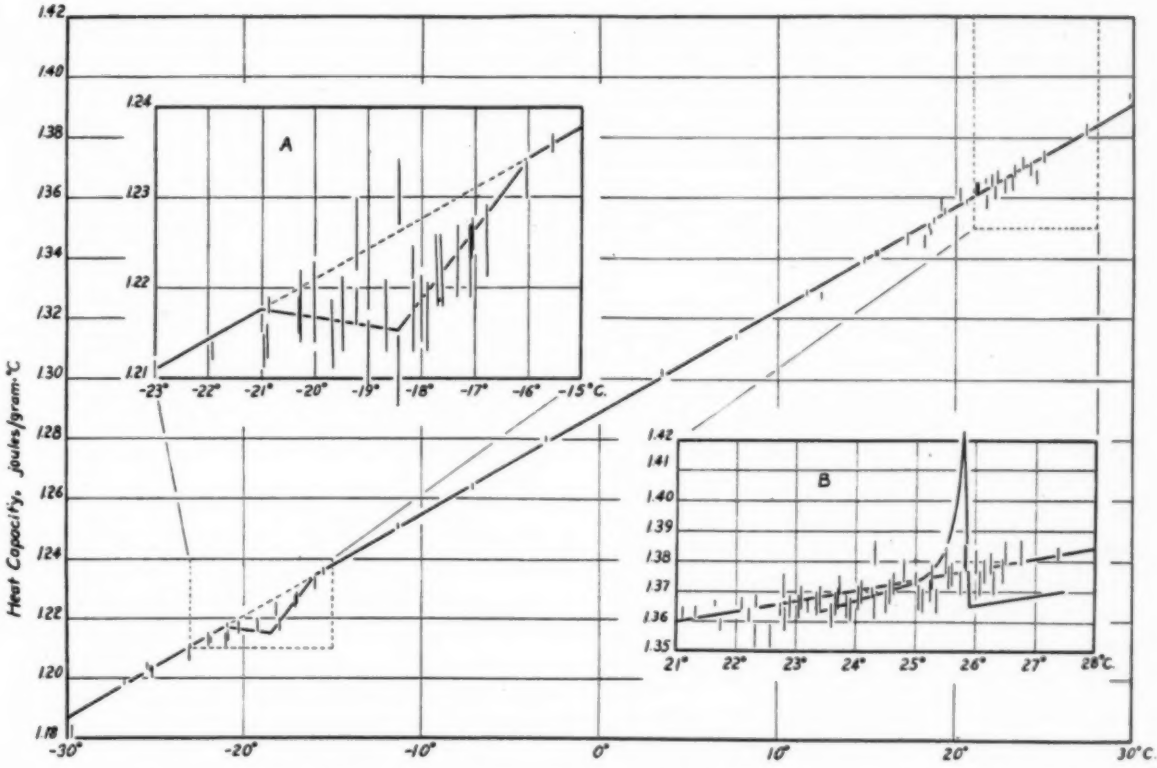

FIG. 3. Heat capacity of the small crystals of Rochelle salt in the range −30 to +30°C.

with temperature intervals of 3° or more from this line is 0.1 percent; the mean deviation of all points is 0.3 percent.

The points near −18° are plotted to a larger scale in inset *A* of the figure. There is a strong suggestion of an anomaly of amplitude somewhat less than 1 percent. It is of the right sign and order of magnitude to agree with the theory mentioned in the introduction but the uncertainties in C_p and $\partial P^2/\partial t$ are large enough to make closer comparison pointless.

The temperature range +22° to +27° was investigated very carefully in a search for the anomaly reported by Kobeko and Nelidow and by Rusterholz. Over 50 measurements were made in this region, most of them with a temperature interval of less than 0.3°. No anomaly was found and it is considered likely that any which may be present has an amplitude less than 1 percent and probably less than ½ percent. Theory does not suggest a larger one. The measurements are plotted in inset *B*, Fig. 3. Rusterholz' curve is superposed for comparison.

The absolute value of the heat capacity found agrees within ½ percent with that found by Kobeko and Nelidow and is about 11 percent smaller than that found by Rusterholz. The large anomaly found by him and by Kobeko and Nelidow would seem to indicate some difference in the properties of Rochelle salt of European and American origin. The differences in absolute value may reasonably be attributed to the method used by Rusterholz. It is perhaps worth mentioning that this work was undertaken in the expectation of finding anomalies as large as those previously reported and that the size to be expected from the theory was not worked out until after measurements at the upper Curie point had shown no appreciable anomaly.

Finally, to show that the apparatus was capable of producing something other than a linear variation of heat capacity with temperature, a magnetic substance containing manganese and arsenic was prepared by heating the powdered metals together at about 700°C. After treatment intended to purify it the substance was put in

the calorimeter and measurements made. They are not included in this paper as it cannot be seriously considered that they represent the temperature variation of the heat capacity of any definite manganese-arsenic compound. They do show, however, a rise to a maximum at about 41.5°C and a rather rapid falling off which is roughly the behavior that Rochelle salt was expected to show.

Discussion of Errors

The errors in the measurements are chiefly of two kinds. The first kind ("systematic") affects all measurements made at a given temperature to the same extent and in the same direction; the second ("accidental") introduces a random scattering. The systematic errors are not affected by the temperature interval used in making a measurement; the accidental errors are more or less inversely proportional to it. When the temperature derivative of the heat capacity does not change rapidly with temperature, the accidental errors may be made small by using large temperature intervals, but small intervals must be used in searching for anomalies near the Curie points.

The vertical lines used in Figs. 2 and 3 to represent the measurements are of lengths intended to cover the "probable" accidental error.

(a) Systematic errors

(i) The calibration of the electrical instruments and stop watch and the measurement of the mass of the salt were done with care that the error introduced by each be not much over 0.01 percent. The total, if all errors affect the result in the same direction, is about 0.1 percent.

(ii) The heat capacity of the second calorimeter was not measured at low temperatures, but measurements made between 18° and 33° were extrapolated parallel to the heat capacity curve of the first calorimeter. It was intended at first to use it only for looking for anomalies near the Curie points and for this use the absolute value of its heat capacity was not important. As the curve is nearly a straight line, the error is probably not much over 0.1 percent at any temperature and vanishes above 18°.

(iii) Non-uniformity of the bath temperature can introduce error if the temperature difference between the position of the thermometer and the position of the jacket junctions of the thermocouples varies systematically with temperature. A constant difference of any amount compatible with the small size of the differences found when the bath was tested with a differential thermocouple would have no appreciable effect. The error from any variation is difficult to estimate but it seems unlikely that it was more than 0.1 percent.

(b) Accidental errors

The errors estimated below are those in measurements made with the second calorimeter. Because of the high heat capacity of the first the errors in measurements made with it are about twice as great.

(i) The smallest division on the platinum thermometer bridge was 0.0001 ohm, the smallest division read on the potentiometer was 0.0001 volt and there was probably a variation of about 0.2 of a second in the times of opening and closing switches. These sources introduce accidental errors totaling 0.1 percent into the measurements made with large temperature intervals (~4°), 0.6 percent into those made with small (~¼°).

(ii) The thermocouple reading could not be kept exactly zero during a measurement. The deflection varied from + to − more or less at random but was rarely more than 0.005°. One may perhaps assume that the effective uncompensated difference in temperature was about 0.002°. A difference of this amount would introduce an error of somewhat less than 0.1 percent in measurements made with large temperature intervals, 0.2 to 0.3 percent in those made with small.

(c) Possible error caused by heat transfer between jacket and calorimeter

One error caused by heat transfer has already been discussed. It is possible, however, that heat transfer could take place even when the differential thermocouple indicated zero. If the transfer is proportional to the rate at which the

calorimeter is heated, it is included in the heat capacity of the empty calorimeter in such a way that it is eliminated in the heat capacity of the salt. If it is independent of the rate of heating the calorimeter, it affects the heat capacity of the salt to an extent depending on the difference between the rate of heating when determining the heat capacity of the empty calorimeter and when determining that of the salt. From observations of the rate of change of temperature of the calorimeter when it was not being heated, it is estimated that the error from this source does not exceed 0.05 percent in measurements made with large temperature intervals, 0.2 percent in those made with small.

It is of some interest to compare the sum of the calculated accidental errors with the mean deviation of the measurements from the straight lines chosen to represent the heat capacities:

	Calculated error	Mean deviation
First calorimeter.		
2° to 4° interval	0.4 percent	0.2 percent
1° interval	1.0 percent	0.3 percent
Second calorimeter.		
3° to 4.5° interval	0.2 percent	0.1 percent
0.2° to 0.5° interval	0.8 percent	0.4 percent

The mean deviations are about half the calculated errors.

ACKNOWLEDGMENTS

The writer desires to express his indebtedness to Professors Mueller and Warren for their help and advice, to Professors Beattie, Bennett, Nottingham and Schumb and Dr. Hicks for the loan of apparatus and to Dr. Gerrish for assistance in the calibration of the stop watch.

The greater part of the work was done with the aid of a Science Research Scholarship of the Royal Commission for the Exhibition of 1851.

DECEMBER 15, 1938 PHYSICAL REVIEW VOLUME 54

Note on the Evaluation of the Earth's Temperatures Arising from Radioactivity*

ARNOLD N. LOWAN**

AND

FREDERICK KING

Columbia University, New York, New York

(Received August 29, 1938)

IN a previous paper,[1] it was shown that the contribution to the temperatures of the earth, arising from radioactivity, is given by

$$T(r,t)=\frac{2R^3}{\pi^2 Kr}\sum_{s=1}^{\infty}\frac{1}{s^2}\sin\frac{s\pi r}{R}\int_0^1 x\phi(Rx)\times\sin s\pi x\,dx-\frac{2R^3}{\pi^2 Kr}\sum_{s=1}^{\infty}e^{-s^2c}\frac{1}{s^2}\times\sin\frac{s\pi r}{R}\int_0^1 x\phi(Rx)\sin s\pi x\,dx$$

$$=T_1(r)-T_2(r,t) \qquad (1)$$

where R is the radius of the earth; r the distance from center; t the time in seconds; K the thermal conductivity in c.g.s. units; k the thermal diffusivity in c.g.s. units; $c=k\pi^2 t/R^2$; and $\phi(r)=$ the heat generated in calories per unit volume per unit time.

It is clear that $T_1(r)$ represents the distribution of temperatures corresponding to the steady state. Accordingly, $T_1(r)$ may be obtained by dropping the term $\partial T(r,t)/\partial t$ in the differential equation of heat conduction, satisfied by $T(r,t)$. Thus, $T_1(r)$ must satisfy the differential equation

$$(\partial/\partial r^2+2/r\cdot\partial/\partial r)T_1(r)=-\phi(r) \qquad (2)$$

and the boundary condition

$$T_1(R)=0. \qquad (3)$$

* Publication assisted by the Ernest Kempton Adams Fund for Physical Research of Columbia University.

** Technical Director, Project for the Computation of Mathematical Tables, W.P.A., New York, New York.

[1] A. N. Lowan, Phys. Rev. **44**, 769 (1933). This paper will be referred to as A.N.L.

TABLE I. *Upper bounds for* $E(n, r)$.

Depth in Miles $=d$	Error after n terms $n=10$	$n=15$	$n=20$	$n=25$
1	0°.6	0°.23	0°.06	0°.01
2	1°.2	0°.45	0°.13	0°.03
3	1°.8	0°.68	0°.19	0°.04
4	2°.4	0°.90	0°.25	0°.05
5	3°.0	1°.1	0°.31	0°.07
10	6°.0	2°.2	0°.63	0°.14
15	9°.1	3°.3	0°.94	0°.20
20	12°	4°.4	1°.3	0°.27
40	24°	8°.9	2°.5	0°.55
60	37°	14°	3°.5	0°.61
80	49°	16°	3°.5	0°.61
100	58°	16°	3°.6	0°.63
300	60°	16°	3°.7	0°.65
400	61°	17°	3°.8	0°.67
500	63°	17°	3°.9	0°.69
1000	74°	20°	4°.6	0°.80
1500	88°	24°	5°.5	0°.96

For $\phi(r)=Ae^{-\alpha(R-r)}$, we get

$$T_1(r)=\frac{A}{K\alpha^2}\left[1-e^{-\alpha d}-\frac{2}{R\alpha}\frac{d}{r}\cdot e^{-R\alpha}-\frac{2}{R\alpha}\left(1-\frac{R}{r}e^{-\alpha d}\right)\right] \quad (4)$$

and

$$T_2(r,t)=\frac{2AR^3}{\pi Kr}\sum_{s=1}^{\infty}e^{-s^2c}\sin\frac{s\pi d}{R}\cdot\frac{1}{s(R^2\alpha^2+s^2\pi^2)}\left(1-\frac{2R\alpha}{R^2\alpha^2+\pi^2s^2}\right), \quad (5)$$

where $d=R-r$ and we have neglected in (5) a term whose order of magnitude is $e^{-R\alpha}$, the exponent of which is approximately equal to 400.

Since $T_1(r)$ is given in closed form, it may be computed as accurately as we wish. Thus the error $E(n, r)$ introduced by truncating the infinite series (5) after n terms, is the error in the value of $T(r, t)$. It is the object of this note to evaluate this error. From (5) we get

$$|E(n,r)|<\frac{2AR^2}{K\pi}\frac{R}{r}\sum_{s=n+1}^{\infty}e^{-s^2c}\left|\sin\frac{s\pi d}{R}\right|\cdot\frac{1}{s(R^2\alpha^2+\pi^2s^2)}\left(1-\frac{2\alpha R}{R^2\alpha^2+s^2\pi^2}\right)$$

and *a fortiori*

$$|E(n,r)|<\frac{2A}{\pi K\alpha^2}\frac{R}{r}\sum_{s=n+1}^{\infty}e^{-s^2c}\frac{1}{s}\left|\sin\frac{s\pi d}{R}\right|. \quad (6)$$

The factor, $|\sin s\pi d/R|$ is never larger than $s\pi d/R$ and also never larger than unity. An upper bound for $E(n, r)$ is obtained below, from each of these limits.

CASE I

Replacing $|\sin s\pi d/R|$ by $s\pi d/R$ and replacing the summation by an integral which exceeds it, we get

$$|E(n,r)|<\frac{2A}{K\alpha^2}\frac{d}{r}\int_n^{\infty}e^{-x^2c}dx, \quad (7)$$

or

$$|E(n,r)|<\frac{A}{K\alpha^2}\left(\frac{\pi}{c}\right)^{\frac{1}{2}}\frac{d}{r}[1-\text{Erf}\,(nc^{\frac{1}{2}})]. \quad (8)$$

Inserting the numerical value of constants of A.N.L. we get

$$|E(n,r)|<8800\frac{d}{4000-d}[1-\text{Erf}\,(nc^{\frac{1}{2}})]. \quad (9)$$

CASE II

In the same way, replacing $|\sin s\pi d/R|$ by unity, we obtain, after putting $y=xc^{\frac{1}{2}}$

$$|E(n,r)|<\frac{A}{\pi K\alpha^2}\frac{R}{r}(-1)\,\text{Ei}\,(-cn^2), \quad (10)$$

where the symbol $\text{Ei}(-cn^2)$ means

$$\int_{cn^2}^{\infty}e^{-y}y^{-1}dy,$$

a function which has been tabulated and given in Table VII in Volume I of the *British Association for the Advancement of Science Mathematical Tables.*

Inserting the numerical values of the constants of A.N.L. we get

$$|E(n,r)|<\frac{487{,}000}{4000-d}\,\text{Ei}\,(-0.006n^2). \quad (11)$$

Table I gives the maximum error of truncation for various values of d and n, from the smaller of the two upper bounds of $E(n, r)$ computed from (9) and (11).

From the table it follows that the error increases with depth. If for instance, we employ 25 terms, the residual error is less than 1°C, up to a depth equal to 1500 miles.

The Nature of Lattice Defects in Silver Bromide Crystals

FREDERICK SEITZ
General Electric Company, Schenectady, New York
(Received November 17, 1938)

IT was first pointed out by Frenkel[1] that ionic crystals may have a volume conductivity only if there are free vacancies, or free interstitial ions in the lattice. He also suggested that the presence of these defects may be explained thermodynamically by the fact that the crystal with vacancies or interstitial ions has a higher entropy than a perfect crystal. Schottky and Wagner[2] and others[3] subsequently investigated the possible types of defects that can occur, and, as a result of this work, it is generally agreed that either one of the following two types occur in the monovalent metal halides with the sodium chloride type of lattice.

I (Cf. Fig. 1a). Positive or negative ions, or both, leave regular lattice sites and enter interstitial positions. It is generally assumed that the entropy S, gained by forming n vacancies and n interstitial ions of a given kind in this way is

$$S=kn \log (n/N_n)+kn \log (n/N_i), \qquad (1)$$

where N_n is the total number of normal sites and N_i is the number of interstitial sites. For simplicity we shall assume that

$$N_n=N_i\equiv N.$$

From this value of the entropy, it is found that the ratio, r_{I}, of the number of vacancies of a given kind to the number of normal ions is

$$r_{\mathrm{I}}=n/N=\exp\left[-\epsilon_{\mathrm{I}}''/2kT\right], \qquad (2)$$

where ϵ_{I}' is the energy required to transfer an ion from a lattice position to an interstitial position.

II (Cf. Fig. 1b). Positive and negative ions leave normal sites in equal number and move to the surface. In this case there are an equal number of vacancies of each kind and there are no interstitial atoms. The equation analogous to (2) is

$$r_{\mathrm{II}}=n/N=\exp\left[-\epsilon_{\mathrm{II}}''/2kT\right], \qquad (3)$$

where ϵ_{II}'' is the energy required to move both a positive and a negative ion to the surface.

Detailed computations of Jost and Nehlep[4] seem to show conclusively that $\epsilon_{\mathrm{I}}-\epsilon_{\mathrm{II}}$ is positive and of the order of 1 ev for the face-centered alkali halides. Hence defects of type II are far more probable than those of type I in these salts. On the other hand, the same workers have given good semi-quantitative evidence to show that $\epsilon_{\mathrm{I}}-\epsilon_{\mathrm{II}}$ probably is negative in AgCl and AgBr because the van der Waals forces between Ag ions and halogen ions are considerably larger than those between alkali metal ions and halogen ions. As a result, they suggest that defects of type I occur more commonly than those of type II in these silver halides.

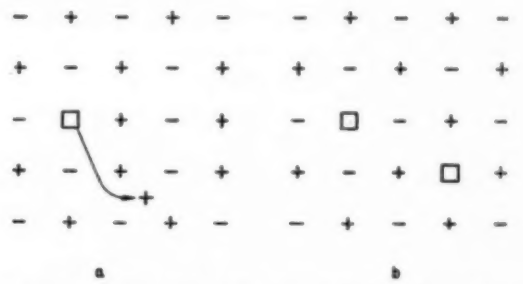

FIG. 1. (a) Lattice defect of type I. Ions leave normal lattice sites and enter interstitial sites. The crystal then has vacancies and interstitial ions. In the case illustrated defects for the positive ion lattice are shown. (b) Lattice defect of type II. There are vacancies in both lattices in equal numbers and no interstitial ions. The ions that leave the lattice to form vacancies go to the surface and extend the crystal. The density of the crystal is the same as for a perfect lattice in case I; it is smaller in case II.

Wagner and Beyer[5] claim to have direct experimental evidence supporting Jost and Nehlep's conclusion concerning the type of defects in AgBr. They assume that r is of the order of unity for the liquid salts at the melting point and compute r for the solid at the same temperature by taking the ratio of the ionic conductivity of the solid to that of the liquid, that is

$$r \text{ (solid)}=\sigma \text{ (solid)}/\sigma \text{ (liquid)}. \qquad (4)$$

[1] I. Frenkel, Zeits. f. Physik **35**, 652 (1926).
[2] C. Wagner and W. Schottky, Zeits. f. physik. Chemie **B11**, 163 (1930), *et. seq.*
[3] Cf. W. Jost, *Diffusion und Chemische Reaction in Festen Stoffen* (Dresden, 1937).
[4] W. Jost and G. Nehlep, Zeits. f. physik. Chemie **B32**, 1 (1936).
[5] C. Wagner and J. Beyer, Zeits. f. physik. Chemie **B32**, 113 (1936).

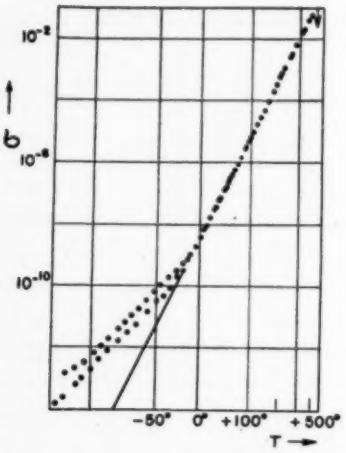

FIG. 2. A log σ *versus* $1/T$ plot of the conductivity, σ, of AgBr (after Lehfeldt). The slope of the high temperature part of the curve, which is precisely reproducible, corresponds to an activation energy of 0.66 ev. The slope of the low temperature position, which depends on the previous history of the specimen, corresponds to one of about 0.30 ev.

This leads to the value 0.16 for r (solid). They then show that, to within the experimental error of about one percent, the observed density at this temperature is the same as that computed from the x-ray lattice constant measurements under the assumption that each cell is fully occupied. Since this can occur only for a crystal of type I if r actually is 0.16, they conclude that AgBr is of this type.

It seems to the writer that the use of Eq. (4) is not well justified because recent investigations on the structure of liquids show that they possess a large amount of local order. Hence r may be considerably less than unity for the liquid at the melting point. The following alternative method of computing r (solid) at the melting points should be somewhat more reliable.

The conductivity of an ionic crystal may be expressed in the form

$$\sigma = ne\mu, \tag{5}$$

where n is the number of potentially free ions or vacancies, given by Eqs. (2) or (3) in the present case, e is the ionic charge, and μ is the mobility of these ions. We shall assume that μ has the form

$$\mu = A \exp[-\epsilon'/kT], \tag{6}$$

where A is practically independent of temperature and ϵ' is the activation energy for motion of the potentially free ions or vacancies. A formal equation could be written for A with the theory of reaction rates, but this is not necessary for the present discussion since we shall be interested only in ϵ'. Eq. (5) may be written in the form

$$\sigma = NeA \exp[-(\tfrac{1}{2}\epsilon''+\epsilon')/kT],$$

using Eqs. (2) or (3) and (6). ϵ'' is one of the energies in case I or II. According to Lehfeldt's[6] measurements of the conductivity of AgBr near the melting point (cf. Fig. 2)

$$(\epsilon''/2+\epsilon') = 0.66 \text{ ev}.$$

The observed slope of the log σ *versus* $1/T$ curve becomes less steep at low temperature. We shall assume that the high temperature value of r is quenched in this low temperature range so that the slope is determined by ϵ' alone. From the experimental curve we find

$$\epsilon' \leqq 0.30 \text{ ev},$$

whence

$$\epsilon''/2 \leqq 0.36 \text{ ev}.$$

Placing this in either (2) or (3) we find

$$r \sim \exp[-4.150/T],$$

which is $10^{-2.6} = 0.0025$ at the melting point (410°C). According to this result the influence of the defects on the density in case II would be less than the experimental error. Moreover, if we assume that the relation

$$r \text{ (solid)}/r \text{ (liquid)} = \sigma \text{ (solid)}/\sigma \text{ (liquid)}$$

is valid at the melting point, we find from Wagner and Beyer's results and the preceding estimate of r (solid), that

$$r \text{ (liquid)} \sim 0.015.$$

To summarize, it may be said that value of ϵ'' computed from the observed conductivity indicate that the fraction of defect ions in AgBr is too small to allow a differentiation between types I and II on the basis of present density and x-ray lattice constant measurements

[6] W. Lehfeldt, Zeits. f. Physik **85**, 717 (1933).

LETTERS TO THE EDITOR

Prompt publication of brief reports of important discoveries in physics may be secured by addressing them to this department. Closing dates for this department are, for the first issue of the month, the eighteenth of the preceding month, for the second issue, the third of the month. Because of the late closing dates for the section no proof can be shown to authors. The Board of Editors does not hold itself responsible for the opinions expressed by the correspondents.

Communications should not in general exceed 600 words in length.

Note on the Fine Structure of Hα and Dα

Various investigators[1] have found that the doublet separations of the Hα and Dα lines are somewhat smaller than the theoretically predicted values. Kemble and Present[2] pointed out that the discrepancy could be accounted for by a deviation from the Coulomb law at small distances from the nucleus, which leads to a displacement of the ^2S levels. However they found that the discrepancy was much too large to be explained on the basis of a finite size of the electron and proton.

Recently R. C. Williams[3] resolved a third component of the Dα line, and obtained the separations 0.319 cm^{-1} between components (1) and (2), and 0.135 cm^{-1} between components (3) and (2). These values are, respectively, 0.009 cm^{-1} less, and 0.027 cm^{-1} greater, than the theoretical values. Unpublished results obtained by Houston and Robinson by means of a Fourier analysis of the Dα line give a similar discrepancy, although the deviations found are not quite as large as those obtained by Williams.

It seems significant that both of these deviations are consistent with a perturbation of the 2^2S level of deuterium. According to theory the component (2) consists of the two transitions $2^2P_{\frac{1}{2}}-3^2D_{\frac{3}{2}}$ and $2^2S_{\frac{1}{2}}-3^2P_{\frac{1}{2}}$, the former having 2.4 times the intensity of the latter. Hence, if the 2^2S level is displaced by an amount x cm^{-1}, the component (2) will undergo an apparent displacement of approximately $0.3x$. On the other hand, the component (3) consists of the transitions $2^2S_{\frac{1}{2}}-3^2P_{\frac{1}{2}}$ and $2^2P_{\frac{1}{2}}-3^2S_{\frac{1}{2}}$, the former being 10.7 times as intense as the latter. Thus its apparent displacement is $0.9x$. Consequently the separation of components (1) and (2) is decreased by an amount $0.3x$, whereas the separation of components (3) and (2) is increased by $0.6x$. This agrees fairly well with the results of Williams, and of Houston and Robinson, if the displacement x is taken to be about 0.03 cm^{-1}.

An S level displacement of this magnitude checks quite well with discrepancies observed in the doublet separations of other Balmer lines of hydrogen, as is seen from Table I.

TABLE I.

	Hα	Hβ	Hγ	Hδ	Hε
$\Delta\nu_{theor}$	0.319	0.344	0.353	0.358	0.360
$\Delta\nu_{obs}$	0.307	0.330	0.339	0.345	0.351
$\Delta\nu_{corr}$	0.308	0.330	0.339	0.343	0.345

The first two rows are the separations in cm^{-1} of the apparent centers of intensity as given by Houston and Hsieh.[4] The third row contains the theoretical separations obtained if a $2S$ level displacement of 0.030 cm^{-1} is assumed.

A displacement of the S levels would seem to point toward some perturbing interaction between the electron and the nucleus. As was indicated by Kemble and Present, the interaction required is much too large to be accounted for by the assumption of a finite size of electron and proton. An estimate of the magnitude of the interaction can be obtained by superposing on the Coulomb field a simple repulsive potential of height D, extending for a distance of r_0 cm from the nucleus. A first-order perturbation treatment raises the energy of the n^3S level of a hydrogen-like atom by an amount

$$\frac{4}{3}D\frac{Z^3}{n^3}\frac{r_0^3}{a_0^3},$$

where a_0 is the Bohr radius. If we assume a displacement of the $2S$ level of deuterium of about 0.3 cm^{-1}, as suggested by Williams' results, we find that Dr_0^3 must be about 5×10^{-42} erg cm^3. Thus if r_0 were taken to be the nuclear radius, 3×10^{-13} cm, D would have to be given the extremely high value of about 100 Mev.

In the case of the ionized helium line λ4686, an S level displacement would shift two of the weaker components toward the red, but would not affect the two main components, which involved transitions between P, D and F levels. Measurements by Leo[5] and by Paschen[6] show deviations from the theoretical values for the two weak components which could be explained by a 3^3S level displacement of 0.04 or 0.05 cm^{-1}. Results soon to be published by Chu, however, show no deviations of this magnitude.

An S level displacement could also be the cause of a slight shift toward the red observed by Edlén[7] in the doubly-ionized lithium line $1s^2S-2p^2P$.

SIMON PASTERNACK

California Institute of Technology,
Pasadena, California,
November 25, 1938.

[1] Houston and Hsieh, Phys. Rev. **45**, 263 (1934); Williams and Gibbs, Phys. Rev. **45**, 475 (1934); Kopfermann, Naturwiss. **22**, 218 (1934); Spedding, Shane and Grace, Phys. Rev. **47**, 38 (1935); Houston, Phys. Rev. **51**, 446 (1937).
[2] Kemble and Present, Phys. Rev. **44**, 1031 (1932).
[3] Williams, Phys. Rev. **54**, 558 (1938).
[4] Houston and Hsieh, reference 1.
[5] Leo, Ann. d. Physik **81**, 757 (1926).
[6] Paschen, Ann. d. Physik **82**, 689 (1927).
[7] Edlén, *Wellenlängen und Termsysteme zu den Atomspektren der Elemente* Li, Be, B, C, N, O (Uppsala, 1934), p. 29.

On The Characteristic Matrices of Covariant Systems

We wish to indicate here how the consideration of certain matrices implicit in a system of tensor equations gives rise to an algebraic formalism both elegant and significant. No attempt to attain generality shall be made at this time, but rather we shall discuss a particular system of current physical interest.

Proca's tensor wave equation[1] is given by the system

$$\begin{aligned} n_{jklm}p_l\varphi_m &= \mu f_{jk}, \\ p_j f_{jk} &= \mu\varphi_k, \end{aligned} \tag{1}$$

where $n_{jklm}=(\delta_{jl}\delta_{km}-\delta_{jm}\delta_{kl})$, $p_k=\hbar\partial/i\partial x_k$ and $\mu=m_0c/\hbar$. Let ψ be a single column matrix whose elements are the components of the vector ϕ_j and the distinct components of the tensor f_{jk}. Then Eq. (1) may be written

$$\Sigma\beta_j p_j\psi=\mu\psi. \tag{2}$$

The symbols β_j are ten-row Hermitian matrices which are found to satisfy the following identities:

$$\begin{aligned} &\beta_j^3=\beta_j, \\ &\beta_j\beta_k^2+\beta_k^2\beta_j=\beta_j, \qquad j\neq k, \\ &\beta_j\beta_k\beta_l+\beta_l\beta_k\beta_j=0, \qquad j\neq k, \qquad l\neq k. \end{aligned} \tag{3}$$

It is easy, then, to deduce this theorem. A necessary and sufficient condition for the existence of Eqs. (3) is that

$$\Sigma_{j,\ k,l}\beta_j\beta_k\beta_l c_{jkl}=\Sigma_{j,\ k}\beta_j c_{jkk} \tag{4}$$

for every c_{jkl} such that $c_{jkl}=c_{lkj}$. The application of this theorem to Eq. (2) gives the relations $\Sigma p_j^2\psi=\mu^2\psi$ and $\Sigma s_{jk}p_k\psi+p_j\psi=\mu\beta_j\psi$. Here s_{jk} is the matrix $\beta_j\beta_k-\beta_k\beta_j$ and it satisfies the identities:

$$\begin{aligned} &s_{jk}^3=-s_{jk}, \\ &s_{jk}\beta_l-\beta_l s_{jk}=\begin{cases}0 & k\neq l\\ \beta_j & k=l.\end{cases} \end{aligned} \tag{5}$$

Another result deducible from Eq. (4) is that, if the symbols β_j are formally transformed as components of a vector, then the relations (3) are covariant under such a transformation.

To attach quantum theoretic significance to these matrices and to the symbol ψ, let us adopt the usual formalism associated with the notation employed here, excepting the postulate that $\psi^*\psi$ is "charge density." Instead we shall suppose that $\psi^*\psi$ is the density of some other mechanical quantity, M, and that if R is an operator, $\int\psi^*R\psi dV$ is the average value of MR. If ψ^* is the matrix adjoint to ψ, then $\psi^*\psi$ when written in terms of ϕ_j and f_{jk} proves to be the expression given by Proca and Kemmer for the relative energy density.

From Eqs. (5) it follows that the operator $(x_1p_2-x_2p_1)-i\hbar s_{12}$ is permutable with the operator of Eq. (2); hence $-i\hbar s_{12}$ is to be interpreted as a component of the spin. The matrix is_{12} has the eigenvalues 1, 0, and -1. The relationship between the spin and the polarization of the vector ϕ_j for plane wave solutions of Eq. (1) is of interest. A circularly polarized wave gives the eigenstates ±1 in the direction of propagation, while a longitudinal wave gives the eigenstate 0 in the same direction. For a wave half-longitudinal and half-plane polarized there are eigenstates ±1 (approximately for low energies) in a direction perpendicular both to the direction of propagation and to the direction of polarization. For all types of low energy waves $-(s_{12}^2+s_{23}^2+s_{31}^2)\psi\cong2\psi$.

The so-called scalar wave equation is given by the system $p_j\phi_j=\mu f$ and $p_j f=\mu\phi_j$ where f is a scalar and ϕ_j is a vector. The matrices here have five rows and again satisfy Eqs. (3) and in addition the relation $\beta_j\beta_k\beta_l=0$. It is again found necessary to add a spin operator to the orbital momentum operator to obtain commutation. However, the spin is "dormant," because for a plane wave solution the average of the spin operator proves to be zero.

Finally we shall give an example of a tensor wave equation with characteristic matrices abstractly isomorphic to the Dirac matrices. This is given by Eqs. (1) if n_{jklm} now signifies the tensor $(\delta_{jl}\delta_{km}-\delta_{jm}\delta_{kl}+\delta_{jk}\delta_{lm}+\epsilon_{jklm})$. Here ϵ_{jklm} is $+1$ or -1, depending on whether or not $jklm$ is an even or an odd permutation of 1234 and is zero otherwise. Because ϵ_{jklm} is not invariant in sign under certain reflections, there is an equipollent set of equations with ϵ_{jklm} replaced by $-\epsilon_{jklm}$. The matrices have eight rows and columns.

R. J. DUFFIN

Department of Mathematics,
Purdue University,
Lafayette, Indiana,
December 1, 1938.

[1] Proca, J. de phys. et le rad. **7**, 347 (1936); Dirac, Proc. Roy. Soc. **A155**, 477 (1936); Kemmer, Proc. Roy. Soc. **A166**, 127 (1938).

Acknowledgment: Direct Determination of Crystal Structure from X-Ray Data*

I regret that my attention was drawn too late to a paper by H. Ott in the Zeits. f. Krist. **66**, 136 (1927), to include mention of it in the paper on the "Direct Determination of Crystal Structure from X-Ray Data," in the August 15 issue of the *Physical Review*. In this paper Ott gives what is essentially the same method that I have used. Though he confines himself explicitly to the special case of lattices with all atoms alike, and to special reflections, he seems to have indicated the generalization in a subsequent note. Other work which I had not seen, based on Ott's but special in treatment, is that of K. Banerjee, Proc. Roy. Soc. **141**, 188 (1933), and H. Seyfarth, Zeits. f. Krist. **67**, 131, 422, 595 (1927).

MELVIN AVRAMI

School of Mines,
Columbia University,
New York, New York,
November 17, 1938.

* Publication assisted by the Ernest Kempton Adams Fund for Physical Research of Columbia University.

On the Paths of Ions in the Cyclotron

Thomas[1] has recently shown that a variation of the magnetic field of a cyclotron with polar angle, together with a radial increase in the field, can produce a focusing effect on the beam while maintaining resonance. For polar angle variations of period 2π or π, the orbits are unstable,

while for period $\pi/2$ they are stable. The calculations have been extended to polar angle variations of period $2\pi/3$; orbits in such a field are stable. The results for the most interesting cases of period $2\pi/3$ and $\pi/2$ are compared here (see Thomas' papers for notation).

For a pure magnetic field of the form

$$H=\frac{m_0c\omega}{e}\left[1+A\frac{\omega r}{c}\cos n(\theta-\beta)+B\left(\frac{\omega r}{c}\right)^2\right], \quad (1)$$

the resonance condition is

$$\begin{aligned} &n=3,\ B=\tfrac{1}{2}-A^2/8;\\ &n=4,\ B=\tfrac{1}{2}-A^2/15. \end{aligned} \quad (2)$$

For the special case of zero focusing, the constants have the values

$$\begin{aligned} &n=3,\ A_0=(4/3)^{\frac{1}{2}},\quad B_0=1/3;\\ &n=4,\ A_0=(30/19)^{\frac{1}{2}},\ B_0=15/38, \end{aligned}$$

and the characteristic exponents of the orbits are

$$n=3,\ D=\pm i\frac{14}{15}\left(\frac{a\omega}{c}\right)^2;\ n=4,\ D=\pm i\frac{105}{152}\left(\frac{a\omega}{c}\right)^2,$$

indicating stability in both cases. Thus the field given by Eq. (1) with $n=3$ would be easier to construct than that with $n=4$, since the field required does not vary as much or as rapidly with polar angle. In general, the required variations in the field increase with increasing n, since the orbits then become more nearly circular; the smallest permissible value of n is fixed by the requirement of stability, and is $n=3$.

For positive focusing with resonance, A must be made greater than A_0, and B correspondingly smaller than B_0, in both cases. As a measure of the degree of focusing, we can compute the number of cycles with mean radius a described per complete oscillation in the z direction; this is smaller the greater the focusing. When the resonance condition (2) is fulfilled, this number is

$$(c/a\omega)[(A/A_0)^2-1]^{-\frac{1}{2}},$$

in both cases.

We have also investigated the nonrelativistic motion of ions in a uniform magnetic field under the action of the electric field due to "triants" operated by three-phase power. The secular variations in the position of the center of the orbit are, in Thomas' notation with $\sigma=\omega$, given approximately by[2]

$$\frac{d\xi}{dt}=\frac{3}{4\pi}\frac{\eta}{a}\frac{eU_0}{m_0a\omega}\sin\alpha,$$

$$\frac{d\eta}{dt}=-\frac{3}{4\pi}\frac{\xi}{a}\frac{eU_0}{m_0a\omega}\sin\alpha.$$

Since these result in a stable oscillation, three-phase triants should be usable.

L. I. SCHIFF

University of California,
Berkeley, California,
November 29, 1938.

[1] L. H. Thomas, Phys. Rev. **54**, 580, 588 (1938). In Eqs. (3.6) and (3.7) of the second paper, σ^2 in the denominators should be replaced by σ.

[2] Professor Thomas has kindly pointed out an error in the derivation of the last result quoted in my abstract in the *Bulletin of the American Physical Society* for the Los Angeles meeting.

Proceedings of the Metropolitan Section of the American Physical Society

Meeting of November 4, 1938

THE first meeting of the Metropolitan Section of the American Physical Society for the season 1938–1939 was held on Friday, November 4, 1938, in the Pupin Physics Laboratories of Columbia University.

The following papers were presented:

Afternoon Session—4 P.M.

The Properties of Gases at Low Temperatures. G. E. Uhlenbeck

The Order-Disorder Transformations in Alloys. F. C. Nix

Evening Session—8 P.M.

The Separation of the Isotopes of Nitrogen. H. C. Urey

E. O. Salant was elected a member of the Executive Committee.

W. S. Gorton, *Secretary-Treasurer*

Author Index to Volume 54

References with (A) are to abstracts of papers presented at meetings of the American Physical Society. References with (L) are to Letters to the Editor; with (T) are to title only.

Adams, Norman I., Jr. (see Kovarik, Alois F.)—413
Ahearn, Arthur J. and Joseph A. Becker. Electron microscope studies of thoriated tungsten—448
Albertson, Walter. Spectrum of neutral iridium, Ir I—183
Alfvén, Hannes. On the sidereal time variation of the cosmic radiation—97
Alleman, R. S. and J. C. Hubbard. Ultrasonic reflection losses in air, helium and CO_2—313(A)
Allison, Samuel K., Lester S. Skaggs and Nicholas M. Smith, Jr. Precise measurement of the energy change in the transmutation of beryllium into lithium by proton bombardment—171
Alvarez, Luis W. Capture of orbital electrons by nuclei—486
——— Collimated, variable energy beam of pure thermal neutrons—235(A)
——— Production of collimated beams of monochromatic neutrons in the temperature range 300–10°K—609
Anderson, Carl D. (see Neddermeyer, Seth H.)—88(L)
Anderson, Paul A. Contact difference of potential between barium and magnesium—753
Andrews, C. Luther. Absorption of x-rays of wave-length $1.5 \leq \lambda \leq 8.3$A—994
Archibald, William J. Process of diffusion in a centrifugal field of force. II—371
Avrami, Melvin. Direct determination of crystal structure from x-ray data—300; Acknowledgment—1114(L)

Bacher, R. F. (see Crittenden, E. C., Jr.)—862(L)
——— (see Hoffman, J. G.)—644
——— (see Tomboulian, D. H.)—446
Bachmann, J. H. (see Glockler, George)—970(L)
Bacon, R. H., E. N. Grisewood and C. W. van der Merwe. β-ray spectrum of I^{128}—315(A)
Bailey, H. H. (see Bollman, V. L.)—792
Ballard, Stanley S. Constitution of the solfataric gases at Kilauea volcano, Hawaii—236(A)
——— Spectrochemical analysis of fertilizers, particularly for the micrometabolic elements—312(A)
Bardeen, John and Eugene Feenberg. Symmetry effects in the spacing of nuclear energy levels—809
Barieau, R. E. (see Giauque, W. F.)—147(L)
Batdorf, Samuel B. and Erich W. Beth. Radiative losses by particles of anomalous magnetic moment—237(A)
Bath, Jean (see Ellis, Joseph W.)—236(A)
Bearden, J. A. Determination of e/m from the refraction of x-rays in a diamond prism—698
——— (see Obert, Leonard)—1000
Becker, Joseph A. (see Ahearn, Arthur J.)—448
Beckman, J. W. and Leonard B. Loeb. Sign preference in cloud condensation on gaseous ions—862(L)
Bender, David. Refractive index of air in the visible and photographic infra-red—179
Bernet, E. J., R. G. Herb and D. B. Parkinson. Gamma-rays from fluorine due to proton bombardment—398
Beth, Erich W. (see Batdorf, Samuel B.)—237(A)
Beth, Richard A. Test for the adequacy of theory in the light of experiment—865(A)
Bethe, H. A. Coulomb energy of light nuclei—436
——— Method for treating large perturbations—955
——— (see Konopinski, E. J.)—130
——— **and C. L. Critchfield.** Formation of deuterons by proton combination—248, 862(L)
Beyer, Harold G. (see Whitaker, Martin D.)—771(L)
Binder, John L. Continuous absorption spectrum of iodine monochloride in the ultraviolet—114
Birge, Raymond T. Present status of the value of e/m—972(L)
Bitter, F. Generalization of the theory of ferromagnetism—79
Blackett, P. M. S. On the instability of the barytron and the temperature effect of cosmic rays—973(L)
Bleakney, Walker (see Sherr, Rubby)—388(L)
Bloomenthal, Sidney. Vibrational analysis for a new CuCl band system excited by active nitrogen—497
Bohn, J. Lloyd and Joseph Morgan. Experiments and theory on the performance of the Geiger point counter—314(A)
Bollman, V. L. and Jesse W. M. DuMond. Evidence for surface layers in cleaved calcite crystals—238(A)
——— **and J. W. M. DuMond.** Further tests of the validity of x-ray crystal methods of determining e—1005
———, **H. H. Bailey and J. W. M. DuMond.** Exploratory study of plural x-ray reflection methods applied to the problem of the diffraction pattern of calcite—792
Bonner, T. W. (see Hudspeth, Emmett)—308(L)
Bracewell, Kent H. Effective cross section of positive alkali ions with respect to gas molecules—639
Bradbury, N. E. and H. J. Meuron. Diurnal variation of atmospheric condensation nuclei—242(A)
Bramley, Arthur. Dirac equation with spin greater than $\frac{1}{2}$—314(A)
Breit, G. (see Hoisington, L. E.)—627
——— **and J. K. Knipp.** Note on K-electron capture in Be^7—652
Brickwedde, F. G., John R. Dunning, Harold J. Hoge and John H. Manley. Neutron scattering cross sections of para- and orthohydrogen, and of N_2, O_2, and H_2O—266
Brillouin, Léon. Thermal dependence of elasticity in solids—916
Brode, Robert B. and Dale R. Corson. Probable ionization of high speed electrons in nitrogen—238(A)
Brown, William Fuller, Jr. Domain theory of ferromagnetics under stress. Part III. Reversible susceptibility—279

Broxon, James W. and George T. Merideth. Analysis of high gradient, high pressure, gamma-ray, air ion current measurements, by Zanstra's adaptation of Jaffé's columnar theory—9
——— **and George T. Merideth.** Application of Clay's new value of the Jaffé-Zanstra coefficient for air to high pressure ion current measurements—605
——— **and George T. Merideth.** Measurements of gamma-ray ionization currents in air at high pressures and high gradients—1
Brož, J. (see Němejcová, A.)—379
Brubaker, Gordon. Scattering of alpha-particles by argon, oxygen, and neon—1011
Bruce, W. A. (see Jauncey, G. E. M.)—163
Buck, John H. Proton induced radioactivities. III. Zinc and selenium targets—1025

Callihan, D. (see Waldman, B.)—543(L), 1017
Carr, Emma P. and Hildegard Stücklen. Ultraviolet absorption spectra of simple hydrocarbons—865(A)
Carroll, Henry and J. R. Dunning. Interaction of slow neutrons with gases—541(L)
Carroll, Kenneth G. (see Margenau, Henry)—705
Cartmel, W. B. Exact solution of Lorentz' pair of triangles—867(A)
——— Michelson-Morley-Miller experiment—315(A)
Cashman, R. J. Comments concerning Anderson's paper on contact difference in potential between barium and magnesium—971(L)
Chapman, Seville. Carrier mobility spectra of liquids electrified by bubbling—520
——— Interpretation of carrier mobility spectra of liquids electrified by bubbling and spraying—528
Ch'en, Shang-Yi (see Ny, Tsi-Zé)—1045
Cobine, J. D., R. B. Power and L. P. Winsor. Electric arc reignition at high pressures—312(A)
Cohn, Willi M. Motion picture polarigraph for sky light investigations—241(A)
Collins, George B. and Victor G. Reiling. Čerenkov radiation—499
Condon, E. U. Note on the external photoelectric effect of semiconductors—1089
——— Simple derivation of the Maxwell-Boltzmann law—937
Coolidge, Albert Sprague, Hubert M. James and E. L. Vernon. On the determination of molecular potential curves from spectroscopic data—726
Cornell, S. D. Ultraviolet band spectra of HgCl, CdCl, and ZnCl—341
Corson, Dale R. (see Brode, Robert B.)—238(A)
Crane, H. R. and J. Halpern. Reply to the above note by L. Wertenstein—306(L)
Crawford, D. P. (see Wilkins, T. R.)—316(A)
Crawford, M. F. (see Stevenson, A. F.)—314(A), 375
———, **A. B. McLay and A. M. Crooker.** Spectrum of doubly ionized lead, Pb III—313(A)
Critchfield, C. L. (see Bethe, H. A.)—248, 862(L)
Crittenden, E. C., Jr. and R. F. Bacher. Nuclear isomerism in rhodium—862(L)
Crooker, A. M. (see Crawford, M. F.)—313(A)
Crudup, Josiah. Absorption of the shower-producing component of cosmic radiation in iron and lead—483

Dancoff, S. M. and P. Morrison. Note on internal conversion of arbitrary multipole order—149(L)
Davidson, W. L., Jr. and Ernest Pollard. Transmutation of titanium by Th C′ alpha-particles—408
Davisson, C. J. Theory of the transverse Doppler effect—90(L)
Delfosse, J. and John A. Hipple, Jr. Dissociation of $C_2H_2D_2$ by electron impact—1060
Delsasso, L. A. (see White, M. G.)—314(A)
Dember, A. (see Gould, W. O.)—240(A)
———, **A. Goetz and W. O. Gould.** Objective quantitative definition of the graininess of photographic emulsions—240(A)
Dempster, A. J. (see Wilkins, T. R.)—315(A)
Dieke, G. H. Bands of H_2 ending on the $2p^1\,\Pi$ level—439
Dow, R. B. Viscosity characteristics of lubricating oils at high pressure at various temperatures—312(A)
——— (see Morgan, H. E.)—312(A)
Drill, H. T. Search for an electrostatic analog to the red shift—240(A)
Duffendack, O. S. (see Lifschutz, Harold)—714
Duffin, R. J. On the characteristic matrices of covariant systems—1114(L)
DuMond, Jesse W. M. (see Bollman, V. L.)—238(A), 792, 1005
——— (see Hirsh, F. R., Jr.)—789
——— (see Kirkpatrick, H. A.)—802
Dunning, John R. (see Brickwedde, F. G.)—266
——— (see Carroll, Henry)—541(L)
——— (see Whitaker, Martin D.)—771(L)

Eckart, Carl. Electrodynamics of material media—920
Ehrenkranz, Florence. Spark breakdown potentials in A, N_2 and H_2 for Pt and Na cathodes—239(A)
Ellett, A. and R. D. Huntoon. Asymmetric distribution of protons from deuteron-deuteron reaction—87(L)
Ellickson, Raymond. Method of calculating fluctuations—572
Ellis, Cecil B. and Harvey Hall. Crystal fields in rare earth ethylsulphates—478(L)
Ellis, Joseph W. and Jean Bath. Alterations in the near infra-red absorption spectra of water and of protein molecules when water is bound to gelatin—236(A)
——— **and E. L. Kinsey.** Vibrational-rotational radiation transitions in water molecules in nonpolar solvents—599
Elmore, W. C. Ferromagnetic colloid for studying magnetic structures—309(L)
——— Magnetization of ferromagnetic colloids—1092
Elsasser, Walter M. Mean absorption and equivalent absorption coefficient of a band spectrum—126
Evans, Robley D. (see Goodman, Clark)—866(A)
——— **and Clark Goodman.** Radioactive air inhalation as a health hazard—866(A)
Ewald, P. P. Force of excitation in the theory of dispersion—893

Farnsworth, H. E. (see Turnbull, John C.)—509
Feenberg, Eugene (see Bardeen, John)—809
——— (see Motz, Lloyd)—1055
Fett, G. H. Ignition potential in a low pressure neon tube—389(L)
Findlay, J. C., A. Pitt, H. Grayson Smith and J. O. Wilhelm. Velocity of sound in liquid helium—506
Fine, Paul. Normal modes of vibration of a body-centered cubic lattice—239(A)
Fleming, G. and J. E. Henderson. Search for temperature changes accompanying field emission at high temperatures—241(A)
Forbush, S. E. On world-wide changes in cosmic-ray intensity—975
Fowler, W. A. Scattering of fast electrons—773(L)
——— **and Jacquenette Oppenheimer.** Scattering and loss of energy of fast electrons and positrons in lead—320
Fox, Francis E. and George D. Rock. Ultrasonic radiation field of a quartz disk radiating into liquid media—223
Frenkel, J. On pre-breakdown phenomena in insulators and electronic semi-conductors—647(L)
Fricke, E. (see Knudsen, V. O.)—238(A)
Fried, B. (see Green, J. B.)—876
——— (see Shortley, George H.)—739, 749
Froehlich, H. Solution of the Schrödinger equation by a perturbation of the boundary conditions—945
Froman, Darol K. and J. C. Stearns. Altitude variation of the relative frequency of occurrence of pairs and larger cosmic-ray showers—315(A)
——— **and J. C. Stearns.** Evidence of neutrons in heavy particle showers—969(L)
Fuller, M. L. Atomic vibrations of a zinc-copper alloy—388(L)
Furry, W. H. Note on the theory of the neutral particle—56

Gamow, G. Tentative theory of novae—480(L)
Giauque, W. F., J. W. Stout and R. E. Barieau. Viscosity of liquid helium II—147(L)
Gilliland, T. R. (see Kirby, S. S.)—234(L)
Glockler, George and J. H. Bachmann. Raman effect of dibromofluoromethane—970(L)
Goetz, A. (see Dember, A.)—240(A)
——— (see Gould, W. O.)—240(A)
——— **and S. Scott Goetz.** Vitrification and crystallization of living cells at low temperature—236(A)
Goetz, S. Scott (see Goetz, Alexander)—236(A)
Goodman, Clark (see Evans, Robley D.)—866(A)
——— **and Robley D. Evans.** Determination of the radon and thoron content of air—866(A)
Goranson, Roy W. and W. A. Zisman. On the electrical properties of multilayers—544(L)
Gould, W. O. (see Dember, A.)—240(A)
———, **A. Goetz and A. Dember.** Instrument for the objective and quantitative determination of photographic graininess—240(A)
Grahame, D. C. Search for long or short-lived radiochlorine—972(L)
——— **and G. T. Seaborg.** Separation of radioactive substances without use of a carrier—240(A)
Granath, L. P. (see Williams, D. T.)—338
Green, J. B. and B. Fried. Zeeman effect in the spectrum of argon—876
——— **and J. A. Peoples, Jr.** Zeeman effect in the spectrum of neon—602
Grisewood, E. N. (see Bacon, R. H.)—315(A)

Hafstad, L. R. (see Rumbaugh, L. H.)—657
——— **and E. Teller.** Alpha-particle model of the nucleus—681
Hale, Donald H. First and second Townsend ionization coefficients for pure H_2—241(A)
Hall, Harvey (see Ellis, Cecil B.)—478(L)
Halpern, J. (see Crane, H. R.)—306(L)
Hardy, T. C. and S. L. Quimby. Change of thermal energy with adiabatic change of magnetization in iron, nickel and carbon steel—217
Harrison, George R. (see Weeks, Dorothy W.)—312(A)
Hartig, Henry E. and Arthur W. Mellon. Transmission of damped electromagnetic waves through small hollow metal tubes—646(L)
——— **and Carl E. Swanson.** "Transverse" acoustic waves in rigid tubes—618
Hatch, Graham T. Yield of alpha-particles from beryllium bombarded by protons—165
Haworth, F. E. An x-ray test of superstructure in Fe-Ni_3—313(A), 693
Haworth, L. J. and L. D. P. King. Excitation function for the disintegration of Li^7 under bombardment by low energy protons—38
——— **and J. D. P. King.** Stopping power of lithium for low energy protons—48
Heaps, C. W. Measurements of magnetic viscosity in iron—288
Heitler, W. Remarks on nuclear disintegrations by cosmic rays—873
Hellund, E. J. (see Uehling, E. A.)—479(L)
Henderson, J. E. (see Fleming, G.)—241(A)
——— (see Rubens, S. M.)—238(A)
——— **and S. M. Rubens.** Probe investigation of anode spots—238(A)
Herb, R. G. (see Bernet, E. J.)—398
Hershey, Allen V. Measurements of the mobility of potassium ions at high field intensity and low pressure—237(A)
——— Mechanism of the positive ion emission from catalysts—242(A)
Herzfeld, Karl F. and Edward Teller. Vapor pressure of isotopes—912
——— (see Lyddane, R. H.)—846
Hicks, J. F. G. (see Wilson, A. J. C.)—87(L)
Hippel, A. von. Electronic conduction in insulating crystals under very high field strength—867(A), 1096
Hipple, John A., Jr. (see Delfosse, J.)—1060
Hirsh, F. R., Jr. Beilby layer on thin ground quartz crystals—238(A)
——— **and J. W. M. DuMond.** X-ray evidence on the nature of the surface layers of thin ground quartz crystals secured with the Cauchois spectrograph—789

Hoffman, J. G. and R. F. Bacher. Photographic effects produced by cadmium and other elements under neutron bombardment—644
Hofstadter, Robert. Photoconductivity in willemite—864(L)
Hoge, Harold J. (see Brickwedde, F. G.)—266
Hoisington, L. E. and G. Breit. Calculation of Coulomb wave functions for high energies—627
Holloway, M. G. and M. Stanley Livingston. Range and specific ionization of alpha-particles—18
Hooley, J. G. (see Wilson, A. J. C.)—87(L)
Houston, W. V. Resonance broadening of spectral lines—237(A), 884
Hubbard, J. C. (see Alleman, R. S.)—313(A)
Hudson, Rosemary. Sources of error in high frequency measurements of the dielectric properties of glass—866(A)
Hudspeth, Emmett and T. W. Bonner. Observation of H^1 and H^3 ranges from the disintegration of deuterium by deuterons—308(L)
Hughes, A. L. and Merle A. Starr. Atomic electron velocities in hydrogen—189
Huntoon, R. D. (see Ellett, A.)—87(L)
Hustrulid, A., P. Kusch and John T. Tate. Dissociation of benzene (C_6H_6), pyridine (C_5H_5N) and cyclohexane (C_6H_{12}) by electron impact—1037
Huxford, W. S. Townsend ionization coefficients in argon photo-tubes—313(A)

Ikawa, M. (see Sagane, R.)—149(L), 542(L), 970(L)

Jacobs, Robert B. Polymorphic transitions in metallic halides—468
——— X-ray diffraction of substances under high pressures—325
James, Hubert M. (see Coolidge, Albert Sprague)—726
——— **and F. L. Yost.** Wave functions for $1s2s\ ^3S$ Li^+—646(L)
Jauncey, G. E. M. and W. A. Bruce. Diffuse scattering of x-rays from piezoelectrically oscillating quartz—163
Jenkins, F. A. (see Worley, R. E.)—305(L)
Jeppesen, C. Rulon. Emission bands in the $3p^1\Pi_{cd}-1s^1\Sigma$ system of the hydrogen molecule—68
Johnson, R. P. Construction of filament surfaces—459
——— Electron optics—867(T)
Johnson, T. H. Cosmic-ray intensity at high elevations in northern latitudes—151
——— Note on the nature of the primary cosmic radiation—385
Jones, A. T. Recent investigations of organ pipes—867(T)
Jordan, W. H. Electrical axis of the heart by direct observation—235(A)

Kakiuchi, Yoshinobu. Increase of x-ray reflection from quartz due to a strong electric field—772(L)
Kalbfell, D. C. Internal conversion of γ-rays in element 43—543(L)
Kamen, Martin D. (see Wilson, Robert R.)—1031
Kamogawa, Hirosi. Structure of oxidized silicon film—91(L)
Kanne, W. R. and G. L. Ragan. Gamma-rays from Li+H—480(L)
Kaplan, Joseph. Identification of auroral radiations—148(L)
——— Preparation and properties of auroral afterflows—176
——— Production of highly vibrating molecules—230(L)
——— Wave-length of the new nitrogen line—541(L)
——— Where does the light of the night sky originate?—241(A)
King, Frederick (see Lowan, Arnold N.)—1109
King, L. D. P. (see Haworth, L. J.)—38, 48
Kinsey, E. L. (see Ellis, J. W.)—599
Kip, Arthur F. Positive-point-to-plane discharge in air at atmospheric pressure—139
Kirby, S. S., N. Smith and T. R. Gilliland. Nature of the ionosphere storm—234(L)
Kirkpatrick, H. A. and J. W. M. DuMond. Shape of the modified Compton line for hydrogen and Ceylon graphite scatterers—802
Knauss, H. P. (see Paul, F. W.)—1072
Knipp, J. K. (see Breit, G.)—652
Knudsen, V. O. and E. Fricke. Absorption of sound in carbon dioxide and in carbon disulphide—238(A)
Kojima, S. (see Sagane, R.)—149(L), 542(L), 970(L)
Konopinski, E. J. and H. A. Bethe. Theory of excitation functions on the basis of the many-body model—130
Kovarik, Alois F. and Norman I. Adams, Jr. Disintegration constant of thorium and the branching ratio of thorium C—413
Krishnan, K. S. and A. Mookherji. Magnetic anisotropy of copper sulphate pentahydrate, $CuSO_4 \cdot 5H_2O$, in relation to its crystal structure. Part II—533: Part III—841
Kroeger, W. J. Binding energy of O^{16}—1048
Kruger, P. Gerald. (see Phillips, L. W.)—839
Kusch, P. (see Hustrulid, A.)—1037
——— (see Millman, S.)—968(L)
Kyropoulos, S. On the viscosity of nonpolar liquids—241(A)

Laird, Elizabeth R. Plan and equipment of Mount Holyoke College—867(T)
Lageman, R. T. (see Slack, F. G.)—358
Landé, Alfred. Transitions between levels spaced almost continuously—940
Langer, Lawrence M. (see Myers, Frank E.)—90(L)
Langer, R. M. Mass of cosmic-ray particles—237(A)
Laporte, Otto. Elastic scattering of Yukawa particles. I.—905
Lifschutz, Harold and O. S. Duffendack. Counting losses in Geiger-Müller counter circuits and recorders—714
Lindsay, George A. (see Whitmer, Robert M.)—988
Livingood, J. J. Investigations in artificial radioactivity—867(T)
——— **and G. T. Seaborg.** Long-lived radioactive silver—88(L)
——— **and G. T. Seaborg.** Long period radioactive zinc—239(A)
——— **and G. T. Seaborg.** Radioactive isotopes of iodine—775

——— **and G. T. Seaborg.** Radioactive isotopes of iron—51
——— **and G. T. Seaborg.** Radioactive manganese isotopes —391
Livingston, M. Stanley (see Holloway, M. G.)—18
Loeb, Leonard B. (see Beckman, J. W.)—862(L)
London, F. On the Bose-Einstein condensation—947
Loughridge, Donald H. (see Trueblood, Harold)—239(A), 545
——— **and N. Kermit Olsen.** Photoelectric long wavelength limit of magnetized iron—239(A)
Lowan, Arnold N. and Frederick King. Note on the evaluation of the earth's temperature arising from radioactivity—1109
Lukens, Charles (see Wood, R. W.)—332
Lyddane, R. H. and K. F. Herzfeld. Lattice vibrations in polar crystals—846

Manley, John H. (see Brickwedde, F. G.)—266
Mann, K. C. (see Smith, H. Grayson)—766
———, **H. Grayson Smith and J. O. Wilhelm.** Effect of magnetic fields on persistent currents in a closed superconducting circuit—314(A)
———, **H. Grayson Smith and J. O. Wilhelm.** Influence of magnetic fields on persistent currents in a closed superconducting circuit—758
Mann, Wilfrid B. Nuclear transformations produced in zinc by alpha-particle bombardment—649
Margenau, Henry. Quadrupole contributions to London's dispersion forces—867(A)
——— **and Kenneth G. Carroll.** Binding energy of Li^8—705
——— **and Warren A. Tyrrell, Jr.** Variational theory of the alpha-particle—422
Maris, H. B. Sidereal daily variation of barometric pressure —478(L)
May, Albert. Potential energies of the alkali halides: Errata and extension of the semi-empirical formula—629
McCormick, W. W. and R. A. Sawyer. Classification of the spectrum of singly ionized tin. Sn II—71
McKeehan, L. W. "Radio"—232(L)
McLay, A. B. (see Crawford, M. F.)—313(A)
McReynolds, A. W. (see B. T. Wright)—231(L)
Mellon, Arthur W. (see Hartig, Henry E.)—646(L)
Merideth, George T. (see Broxon, James W.)—1, 9, 605
Merwe, C. W. van der (see Bacon, R. H.)—315(A)
Meuron, H. J. (see Bradbury, N. E.)—242(A)
Millman, S., P. Kusch and I. I. Rabi. Nuclear magnetic moment of N^{14}—968(L)
Mimno, H. R. (see Pierce, John Alvin)—475
Miyamoto, G. (see Sagane, R.)—542(L), 970(L)
Mohler, Fred L. Number of lines in a series as a function of electron concentration—313(A)
Mookherji, A. (see Krishnan, K. S.)—533, 841
More, Kenneth R. Spectra of the monochlorides of nickel, cobalt and iron—122
Morgan, H. E. and R. B. Dow. Effects of pressure and temperature on the viscosity of monosubstituted toluenes—312(A)
Morgan, Joseph (see Bohn, J. Lloyd)—314(A)
Morgan, K. Z. (see Nielsen, W. H.)—245
Morrison, P. (see Dancoff, S. M.)—149(L)
Morse, Philip M. and Pearl J. Rubenstein. Diffraction of waves by ribbons and by slits—895
Motz, Lloyd and Eugene Feenberg. Spacing of energy levels in light nuclei—1055
Myers, Frank E. and Lawrence M. Langer. Search for an excited state of the H^3 nucleus—90(L)
Myers, R. D. Angular distribution of resonance disintegration products—361

Neddermeyer, Seth H. and Carl D. Anderson. Cosmic-ray particles of intermediate mass—88(L)
Nelson, E. B. (see Underwood, N.)—355
Němejcová, A. and J. Brož. Effect of a direct electric field on Laue diffraction photograms—379
Nielsen, Alvin H. and Harald H. Nielsen. Infra-red absorption spectrum of CD_4—118
Nielsen, Harald H. (see Nielsen, Alvin H.)—118
Nielsen, W. M. and K. Z. Morgan. Absorption of the penetrating component of the cosmic radiation—245
Nier, Alfred O. Isotopic constitution of strontium, barium, bismuth, thallium and mercury—275
Nix, F. C. Order-disorder transformations in alloys—1116(T)
Nordheim, G. (see Nordheim, L. W.)—254
Nordheim, L. W. and G. Nordheim. On the production of heavy electrons—254
Ny, Tsi-Zé and Shang-Yi Ch'en. Pressure shifts of the high terms of the absorption series of Na, Rb, and Cs produced by hydrogen and nitrogen—1045

Obert, Leonard and J. A. Bearden. Effect of chemical combination of *K*-fluorescent x-ray emission lines—1000
Oliphant, M. L. Helium-deuteron and deuteron-deuteron nuclear reactions—corrections—772(L)
Olsen, N. Kermit (see Loughridge, Donald H.)—239(A)
Onsager, L. Initial recombination of ions—554
Oppenheimer, Jacquenette (see Fowler, W. A.)—320
Oppenheimer, J. R. and Robert Serber. On the stability of stellar neutron cores—540(L)

Parkinson, D. B. (see Bernet, E. J.)—398
Parratt, Lyman G. Silver *L* series x-ray spectrum: line widths, wave-lengths, relative intensities, satellites, and widths of energy levels—99
Pasternack, Simon. Note on the fine structure of Hα and Dα—1113(L)
Paul, F. W. and H. P. Knauss. Rotational structure of the $^2\Sigma - {}^2\Pi$ bands of BF—1072
Pauli, W. On asymptotic series for functions in the theory of diffraction of light—924
Pauling, Linus. Nature of the interatomic forces in metals —899
Peierls, R. On a minimum property of the free energy—918
Peoples, J. A., Jr. (see Green, J. B.)—602
Phillips, L. W. and P. Gerald Kruger. Deep terms in Co VI and Ni VII—839
Pierce, John Alvin and H. R. Mimno. Unusual range of radio signals—475
Pitt, A. (see Findlay, J. C.)—506

Pollard, Ernest. Transmutation of scandium by Th C′ alpha-particles—411
——— (see Davidson, W. L., Jr.)—408
Pontecorvo, Bruno. Nuclear isomerism and internal conversion—542(L)
Power, R. B. (see Cobine, J. D.)—312(A)
Powers, Philip N. Magnetic scattering of neutrons—827
Purcell, Edward M. Focusing of charged particles by a spherical condenser—818

Quimby, S. L. (see Hardy, T. C.)—217
——— (see Siegel, Sidney)—76
——— **and Sidney Siegel.** Variation of the elastic constants of crystalline sodium with temperature between 80°K and 210°K—293

Rabi, I. I. (see Millman, S.)—968(L)
Ragan, G. L. (see Kanne, W. R.)—480(L)
Raines, Barbara. Variation with heat treatment of the cold resistance of nickel—481(L)
Ramsey, W. E. (see Swann, W. F. G.)—229(L)
Rarita, William and Zaka I. Slawsky. Nuclear two-body variational problem—1053
Read, T. A. Internal friction of metallic crystals—389(L)
Reiling, Victor G. (see Collins, George B.)—499
Ridenour, L. N. (see White, M. G.)—314(A)
Roberts, R. B. (see Rumbaugh, L. H.)—657
Rock, George D. (see Fox, Francis E.)—223
Rosenthal, Jenny E. Virtual levels of Be^8 and the alpha-particle model—315(A)
Rubens, S. M. (see Henderson, J. E.)—238(A)
——— **and J. E. Henderson.** Spherical ground joints for vacuum systems—238(A)
Rubenstein, Pearl J. (see Morse, Philip M.)—895
Rubinowicz, A. On the anomalous propagation of phase in the focus—931
Ruhlig, Arthur J. Search for gamma-rays from the deuteron-deuteron reaction—308(L)
Rumbaugh, L. H., R. B. Roberts and L. R. Hafstad. Nuclear transmutations of the lithium isotopes—657
Rusk, Rogers D. Collector electrode currents in discharges of different current density—865(A)

Sagane, R., S. Kojima and M. Ikawa. Radioactive As isotopes—149(L)
———, **Shoji Kojima, Goro Miyamoto and M. Ikawa.** Neutron induced radioactivity in columbium—970(L)
———, **S. Kojima, G. Miyamoto and M. Ikawa.** Preliminary report on the radioactivity produced in Y, Zr and Mo—542(L)
St. Helens, N. J. (see Wilkins, T. R.)—783
Sargent, B. W. β-rays of actinium B and actinium C″ particle spectra—232(L)
Sawyer, R. A. (see McCormick, W. W.)—71
Schein, Marcel and Volney C. Wilson. Evidence for the production of penetrating secondary cosmic-ray particles in the atmosphere—304(L)
Schiff, L. I. Excited state of He^3—92(L), 235(A)
——— On the paths of ions in the cyclotron—1114(L)
Schneider, Edwin G. Secondary emission of beryllium—185
Schneider, W. A. (see Waldman, B.)—543(L), 1017
Schremp, E. J. I. General theory of the earth's shadow effect of cosmic radiation—153
——— II. Simple shadow cone of cosmic radiation—158
Schultz, H. L. Vacuum tube high voltage stabilizing circuit of d.c. sources—314(A)
Seaborg, G. T. (see Grahame, D. C.)—240(A)
——— (see Livingood, J. J.)—51, 88(L), 239(A), 391, 775
——— (see Segrè, E.)—772(L)
Seeger, R. J. and E. Teller. On the electrical breakdown of the alkali halides—515
Segrè, E. and G. T. Seaborg. Nuclear isomerism in element 43—772(L)
Seitz, Frederick. Nature of lattice defects in silver bromide crystals—1111
Serber, R. Transition effects of cosmic rays in the atmosphere—317
——— (see Oppenheimer, J. R.)—540(L)
Shaw, A. E. New precision method for the determination of e/m for electrons—193
Sherr, Rubby (see White, M. G.)—314(A)
———, **Lincoln G. Smith and Walker Bleakney.** On the existence of H^3—388(L)
Shortley, George H. and Bernard Fried. Extension of the theory of complex spectra—739
——— **and Bernard Fried.** Structure of the configurations of high azimuthal quantum number in Cu II and the rare gases—749
Siegel, Sidney (see Quimby, S. L.)—293
——— **and S. L. Quimby.** Thermal expansion of crystalline sodium between 80°K and 290°K—76
Skaggs, Lester S. (see Allison, Samuel K.)—171
Slack, F. G. (see Underwood, N.)—355
———, **R. T. Lageman and N. Underwood.** Magneto-optical activity of crystalline nickel sulfate, α-hexahydrate—358
Slawsky, Zaka I. (see Rarita, William)—1053
Smith, H. Grayson (see Findlay, J. C.)—506
——— (see Mann, K. C.)—314(A), 758
——— **and K. C. Mann.** Relaxation effects connected with the transition between the superconducting and normal states—766
Smith, Lincoln G. (see Sherr, Rubby)—388 (L)
Smith, N. (see Kirby, S. S.)—234(L)
Smith, Nicholas M., Jr. (see Allison, Samuel K.)—171
Starr, Chauncey. Pressure coefficient of thermal conductivity of metals—210
Starr, Merle A. (see Hughes, A. L.)—189
Staub, H. (see Stephens, W. E.)—237(A)
——— **and W. E. Stephens.** α-Particles from the disintegration of lithium by deuterons—236(A)
Stearns, J. C. (see Froman, Darol K.)—315(A), 969(L)
Stephens, W. E. (see Staub, H.)—236(A)
——— **and H. Staub.** Neutrons from the break-up of He^5—237(A)
Stevenson, A. F. and M. F. Crawford. Lower limit for the theoretical energy of the normal state of helium—375
——— **and M. F. Crawford.** Theoretical lower bound for the energy of the normal state of helium—314(A)
Stout, J. W. (see Giauque, W. F.)—147(L)

Strain, Charles V. Proton induced radioactivities. II. Nickel and copper targets—1021
Strong, John. New radiation pyrometer for the measurement of low and high temperatures—242(A)
Stueckelberg, E. C. G. Rigorous theory of interaction between nuclear particles—889
Stücklen, Hildegard (see Carr, Emma P.)—865(A)
Swann, W. F. G. Hard and soft component of cosmic radiation in terms of a common primary background—307(L)
——— **and W. E. Ramsey.** Cosmic-ray electron showers in a mine 100 feet below sea level—229(L)
Swanson, Carl E. (see Hartig, Henry E.)—618
Szczeniowski, S. and St. Ziemecki. Fluctuations of residual ionization current at great depths—233(L)

Tappert, J. G. Experimental investigation of de Broglie's equation—1085
Tate, John T. (see Hustrulid, A.)—1037
Teller, E. (see Hafstad, L. R.)—681
——— (see Herzfeld, K. F.)—912
——— (see Seeger, R. J.)—515
Thomas, Charles D. Static interaction of charged particles—367
Thomas, L. H. Paths of ions in the cyclotron. I. Orbits in the magnetic field—580
——— Paths of ions in the cyclotron. II. Paths in the combined electric and magnetic fields—588
Thompson, Julian L. Solar diurnal variation of cosmic-ray intensity as a function of latitude—93
Thosar, B. V. Physical state of chromium impurity in corundum—233(L)
Tomboulian, D. H. New terms in the spectrum of Na III—347
——— Spectra of Rb III and Sr IV—350
——— **and R. F. Bacher.** On the hyperfine structure interval rule in indium—446
Tonks, L. New form of the electromagnetic energy equation when free charged particles are present—863(L)
——— Rate of vaporization of mercury from an anchored cathode spot—634
Trichel, G. W. Mechanism of the negative point to plane corona near onset—1078
——— Mechanism of the positive and negative point coronas in air at atmospheric pressure—242(A)
Trueblood, Harold and Donald H. Loughridge. Angular distributions of recoil and photoelectrons produced by 300 to 800 kv x-rays in nitrogen—239(A)
——— **and Donald H. Loughridge.** Scattering and photoelectric absorption of high voltage x-rays in nitrogen—545
Turnbull, John C. and H. E. Farnsworth. Inelastic scattering of slow electrons from a silver single crystal—509
Tyrrell, Warren A., Jr. (see Margenau, Henry)—422

Uehling, E. A. and E. J. Hellund. Viscosity of helium—479(L)
Uhlenbeck, G. E. Properties of gases at low temperatures—1116(T)
Underwood, N. (see Slack, F. G.)—358
———, **F. G. Slack and E. B. Nelson.** Optical activity of crystalline nickel sulfate α-hexahydrate—355
Urey, H. C. Separation of the isotopes of nitrogen—1116(T)

Vernon, E. L. (see Coolidge, Albert Sprague)—726

Waddel, R. C. (see Waldman, B.)—543(L), 1017
Waldman, B., R. C. Waddel, D. Callihan and W. A. Schneider. Location of resonances in boron plus proton reactions—543(L)
———, **R. C. Waddel, D. Callihan and W. A. Schneider.** Resonance processes in the disintegration of boron by protons—1017
Wall, C. N. Atomic distribution function for liquid sodium—1062
Watson, W. W. High pressure arc as spectroscopic source—865(A)
——— Spectrum of lead hydride—1068
Weeks, Dorothy W. and George R. Harrison. New survey of the spectrum of the international iron arc in the range 10,000 to 2000A—312(A)
Wentzel, G. Angular spread of hard cosmic-ray showers—869
Wertenstein, L. Remarks on the article by H. R. Crane and J. Halpern—"New experimental evidence for the neutrino"—306(L)
Wheeler, Mary A. Paramagnetic susceptibility of copper-nickel and zinc-nickel alloys—867(A)
Whitaker, Martin D., Harold G. Beyer and John R. Dunning. Scattering of slow neutrons by paramagnetic salts—771(L)
White, M. G., L. A. Delsasso, Rubby Sherr and L. N. Ridenour. Threshold energies for some (p,n) reactions—314(A)
Whitmer, Robert M. and George A. Lindsay. Anomalous dispersion of x-rays in calcite—988
Wilhelm, J. O. (see Findlay, J. C.)—506
——— (see Mann, K. C.)—314(A), 758
Wilkins, T. R. and D. P. Crawford. Cloud-chamber study of the alpha-rays of actino-uranium—316(A)
——— **and A. J. Dempster.** Radioactive isotope of samarium—315(A)
——— **and H. J. St. Helens.** Grain-spacing of alpha-ray, proton and deuteron tracks in photographic emissions—783
Williams, D. T. and L. P. Granath. Hyperfine structure of boron, yttrium, rhodium and palladium—338
Williams, Dudley. S–H frequency of the mercaptans—504
Williams, Robley C. Determination of e/m from the Hα − Dα interval—568
——— Fine structure of Hα and Dα under varying discharge conditions—558
Wilson, Arthur J. C. Heat capacity of Rochelle salt between −30° and +30°C—1103
———, **J. F. G. Hicks and J. G. Hooley.** Heat capacity of Rochelle salt—87(L)
Wilson, Robert R. Magnitude of accelerated current in the cyclotron—240(A)
——— **and Martin D. Kamen.** Internal targets in the cyclotron—1031
Wilson, Volney C. (see Schein, Marcel)—304(L)

Winsor, L. P. (see Cobine, J. D.)—312(A)
Wood, R. W. and Charles Lukens. Optical properties of the alkali metals—332
Worley, R. E. and F. A. Jenkins. New Rydberg series in N_2—305(L)
Wright, B. T. and A. W. McReynolds. Beta-rays from radium E—231(L)
Yost, F. L. (see James, Hubert M.)—646(L)
Young, R. T., Jr. Transparency of sea-water in the Pacific Ocean—866(A)

Ziemecki, St. (see Szczeniowski, S.)—233(L)
Zisman, W. A. (see Goranson, Roy W.)—544(L)
Zwicky, F. On neutron stars—242(A)

Analytic Subject Index to Volume 54

References with (A) are to abstracts of papers presented at meetings of the American Physical Society. References with (L) are to Letters to the Editor.

Absorption and reflection of light (see also **Spectra, absorption**)
Transparency of sea-water, R. T. Young, Jr.—866(A)
Acoustics
Absorption in CO_2 and CS_2, V. O. Knudsen, E. Fricke—238(A)
Diffraction of waves by ribbons and slits, P. M. Morse, P. J. Rubenstein—895
"Transverse" waves in rigid tubes, H. E. Hartig, C. E. Swanson—618
Ultrasonic radiation field in liquid media, F. E. Fox, G. D. Rock—223
Ultrasonic reflection losses, R. S. Alleman, J. C. Hubbard—313(A)
Velocity of sound in liquid He, J. C. Findlay, A. Pitt, H. G. Smith, J. O. Wilhelm—506
Afterglow
Highly vibrating molecules, J. Kaplan—230(L)
Arcs (see **Discharge of electricity in gases**)
Astrophysics
Deuterons by $_1H^1$ combination, H. A. Bethe, C. L. Critchfield—248; 862(L)
Neutron stars, F. Zwicky—242(A)
Stability of stellar neutron cores, J. R. Oppenheimer, R. Serber—540(L)
Theory of novae, G. Gamow—480(L)
Atomic structure (see also **Energy states of atoms; Spectra**)
Atomic electron velocities in hydrogen, A. L. Hughes, M. A. Starr—189
Aurora
Identification of radiations, J. Kaplan—148(L)
Preparation and properties of afterglows, J. Kaplan—176; 230(L)

Biophysics
Electrical axis of heart, W. H. Jordan—235(A)
Inhalation of radioactive air, R. D. Evans, C. Goodman—866(A)
Vitrification and crystallization of living cells, A. Goetz, S. S. Goetz—236(A)
Broadening of spectral lines
Resonance broadening, W. V. Houston—237(A); 884

Compton effect (see **X-rays, diffraction, scattering**)
Conductivity, electrical (see **Electrical conductivity; Discharge of electricity in gases**)
Constants, physical, standards
Evaluation of, R. A. Beth—865(A)
Validity of x-ray methods of determining e, V. L. Bollman, J. W. M. DuMond—1005
Contact potentials
Between Ba and Mg, P. A. Anderson—753; R. J. Cashman—971(L)
And photoelectric effect of semi-conductors, E. U. Condon—1089

Cosmic radiation
Absorption of shower-producing component in Fe and Pb, J. Crudup—483
Angular spread of showers, G. Wentzel—869
Diurnal variation, function of latitude, J. L. Thompson—93
Earth's shadow, theory of, E. J. Schremp—153; 158
At great depths, S. Szczeniowski, St. Ziemecki—233(L)
Hard and soft components common, primary background, W. F. G. Swann—307(L)
Heavy electrons, production of, L. W. Nordheim, G. Nordheim—254
At high elevations in northern latitudes, T. H. Johnson—151
Ionization in air at high pressures, J. W. Broxon, G. T. Merideth—1; 9; 605
Mass of particles, R. M. Langer—237(A)
Nature of primary radiation, T. H. Johnson—385
Neutrons in showers, D. K. Froman, J. C. Stearns—969(L)
Particles of intermediate mass, S. H. Neddermeyer, C. D. Anderson—88(L)
Penetrating component, absorption of, W. M. Nielsen, K. Z. Morgan—245
Penetrating secondary particles, M. Schein, V. C. Wilson—304(L)
Radiative losses by particles, S. B. Batdorf, E. W. Beth—237(A)
Showers, altitude variation of, D. K. Froman, J. C. Stearns—315(A)
Showers in a mine, W. F. G. Swann, W. E. Ramsey—229(L)
Sidereal time variation, H. Alfvén—97
Temperature of cosmic rays, P. M. S. Blackett—973(L)
Transition effects, R. Serber—317
World-wide changes, S. E. Forbush—975
Crystal structure
Beilby layer on quartz crystals, F. R. Hirsh, Jr.—238(A)
Direct determination of crystal structure, M. Avrami—300; 1114(L)
Nature of surface layers of ground quartz, F. R. Hirsh Jr., J. W. M. DuMond—789
Superstructure in $FeNi_3$, F. E. Haworth—313(A); 693
Surface layers in calcite crystals, V. L. Bollman, J. W. M. DuMond—238(A)
Crystalline state
Atomic vibrations of Zn-Cu alloy, M. L. Fuller—388(L)
Crystal fields in ethylsulphates, C. B. Ellis, H. Hall—478(L)
Defect in AgBr crystals, F. Seitz—1111
Electrical breakdown of alkali halides, R. J. Seeger, E. Teller—515
Electronic conduction in insulating crystals, A. von Hippel—867(A); 1096

Crystalline state (continued)
Filament surfaces; nature of, R. P. Johnson—459
Heat capacity of Rochelle salt, A. J. C. Wilson—1103
Heat capacity of Rochelle salt, A. J. C. Wilson, J. F. G Hicks, J. G. Hooley—87(L)
Interatomic forces in metals, L. Pauling—899
Internal friction of metallic crystals, T. A. Read—389(L)
Magnetic anisotropy of $CuSO_4 \cdot 5H_2O$, K. S. Krishnan, A. Mookherji—533; 841
Polymorphic transitions in metallic halides, R. B. Jacobs—468
Potential energies of alkali halides, A. May—629
State of Cr impurity in corundum, B. V. Thosar—233(L)
Temperature changes accompanying field emission, G. Fleming, J. E. Henderson—241(A)
Vibration of a body-centered cubic lattice, P. Fine—239(A)
Vibrations in polar crystals, R. H. Lyddane, K. F. Herzfeld—846
X-ray diffraction under high pressures, R. B. Jacobs—325

Dielectrics and dielectric properties
Errors in measurement at high frequencies, R. Hudson—866(A)
Diffraction of light
Asymptotic series for functions in the theory, W. Pauli—924
By ribbons and by slits, P. M. Morse, P. J. Rubenstein—895
Diffusion
In centrifugal force field, W. J. Archibald—371
Discharge of electricity in gases
Currents to collector electrodes, R. D. Rusk—865(A)
Ignition potential at low pressure, G. H. Fett—389(L)
Initial recombination of ions, L. Onsager—554
Ion currents in air at high pressure, J. W. Broxon, G. T. Merideth—1; 9; 605
Point to plane corona, G. W. Trichel—242(A); 1078
Positive ion emission from catalysts, A. V. Hershey—242(A)
Positive-point-to-plane discharge, A. F. Kip—139
Probe investigation of anode spots, J. E. Henderson, S. M. Rubens—238(A)
Reignition at high pressures, J. D. Cobine, R. B. Power, L. P. Winsor—312(A)
Spark breakdown potentials in A, N_2, and H_2, F. Ehrenkranz—239(A)
Townsend coefficients for pure H_2, D. H. Hale—241(A)
Townsend ionization coefficients, W. S. Huxford—313(A)
Vaporization of Hg from cathode spot, L. Tonks—634
Disintegration of nucleus, transmutations (see also **Radioactivity**)
α-particles from Li^7 (d,n) Be^8 reaction, H. Staub, W. E. Stephens—236(A)
Angular distribution of products, R. D. Myers—361
By cosmic rays, W. Heitler—873
Capture of orbital electrons, L. W. Alvarez—486
Distribution of H^1 from $d-d$ reaction, A. Ellett, R. D. Huntoon—87(L)
Energy change in $_4Be^9$ $(p,\alpha)_3Li^6$ reaction, S. K. Allison, L. S. Skaggs, N. M. Smith, Jr.—171
Excitation function of $_4Be^9$ $(p,\alpha)_3Li^6$ reactions, G. T. Hatch—165
γ-rays from the $_1H^2$ $_1H^2$ reaction, A. J. Ruhlig—308(L)
γ-rays from F+H, E. J. Bernet, R. G. Herb, D. B. Parkinson—398
γ-rays from Li+H^1, W. R. Kanne, G. L. Ragan—480(L)
$_2He^3-{}_1H^2$ and $_1H^2-{}_1H^2$ reactions, M. L. Oliphant—772(L)
K-electron capture in Be^7, G. Breit, J. K. Knipp—652
Of Li isotopes, yield curves, L. H. Rumbaugh, R. B. Roberts, L. R. Hafstad—657
Of Li^7; excitation function for protons, L. J. Haworth, L. D. P. King—38
Neutrons from break-up of He^5, W. E. Stephens, H. Staub—237(A)
H^1 and H^2 ranges from H^2+H^2, E. Hudspeth, T. W. Bonner—308(L)
Range and specific ionization of α-particles, M. G. Holloway, M. S. Livingston—18
Resonance processes in B+H reaction, B. Waldman, R. C. Waddel, D. Callihan, W. A. Schneider—543(L), 1017
Of Sc by α-particles, E. Pollard—411
Stopping power of Li for protons, L. J. Haworth, L. D. P. King—48
Theory of excitation, E. J. Konopinski, H. A. Bethe—130
Threshold energies (p,n) reactions, M. G. White, L. A. Delsasso, R. Sherr, L. N. Ridenour—314(A)
Of Ti by α-particles, W. L. Davidson, Jr., E. Pollard—408
Dissociation
Of C_6H_6, C_5H_5N and C_6H_{12} by electron impact, A. Hustrulid, P. Kusch, J. T. Tate—1037
Of C_2H_2D by electron impact, J. Delfosse, J. A. Hipple, Jr.—1060
Doppler effect
Transverse effect; theory of relativity, C. J. Davisson—90(L)

Elasticity
Coefficients, dependence on temperature, L. Brillouin—916
Constants of crystalline Na variation with temperature, S. L. Quimby, S. Siegel—293
Electrical conductivity and resistance
Breakdown phenomena in semi-conductors, J. Frenkel—647(L)
Electrical breakdown of alkali halides, R. J. Seeger, E. Teller—515
In crystals at high fields, A. von Hippel—867(A)
Of insulating crystals, A. von Hippel—867(A); 1096
Magnetic fields and persistent currents in superconducting circuit, K. C. Mann, H. G. Smith, J. O. Wilhelm—314(A); 758

Relaxation effects in superconductivity, H. G. Smith, K. C. Mann—766
Resistance of Ni, variation with heat treatment, B. Raines—481(L)
Electrical oscillations and waves
Transmission of damped waves through tubes, H. E. Hartig, A. W. Mellon—646(L)
Electromagnetic theory
Energy equation for field and free charges, L. Tonks—863(L)
Of material media, C. Eckart—920
Electron diffraction (see also **Electrons, scattering of**)
Test of de Broglie's equation, J. G. Tappert—1085
Electron optics
Studies of thoriated W, A. J. Ahearn, J. A. Becker—448
Electrons (see also E/m)
Heavy electrons, production of, L. W. Nordheim, G. Nordheim—254
Spin greater than $\frac{1}{2}$, Dirac equation, A. Bramley—314(A)
Electrons in metals (see **Crystalline state**)
Electrons, scattering of (see **Scattering of electrons, neutrons and ions, Electron diffraction**)
Electrons, secondary
From Be films, E. G. Schneider—185
Electrostatics
Interaction of charged particles; Born-Infeld equations, C. D. Thomas—367
E/m
β-rays from RaE, B. T. Wright, A. W. McReynolds—231(L)
Focusing of charged particles by a spherical condenser, E. M. Purcell—818
From the $H\alpha - D\alpha$ interval, R. C. Williams—568
Method for its determination, A. E. Shaw—193
From refraction of x-rays in diamond, J. A. Bearden—698
Value from recent data, R. T. Birge—972(L)
Energy states of atoms (see also **Spectra, atomic**)
Of He, theoretical lower bound, A. F. Stevenson, M. F. Crawford—314(A); 375
Energy states of nucleus (see also **Nucleus**)
Binding energy of Li^6, H. Margenau, K. G. Carroll—705
Binding energy of O^{16}, W. J. Kroeger—1048
Coulomb energy of light nuclei, H. A. Bethe—436
Excited state of He^3, L. I. Schiff—92(L); 235(A)
Of H^3 nucleus, F. E. Myers, L. M. Langer—90(L)
Levels in light nuclei, spacing of, L. Motz, E. Feenberg—1055
Symmetry effects in spacing levels, J. Bardeen, E. Feenberg—809
Two-body variational problem, W. Rarita, Z. I. Slawsky—1053
Variation theory of α-particle, H. Margenau, W. A. Tyrrell, Jr.—422
Errors of measurement
Physical constants, R. A. Beth—865(A)
Evaporation
Latent heat for liquid Na, C. N. Wall—1062
Of Hg from cathode spot, L. Tonks—634
Ferromagnetism (see **Magnetic properties**)
Field currents
Temperature changes, G. Fleming, J. E. Henderson—241(A)
Films, properties of
Electrical properties of multilayers, R. W. Goranson, W. A. Zisman—544(L)
Of SiO_2, Structure of films, Hirosi Kamogawa—91(L)
Fine structure (see **Spectra, etc. and Hyperfine structure**)
Of $H\alpha$ and $D\alpha$, R. C. Williams—558

Geophysics
Constitution of gases at Kilauea volcano, S. S. Ballard—236(A)
Disintegration constant of Th, A. F. Kovarik, N. I. Adams, Jr.—413
Earth's temperature, A. N. Lowan, F. King—1109

High voltage tubes and machines
Internal targets in cyclotrons, R. R. Wilson, M. D. Kamen—1031
Magnitude of current in cyclotron, R. R. Wilson—240(A)
Paths of ions in cyclotron, L. H. Thomas—580; 588; L. I. Schiff—1114(L)
Hyperfine structure
Of B, Y, Rh and Pd, D. T. Williams, L. P. Granath—338
Interval rule in In, D. H. Tomboulian, R. F. Bacher—446

Instruments (see **Methods and instruments**)
Ionization by particles (see also **Ionization potentials**)
By high speed electrons in N_2, R. B. Brode, D. R. Corson—238(A)
Range and specific ionization of α-particles, M. G. Holloway, M. S. Livingston—18
Townsend ionization coefficients, W. S. Huxford—313(A)
Ionization potentials
Of C_6H_6, C_5H_5N and C_6H_{12} by electron impact, A. Hustrulid, P. Kusch, J. T. Tate—1037
Ionization by radiation (see **Photoionization**)
Ionosphere
Nature of ionosphere storm, S. S. Kirby, N. Smith, T. R. Gilliland—234(L)
Ions, mobility
Of liquids electrified by bubbling, S. Chapman—520; 528
Of K ions at low pressure, A. V. Hershey—237(A)
Isomerism in nuclei
In element 43, E. Segrè, G. T. Seaborg—772(L)
And internal conversion, B. Pontecorvo—542(L)
In Rh, E. C. Crittenden, Jr., R. F. Bacher—862(L)
Isotopes
Existence of H^3, R. Sherr, L. G. Smith, W. Bleakney—388(L)
Of Sr, Ba, Bi, Tl and Hg, A. O. Nier—275
Vapor pressure of, K. F. Herzfeld, E. Teller—912

Liquid
Atomic distribution function for Na, C. N. Wall—1062
Velocity of sound in liquid He, J. C. Findlay, A. Pitt, H. G. Smith, J. O. Wilhelm—506

Liquid (continued)
Vibrational-rotational transitions in H_2O in solvents, J. W. Ellis, E. L. Kinsey—599

Magnetic properties
Anisotropy of $CuSO_4 \cdot 5H_2O$, K. S. Krishnan, A. Mookherji—533; 841
Domain theory, reversible susceptibility, W. F. Brown, Jr.—279
Ferromagnetic colloid, magnetic structures, W. C. Elmore—309(L); 1092
Generalization of theory, F. Bitter—79
Magnetic viscosity in Fe, C. W. Heaps—288
Susceptibility of Cu-Ni and Zn-Ni alloys, M. A. Wheeler 807(A)
Thermal energy change with magnetization, T. C. Hardy, S. L. Quimby—217

Magneto-optical effects
Of α-$NiSO_4 \cdot 6H_2O$, F. G. Slack, R. T. Lageman, N. Underwood—358

Mechanics, quantum—general
Calculation of Coulomb wave functions, L. E. Hoisington, G. Breit—627
Derivation of Maxwell-Boltzmann law, E. U. Condon—937
Matrices for covariant systems, R. J. Duffin—1114
Method for large perturbations, H. A. Bethe—955
Perturbation method, use of boundary conditions, H. Froehlich—945
Theory of neutral particle, W. H. Furry—56
Wave functions for $1s2s\,^3S$ Li^+, H. M. James, F. L. Yost—646(L)

Mechanics, quantum—molecular structure and spectra
Transitions between levels, A. Landé—940

Mechanics, statistical
Bose-Einstein condensation, F. London—947
Derivation of Maxwell-Boltzmann law, E. U. Condon—937
Minimum property of free energy, R. Peierls—918

Metals (see **Crystalline state**)

Meteorology
Atmospheric condensation nuclei, N. E. Bradbury, H. J. Meuron—242(A)
Nature of ionosphere storm, S. S. Kirby, N. Smith, T. R. Gilliland—234(L)
Polarigraph for sky light investigations, W. M. Cohn—241(A)
Sidereal variation of barometric pressure, H. B. Maris—478(L)
Source of night sky light, J. Kaplan—241(A)

Methods and instruments
Analysis of fertilizers, S. S. Ballard—312(A)
Calculation of Coulomb wave functions, L. E. Hoisington, G. Breit—627
Calculation of fluctuations, R. Ellickson—572
Condensation in cloud chamber, J. W. Beckman, L. B. Loeb—862(L)
Counting losses in G-M counters, H. Lifschutz, O. S. Duffendack—714
Dielectric constants at high frequencies, R. Hudson—866(A)
Diffusion in centrifugal force field, W. J. Archibald—371
Direct determination of crystal structure, M. Avrami—300
Electrical axis of heart by direct observation, W. H. Jordan—235(A)
E/m, determination of, A. E. Shaw—193
Ferromagnetic colloid, magnetic structure, W. C. Elmore—309(L)
Focusing of charged particles by a spherical condenser, E. M. Purcell—818
Geiger point counter, performance of, J. L. Bohn, J. Morgan—314(A)
Grain-spacing of α-ray, tracks in photographic emulsions, T. R. Wilkins, H. J. St Helens—783
Ground joints for vacuum systems, S. M. Rubens, J. E. Henderson—238(A)
High voltage stabilizing circuit, H. L. Schultz—314(A)
Internal targets in cyclotrons, R. R. Wilson, M. D. Kamen—1031
Large perturbations; treatment of, H. A. Bethe—955
Magnitude of current in cyclotron, R. R. Wilson—240(A)
Motion picture polarigraph, W. M. Cohn—241(A)
Paths of ions in cyclotron, L. H. Thomas—580; 588; L. I. Schiff—1114(L)
Photographic graininess, W. O. Gould, A. Goetz, A. Dember—240(A)
Potential curves from spectroscopic data, A. S. Coolidge, H. M. James, E. L. Vernon—726
Production of collimated beams of slow neutrons, L. W. Alvarez—609
Radiation pyrometer for low and high temperatures, J. Strong—242(A)
Separation of radioactive substances, D. C. Grahame, G. T. Seaborg—240(A)
Thermal expansion; low temperatures, S. Siegel, S. L. Quimby—76

Mobility of ions (see **Ions, mobility**)

Molecular structure and constants (see also **Spectra molecular**)
Potential curves from spectroscopic data, A. S. Coolidge H. M. James, E. L. Vernon—726

Neutrino (see also **Radioactivity**)
Experimental evidence for it, H. R. Crane, J. Halpern—306(L); L. Wertenstein—306(L)
Theory of neutral particle, W. H. Furry—56

Neutrons
From break-up of He^5, W. E. Stephens, H. Staub—237(A)
Neutron stars, F. Zwicky—242(A)
Photographic effects of elements under neutron bombardment, J. G. Hoffman, R. F. Bacher—644
Production of collimated beams, L. W. Alvarez—235(A); 609
Scattering cross sections of H_2, N_2 and H_2O, F. G. Brickwedde, J. R. Dunning, H. J. Hoge, J. H. Manley—266

Nuclear moments and spin (see also **Hyperfine structure**)
Of N^{14}, S. Millman, P. Kusch, I. I. Rabi—968(L)
Nucleus (see also **Disintegration of nucleus; Energy states of nucleus**)
α-particle model, L. R. Hafstad, E. Teller—681
Be^8 and α-particle model, J. E. Rosenthal—315(A)
Deuterons by $_1H^1$ combination, H. A. Bethe, C. L. Critchfield—248; 862(L)
Energy levels in light nuclei, L. Motz, E. Feenberg—1055
Interaction between nuclear particles, theory of, E. C. G. Stueckelberg—889
Isomerism and internal conversion, B. Pontecorvo—542(L)
Symmetry effects in spacing levels, J. Bardeen, E. Feenberg—809
Theory of excitation, E. J. Konopinski, H. A. Bethe—130
Two-body variational problem, W. Rarita, Z. I. Slawsky—1053
Variation theory of α-particle, H. Margenau, W. A. Tyrrell, Jr.—422

Optical constants and properties
Activity of crystalline α-$NiSO_4 \cdot 6H_2O$, N. Underwood, F. G. Slack, E. B. Nelson—355
Of alkali metals, R. W. Wood, C. Lukens—332
Refractive index of air, D. Bender—179
Optical theory (see also **Diffraction of light**)
Anomalous propagation of phase, A. Rubinowicz—931
Diffraction theory, W. Pauli—924
Theory of dispersion, force of excitation, P. P. Ewald—893

Photoconductivity
In willemite, R. Hofstadter—864(L)
Photoelectric effect and properties; cells
Long wave-length limit of magnetized iron, D. H. Loughridge, N. K. Olsen—239(A)
In semi-conductors, effect of contact potentials, E. U. Condon—1089
Photography
Graininess of photographic emulsions, A. Dember, A. Goetz, W. O. Gould—240(A)
Grain-spacing of α-ray tracks in photographic emulsions, T. R. Wilkins, H. J. St Helens—783
Instrument for determining graininess, W. O. Gould, A. Goetz, A. Dember—240(A)
Photoionization
Analysis of high gradient, high pressure, γ-ray ionization in air, J. W. Broxon, G. T. Merideth—9
γ-rays in air at high pressures, J. W. Broxon, G. T. Merideth—1

Quantum mechanics (see **Mechanics, quantum**)

Radiation
Čerenkov radiation; two million volt electrons, G. B. Collins, V. G. Reiling—499
Radio
Unusual range of signals, J. A. Pierce, H. R. Mimno—475
Radioactivity (see also **Disintegration of nucleus**)
α-rays of actino-uranium, T. R. Wilkins, D. P. Crawford—316(A)
β-ray spectrum of I^{128}, R. H. Bacon, E. N. Grisewood, C. W. van der Merwe—315(A)
β-rays of Ac B and Ac C″, B. W. Sargent—232(L)
β-rays from Ra E, B. T. Wright, A. W. McReynolds—231(L)
Calculation of fluctuations, R. Ellickson—572
Capture of orbital electrons, L. W. Alvarez—486
In Co, neutron induced, R. Sagane, S. Kajima, G. Miyamoto, M. Ikawa—970(L)
Disintegration constant of Th, branching ratio of Th C, A. F. Kovarik, N. I. Adams, Jr.—413
Earth's temperatures, A. N. Lowan, F. King—1109
Grain-spacing of α-ray tracks in photographic emulsions, T. R. Wilkins, H. J. St Helens—783
Inhalation of radioactive air, R. D. Evans, C. Goodman—866(A)
Internal conversion of arbitrary multipole order, S. M. Dancoff, P. Morrison—149(L)
Internal conversion in element 43, D. C. Kalbfell—543(L)
Of I isotopes, J. J. Livingood, G. T. Seaborg—775
Of Fe isotopes, J. J. Livingood, G. T. Seaborg—51
Isomerism in element 43, E. Segrè, G. T. Seaborg—772(L)
Isomerism and internal conversion, B. Pontecorvo—542(L)
Isomerism in Rh, E. C. Crittenden, Jr., R. F. Bacher—862(L)
Isotopes of As, R. Sagane, S. Kojima, M. Ikawa—149(L)
K-electron capture in Be^7, G. Breit, J. K. Knipp—652
Of Mn isotopes, J. J. Livingood, G. T. Seaborg—391
In Ni and Cu by $_1H^1$, C. V. Strain—1021
Ra and Th in air, C. Goodman, R. D. Evans—866(A)
Of Ra-Cl, D. C. Grahame—972(L)
Range and specific ionization of α-particles, M. G. Holloway, M. S. Livingston—18
Of Sm^{148}, T. R. Wilkins, A. J. Dempster—315(A)
Separation of radioactive substances, D. C. Grahame, G. T. Seaborg—240(A)
Of Ag, J. J. Livingood, G. T. Seaborg—88(L)
Use of term "radio," L. W. McKeehan—232(L)
In Y, Zr and Mo, R. Sagane, S. Kojima, G. Miyamoto, M. Ikawa—542(L)
Of Zn, J. J. Livingood, G. T. Seaborg—239(A)
In Zn by α-particle bombardment, W. B. Mann—649
In Zn and Se by $_1H^1$, J. H. Buck—1025
Raman effect
In dibromofluoromethane, G. Glockler, J. H. Bachmann—970(L)
Recombination
Initial recombination of ions, L. Onsager—554
Relativity
Electrostatic analog to red shift, H. T. Drill—240(A)
Lorentz' triangles and fringe shift, W. B. Artmel—867(A)
Michelson-Morley-Miller experiment, W. B. Cartmel—315(A)
Transverse Doppler effect, C. J. Davisson—90(L)

Scattering of electrons, neutrons and ions (see also **Electrons, scattering of; Electron diffraction**)
Of alkali ions in gases, K. H. Bracewell—639
Of α-particles by A, O_2 and Ne, G. Brubaker—1011
Angular distribution of photoelectrons, H. Trueblood, D. H. Loughridge—239(A); 545
Of electrons from Ag crystal, J. C. Turnbull, H. E. Farnsworth—509
Of fast electrons and positrons in Pb, W. A. Fowler, J. Oppenheimer—320; W. A. Fowler—773(L)
In H and atomic electron velocities, A. L. Hughes, M. A. Starr—189
Magnetic scattering of neutrons, P. N. Powers—827
Neutrons by H_2, N_2 and H_2O, F. G. Brickwedde, J. R. Dunning, H. J. Hoge, J. H. Manley—266
Of neutrons by paramagnetic salts, M. D. Whitaker, H. G. Beyer, J. R. Dunning—771(L)
Of slow neutrons with gases, H. Carroll, J. R. Dunning—541(L)
Of Yukawa particles I, O. Laporte—904
Secondary electrons (see **Electrons, secondary**)
Solid state (see **Crystalline state**)
Specific heat
Of Rochelle salt between $-30°$ and $+30°$C, A. J. C. Wilson, J. F. G. Hicks, J. G. Hooley—87(L); A. J. C. Wilson—1103
Spectra, absorption
Alterations in near infra-red spectra of water and protein molecules in gelatine, J. W. Ellis, J. Bath—236(A)
Of CD_4 in infra-red, A. H. Nielsen, H. H. Nielsen—118
Equivalent absorption coefficient, W. M. Elsasser—126
Of hydrocarbons, ultraviolet, E. P. Carr. H. Stücklen—865(A)
Of I Cl in ultraviolet, J. L. Binder—114
Of N_2, new Rydberg series, R. E. Worley, F. A. Jenkins—305(L)
Pressure shifts of high terms of Na, Rb, and Cs, Ny Tsi-Zé, Ch'en Shang-Yi—1045
S–H frequency of mercaptans, D. Williams—504
Vibrational-rotational transitions in H_2O in solvents, J. W. Ellis, E. L. Kinsey—599
Spectra, atomic
Of Co VI and Ni VII, L. W. Phillips, P. G. Kruger—839
Complex spectra, theory of, G. H. Shortley, B. Fried—739
Configurations in Cu II and rare gases, G. H. Shortley, B. Fried—749
Fine structure of Hα and Dα, S. Pasternack—1113(L)
Of Ir I, W. Albertson—183
Of Pb III, M. F. Crawford, A. B. McLay, A. M. Crooker—313(A)
Of Rb III and Sr IV, D. H. Tomboulian—350
Of Na III, D. H. Tomboulian—347
Of Sn II, W. W. McCormick, R. A. Sawyer—71
Spectra, general
Electrostatic analog to red shift, H. T. Drill—240(A)
New survey of the international Fe arc, D. W. Weeks, G. R. Harrison—312(A)
Nitrogen afterglow, J. Kaplan—176
Number of lines in a series, F. L. Mohler—313(A)
Resonance broadening, W. V. Houston—237(A); 884
Transitions between closely spaced levels, A. Landé—940
Wave-length of N_2 line, J. Kaplan—541(L)
Spectra, molecular (see also **Molecular structure and constants**)
Of BF, rotational structure of $^1\Sigma - {}^3\Pi$ bands, F. W. Paul, H. P. Knauss—1072
Of chlorides of Ni, Co, and Fe, K. R. More—122
Of CuCl excited by active nitrogen, S. Bloomenthal—497
Of H_2, bands ending on $2p^1$ II level, G. H. Dieke—439
Of H_2, emission bands, C. R. Jeppesen—68
Of HgCl, CdCl, and ZnCl, S. D. Cornell—341
Of PbH, W. W. Watson—1068
Spectroscopy, technique
Analysis of fertilizers, S. S. Ballard—312(A)
New survey of the international Fe arc, D. W. Weeks, G. R. Harrison—312(A)
Source, high pressure arc, W. W. Watson—865(A)
Statistical mechanics (see **Mechanics, statistical**)
Superconductivity (see **Electrical conductivity and resistance**)
Supersonics (see **Acoustics**)

Thermal conductivity
Of metals, pressure coefficient, C. Starr—210
Thermal expansion
Of crystalline Na between 80°K and 290°K, S. Siegel, S. L. Quimby—76
Thermionic emission of electrons; emitting surfaces
Studies of thoriated W, A. J. Ahearn, J. A. Becker—448
Thermodynamics
Minimum property of free energy, R. Peierls—918

Van der Waals forces
Quadrupole contributions, H. Margenau—867(A)
Vaporization (see **Evaporation**)
Vapor pressure
Of isotopes, K. F. Herzfeld, E. Teller—912
Viscosity
Effects of pressure and temperature on toluenes, H. E. Morgan, R. B. Dow—312(A)
Of helium, E. A. Uehling, E. J. Hellund—479(L)
Of liquid He II, W. F. Giauque, J. W. Stout, R. E. Barieau—147(L)
Of lubricating oils at various temperatures, R. B. Dow—312(A)
Of nonpolar liquids, S. Kyropoulos—241(A)

X-rays, absorption
Of wave-length $1.5 \leq \lambda \leq 8.3$A, C. L. Andrews—994
X-rays, diffraction, scattering, reflection, refraction and polarization
Anomalous dispersion in calcite, R. M. Whitmer, G. A. Lindsay—988
Beilby layer on quartz crystals, F. R. Hirsh, Jr.—238(A)
Diffraction under high pressures, R. B. Jacobs—325
Diffuse scattering from oscillating quartz, G. E. M. Jauncey, W. A. Bruce—163

Electric field on Laue pattern, A. Němejcová, J. Brož—379
Plural x-ray reflection, diffraction pattern of calcite, V. L. Bollman, H. H. Bailey, J. W. M. DuMond—792
Reflection from quartz in electric field, Y. Kakiuchi—772(L)
Scattering and absorption in N_2, H. C. Trueblood, D. H. Loughridge—239(A); 545
Shape of Compton line, H. A. Kirkpatrick, J. W. M. DuMond—802
Surface layers in calcite crystals, V. L. Bollman, J. W. M. DuMond—238(A)
Validity of x-ray methods of determining e, V. L. Bollman, J. W. M. DuMond—1005

X-rays, emission
Chemical combination and K-fluorescent lines, L. Obert, J. A. Bearden—1000
L series data, L. G. Parratt—99

Zeeman effect
In argon, J. B. Green, B. Fried—876
Of Cr lines, B. V. Thosar—233(L)
In Ne, J. B. Green, J. A. Peoples, Jr.—602

DEC 27 1938

THE PHYSICAL REVIEW

VOLUME 54 *Second Series* NUMBER 12

DECEMBER 15, 1938

Published for the

AMERICAN PHYSICAL SOCIETY

by the

AMERICAN INSTITUTE OF PHYSICS
Incorporated

LANCASTER, PA., AND NEW YORK, N. Y.

THE AMERICAN INSTITUTE OF PHYSICS

INCORPORATED

ADMINISTRATIVE STAFF

HERBERT A. BARTON, *Director*

MADELINE M. MITCHELL, *Publications Manager*

Office: 175 Fifth Avenue, New York, New York

JOURNALS

THE PHYSICAL REVIEW
REVIEWS OF MODERN PHYSICS
JOHN T. TATE, *Editor*
J. W. BUCHTA, *Assistant Editor*

JOURNAL OF APPLIED PHYSICS
ELMER HUTCHISSON, *Editor*

THE JOURNAL OF THE OPTICAL SOCIETY OF AMERICA
THE REVIEW OF SCIENTIFIC INSTRUMENTS
F. K. RICHTMYER, *Editor*

JOURNAL OF THE ACOUSTICAL SOCIETY OF AMERICA
F. R. WATSON, *Editor*

THE JOURNAL OF CHEMICAL PHYSICS
HAROLD C. UREY, *Editor*

THE AMERICAN PHYSICS TEACHER
DUANE ROLLER, *Editor*

GOVERNING BOARD

For The American Physical Society:

JOHN T. TATE, *Chairman*
University of Minnesota

GEORGE B. PEGRAM, *Secretary*
Columbia University

KARL T. COMPTON
Massachusetts Institute of Technology

For The Optical Society of America:

E. C. CRITTENDEN
National Bureau of Standards

A. C. HARDY
Massachusetts Institute of Technology

W. B. RAYTON
Bausch & Lomb Optical Company

For The Acoustical Society of America:

HARVEY FLETCHER
Bell Telephone Laboratories

VERN O. KNUDSEN
University of California at Los Angeles

WALLACE WATERFALL
The Celotex Corporation

For The Society of Rheology:

WHEELER P. DAVEY
Pennsylvania State College

MELVIN MOONEY
United States Rubber Products, Inc.

R. L. PEEK, JR.
Bell Telephone Laboratories

For The American Association of Physics Teachers:

HOMER L. DODGE
University of Oklahoma

FREDERIC PALMER, JR.
Haverford College

F. K. RICHTMYER
Cornell University

The American Institute of Physics is a membership corporation of which five societies are the founding members. These five societies are the principal national societies devoted to pure and applied physics in America. Their names, and those of their representatives who form the Governing Board of the Institute, are given above. The principal work of the Institute is the publication of journals sponsored by the societies or by itself. The names and the editors of the journals are also listed above.

The broad purpose of the Institute is to represent, in all matters of wide or common interest, the five thousand or more members and subscribers associated with the Founder Societies and the journals. It aims to advance the science and profession of physics, and to promote cooperation between pure research, the applied sciences and the industries. To achieve these aims, it is greatly in need of an endowment and is empowered by law to administer grants and funds of any kind.

CONTENTS

PHYS. REV. 54 (1938) DECEMBER 15

On World-Wide Changes in Cosmic-Ray Intensity . . . . . S. E. FORBUSH 975

Anomalous Dispersion of X-Rays in Calcite . ROBERT M. WHITMER AND GEORGE A. LINDSAY 988

Absorption of X-Rays of Wave-Length $1.5 \leq \lambda \leq 8.3$A . . . . . C. LUTHER ANDREWS 994

Effect of Chemical Combination on K Fluorescent X-Ray Emission Lines . . . . . LEONARD OBERT AND J. A. BEARDEN 1000

Further Tests of the Validity of X-Ray Crystal Methods of Determining e . . . . . V. L. BOLLMAN AND J. W. M. DUMOND 1005

Scattering of Alpha-Particles by Argon, Oxygen and Neon . . . . GORDON BRUBAKER 1011

Resonance Processes in the Disintegration of Boron by Protons . . . . . B. WALDMAN, R. C. WADDEL, D. CALLIHAN AND W. A. SCHNEIDER 1017

Proton Induced Radioactivities II. Nickel and Copper Targets . . . CHARLES V. STRAIN 1021

Proton Induced Radioactivities III. Zinc and Selenium Targets . . . . JOHN H. BUCK 1025

Internal Targets in the Cyclotron . . . . . ROBERT R. WILSON AND MARTIN D. KAMEN 1031

Dissociation of Benzene (C_6H_6), Pyridine (C_5H_5N) and Cyclohexane (C_6H_{12}) . . . . . A. HUSTRULID, P. KUSCH AND JOHN T. TATE 1037

Pressure Shifts of the High Terms of the Absorption Series of Na, Rb and Cs Produced by Hydrogen and Nitrogen . . . . . NY TSI-ZE AND CH'EN SHANG-YI 1045

Binding Energy of O^{16} . . . . . W. J. KROEGER 1048

Nuclear Two-Body Variational Problem . . . . WILLIAM RARITA AND ZAKA I. SLAWSKY 1053

Spacing of Energy Levels in Light Nuclei . . . . LLOYD MOTZ AND EUGENE FEENBERG 1055

Dissociation of $C_2H_2D_2$ by Electron Impact . . . . J. DELFOSSE AND JOHN A. HIPPLE, JR. 1060

Absolute Distribution Function for Liquid Sodium . . . . . C. N. WALL 1062

Spectrum of Lead Hydride . . . . . W. W. WATSON 1068

Rotational Structure of the $^2\Sigma \rightarrow {}^2\Pi$ Bands of BF . . . . F. W. PAUL AND H. P. KRAUSS 1072

Mechanism of the Negative Point to Plane Corona Near Onset . . . . G. W. TRICHEL 1078

Experimental Investigation of de Broglie's Equation . . . . . J. G. TAFFERY 1085

Note on the External Photoelectric Effect of Semi-Conductors . . . . E. U. CONDON 1089

Magnetization of Ferromagnetic Colloids . . . . . W. C. ELMORE 1092

Electronic Conduction in Insulating Crystals Under Very High Field Strength . A. VON HIPPEL 1096

Heat Capacity of Rochelle Salt Between $-50°$ and $+30°$C . . . . ARTHUR J. C. WILSON 1103

Note on the Production of the Earth's Temperatures Arising from Radioactivity . . . . . ARNOLD N. LOWAN AND FREDERICK KING 1109

Energy of Lattice Defects in Silver Bromide Crystals . . . . . FREDERICK SEITZ 1111

Letters to the Editor:

Note on the Fine Structure of He^+ and Be^{++} . . . . . SIDNEY PFEIFFERBECK 1113

On the Characteristic Matrices of Covariant Systems . . . . . R. J. DUFFIN 1114

Acknowledgment: Direct Determination of Crystal Structure from X-Ray Data . MELVIN AVRAMI 1114

On the Radius of Ions in the Cyclotron . . . . . L. L. SCHIFF 1114

Proceedings of the Metropolitan Section of the American Physical Society 1116

Author Index to Volume 54 1117

Analytic Subject Index to Volume 54 1125

Volume Table of Contents III

LANCASTER PRESS, INC., LANCASTER, PA.